UNIVERSITÀ DEGLI STUDI DI PADOVA

Faculty of Civil Engineering

Master's degree in Structural Engineering

DYNAMIC ANALYSIS OF AN HIGHWAY BRIDGE IN PRAGUE LANOVY MOST

Supervisors: *Prof. Claudio Modena (University of Padova)*

Prof. Jiri Maca (University of Prague CTU)

Prof. Thomas Plachy (University of Prague CTU)

Prof. Michal Polak (University of Prague CTU)

Student: Baret Eleonora

Academic year 2012/2013

Abstract

The main goal of the current research is to study the dynamic behaviour of the curved cable-stayed bridge constructed in Prague by full-scale testing and analytical models, through which the traffic flow vibration has been studied.

The finite element method with the Software Straus 7 has been employed in this study to obtain a three-dimensional numerical model for the bridge system and it is validated by a direct comparison with acceleration and displacement's measurements. The developed three-dimensional finite element model of the bridge has achieved a good correlation with the measured natural frequencies and mode shapes identified from field ambient vibration tests.
Comparison of test results and free vibration analyses shows that modelling of the deck end fixity is an important factor, while correct modelling of stay cables and stress-stiffening effects is not so important except for identifying cable modes with weak superstructure interaction.

The calibrate model is used for the simulation of a cable break and for the roadway traffic.

Moving vehicle loads can induce significant dynamic effects on the structural behaviours of bridges, especially for long-span bridges.
The bridge-vehicle interaction is affected by many factors. The current study has been focused on such factors as: vehicle speed, vehicle damping ratio, multiple traffic lanes, mass ratio of vehicle and bridge, and dynamic characteristics of bridge.
The dynamic characteristics of a box-girder bridge, including its natural frequencies, vibration mode shapes, and mechanical damping properties' are important factors which can significantly affect its stability behavior under traffic loads.

Contents

Chapter I - INTRODUCTION ABOUT THE STRUCTURE 21

1. General characteristics of bridges 23

1.1 Cable stayed bridge 23

1.2 Bridge monitoring 24

2. Location of the bridge 25

3. Bridge's description 29

Chapter II - FEM MODELS 39

1. Finite element modeling of the bridge 41

1.1 Simplified 3D finite element models of cable-stayed bridges 41

1.2 Full 3D finite element modeling of cable-stayed bridges 42

1.3 Initial equilibrium configuration 42

2. Type of elements in the models 43

2.1 Plate elements 43

2.2 Beam elements 45

2.3 Links 47

2.4 Cable and truss elements 47

2.5 Bridge bearings 49

2.6 Non structural masses 49

3. Design and import of the track 51

4. Simple beams model 53

4.1 Deck 53

4.2 Bearings 54

4.3 Pylon 54

4.4 Cables 57

5. Beams model with torsional d.o.f. 59

6. Plates model 63

6.1 Local plate results 71
6.2 Global plate results 71
6.3 Checking the quality of the plates model 72
6.3.1 Free edges 72
6.3.2 Orientation 72
6.3.3 Element aspect ratio 73
6.3.4 Plate warping ratio 75
7. Comparison of the three models 77
Chapter III - ANALYSIS 79
1. Static analysis 81
2. Natural frequency analysis 87
2.1 Pre-stressed modal analysis 88
2.2 Results from the three different models 89
2.3 Measured values of vibrations 101
2.4 Finite element model validation 111
3. Linear buckling solver 117
4. Linear dynamic analysis 123
4.1 Single degree of freedom systems 123
4.1.1 Case f = 0, c = 0 124
4.1.2 Case f = 0, c ≠ 0 125
4.1.3 Case f = cost, c = 0 129
4.2 Case f = cost, c ≠ 0, $\xi < 1$ 130
4.3 Straus analysis 132
4.4 Forcing function 134
4.5 Initial conditions 134
4.6 Solution techniques 134
4.7 Rayleigh damping 136
5. Vehicles vibration 143

5.1 Introduction to Program Prejezdy 144
5.1.1 Model of vehicle 144
5.1.2 Procedure of calculation of the bridge response 145
5.2 Applications of Program Prejezdy 146
5.3 Analyzed cases of traffic 149
5.3.1 Case 1: two vehicles in the same direction at 50 Km/h 150
5.3.2 Case 2: two vehicles in the same direction at 100 Km/h 158
5.3.3 Case 3: traffic flow 163
6. Conclusions 173

List of figures

Fig. 1 - Location of the bridge in Czech Republic 25
Fig. 2 - Prague's map 25
Fig. 3 - Bridge's position in Prague, aerial's view 26
Fig. 4 - Aerial view of Lanovy most 26
Fig. 5 - Track's shape of the bridge 27
Fig. 6 - Center of the roadway 29
Fig. 7 - Bridge's view 30
Fig. 8 - Photos' view 30
Fig. 9 - Photo from corner 1 31
Fig. 10 - Photo from corner 2 31
Fig. 12 - Render of the cables part of the bridge 32
Fig. 13 - Particular of the concrete box section 33
Fig. 14 - Cross section 33
Fig. 15 - Geometrical properties of the schematized cross section 34
Fig. 16 - Cross section's renders 34
Fig. 17 - Top of the pylon 35
Fig. 18 - Blueprint of the second part of the pylon 36
Fig. 19 - Blueprint of the third part of the pylon 37
Fig. 20 - Blueprint of the forth part of the pylon 37
Fig. 21 - Cables connection to the deck 38
Fig. 22 - Simple and double bearings 38
Fig. 23 - 4 nodes quadrilateral element 43
Fig. 24 - Local coordinates system of a plate element 44
Fig. 25 - Plates displacements 44
Fig. 26 - Beam forces associated with d.o.f 45
Fig. 27 - Principal coordinate system of a beam 46
Fig. 28 - Default principal axes of a beam element 47
Fig. 29 - Degrees of freedom of a truss element in global coordinates 48
Fig. 30 - Track of the bridge (mm) 51
Fig. 31 - Track's subdivision 51
Fig. 32 - Simple schematization of the cross section 53
Fig. 33 - Deck's subdivision 53
Fig. 34 - Number of bearings 53

Fig. 35 - Types of support 54
Fig. 36 - Pylon (dimensions in cm) 54
Fig. 37 - Pylon part I 55
Fig. 38 - Pylon part II 55
Fig. 39 - Pylon part III 56
Fig. 40 - Pylon part IV 56
Fig. 41 - Front of the bridge 57
Fig. 42 - Dimensions of the cables 57
Fig. 43 - Beam's degree of freedom 59
Fig. 44 - Schematization of the deck part 1 59
Fig. 45 - Schematization of the deck part 2 60
Fig. 46 – Bridge's model with non-structural masses 61
Fig. 47 - Particular of the masses' connection 61
Fig. 48 - Displacements vs number of plates 63
Fig. 49 - Complete plates model 64
Fig. 50 - Insole 1 64
Fig. 51 - Insole 2 65
Fig. 52 - Insole 3 65
Fig. 53 - Low plane 1 65
Fig. 54 - Low plane 2 66
Fig. 55 - Low plane 3 66
Fig. 56 - Inclined plates 1 66
Fig. 57 - Inclined plates 2 67
Fig. 58 - Inclined plates 3 67
Fig. 59 - Vertical planes 1 67
Fig. 62 - Bearings 69
Fig. 63 - Internal wind bracings 69
Fig. 64 - Wind bracings 69
Fig. 65 - Material and structural properties of the wind bracings 70
Fig. 66 - Convention for moments 71
Fig. 67 - Positive stress directions 71
Fig. 68 - Mid plane's forces 71
Fig. 69 - Free edges 72
Fig. 70 - Different orientations of the plates 72
Fig. 71 - Common orientation of the plates 73

Fig. 72 - Aspect ratios for a square and a rectangle 73
Fig. 73 - Contour type 74
Fig. 74 - Element aspect ratio 74
Fig. 75 - Element aspect ratio's detail 74
Fig. 76 - Warped plate element 75
Fig. 77 - Plate warping ratio 75
Fig. 78 - Static analysis displacements, self weight 81
Fig. 79 - Static analysis displacements, cables pretension 81
Fig. 80 - Static analysis displacements, linear load combination 81
Fig. 81 - Static analysis displacements, SLU combination 82
Fig. 82 - Central points of the deck 82
Fig. 83 - Vertical displacements SLU, centre of the deck 82
Fig. 84 - Cross sections along the slab 83
Fig. 85 - Vertical displacements in the cross sections 83
Fig. 86 - Vectors Dx of the pylon, SLU static 84
Fig. 87 - Pylon's displacements Dx, SLU static 84
Fig. 88 - Vectors Dz of the pylon, SLU static 85
Fig. 89 - Pylon's vertical displacements Dz, SLU static 85
Fig. 90 - Vectors D(xyz) of the pylon SLU static 86
Fig. 91 - Displacements' magnitude of the pylon, SLU static 86
Fig. 92 - First natural mode (beams model) 89
Fig. 93 - Second natural mode (beams model) 89
Fig. 94 - Third natural mode (beams model) 90
Fig. 95 - Forth natural mode (beams model) 90
Fig. 96 - Fifth natural mode (beams model) 90
Fig. 97 - Sixth natural mode (beams model) 91
Fig. 98 - Seventh natural mode (beams model) 91
Fig. 99 - Eighth natural mode (beams model) 91
Fig. 100 - Comparison of natural frequencies (beams model) 92
Fig. 101 - First natural mode (beams model with masses) 93
Fig. 102 - Second natural mode (beams model with masses) 93
Fig. 103 - Third natural mode (beams model with masses) 93
Fig. 104 - Forth natural mode (beams model with masses) 94
Fig. 105 - Fifth natural mode (beams model with masses) 94
Fig. 106 - Sixth natural mode (beams model with masses) 94

Fig. 107 - Seventh natural mode (beams model with masses) 95
Fig. 108 - Eighth natural mode (beams model with masses) 95
Fig. 109 - Ninth natural mode (beams model with masses) 95
Fig. 110 - Tenth natural mode (beams model with masses) 96
Fig. 111 - Comparison of natural frequencies (beams model with masses) 97
Fig. 112 - First natural mode (plates model) 97
Fig. 113 - Second natural mode (plates model) 98
Fig. 114 - Third natural mode (plates model) 98
Fig. 115 - Forth natural mode (plates model) 98
Fig. 116 - Fifth natural mode (plates model) 99
Fig. 117 - Sixth natural mode (plates model) 99
Fig. 118 - Seventh natural mode (plates model) 99
Fig. 119 - Eighth natural mode (plates model) 100
Fig. 120 - Ninth natural mode (plates model) 100
Fig. 121 - Tenth natural mode (plates model) 100
Fig. 122 - Comparison of natural frequencies (plates model) 101
Fig. 123 - Acceleration, velocity and displacement of an harmonic wave 102
Fig. 124 - Vibration amplitude and frequency 102
Fig. 125 - Evaluated points along the span 103
Fig. 126 - Identification of the pillars 104
Fig. 127 - Studied points in the last cross section (Pillar No. 10) 104
Fig. 128 - Location of monitored points in the Pillar No. 9 104
Fig. 129 - Placing the monitored points in the pillar No. 8 105
Fig. 130 - Measuring the vertical displacement expansion joints in section R111 of pier 10 on the left edge of the bridge 105
Fig. 131 - View of the sensors placed in sections R92 and R93 in Pillar No. 9 106
Fig. 132 - View of the sensors placed in sections R81 and R82 on pillars No. 8 106
Fig. 133 - The sensor tracks IWT 102 in the reporting point structure R102 106
Fig. 134 - View of the device for measuring relative deflection KSM-R sensor tracks WA50 captured in section R91 107
Fig. 135 - Measuring DEWE exchange 5000 107
Fig. 136 - Extreme vertical deflections in the point R101 caused by traffic flow 108
Fig. 137 - Extreme vertical deflections in the point R104 caused by traffic flow 109
Fig. 138 - Extreme vertical deflections in the point R102 caused by traffic flow 110
Fig. 139 - Extreme vertical deflections in the point R103 caused by traffic flow 110

Fig. 140 - Comparison of empirical results 112
Fig. 141 - Comparison of principal natural modes with measured results 113
Fig. 142 - Comparison plates model vs measured values (error %) 114
Fig. 143 - 1 vertical bending f = 1,07 Hz (measured) and 1,03 Hz 115
Fig. 144 - 2 vertical bending f = 2,1 Hz (measured) and 2,25 Hz 115
Fig. 145 - 3 vertical bending f = 2,8 Hz (measured) and 3,11 Hz 116
Fig. 146 - Cantilever with axial force 117
Fig. 147 - Equilibrium path of cantilever with axial force 118
Fig. 148 - Displacement with increasing load 119
Fig. 149 - Unitary force at the top of the pylon 121
Fig. 150 - First buckling load factor 121
Fig. 151 - Displacement DY from the base to the top of the pylon 122
Fig. 152 - Single d.o.f. dynamic system 123
Fig. 153 - Free body diagram 123
Fig. 154 - u(t) with f=0, c=0 125
Fig. 155 - u(t) with f = 0, c = c_{cr} 127
Fig. 156 - u(t) with f = 0, c $\geq$ c_{cr} 128
Fig. 157 - u(t) with f = 0, c $<$ c_{cr} 129
Fig. 158 - u(t) with $f = f = \cos t, c = 0$ 130
Fig. 159 - u(t) with f = $\bar{f}$=cost, c $<$ c_{cr} 130
Fig. 160 - Oscillatory motions 131
Fig. 161 - Undamped and damped oscillator 131
Fig. 162 - Load's law 132
Fig. 163 - Time step too large 133
Fig. 164 - Reaction force applied instead of the cable 136
Fig. 165 - Load vs time table 136
Fig. 166 - Linear transient dynamic solver (plates model) 138
Fig. 167 - Points of study in the cross section (beams model) 139
Fig. 168 - Displacements of different points in the deck (beams model) 139
Fig. 169 - Displacements of different points in the deck (beams model with masses) 140
Fig. 170 - Some studied points for the dynamic analysis (plates model) 140
Fig. 171 - Displacements of node 181 in the linear dynamic analysis (plates model) 141
Fig. 172 - Displacements of different points in the deck (plates model) 141
Fig. 173 - Points of study in the pylon 142
Fig. 174 - Displacements of different points in the pylon 142

Fig. 175 - Plane and space model of the truck type TATRA T815 145
Fig. 176 - Main screen of Polàk software 146
Fig. 177 - Importation screen 147
Fig. 178 - Vehicles motion 147
Fig. 179 - Road roughness and obstacles 148
Fig. 180 - Definition of simulation parameters 148
Fig. 181 - Analyzed sections for the vibration 149
Fig. 182 - Output points in each cross section 149
Fig. 183 - Traffic's direction 150
Fig. 184 - Definition of the spans 150
Fig. 185 - Vertical displacements of the cross section in the middle of the 1st span (case 1) 150
Fig. 186 - Vertical displacements of the cross section in the middle of the 2nd span (case 1) 151
Fig. 187 - Vertical displacements of the cross section in the middle of the 3rd span (case 1) 151
Fig. 188 - Vertical displacements along the deck - Points in position 01 (case 1) 152
Fig. 189 - Max e min vertical displacements - Points 01 (case 1) 152
Fig. 190 - Vertical displacements along the deck in different times - position 01 (case 1) 153
Fig. 191 - Vertical displacements along the deck - Points in position A (case 1) 153
Fig. 192 - Max e min vertical displacements - Points A (case 1) 154
Fig. 193 - Vertical displacements along the deck in different times - position A (case 1) 154
Fig. 194 - Vertical displacements along the deck - Points in position B (case 1) 155
Fig. 195 - Max e min vertical displacements - Points B (case 1) 155
Fig. 196 - Vertical displacements along the deck in different times - position B (case 1) 156
Fig. 197 - Vertical displacements along the deck - Points in position 04 (case 1) 156
Fig. 198 - Max e min vertical displacements - Points 04 (case 1) 157
Fig. 199 - Vertical displacements along the deck in different times - positions 04 (case 1) 157
Fig. 200 - Vertical displacements of the cross section in the middle of the 1st span (case 2) 158
Fig. 201 - Vertical displacements of the cross section in the middle of the 2nd span (case 2) 158
Fig. 202 - Vertical displacements of the cross section in the middle of the 3rd span (case 2) 159
Fig. 203 - Vertical displacements along the deck - Points in position 01 (case 2) 159
Fig. 204 - Max e min vertical displacements - Points 01 (case 2) 160
Fig. 205 - Vertical displacements along the deck - Points in position A (case 2) 160
Fig. 206 - Max e min vertical displacements - Points A (case 2) 161
Fig. 207 - Vertical displacements along the deck - Points in position B (case 2) 161
Fig. 208 - Max e min vertical displacements - Points B (case 2) 162
Fig. 209 - Vertical displacements along the deck - Points in position 04 (case 2) 162

Fig. 210 - Max e min vertical displacements - Points 04 (case 2) 163
Fig. 211 - Vertical displacements of the cross section in the middle of the 1st span (case 3) 164
Fig. 212 - Vertical displacements of the cross section in the middle of the 2nd span (case 3) 164
Fig. 213 - Vertical displacements of the cross section in the middle of the 3rd span (case 3) 165
Fig. 214 - Vertical displacements along the deck - Points in position 01 (case 3) 165
Fig. 215 - Max e min vertical displacements - Points 01 (case 3) 166
Fig. 216 - Vertical displacements along the deck in different times - position 01 (case 3) 166
Fig. 217 - Vertical displacements along the deck - Points in position A (case 3) 167
Fig. 218 - Max e min vertical displacements - Points A (case 3) 167
Fig. 219 - Vertical displacements along the deck in different times - position A (case 3) 168
Fig. 220 - Vertical displacements along the deck - Points in position B (case 3) 168
Fig. 221 - Max e min vertical displacements - Points B (case 3) 169
Fig. 222 - Vertical displacements along the deck in different times - position B (case 3) 169
Fig. 223 - Vertical displacements along the deck - Points in position 04 (case 3) 170
Fig. 224 - Max e min vertical displacements - Points 04 (case 3) 170
Fig. 225 - Vertical displacements along the deck in different times - position 04 (case 3) 171
Fig. 226 - Comparison measured and numerical values (Points 01) 171
Fig. 227 - Comparison measured and numerical values (Points 04) 172
Fig. 228 - Comparison of natural frequencies "plates model" and measured values 175
Fig. 229 - 2 axle space system for the vehicle 176

List of tables

Tab. 1 - Types of plate elements 43
Tab. 2 - Available material models 45
Tab. 3 - Geometrical characteristics of the deck 53
Tab. 4 - Density of the three groups of beams 54
Tab. 5 - Geometric characteristics of the cables 57
Tab. 6 - Cables' pretension values 58
Tab. 7 - Bill of materials (beams model) 58
Tab. 8 - Global inertia (beams model) 58
Tab. 9 - Central beams' properties 60
Tab. 10 - Bill of materials (beams model with masses) 62
Tab. 11 - Global inertia (beams model with masses) 62
Tab. 12 - Densities of the deck 64
Tab. 13 - Summary of the plates' properties 68
Tab. 14 - Bill of materials (plates model) 70
Tab. 15 - Global inertia (plates model) 70
Tab. 16 - Properties of the models 77
Tab. 17 - Modes of vibration (beams model) 92
Tab. 18 - Modes of vibration (beams model with masses) 96
Tab. 19 - Modes of vibration (plates model) 101
Tab. 20 - Measured values for the points R101 and R104 108
Tab. 21 - Measured values for the points R102 and R103 109
Tab. 22 - Measured results of natural modes 111
Tab. 23 - Empirical results 112
Tab. 24 - Principal natural modes with measured results 113
Tab. 25 - Inertia of the pylon 120
Tab. 26 - Calculation of the critical load 121
Tab. 27 - Static forces applied in the models 136
Tab. 28 - Frequencies used for Rayleigh coefficients 138
Tab. 29 - Rayleigh coefficients 138
Tab. 30 - Vehicles motion (traffic flow) 163

Introduction

Civil infrastructures serve as the underpinnings of our present highly industrialized society. It is an important issue how to monitor these widely used infrastructures in order to prevent potential catastrophic events.

Empirical dynamic analysis and permanent monitoring are really useful instruments for a proper evaluation of the real dynamic behavior of civil engineering structures and, therefore, to obtain an efficient structural modeling and a reliable evaluation of seismic forces.

Bridges, a type of important civil infrastructures, are normally designed to have long life span. Service loads, environmental and accidental actions may cause damage to bridges.

Continuous health monitoring or regular condition assessment of important bridges is necessary so that early identification and localization of any potential damage can be made.

The increasing popularity of cable-stayed bridges are attributed to the appealing aesthetics, the full and efficient utilization of structural materials, the increased stiffness over suspension bridges and the relatively small size of the bridge elements. They are normally sensitive to dynamic loadings such as earthquakes, winds and vehicles.

The health monitoring and condition assessment of large span cable-stayed bridges is a crucial issue to ensure safety during the bridge service life. One way to carry out the health monitoring or structural assessment is through changes in vibration characteristics (natural frequencies, damping ratios, and mode shapes) of bridges.

Due to the structural complexity of large span cable-stayed bridges, the finite element (FE) method is currently a common way to perform the modal analysis and dynamic response analysis under earthquake, wind and vehicle loadings. Starting from the knowledge of the structure geometry, the boundary conditions and material properties, the mass, stiffness and damping distribution of the structure are expressed in a matrix form.

To identify changes in the dynamic characteristics of a bridge, a baseline finite element is often required. Bridge health can be monitored or assessed when the baseline model is compared against a finite element model of the updated bridge. However, the success of finite element method application strongly depends on the reliability of the model since many simplifying assumptions are made in modeling the complicated structures, and there are many uncertainties in the material and geometric properties. The calculated results are often questionable if the finite element model is not properly validated by the field test results.

There are three main types of bridge dynamic tests: forced vibration tests; free vibration tests; and ambient vibration tests.

In the forced vibration method, the bridge is excited by artificial means and correlated input - output measurements are performed. In the case of large and flexible bridges, like cable-stayed bridges, it often requires very heavy equipment and involves significant resources to provide controlled excitation at sufficiently high levels, which becomes difficult and costly.

Free vibration tests of bridges is carried out by a sudden release of a heavy load or mass appropriately connected to the bridge deck. Both forced and free vibration tests, however, need an artificial means to excite the bridge, additionally traffic has to be shut down during the tests.

Ambient vibration tests have an advantage of being inexpensive since no equipment is needed to excite the bridge. It corresponds to the real operating condition of the bridge. The service state need not have to be interrupted to use this technique. Ambient vibration tests have been successfully applied to several large scale cable-supported bridges. In case of ambient vibration tests, only response data are measured while actual loading conditions are not measured.

An initial full three-dimensional finite element model of the cable-stayed bridge is first conceived according to the original blue prints.

The initial finite element model is then verified with the field test results in terms of frequencies and mode shapes.

The finite element method has been employed in this study to obtain an analytical model for the bridge and vehicle systems. Both the natural frequencies and the dynamic response of the box-girder bridge will be assessed using this analytical model.

Chapter I

INTRODUCTION ABOUT THE STRUCTURE

1. GENERAL CHARACTERISTICS OF BRIDGES

A bridge can be categorized by what it is designed to carry, such as trains, pedestrian or road traffic, a pipeline or waterway for water transport or large traffic.

1.1 Cable stayed bridge

A cable-stayed bridge is a bridge that consists of one or more columns (normally referred to as towers or pylons), with cables supporting the bridge deck.

There are two major classes of cable-stayed bridges:

- in a harp design, the cables are made nearly parallel by attaching them to various points on the tower so that the height of attachment of each cable on the tower is similar to the distance from the tower along the roadway to its lower attachment;
- in a fan design, the cables all connect to or pass over the top of the tower.

Compared to other bridge types, the cable-stayed is optimal for spans longer than typically seen in cantilever bridges, and shorter than those typically requiring a suspension bridge. This is the range in which cantilever spans would rapidly grow heavier if they were lengthened, and in which suspension cabling does not get more economical, were the span to be shortened.

A multiple-tower cable-stayed bridge may appear similar to a suspension bridge, but in fact is very different in principle and in the method of construction. In the suspension bridge, a large cable hangs between two towers, and is fastened at each end to anchorages in the ground or to a massive structure. These cables form the primary load-bearing structure for the bridge deck. Before the deck is installed, the cables are under tension from only their own weight. Smaller cables or rods are then suspended from the main cable, and used to support the load of the bridge deck, which is lifted in sections and attached to the suspender cables. As this is done the tension in the cables increases, as it does with the live load of vehicles or persons crossing the bridge. The tension on the cables must be transferred to the earth by the anchorages, which are sometimes difficult to construct owing to poor soil conditions.

In the cable-stayed bridge, the towers form the primary load-bearing structure. A cantilever approach is often used for support of the bridge deck near the towers, but areas further from them are supported by cables running directly to the towers. This has the disadvantage, compared to the suspension bridge, of the cables pulling to the sides as opposed to directly up, requiring the bridge deck to be stronger to resist the resulting horizontal compression loads; but has the advantage of not requiring firm anchorages to resist a horizontal pull of the cables, as in the suspension bridge. All

static horizontal forces are balanced so that the supporting tower does not tend to tilt or slide, needing only to resist such forces from the live loads.

Key advantages of the cable-stayed form are as follows:

- much greater stiffness than the suspension bridge, so that deformations of the deck under live loads are reduced;
- can be constructed by cantilevering out from the tower - the cables act both as temporary and permanent supports to the bridge deck;
- for a symmetrical bridge (i.e. spans on either side of the tower are the same), the horizontal forces balance and large ground anchorages are not required.

1.2 Bridge monitoring

There are several methods used to monitor the stress on large structures like bridges.
The most common method is the use of an accelerometer, which is integrated into the bridge while it is being built. This technology is used for long-term surveillance of the bridge.
Another option for structural-integrity monitoring is "non-contact monitoring", which uses the Doppler effect (Doppler shift). A laser beam from a Laser Doppler Vibrometer is directed at the point of interest, and the vibration amplitude and frequency are extracted from the Doppler shift of the laser beam frequency due to the motion of the surface. The advantage of this method is that the setup time for the equipment is faster and, unlike an accelerometer, this makes measurements possible on multiple structures in as short a time as possible. Additionally, this method can measure specific points on a bridge that might be difficult to access.

2. LOCATION OF THE BRIDGE

The bridge studied is situated in the East part of the river Moldava of Prague in Czech Republic; in particular it is placed along the highway E55 Jizni Spojka over the railway station.

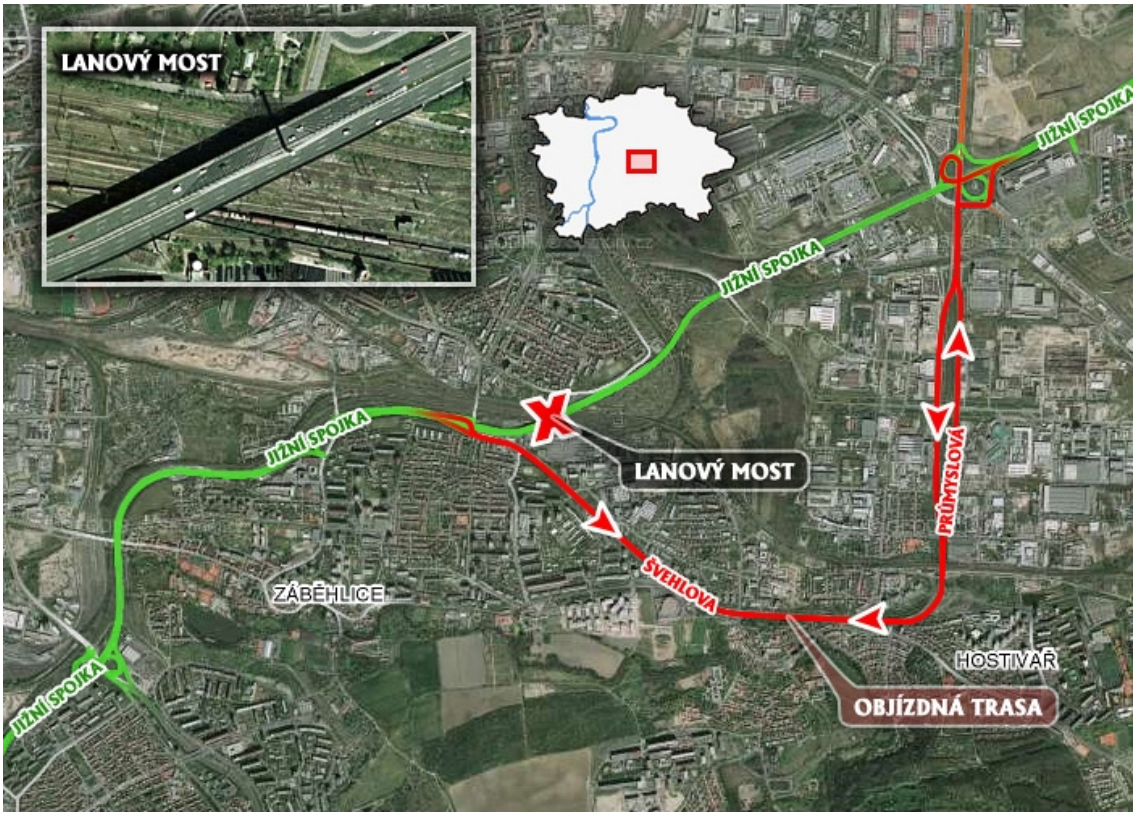

Fig. 1 - Location of the bridge in Czech Republic

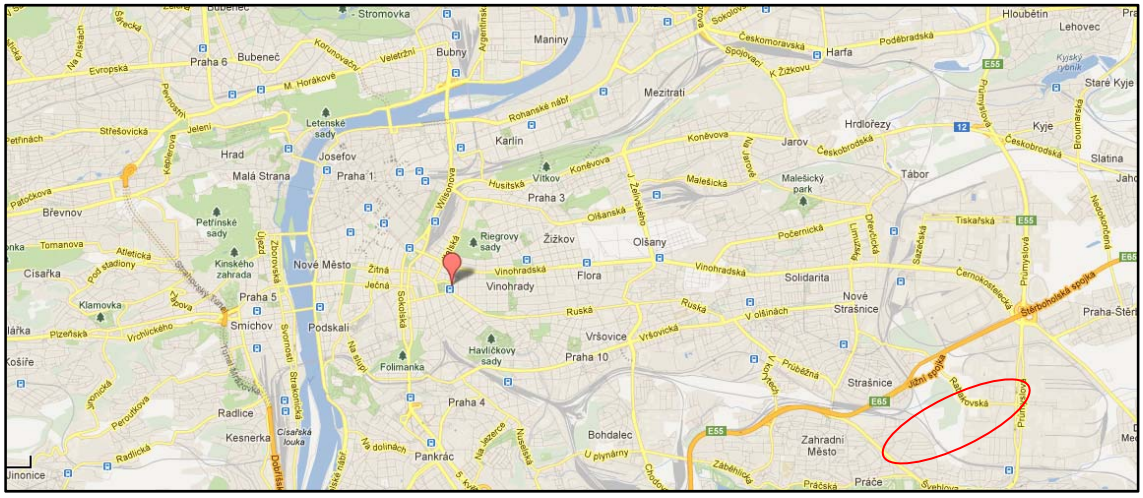

Fig. 2 - Prague's map

Lanovy Most is one of the most important and busiest bridges for traffic in the Capital, it is part of the South clutch on a street circuit and converts traffic across the railway line Prague - Czech

Budejovice and marshalling station Praha-Vršovice (or Praha-Strašnice), following the edge scattered neighborhoods Skalka (street Pretlucká and Dolinecká) and land belongs to the most part to Strašnice.

This highway bridge is not officially named, professional organizations (such as operating on radar tracking operation) and motoring journalist often referred to it as a rope bridge.

Fig. 3 - Bridge's position in Prague, aerial's view

Fig. 4 - Aerial view of Lanovy most

Fig. 5 - Track's shape of the bridge

3. BRIDGE'S DESCRIPTION

Most parts of the bridge were designed by George Stráský, Ilja thick, Slavomir Kolčava in the years 1991 - 1993. The bridge was opened to the traffic in December 1997.

"Beam bridges" are composed by horizontal beams supported at each end by substructure units and can be either simply supported, when the beams only connect across a single span, or continuous supported, when the beams are connected across two or more spans. When there are multiple spans, the intermediate supports are known as piers.

The bridge inspected has a single continuous span, single and double bearings on the piers and at the end the span is suspended by cables fixed at the top of one tower. The tower and the relative cables are situated in the middle of the roadway into two lines in both sides.

Fig. 6 - Center of the roadway

The span consists of a series of longitudinal box girders, floor beams, and a concrete deck with transverse beams.

Cable-stayed bridges, like suspension bridges, are held up by cables. However, in a cable-stayed bridge, less cables are required and the towers holding the cables are proportionately shorter.

Fig. 7 - Bridge's view

Fig. 8 - Photos' view

In the following pictures are presented different views of the bridge from all around the highway junction.

Fig. 9 - Photo from corner 1

Fig. 10 - Photo from corner 2

Fig. 11 - Photo from the corner 3

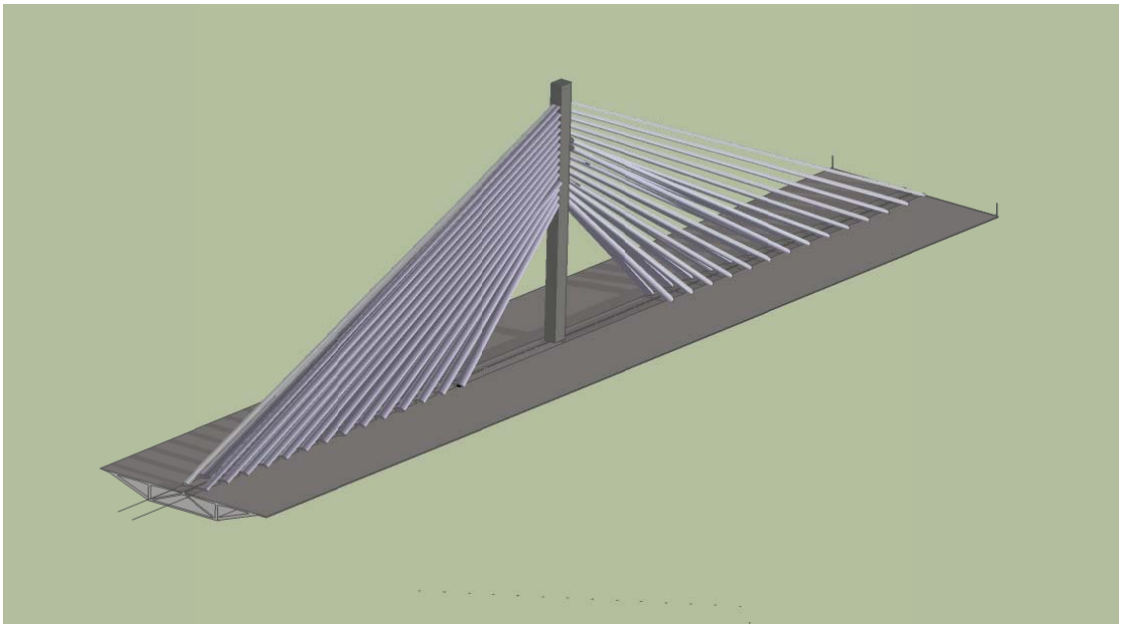

Fig. 12 - Render of the cables part of the bridge

- **Cross section**

The cross section is composed by concrete slabs to create a rigid box with torsional stiffness. In the middle of the section there are two beams, introduced to increase the rigidity of the section.

Fig. 13 - Particular of the concrete box section

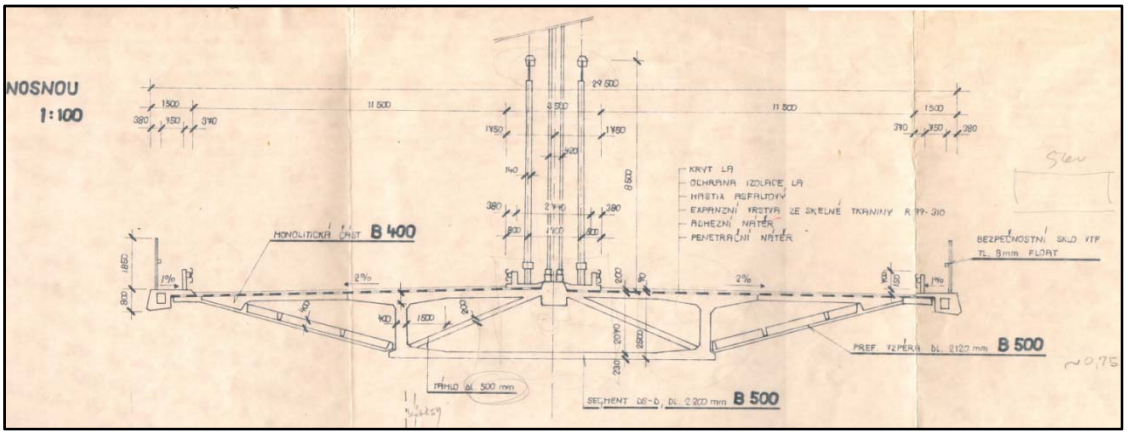

Fig. 14 - Cross section

In the following figure the schematization of the cross section is reported with all the information about area, perimeter and moments of inertia

.

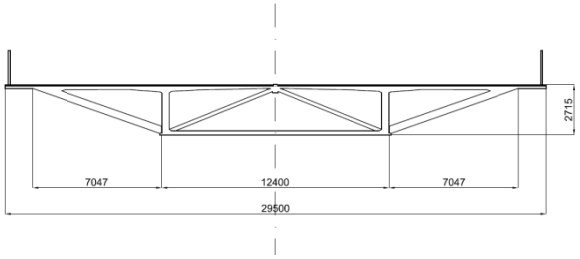


```
Area:                           18321531.4892
Perimeter:                      136268.7145
Bounding box:           X:  105380.2536  --  134880.2536
                        Y:  -1567.5732  --  1083.7715
Centroid:               X:  120130.2932
                        Y:  -20.0040
Moments of inertia:     X:  1.6152E+13
                        Y:  2.6542E+17
Product of inertia:     XY: -4.4016E+13
Radii of gyration:      X:  938.9326
                        Y:  120360.7331
Principal moments and X-Y directions about centroid:
                        I:  1.6145E+13 along [1.0000 0.0000]
                        J:  1015356010197388 along [0.0000 1.0000]
```

Fig. 15 - Geometrical properties of the schematized cross section

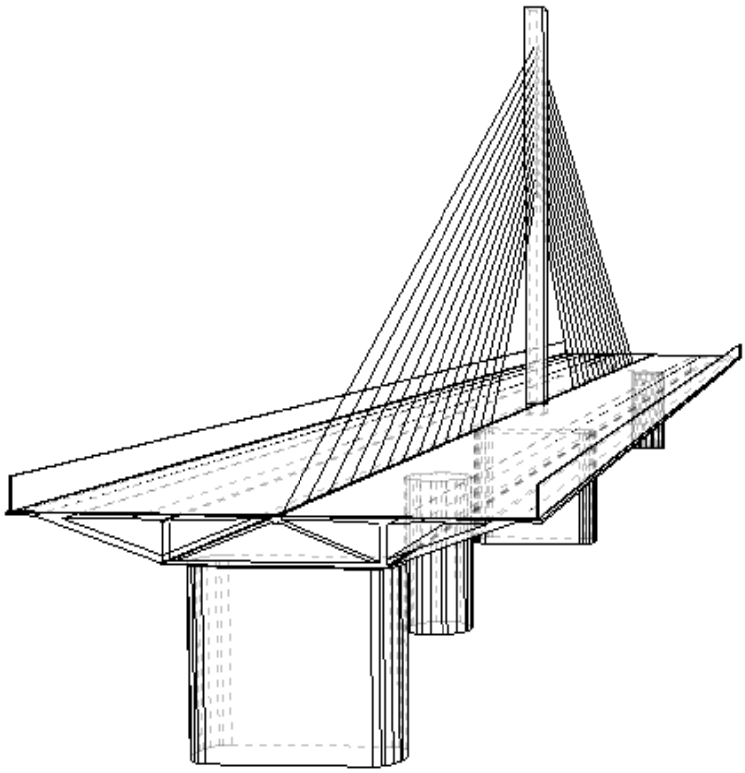

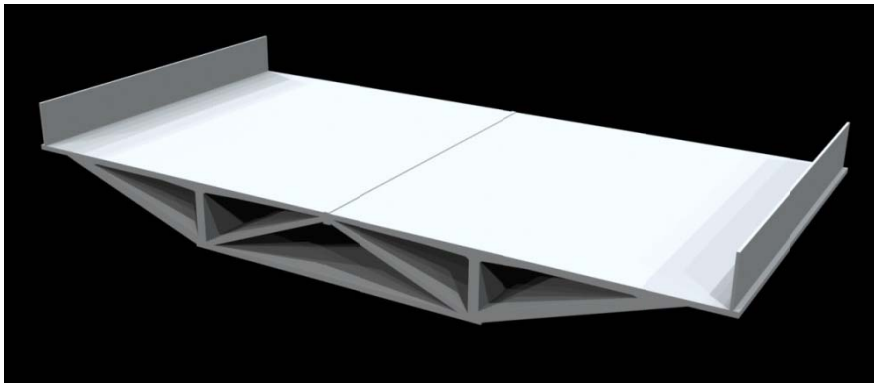

Fig. 16 - Cross section's renders

- **Pylon**

The pylon is situated in the middle of the roadway and on the top it is characterized by two rows of cables in both sides.

Fig. 17 - Top of the pylon

The position of the pylon is in the center of gravity of the cross section, so the deck has to be characterized by high torsional stiffness and it is necessary to insert a traffic island to divide the roadways.

From the bottom to the top the tower is composed by four parts with different peculiarities about the geometry and the material. In the following figures, drawings and properties of each part are reported.

Pylon 1 - steel part

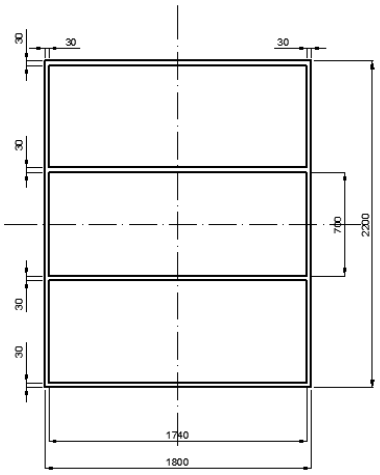


```
Area:                              340800.0000
Perimeter:                          22600.0000
Bounding box:                X: 1878.3003  --  3678.3003
                             Y: 598.2672  --  2798.2672
Centroid:                    X: 2778.3003
                             Y: 1698.2672
Moments of inertia:          X: 1.1730E+12
                             Y: 2.7867E+12
Product of inertia:           XY: 1.6080E+12
Radii of gyration:           X: 1855.2140
                             Y: 2859.5317
Principal moments and X-Y directions about centroid:
                             I: 1.9007E+11 along [1.0000 0.0000]
                             J: 1.5608E+11 along [0.0000 1.0000]
```

Pylon 1 - concrete part

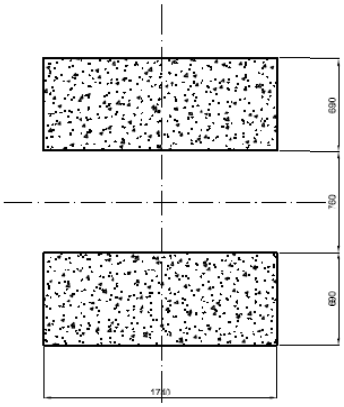


```
Area:                              2401200.0000
Perimeter:                          9720.0000
Bounding box:                X: 6101.8327  --  7841.8327
                             Y: 628.2672  --  2768.2672
Centroid:                      X: 6971.8327
                             Y: 1698.2672
Moments of inertia:          X: 8.2827E+12
                             Y: 1.1732E+14
Product of inertia:          XY: 2.8430E+13
Radii of gyration:           X: 1857.2592
                             Y: 6989.9035
Principal moments and X-Y directions about centroid:
                             I: 1.3574E+12 along [1.0000 0.0000]
                             J: 6.0582E+11 along [0.0000 1.0000]
```

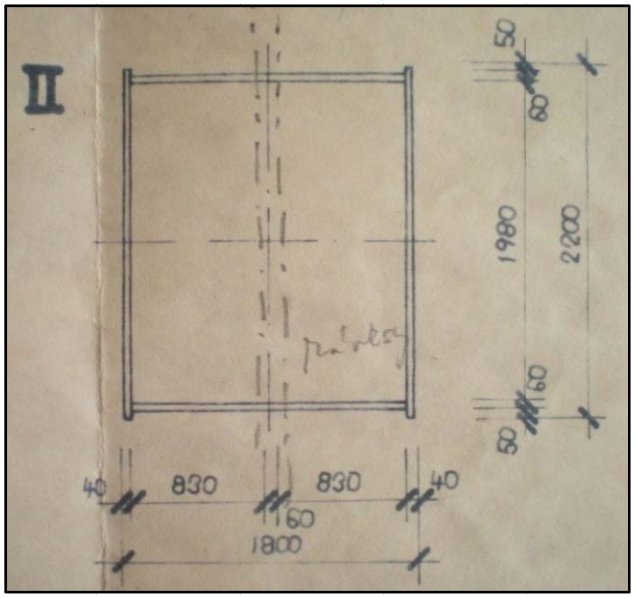

Fig. 18 - Blueprint of the second part of the pylon

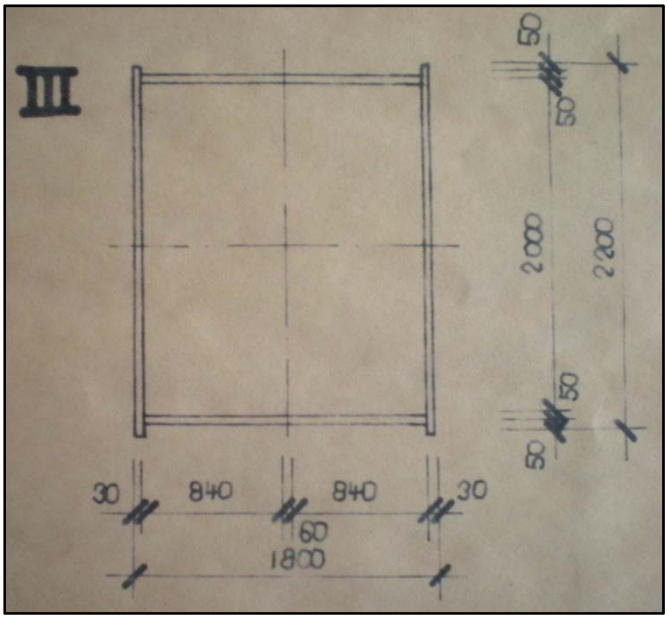

Fig. 19 - Blueprint of the third part of the pylon

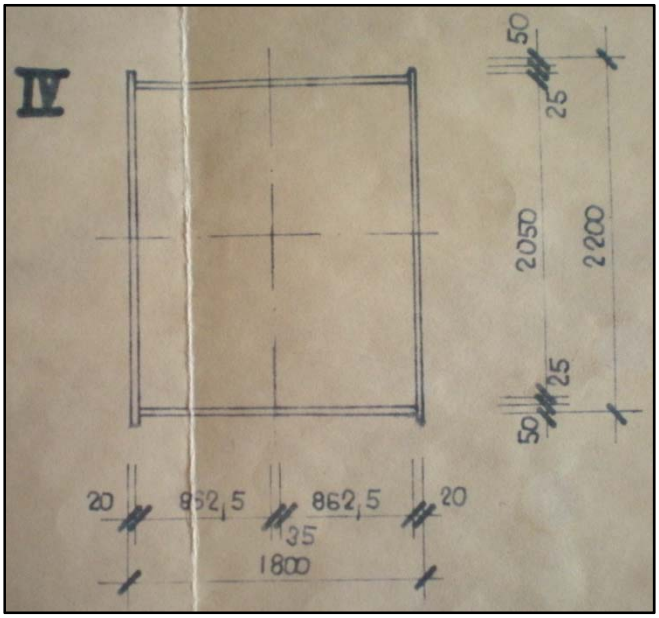

Fig. 20 - Blueprint of the forth part of the pylon

- **Cables**

The cable is considered to have no stiffness in compression. An initial stress is applied to the cable elements to provide the necessary pretension that keeps the deck from sagging under the dead load.

Fig. 21 - Cables connection to the deck

- **Bearings**

The figure below shows the two different kinds of pier with the corresponding bearings.

Fig. 22 - Simple and double bearings

Chapter II

FEM MODELS

1. FINITE ELEMENT MODELING OF THE BRIDGE

In general, the modal analysis procedure for more complicated structures includes analytical and experimental modal analysis. Analytical modal analysis is the process of determining the dynamic properties of a structure based on the free vibration solution of the equations of motion.

The finite element (FE) method is currently a common way to perform an analytical modal analysis of cable-stayed bridges, starting from the knowledge of the structural geometry, boundary conditions and material properties.

Contemporary cable-stayed bridges are complex, efficient and aesthetically pleasing structures which are appearing in various exotic forms. They involve a variety of decks, towers and stay cables that are connected together in different ways. To reduce the degrees of freedom and simplify the dynamic analysis, several simplified three-dimensional finite element models of cable-stayed bridges were developed using elastic beam elements to model the towers and the deck, and truss elements to model the cables.

1.1 Simplified 3D finite element models of cable-stayed bridges

The single-girder (spine) model is probably the earliest three-dimensional finite element model of cable-stayed bridges in structural dynamics. The bridge deck was modeled using a single central spine with offset rigid links to accommodate cable anchor points. The deck stiffness was assigned to the spine, and mass (translational and rotational) was assigned to the spine nodes.

This simplified model neglects the floor beam stiffness and girder warping, so it is suitable for a box section girder with relatively large pure torsional stiffness but small warping stiffness.

The double-girder beam element model consists of two girders located in each cable plane coupled to floor beams. This model may include part of torsional stiffness through the opposite vertical bending of the two girders.

The modeling of a deck system is relatively ambiguous by using simplified beam element models.

The adequacy of the simplified models is particularly questionable when representing the bridge deck system in the lateral and torsional vibration. The lateral vibration modes may be distorted to some extent if the deck stiffness equivalence is treated improperly.

To represent the bridge dynamic behavior well, instead of simplified beam element models, a full three-dimensional finite element model is required with several types of elements such as beam elements, truss elements, shell elements, solid elements and link elements representing different components of cable-stayed bridges.

1.2 Full 3D finite element modeling of cable-stayed bridges

Creating a good three-dimensional dynamic finite element model for cable-stayed bridges is not an easy task. Many different modeling strategies (which element types, how many degrees of freedom, etc.) are possible; the choice of strategy depends on the skill and experience of the analyst and on the intended application of the model. The baseline finite element model for structural dynamics needs an accurate representation of the bridge dynamic behavior.

The geometry and member details of the model are based on the design information and design blue prints of the bridge. The main structural members are composed of stay cables, girders, floor beams, concrete slab and towers, all of which are discretized by different finite element types.

No bending stiffness is included, whereas the pre-tensions of the cables can be incorporated by the initial strains of the element. The stress-stiffening capability is needed for analysis of structures with a low or non existing bending stiffness as is the case with cables. The cable sagging effect can be considered with the stress-stiffening capability.

1.3 Initial equilibrium configuration

One of the important features of a large span cable-stayed bridge is that the dead load (self weight) is often dominant. The pre-tensions in the stay cables control the internal force distribution in the deck and towers as well as the bridge alignment. The initial equilibrium configuration of cable-stayed bridges is therefore the equilibrium position due to dead load and tension forces in the stay cables. The initial equilibrium configuration is important in cable-stayed bridges since it is a starting position to perform the succeeding analysis.

Inspection of the initial equilibrium configuration of the cable-stayed bridge obtained from both small deflection and large deflection analysis demonstrates that the deflection and member force differences are small. It is again verified that the small deflection analysis can be used to calculate the static initial equilibrium configuration of large span cable-stayed bridges. However, the static analysis of cable-stayed bridges is always a geometrical analysis due to the pre-tensions in the stay cables.

Base on previous research and static analysis of the bridge, three 3-dimensional numerical models are created using Straus 7.

2. TYPE OF ELEMENTS IN THE MODELS

The finite element mesh is divided into five element groups:

- Group 1: Concrete deck, modeled using 4-nodes shell elements in the “plates model” and beam elements in the other two models.
- Group 2: Tower, modeled using a sequence of beam elements.
- Group 4: Transverse box girders, modeled composing different types of shell elements in the “plates model”.
- Group 5: Cables, modeled using truss elements with specified initial stress; each cable is modeled with one truss element, to avoid cable vibration modes in the response spectrum analysis.

2.1 Plate elements

Plate is a generic name for a group of two-dimensional surface elements, that include the three and six node triangular elements, and four, eight and nine node quadrilateral elements. These elements can be used for plane stress and plane strain analysis, axial-symmetric solid problems, plate and shell analysis, as shear panels, 3D membranes and for heat flow analysis. The following table shows the way in which plate elements may be used in Strand7.

	2D Plane Stress	2D Plane Strain	Axisymmetric	Thin Plate/Shell	Thick Plate/Shell	Shear Panel	3D Membrane	Heat Transfer
Tri3	•	•	•	•			•	•
Quad4	•	•	•	•		•	•	•
Tri6	•	•	•	•	•		•	•
Quad8	•	•	•	•	•		•	•
Quad9	•	•	•	•	•		•	•

Tab. 1 - Types of plate elements

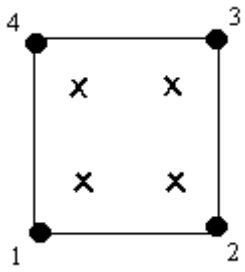

Fig. 23 - 4 nodes quadrilateral element

A plate element will account for bending with transverse shear effects in thick plates and rotational drilling degrees of freedom. It is important to note that these formulations are not coupled during the initial analysis. The stiffness matrix for each formulation is computed separately in local coordinate space. The two formulations are assembled into a total 6 degree of freedom (d.o.f) global element matrix. Once assembled into the global element matrix, the element is combined into the total structural stiffness matrix. Membrane and bending coupling is achieved with the addition of geometric stiffness terms in the overall stiffness matrix. The additional stiffness terms result from membrane strains which are calculated during the initial analysis. Once the membrane strains are found the element stiffness is automatically updated to account for the extra stiffness terms resulting from membrane strains.

Plate elements have their own local coordinate systems. The local system has its origin at the centroid of the plate. The local x-axis is parallel to and in the direction of a vector from the first node to the second. The y-axis is perpendicular to the x-axis and in the plane of the plate. Note the right-hand rule where the local z-axis points out of the plane defined by the counter-clockwise node ordering. The picture below clarifies this, using a triangular plate element as an example.

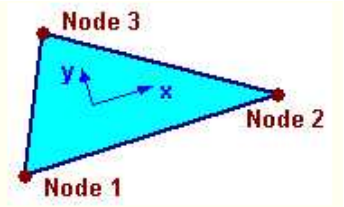

Fig. 24 - Local coordinates system of a plate element

For plate elements, the local systems are used for directing pressure loads. Local forces and stresses are also reported in these directions.

It is the only plate element that permits out of plane displacements associated with bending behavior, see the figure below.

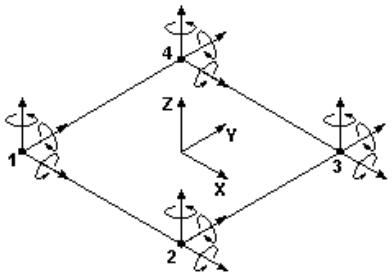

Fig. 25 - Plates displacements

The following table summarizes the different types of plate elements and the available material models for each type.

	Isotropic	Orthotropic	Anisotropic	Laminate	Rubber	Soil	Fluid	User Defined
2D Plane Stress	✓	✓	✓	✓	✓			
2D Plane Strain	✓	✓	✓		✓	✓	✓	
Axisymmetric	✓	✓			✓	✓	✓	
Plate/Shell	✓	✓	✓	✓	✓			✓
Shear Panel	✓							
3D Membrane	✓	✓		✓	✓			
Load Patch								

Tab. 2 - Available material models

For all the plates an isotropic material is chosen; an isotropic material has the same elastic modules in all directions.

2.2 Beam elements

Beam is a generic name for a group of one-dimensional or line elements that are all connected between two nodes at their ends and the single dimension is length.

The conventional beam element has six degrees of freedom at each node: three translations and three rotations. The beam carries axial force, torque, shear forces and bending moments in its principal planes.

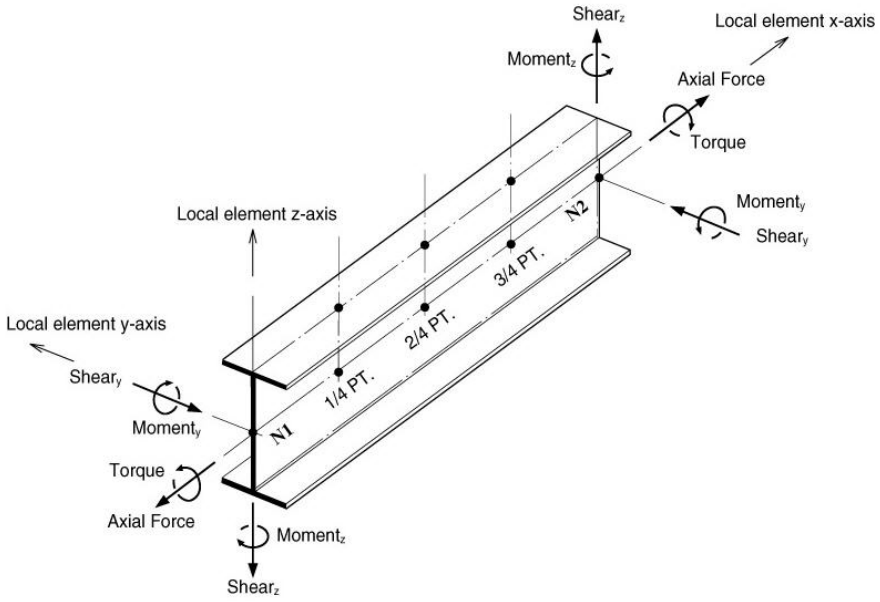

Fig. 26 - Beam forces associated with d.o.f

The undeformed element is a straight line between the two nodes to which it is connected.
For slender beams all the transverse deflection is due to bending and Engineers Theory of Bending is used to determine the stiffness matrix.
For deep beams there can be additional linear transverse deflection and Timoshenko beam theory is used. The axial deformation and the twist are linear along the beam.

The beam element requires the selection of two nodes as the end nodes. An optional third node called the Reference Node may also be specified. The reference node is only used for the definition of the principal axis direction on the beam. A beam without a reference node is called Beam2 in Strand7; a beam with a reference node is called a Beam3.
The beam element is defined by nodes N1 and N2 as shown in Fig. 27 and this also defines the principal coordinate system. The axis system is used to define section properties and to define the force, moment, stress and strain results.

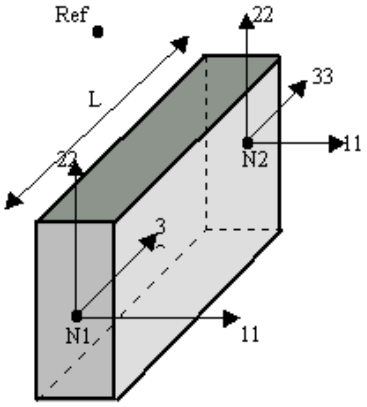

Fig. 27 - Principal coordinate system of a beam

For a beam with a reference node, the principal axis system, shown in Fig. 27, is defined as follows:

- 3rd axis is directed from node N1 to node N2.
- 2nd axis is normal to the 3rd axis and lies in the plane formed by nodes N1, N2 and the reference node Ref N. It is positive towards the side on which node Ref N lies.
- 1st axis completes the right-hand axis system.

If none method is used to align the principal axes, then the default axes are shown in Fig. 28.

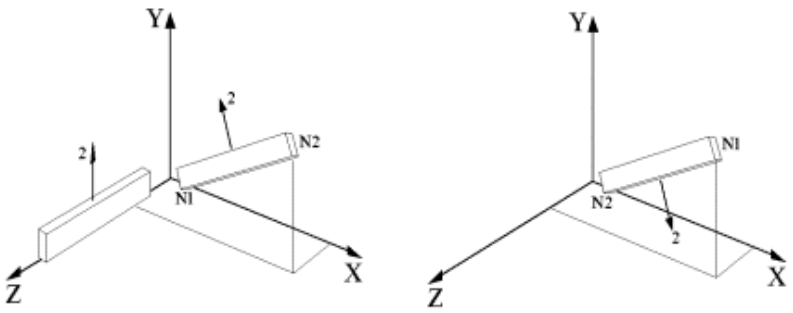

Fig. 28 - Default principal axes of a beam element

The figure shows that if the beam is parallel to the global Z axis, then the 2nd direction is always in the positive Y direction. Otherwise, the 2nd direction is given by the vector cross product of the Z axis and a vector defined by nodes N1-N2. The 3rd direction is directed from node N1 to node N2, with the 1 direction completing a right hand system.

2.3 Links

The link elements define how the displacements/rotations of one node are related to the displacements/rotations of another one. Strand7 has the following types of links:

- Master-Slave link
- Sector Symmetry link
- Coupling link
- Pinned link
- Rigid link
- Shrink link
- 2-Point link
- Attachment link
- Multi-Point link

Rigid links provide an infinitely stiff connection between two nodes, this means that the distance between the 2 nodes will always remain constant and equal to the initial distance between the nodes. However, the rigid link also provides constraints on the nodal rotation such that there is no relative rotation between the connected nodes. The Rigid link may act in any one of the Cartesian planes (XY, YZ, ZX, XYZ).

2.4 Cable and truss elements

Cable elements have particular characteristics: they don’t transfer moment and torsion, they don’t react to compression forces, only to tensile forces and a pretension value for each cable must be defined (a zero value can be chosen).

The software has to consider large deformation analysis to use this kind of elements, it means that it has to take in consideration the second order displacements. Besides it is not possible to use a linear analysis with cable elements because they need a non linear analysis step by step, conversely the structure is going to be more stiff than the real one.
A cable can be considered as a bar element with equivalent tangent modulus of elasticity to account for sag effect. A cable can be considered as a combination of large numbers of straight beam segment with very small moment of inertia adequately modeling the curved geometry of the cable. Isoparametric element, which include the element curvature are also tried. The last two modeling approaches are found to be superior to the bar element approach and have almost similar performances.

Furthermore in simple models two different approaches can be used instead of cable elements: bars with low inertia properties and only tension reagent or trusses with pretension values.
In this project truss elements are used for the linear solver. To use this method it was necessary to verify that no cables were compressed and then to calibrate the Dischinger stiffness of the cables. This because the cable is schematized like a single straight element, but in the reality the cable has a non straight shape, this approximation influences the behavior of the total structure.

A truss element can carry axial force and/or torque. The element may contribute to the three translational degrees of freedom at each node, depending on its orientation, and behaves like a pin-jointed rod element.

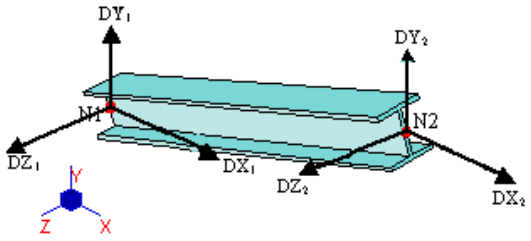

Fig. 29 - Degrees of freedom of a truss element in global coordinates

Torsional stiffness is included in the element when both its shear modulus and torsion constant are non-zero.

When using this element to carry only axial force, the rotational degrees of freedom should be fixed in the global freedom cases. So the element has only three translational degrees of freedom at each node and behaves like a pin jointed beam element. The solver automatically detects nodes that are connected only to truss elements and suppresses the rotational degrees of freedom.

If the element is parallel to one of the global axes, and the element is used only in linear analysis (static or dynamic), then it is easy to suppress the missing rotational degrees of freedom.

2.5 Bridge bearings

The modeling of bridge boundary conditions is an important issue in the dynamic analysis.
Two types of bridge bearings are used in the current models of cable-stayed bridge: all fixed bearings are applied to both ends of the slab and in one point in the middle of it, under the pylon; simple bearings are used for the rest of the piers.

2.6 Non structural masses

Non-structural mass attributes are mainly used for modeling live and non-structural dead loads which may vary across a range of operation conditions. For example, furniture not fixed to a building will generate gravity load on the building slab and therefore can be modeled with a plate/patch non-structural mass attribute. The non-structural mass attribute is load case dependent, and each attribute may be active only for the load case it has been assigned to.

From the solver's perspective, the difference between a structural mass and a non-structural mass is that non-structural masses are element attributes that are load case specific whereas a structural mass is active across all load cases. Strand7 allows the user to set the options for each load case to include/exclude structural mass and/or non-structural mass.

A non-structural mass attribute is also associated with a dynamic factor with a default unit value. This factor can be used to change the effective contribution of the prescribed mass in dynamic analysis. A dynamic factor will be used for natural frequency, spectral response, harmonic response, linear and nonlinear transient analyses, so that the effective mass in these analyses is the product of the mass value and the dynamic factor.

For any static analysis (including linear, non linear and linear buckling), the non-structural mass may generate inertia force based on the global load case setting.
Non-structural mass attributes generate gravity loads on the model when non-zero global accelerations are applied. When no global accelerations are applied or the applied values are zero, non-structural mass attributes will have no effect on the analysis results.
The global load case setting contains acceleration definition parameters and structural and non-structural mass options. When global acceleration is defined, the user may choose to include or exclude the inertia forces due to the structural masses and non-structural masses.

For dynamic analysis, the non-structural masses in a selected load case may be included in addition to the structural mass. For mode superposition based solvers, such as harmonic response, spectral response and linear transient dynamics with mode superposition, the non-structural mass that is included is determined by the natural frequency analysis conducted to determine the natural vibration modes.

3. DESIGN AND IMPORT OF THE TRACK

The first step in the creation of the geometry of the bridge is drawing the track in the software Autocad.

Fig. 30 - Track of the bridge (mm)

The whole track is divided by dots in segments with the same length of 2.20 m, so the track is imported in the fem software Straus only by a series of dots and all the geometry of the bridge is built through the fem elements.

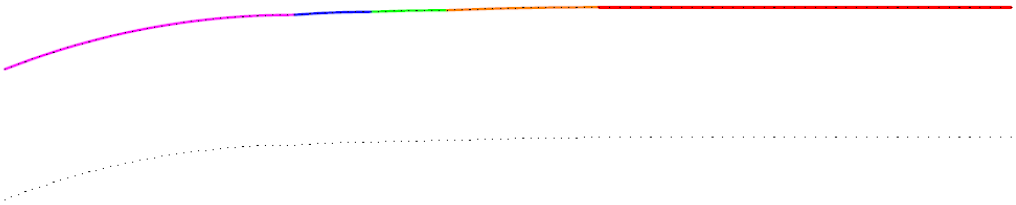

Fig. 31 - Track's subdivision

4. SIMPLE BEAMS MODEL

The first step of the study was create a simple fem model composed by only beam elements.

The same approach was used by the Engineers of the bridge, M. Studničková, J. Máca and J. Král, in 1989.

In the following lines the geometrical characteristics of all the components of the bridge are shown.

4.1 Deck

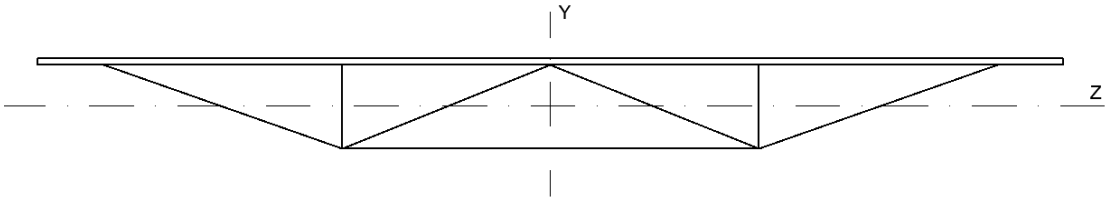

Fig. 32 - Simple schematization of the cross section

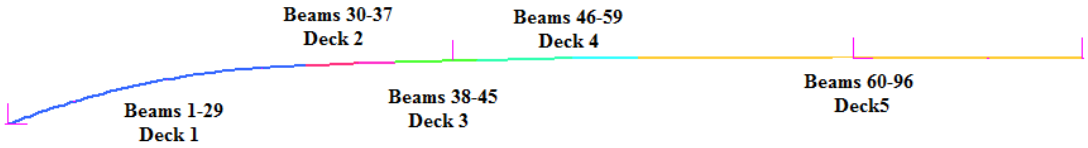

Fig. 33 - Deck's subdivision

Beams 1 - 29	Beams 30 - 37	Beams 38 - 45	Beams 46 - 59	Beams 60 - 96
A = 12,863 e6 mm2	A = 12,591 e6 mm2	A = 12,318 e6 mm2	A = 12,046 e6 mm2	A = 11,774 e6 mm2
Iz = 11,702 e12 mm4	Iz = 11,381 e12 mm4	Iz = 11,060 e12 mm4	Iz = 10,739 e12 mm4	Iz = 10,417 e12 mm4
Iy = 664,622 e12 mm4	Iy = 638,622 e12 mm4	Iy = 612,622 e12 mm4	Iy = 586,622 e12 mm4	Iy = 560,432 e12 mm4
J = 22,575 e12 mm4	J = 22,575 e12 mm4	J = 22,575 e12 mm4	J = 22,575 e12 mm4	J = 22,575 e12 mm4

Tab. 3 - Geometrical characteristics of the deck

The deck of the bridge is further subdivided in three parts which have different values of density.

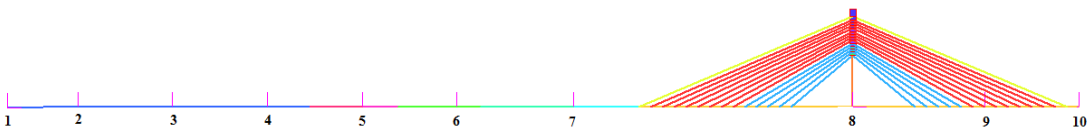

Fig. 34 - Number of bearings

Bearings	Permanent load	Area cross section	Mass	Density
1 - 5	547,7 KN/m	12,86 m2	55,89 Kg	4,346 e-9 T/mm2
5 - 7	514,0 KN/m	12,05 m2	52,45 Kg	4,353 e-9 T/mm2
7 - 10	480,2 KN/m	11,77 m2	49 Kg	4,163 e-9 T/mm2

Tab. 4 - Density of the three groups of beams

4.2 Bearings

The modeling of bridge boundary conditions is an important issue in the modal analysis.

Two types of bridge bearings are used in this cable-stayed bridge:

- simple bearings, that allow the torsional degree of freedom, are used in supports number 2, 3, 4, 5, 7 and 9;
- double bearings in 1, 6, 8, 10 (see Fig. 34).

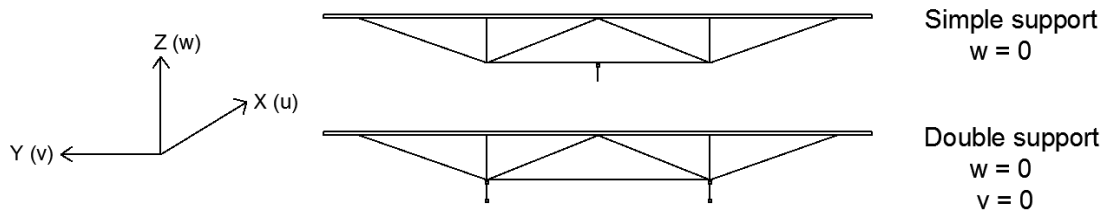

Fig. 35 - Types of support

4.3 Pylon

The pylon is composed by 4 parts:

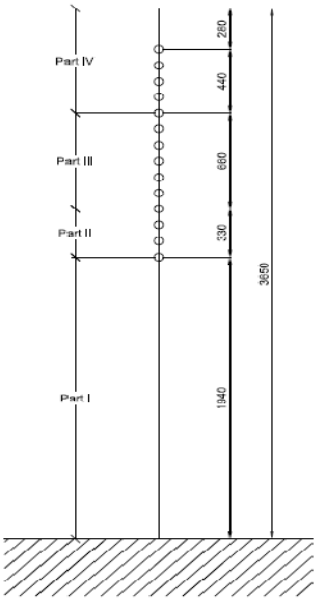

Fig. 36 - Pylon (dimensions in cm)

The first part of the pylon is composed by an external box of steel and an internal portion of concrete; this part is considered as an idealized steel section with the following characteristics taken from the CVUT report.

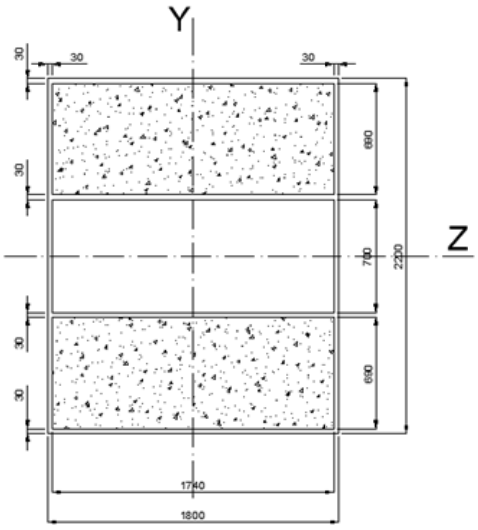

Pylon I (101 - 105)
A = 0,8162 e6 mm2
Iz = 0,727325 e12 mm12
Iy = 0,257683 e12 mm12
J = 0,139293 e12 mm12

Fig. 37 - Pylon part I

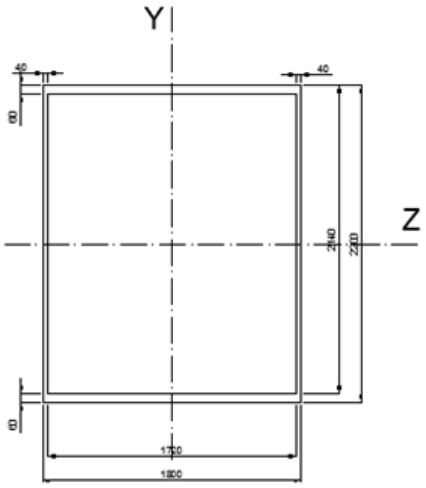

Pylon II (106 - 110)
A = 0,5012 e6 mm2
Iz = 0,324599 e12 mm12
Iy = 0,18738 e12 mm12
J = 0,320937 e12 mm12

Fig. 38 - Pylon part II

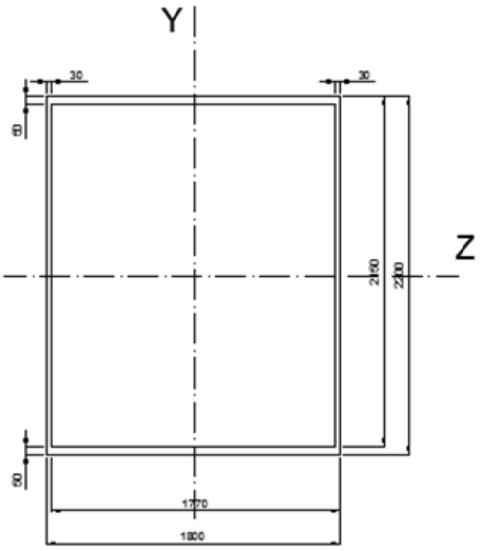

Pylon III (101 - 105)
A = 0,426 e6 mm2
Iz = 0,276085 e12 mm12
Iy = 0,147332 e12 mm12
J = 0,253843 e12 mm12

Fig. 39 - Pylon part III

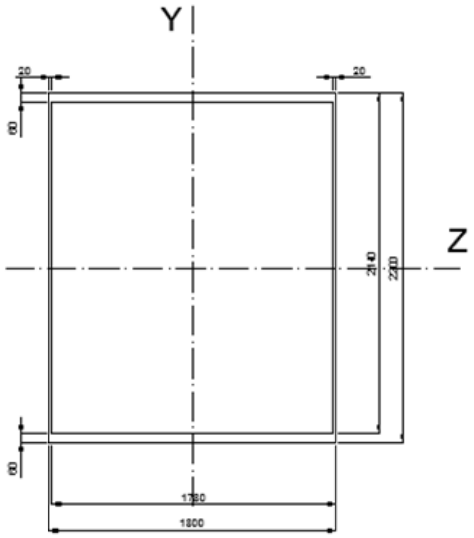

Pylon IV (97 - 100)
A = 0,24775 e6 mm2
Iz = 0,155349 e12 mm12
Iy = 0,092431 e12 mm12
J = 0,155952 e12 mm12

Fig. 40 - Pylon part IV

The material used for the four parts of the pylon is structural steel with the following properties:

E = 210000 MPa
ν = 0,3
ρ = 7,8 e-9 T/mm3

4.4 Cables

In the analysis of cable-stayed bridges, a common practice is to model each cable as a single truss element with an equivalent modulus. However, to model the stay cables as truss elements with equivalent modulus is simple, but inadequate for accurate dynamic analysis of a cable-stayed bridge because it essentially precludes the transverse cable vibrations.

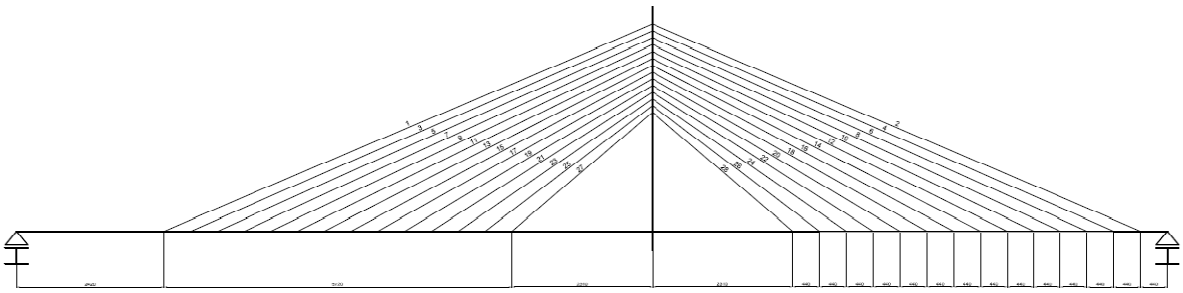

Fig. 41 - Front of the bridge

There are three different groups of cables subdivided by geometrical characteristics.

Cables 1,2	Cables 3 - 18	Cables 19 - 28
A = 8980 mm2	A = 17960 mm2	A = 16430 mm2
D = 106,93 mm	D = 151,22 mm	D = 144,635 mm

Tab. 5 - Geometric characteristics of the cables

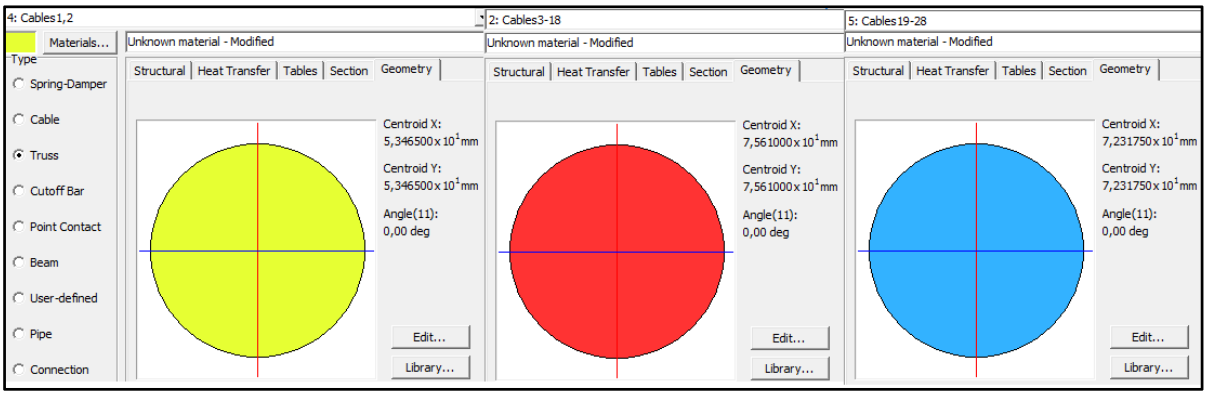

Fig. 42 - Dimensions of the cables

The material of the cables is steel with the following properties:

E = 195000 MPa
ν = 0,3
ρ = 7,8 e-9 T/mm3

All the cables are pretensioned with the following values:

Cables	Pretension loads (KN)	Cables	Pretension loads (KN)
1	2691	**28**	1528
3	5230	**26**	3290
5	5103	**24**	3512
7	4969	**22**	3724
9	4827	**20**	3924
11	4677	**18**	4115
13	4517	**16**	4294
15	4348	**14**	4463
17	4167	**12**	4623
19	3976	**10**	4772
21	3775	**8**	4913
23	3561	**6**	5047
25	3337	**4**	5174
27	1551	**2**	2663

Tab. 6 - Cables' pretension values

The model summary option in Straus provides a complete account of the bill of materials, mass distribution and moments of inertia on separate tabs.

	Mass T	Volume mm^3	Length mm	Area mm^2	Count	Material	Type
Grand total:	**$2{,}121733\times10^{4}$**	**$4{,}943494\times10^{12}$**	**$2{,}069926\times10^{6}$**				
Beam properties:							
1: Deck1	$6{,}308561\times10^{3}$	$1{,}451579\times10^{12}$	$1{,}128504\times10^{5}$		51		Beam
2: Cables3-18	$1{,}515598\times10^{2}$	$1{,}925792\times10^{10}$	$1{,}072262\times10^{6}$		16		Truss
3: Deck 3	$1{,}651570\times10^{3}$	$3{,}794359\times10^{11}$	$3{,}080262\times10^{4}$		14		Beam
4: Cables1,2	$1{,}230939\times10^{1}$	$1{,}564090\times10^{9}$	$1{,}741698\times10^{5}$		2		Truss
5: Cables19-28	$4{,}989888\times10^{1}$	$6{,}340392\times10^{9}$	$3{,}859041\times10^{5}$		10		Truss
7: Pilon2	$9{,}931310\times10^{0}$	$1{,}261920\times10^{9}$	$3{,}300000\times10^{3}$		3		Beam
8: Pilon1 steel	$5{,}203266\times10^{1}$	$6{,}611520\times10^{9}$	$1{,}940000\times10^{4}$		1		Beam
9: Pilon4	$9{,}972864\times10^{0}$	$1{,}267200\times10^{9}$	$7{,}200000\times10^{3}$		5		Beam
10: Deck 2.1	$1{,}085063\times10^{3}$	$2{,}496693\times10^{11}$	$1{,}982982\times10^{4}$		9		Beam
11: Deck 4.2	$1{,}845741\times10^{3}$	$4{,}240451\times10^{11}$	$3{,}520215\times10^{4}$		16		Beam
12: Deck5	$8{,}087524\times10^{3}$	$1{,}942669\times10^{12}$	$1{,}650000\times10^{5}$		76		Beam
13: Pilon3	$1{,}589425\times10^{1}$	$2{,}019600\times10^{9}$	$6{,}600000\times10^{3}$		6		Beam
14: Deck 2.2	$7{,}236034\times10^{2}$	$1{,}662424\times10^{11}$	$1{,}320369\times10^{4}$		6		Beam
15: Deck 4.3	$1{,}213672\times10^{3}$	$2{,}915308\times10^{11}$	$2{,}420146\times10^{4}$		11		Beam
Total	**$2{,}121733\times10^{4}$**	**$4{,}943494\times10^{12}$**	**$2{,}069926\times10^{6}$**		**226**		

Tab. 7 - Bill of materials (beams model)

	IXX $T.mm^2$	IYY $T.mm^2$	IZZ $T.mm^2$	IXY $T.mm^2$	IYZ $T.mm^2$	IZX $T.mm^2$
AutoCAD import: "Track_newEXP.dxf"	$0{,}000000\times10^{0}$	$0{,}000000\times10^{0}$	$0{,}000000\times10^{0}$	$0{,}000000\times10^{0}$	$0{,}000000\times10^{0}$	$0{,}000000\times10^{0}$
Model	$1{,}124167\times10^{17}$	$1{,}090874\times10^{17}$	$2{,}215039\times10^{17}$	$-1{,}105840\times10^{17}$	$-1{,}014751\times10^{13}$	$1{,}052872\times10^{13}$
Total:	**$1{,}124167\times10^{17}$**	**$1{,}090874\times10^{17}$**	**$2{,}215039\times10^{17}$**	**$-1{,}105840\times10^{17}$**	**$-1{,}014751\times10^{13}$**	**$1{,}052872\times10^{13}$**

Tab. 8 - Global inertia (beams model)

5. BEAMS MODEL WITH TORSIONAL D.O.F.

The 3D space beam stands for an element orientated in any direction in the space and that can be stressed by four kind of load: axial forces, perpendicular forces, bending moments along the two principal inertia axis of the section and torque moment along the longitudinal axis.

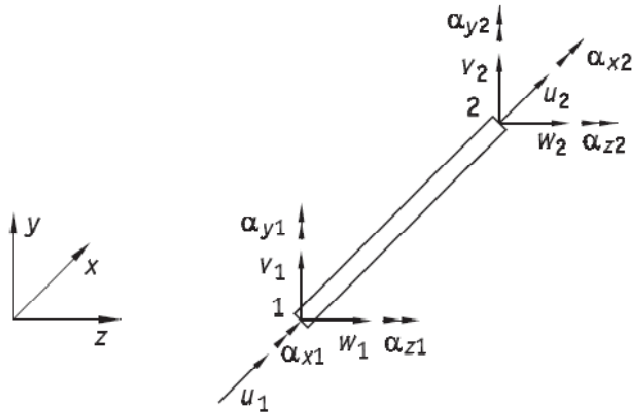

Fig. 43 - Beam's degree of freedom

The system natural frequency is observed to be dependent on several parameters such as the magnitude of the tip mass, the location of the tip mass centre of gravity relative to the point of attachment, the moments of inertia of the tip mass about its centre of gravity, the length of the beam, the slenderness ratio, and the bending stiffness and torsional rigidity of the beam.

The non structural added masses are calculated subdividing the cross section in two parts.
The area of the following part of the cross section (Fig. 44) is assigned to the central beams but the inertias are maintained the same as in the simple beams model. This because the torsional inertia of the central part of the deck, close section, is higher than the total cross section, so it's necessary to maintain this characteristic.

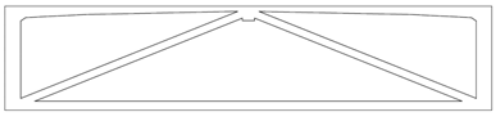

```
Area:                          9532895.8706
Perimeter:                     79782.8800
Bounding box:            X: 113930.2536  --  126330.2536
                         Y: -8857.2156  --  -6205.8710
Centroid:                X: 120130.3297
                         Y: -7563.6126
Moments of inertia:      X: 5.5500E+14
                         Y: 1.3774E+17
Product of inertia:     XY: -8.6618E+15
Radii of gyration:       X: 7630.1342
                         Y: 120201.8365
Principal moments and X-Y directions about centroid:
                         I: 9.6350E+12 along [1.0000 0.0001]
                         J: 1.6383E+14 along [-0.0001 1.0000]
```

Fig. 44 - Schematization of the deck part 1

In the following table the properties of the central beams are summarized, divided as before into three different density properties.

	Density (T/mm^2)	Area cross section (mm^2)	I11 (mm^4)	I22 (mm^4)	J (mm^4)
Deck 1	4,3460E-09	9,532896E+06	6,646217E+14	1,170242E+13	2,257500E+13
Deck 2.1	4,3460E-09	9,532896E+06	6,386217E+14	1,138120E+13	2,257500E+13
Deck 2.2	4,3527E-09	9,532896E+06	6,386217E+14	1,138120E+13	2,257500E+13
Deck 3	4,3527E-09	9,532896E+06	6,126217E+14	1,105990E+13	2,257500E+13
Deck 4.2	4,3527E-09	9,532896E+06	5,866217E+14	1,073870E+13	2,257500E+13
Deck 4.3	4,1631E-09	9,532896E+06	5,866217E+14	1,073870E+13	2,257500E+13
Deck 5	4,1631E-09	9,532896E+06	5,604320E+14	1,041740E+13	2,257500E+13

Tab. 9 - Central beams' properties

The non structural masses are connected to the central beams by rigid link and they are calculated using an approximate density of 4*E-09 T/mm^2 for all the beams, the areas of the part in Fig. 45 and the lengths of the beams, see the following expression.

$$M = \rho * A * l$$

Where: ρ is the density of the beams' material

A is the area of the second part of the schematization of the cross section

l is the length of the referred beams

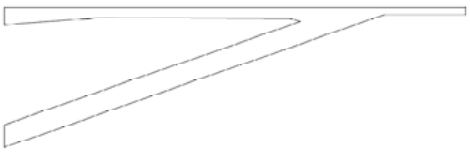

```
Area:                              4384560.3793
Perimeter:                         29710.2457
Bounding box:                X: 128661.0284  --  137211.0284
                             Y: -8811.3121  --  -6205.8710
Centroid:                    X: 132079.5397
                             Y: -7031.3190
Moments of inertia:          X: 2.1936E+14
                             Y: 7.6508E+16
Product of inertia:          XY: -4.0679E+15
Radii of gyration:           X: 7073.1864
                             Y: 132096.5837
Principal moments and X-Y directions about centroid:
                             I: 1.7074E+12 along [0.9764 0.2159]
                             J: 2.0624E+13 along [-0.2159 0.9764]
```

Fig. 45 - Schematization of the deck part 2

The calculated masses are equal to 38,58 Kg in the most part of the deck; in correspondence of the pylon and in the lasts part of the bridge, where the distance between the plates is lower, the masses are equal to 19,29 Kg; in the two sides of the pylon the masses are equivalent to 28,94 Kg.

All the non structural masses have a dynamic factor of 1.

The values quoted before are used to represent the real total mass of the structure.

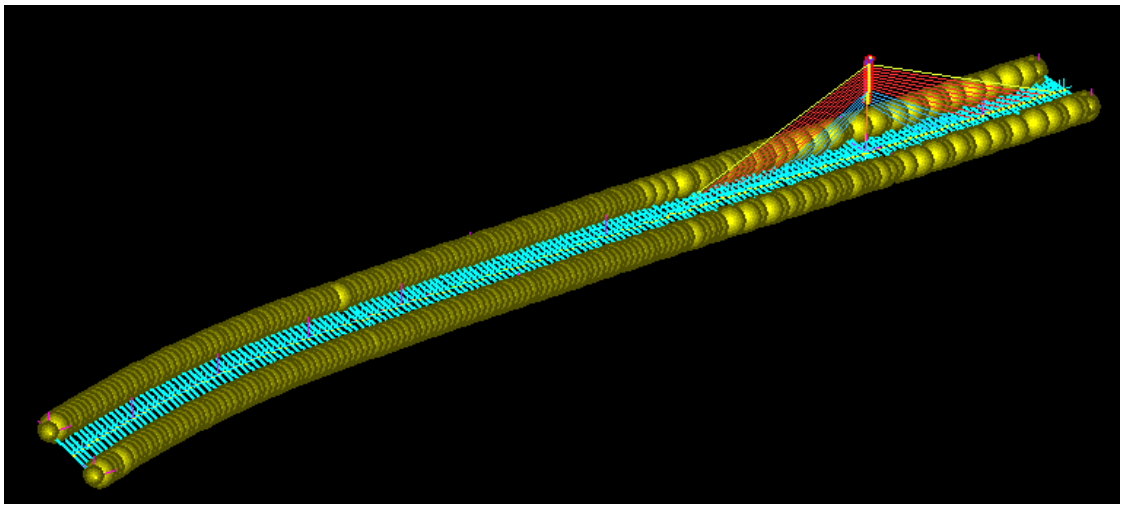

Fig. 46 – Bridge's model with non-structural masses

The non structural masses are added at the simple beam model by rigid links in the plane xyz to simulate the torsional behavior of the structure.

All the characteristics of the pylon, cables and bearings remain the same as in the simple beam model.

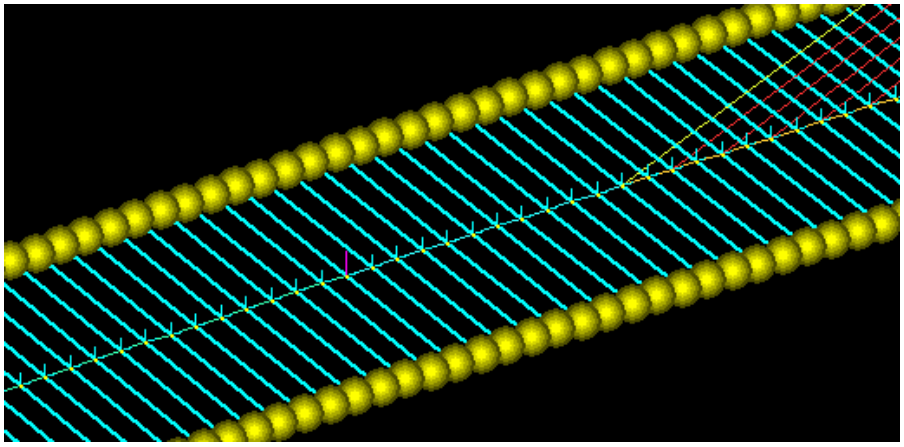

Fig. 47 - Particular of the masses' connection

The following tables report the characteristics of the total bridge.

	Mass T	Volume mm^3	Length mm	Area mm^2	Count	Material	Type
Grand total:	**$3{,}063706 \times 10^4$**	**$3{,}861873 \times 10^{12}$**	**$2{,}069926 \times 10^6$**				
Node mass:	**$1{,}404314 \times 10^4$**						
Beam properties:							
1: Deck1	$4{,}675387 \times 10^3$	$1{,}075791 \times 10^{12}$	$1{,}128504 \times 10^5$		51		Beam
2: Cables3-18	$1{,}515598 \times 10^2$	$1{,}925792 \times 10^{10}$	$1{,}072262 \times 10^6$		16		Truss
3: Deck 3	$1{,}278119 \times 10^3$	$2{,}936381 \times 10^{11}$	$3{,}080262 \times 10^4$		14		Beam
4: Cables1,2	$1{,}230939 \times 10^1$	$1{,}564090 \times 10^9$	$1{,}741698 \times 10^5$		2		Truss
5: Cables19-28	$4{,}989888 \times 10^1$	$6{,}340392 \times 10^9$	$3{,}859041 \times 10^5$		10		Truss
7: Pilon2	$9{,}931310 \times 10^0$	$1{,}261920 \times 10^9$	$3{,}300000 \times 10^3$		3		Beam
8: Pilon1 steel	$5{,}203266 \times 10^1$	$6{,}611520 \times 10^9$	$1{,}940000 \times 10^4$		1		Beam
9: Pilon4	$9{,}972864 \times 10^0$	$1{,}267200 \times 10^9$	$7{,}200000 \times 10^3$		5		Beam
10: Deck 2.1	$8{,}215486 \times 10^2$	$1{,}890356 \times 10^{11}$	$1{,}982982 \times 10^4$		9		Beam
11: Deck 4.2	$1{,}460672 \times 10^3$	$3{,}355784 \times 10^{11}$	$3{,}520215 \times 10^4$		16		Beam
12: Deck5	$6{,}548256 \times 10^3$	$1{,}572928 \times 10^{12}$	$1{,}650000 \times 10^5$		76		Beam
13: Pilon3	$1{,}589425 \times 10^1$	$2{,}019600 \times 10^9$	$6{,}600000 \times 10^3$		6		Beam
14: Deck 2.2	$5{,}478719 \times 10^2$	$1{,}258694 \times 10^{11}$	$1{,}320369 \times 10^4$		6		Beam
15: Deck 4.3	$9{,}604690 \times 10^2$	$2{,}307100 \times 10^{11}$	$2{,}420146 \times 10^4$		11		Beam
Total	**$1{,}659392 \times 10^4$**	**$3{,}861873 \times 10^{12}$**	**$2{,}069926 \times 10^6$**		**226**		

Tab. 10 - Bill of materials (beams model with masses)

	IXX $T.mm^2$	IYY $T.mm^2$	IZZ $T.mm^2$	IXY $T.mm^2$	IYZ $T.mm^2$	IZX $T.mm^2$
AutoCAD import: "Track_newEXP.dxf"	$0{,}000000 \times 10^0$	$0{,}000000 \times 10^0$	$0{,}000000 \times 10^0$	$0{,}000000 \times 10^0$	$0{,}000000 \times 10^0$	$0{,}000000 \times 10^0$
Model	$1{,}623035 \times 10^{17}$	$1{,}581592 \times 10^{17}$	$3{,}204625 \times 10^{17}$	$-1{,}599937 \times 10^{17}$	$-1{,}014751 \times 10^{13}$	$1{,}052872 \times 10^{13}$
Total:	**$1{,}623035 \times 10^{17}$**	**$1{,}581592 \times 10^{17}$**	**$3{,}204625 \times 10^{17}$**	**$-1{,}599937 \times 10^{17}$**	**$-1{,}014751 \times 10^{13}$**	**$1{,}052872 \times 10^{13}$**

Tab. 11 - Global inertia (beams model with masses)

6. PLATES MODEL

Determining a plate element size that gives accurate results and minimizes the model and the time is critical. It is useful to follow the next procedure to minimize the number of plates in a general model:

1. Start with an element size that matches the natural geometry in the model. Use nodes at locations where other plates connect or where members connect. Try to minimize the number of plate elements in a reasonable way.
2. Run the analysis and record your results. If you have reason to question the results or if you have no way of knowing whether or not they are reasonable, proceed to step 3.
3. Subdivide your initial element meshes into smaller elements and analyze again with the refined model.
4. Compare the results of step 3 with the previous analysis. If the results are similar, assume you are near the converged solution and feel somewhat confident of your results. Otherwise, if the results differ substantially, return to step 3.

The following picture shows what happens as you "refine" your model by using smaller elements. Your goal is to get into the "flat area" for the model, the area where results do not change much as you refine the model further.

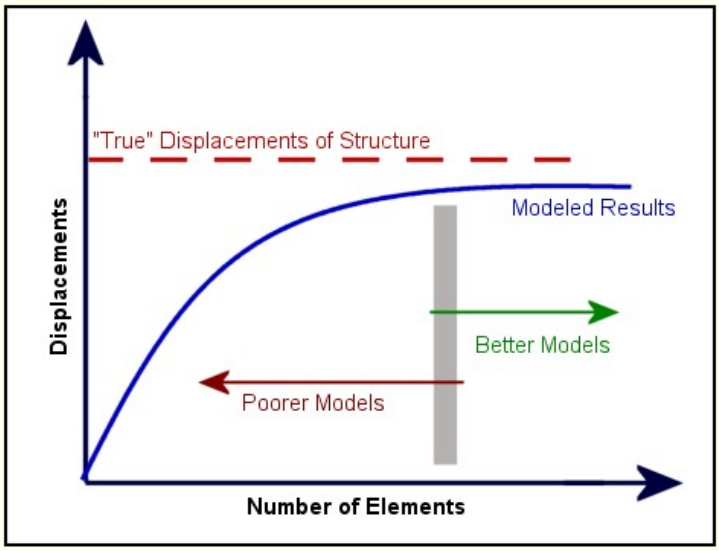

Fig. 48 - Displacements vs number of plates

As a general rule it is useful to place more elements in areas where stresses and forces in the plates are changing the most per unit length of mesh. Stress concentrations or locations near concentrated loads may require smaller element size. At locations under uniform loading/no loading, and away from geometric irregularities, large elements may be sufficient.

This model is composed by plates, beams and trusses. Plates are used to create the cross section of the deck, beams are used to schematized the pylon and the wind bracings, trusses for the cables.
All the portions of the deck are divided in three parts with different density's properties of the material, taken from the permanent loads applied at the structure.

	Permanent load (KN/m)	Area cross section (m^2)	Mass (Kg)	Density (T/mm^2)
Part 1	547,7	12,86	55,89	4,3460E-09
Part 2	514,0	12,05	52,45	4,3527E-09
Part 3	480,2	11,77	49	4,1631E-09

Tab. 12 - Densities of the deck

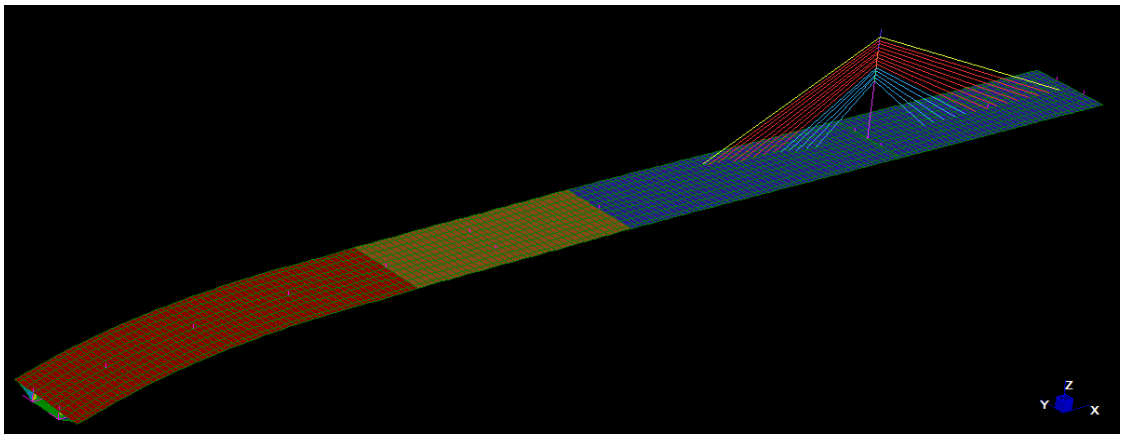

Fig. 49 - Complete plates model

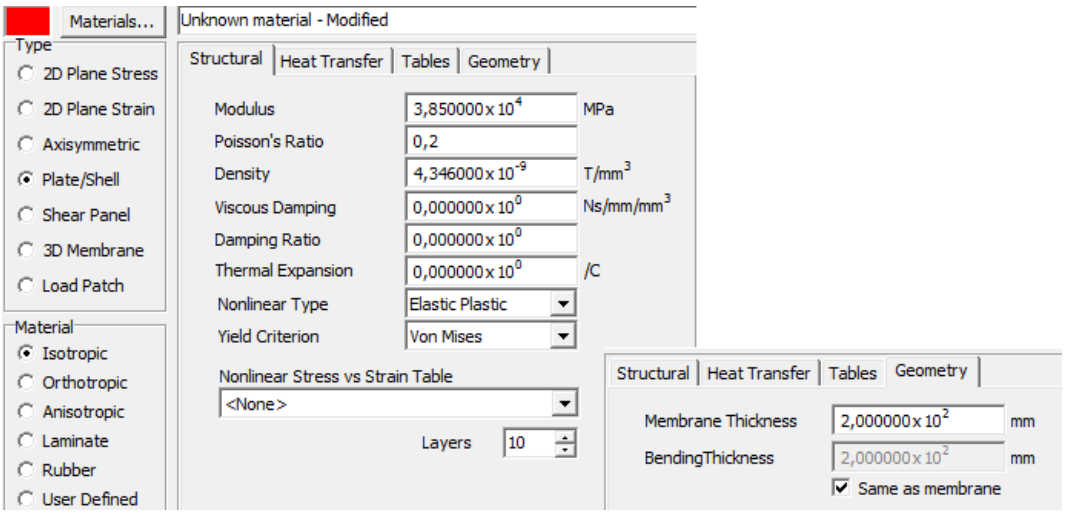

Fig. 50 - Insole 1

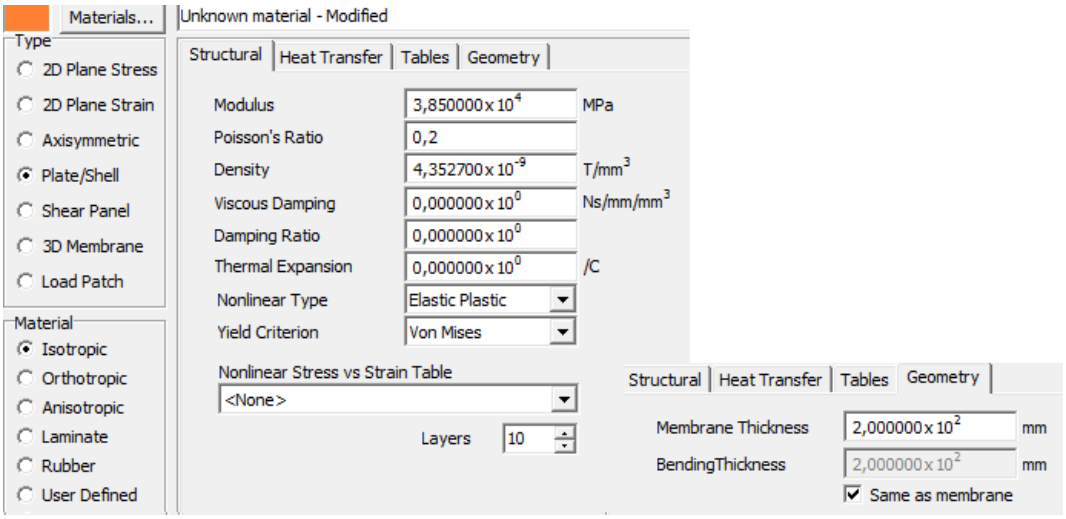

Fig. 51 - Insole 2

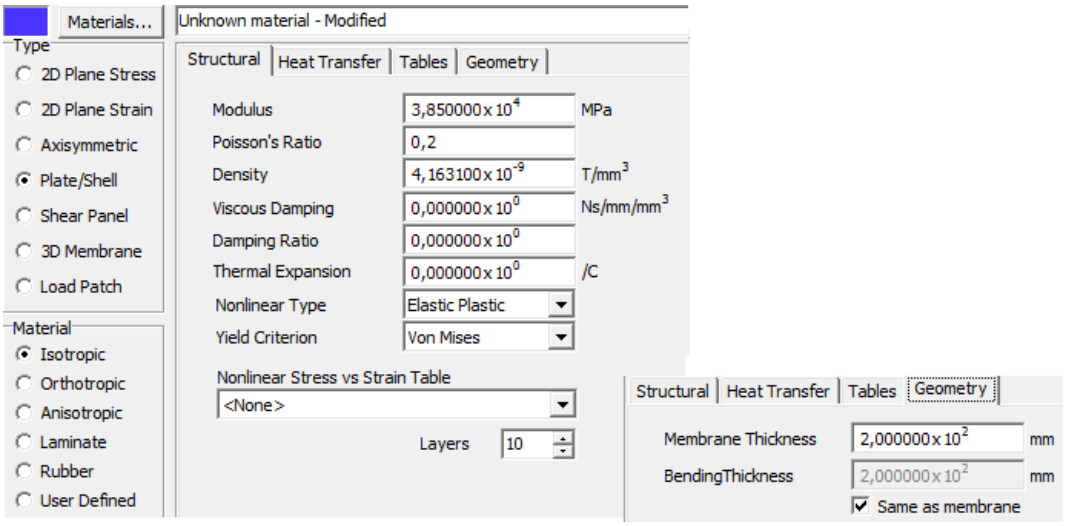

Fig. 52 - Insole 3

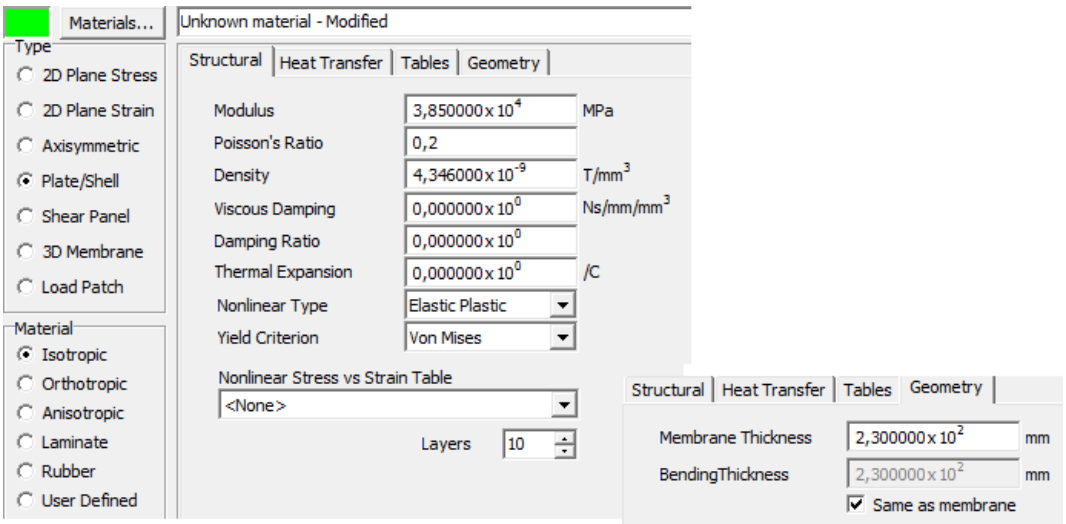

Fig. 53 - Low plane 1

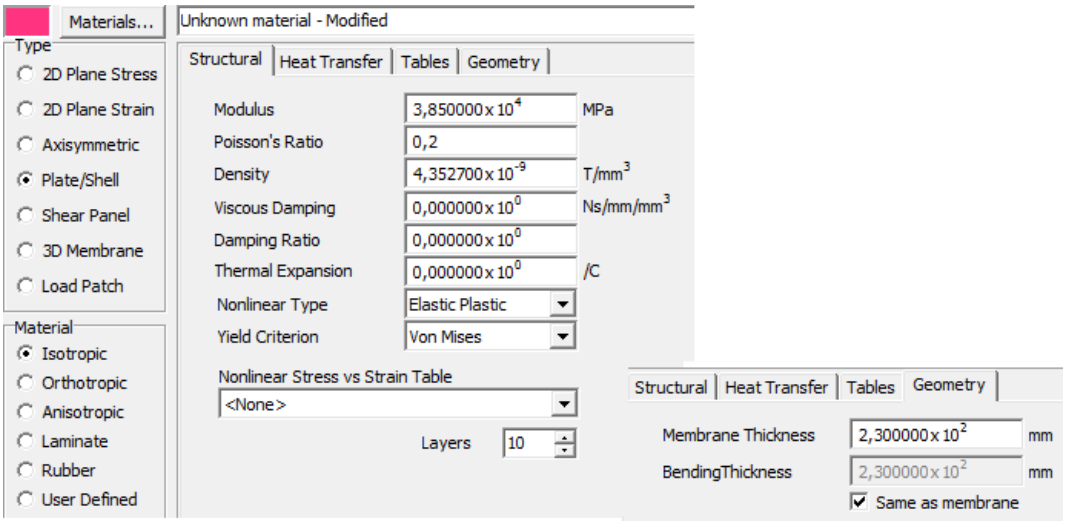

Fig. 54 - Low plane 2

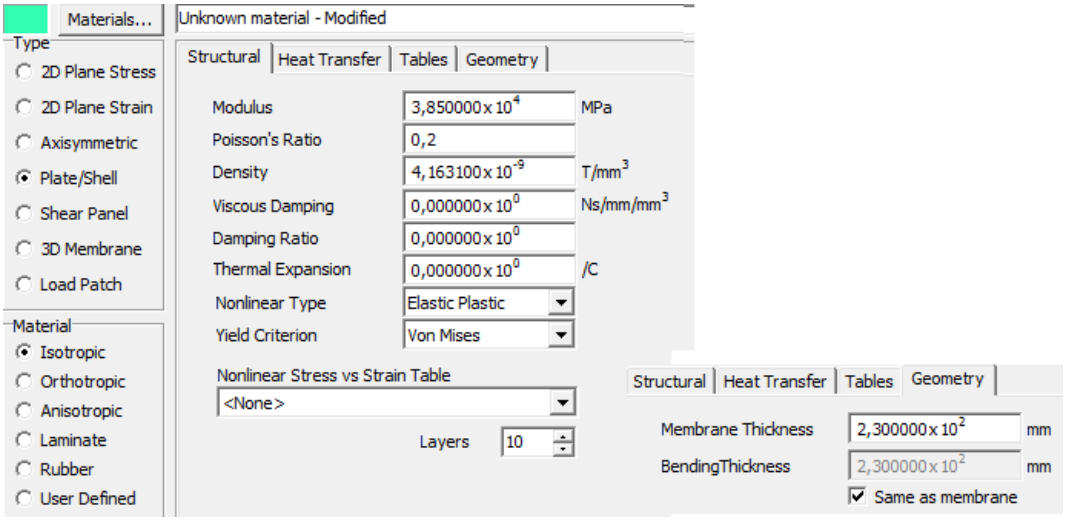

Fig. 55 - Low plane 3

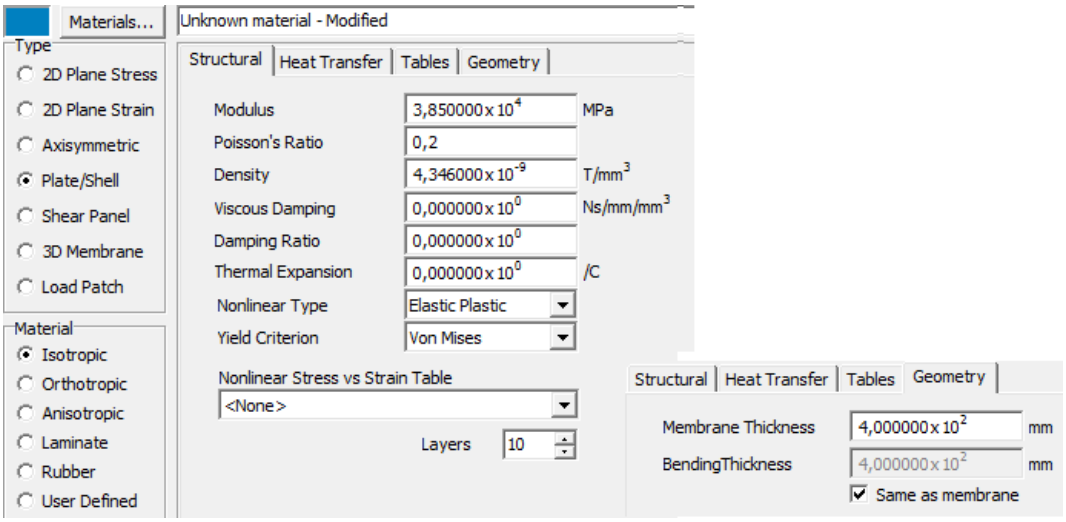

Fig. 56 - Inclined plates 1

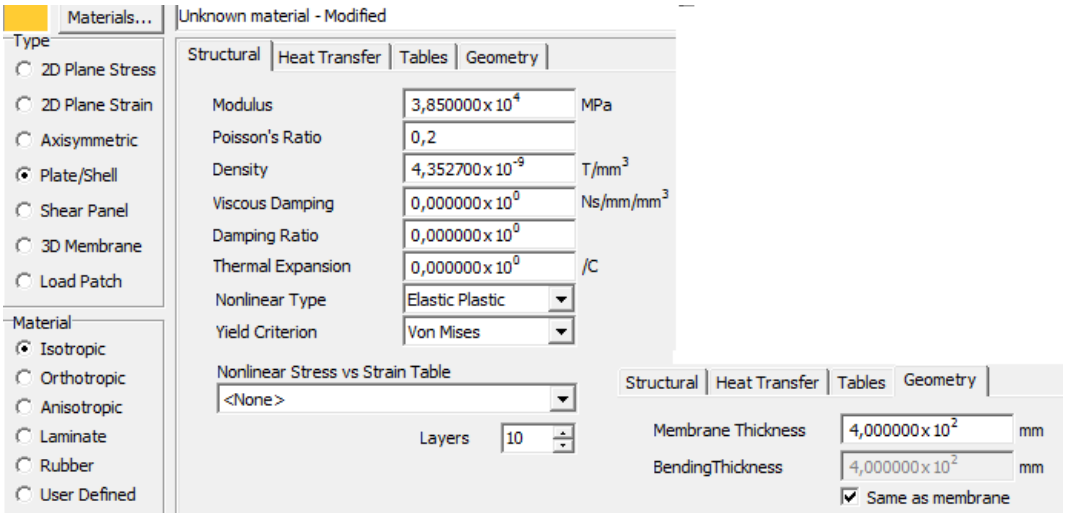

Fig. 57 - Inclined plates 2

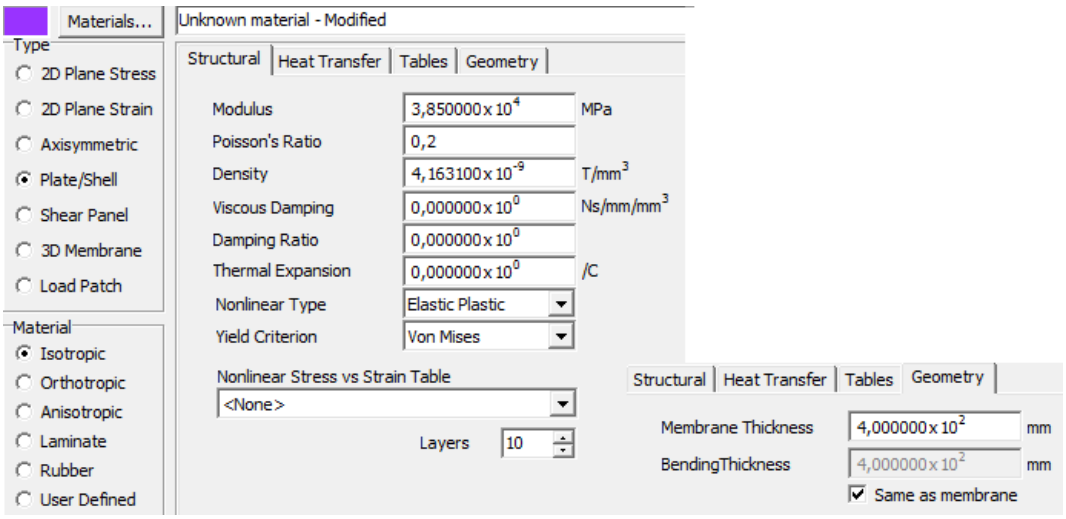

Fig. 58 - Inclined plates 3

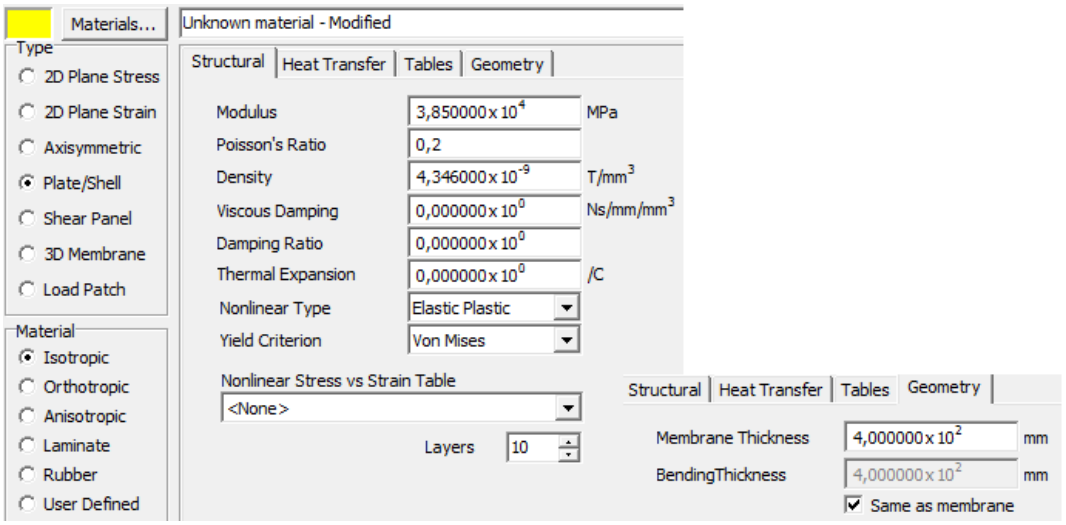

Fig. 59 - Vertical planes 1

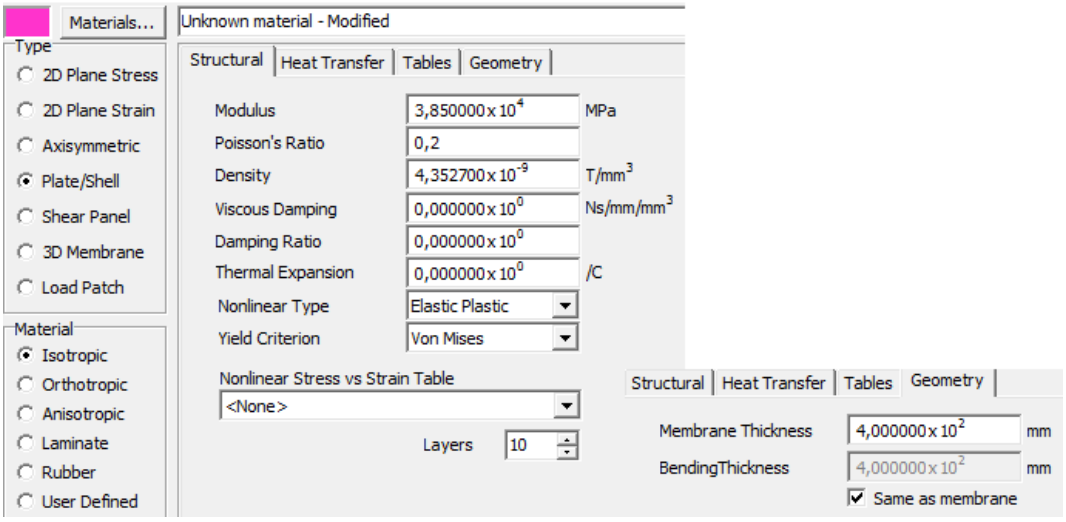

Fig. 60 - Vertical planes 2

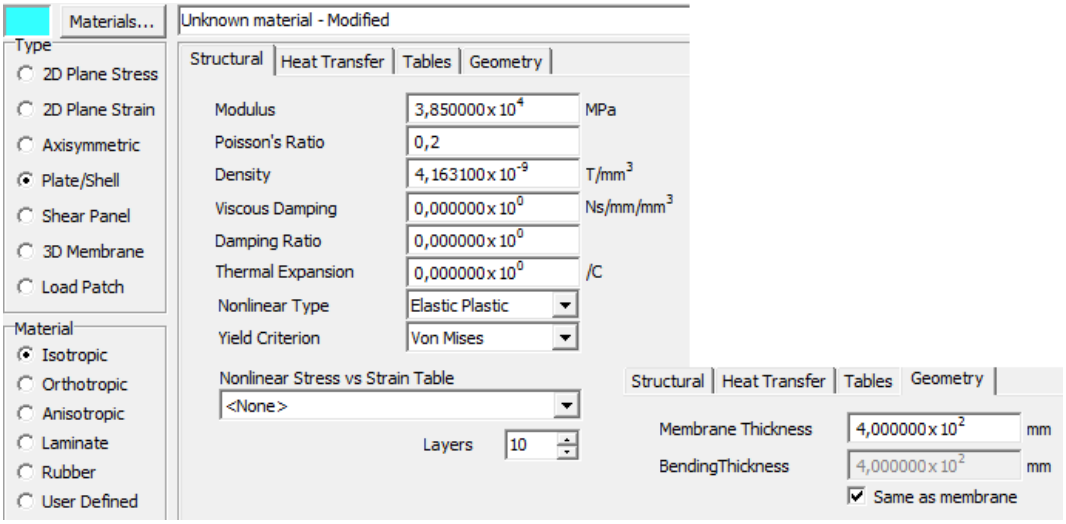

Fig. 61 - Vertical planes 3

	E (MPa)	ν	Density (T/mm3)	Thickness (mm)
Insole 1	3,85E+04	0,2	4,3460E-09	2,00E+02
Low plane 1	3,85E+04	0,2	4,3460E-09	2,30E+02
Inclined plates 1	3,85E+04	0,2	4,3460E-09	4,00E+02
Vertical plates 1	3,85E+04	0,2	4,3460E-09	4,00E+02
Insole 2	3,85E+04	0,2	4,3527E-09	2,00E+02
Low plane 2	3,85E+04	0,2	4,3527E-09	2,30E+02
Inclined plates 2	3,85E+04	0,2	4,3527E-09	4,00E+02
Vertical plates 2	3,85E+04	0,2	4,3527E-09	4,00E+02
Insole 3	3,85E+04	0,2	4,1631E-09	2,00E+02
Low plane 3	3,85E+04	0,2	4,1631E-09	2,30E+02
Inclined plates 3	3,85E+04	0,2	4,1631E-09	4,00E+02
Vertical plates 3	3,85E+04	0,2	4,1631E-09	4,00E+02

Tab. 13 - Summary of the plates' properties

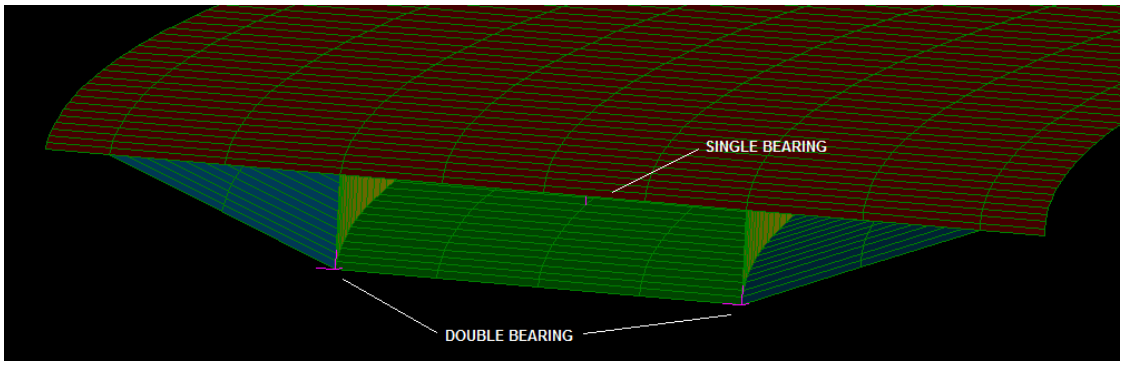

Fig. 62 - Bearings

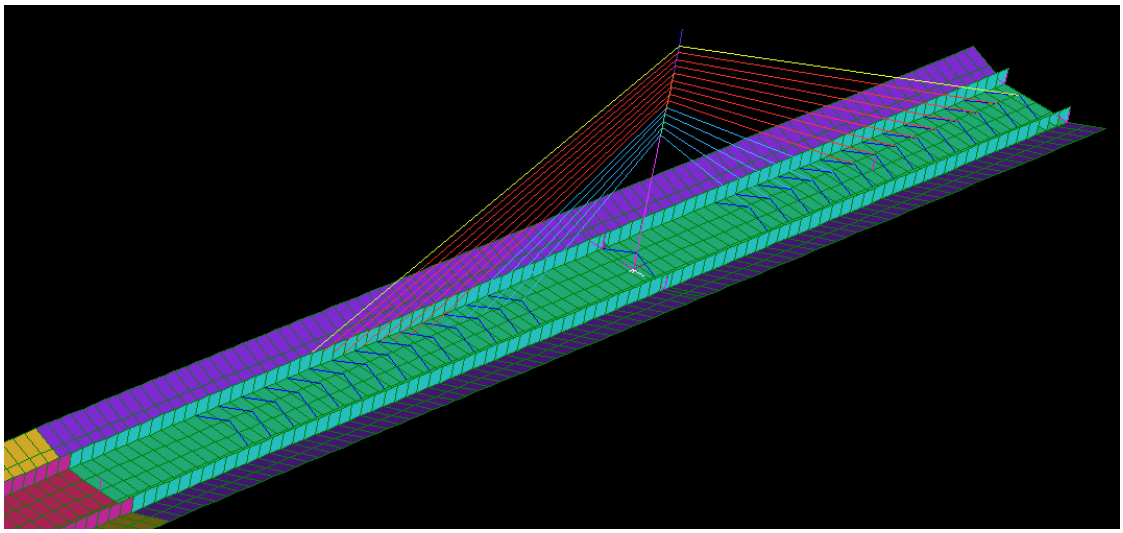

Fig. 63 - Internal wind bracings

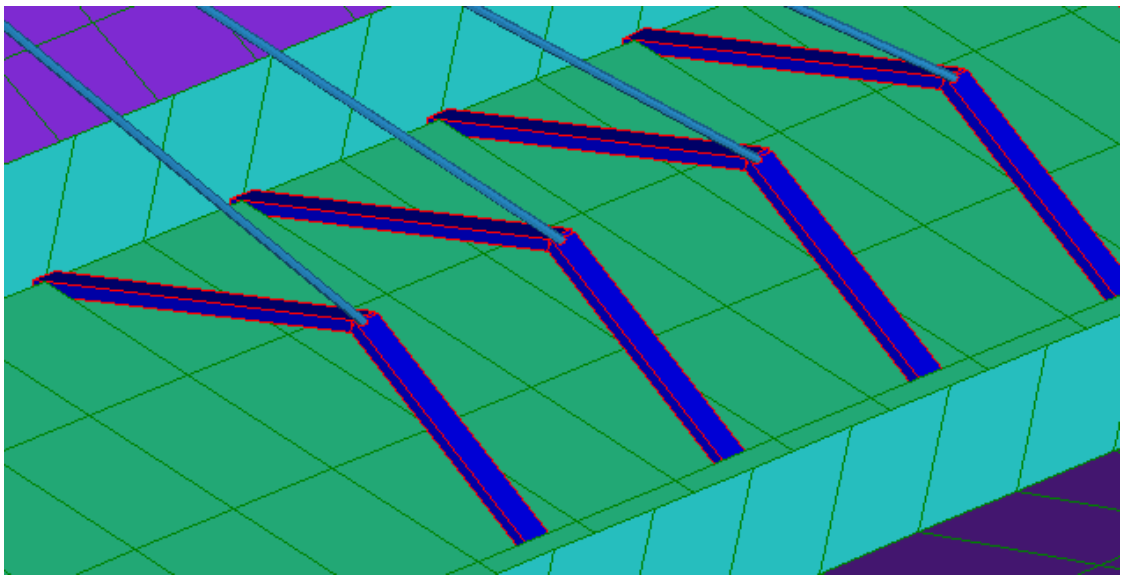

Fig. 64 - Wind bracings

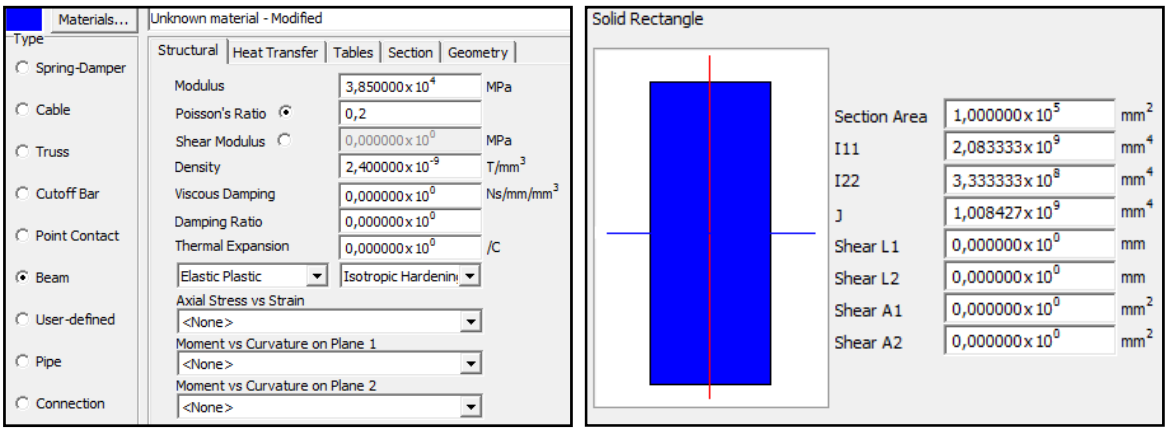

Fig. 65 - Material and structural properties of the wind bracings

	Mass T	Volume mm³	Length mm	Area mm²	Count	Material	Type
Grand total:	**2,860814x10⁴**	**6,697989x10¹²**	**2,050705x10⁶**	**2,445924x10¹⁰**			
Beam properties:							
2: Cables3-18	1,515598x10²	1,925792x10¹⁰	1,072262x10⁶		16		Truss
4: Cables1,2	1,230939x10¹	1,564090x10⁹	1,741698x10⁵		2		Truss
5: Cables19-28	4,989888x10¹	6,340392x10⁹	3,859041x10⁵		10		Truss
6: Pilon1 acciaio	5,900611x10¹	7,497600x10⁹	2,200000x10⁴		2		Beam
7: Pilon2	9,931310x10⁰	1,261920x10⁹	3,300000x10³		3		Beam
8: Pilon3	1,589425x10¹	2,019600x10⁹	6,600000x10³		6		Beam
9: Pilon4	9,972864x10⁰	1,267200x10⁹	7,200000x10³		5		Beam
10: Controv	9,102445x10¹	3,792686x10¹⁰	3,792686x10⁵		58		Beam
Total	**3,995971x10²**	**7,713558x10¹⁰**	**2,050705x10⁶**		**102**		
Plate properties:							
1: Soletta1	3,332346x10³	7,667616x10¹¹		3,833808x10⁹	600	Isotropic	Plate/Shell
4: Low Plane1	1,558860x10³	3,586885x10¹¹		1,559515x10⁹	240	Isotropic	Plate/Shell
5: Inclinati 1	3,319472x10³	7,637993x10¹¹		1,909498x10⁹	240	Isotropic	Plate/Shell
7: Vertical plane 1	1,199386x10³	2,759748x10¹¹		6,899370x10⁸	120	Isotropic	Plate/Shell
8: Soletta2	2,033485x10³	4,671779x10¹¹		2,335889x10⁹	360	Isotropic	Plate/Shell
9: Soletta3	4,647195x10³	1,116282x10¹²		5,581412x10⁹	870	Isotropic	Plate/Shell
10: Low plane2	9,512575x10²	2,185442x10¹¹		9,501923x10⁸	144	Isotropic	Plate/Shell
11: Low plane 3	2,173942x10³	5,221931x10¹¹		2,270405x10⁹	348	Isotropic	Plate/Shell
12: Inclinati 2	2,020287x10³	4,641458x10¹¹		1,160364x10⁹	144	Isotropic	Plate/Shell
13: Inclinati 3	4,616848x10³	1,108993x10¹²		2,772482x10⁹	348	Isotropic	Plate/Shell
14: Vertical plane 2	7,171230x10²	1,647536x10¹¹		4,118840x10⁸	72	Isotropic	Plate/Shell
15: Vertical plane 3	1,638342x10³	3,935390x10¹¹		9,838476x10⁸	174	Isotropic	Plate/Shell
Total	**2,820855x10⁴**	**6,620853x10¹²**		**2,445924x10¹⁰**	**3660**		

Tab. 14 - Bill of materials (plates model)

	IXX T.mm²	IYY T.mm²	IZZ T.mm²	IXY T.mm²	IYZ T.mm²	IZX T.mm²
AutoCAD import: "Track_newEXP.dxf"	0,000000x10⁰	0,000000x10⁰	0,000000x10⁰	0,000000x10⁰	0,000000x10⁰	0,000000x10⁰
Model	1,515476x10¹⁷	1,477271x10¹⁷	2,992745x10¹⁷	-1,494177x10¹⁷	5,860363x10¹³	-5,722753x10¹³
Total:	**1,515476x10¹⁷**	**1,477271x10¹⁷**	**2,992745x10¹⁷**	**-1,494177x10¹⁷**	**5,860363x10¹³**	**-5,722753x10¹³**

Tab. 15 - Global inertia (plates model)

6.1 Local plate results

The sign convention for moments is: a positive moment produces tensile stresses on the +z local coordinate face of the element, as shown in the sketch.

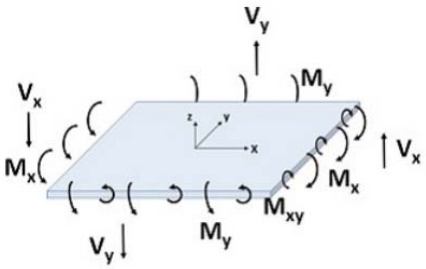

Fig. 66 - Convention for moments

The picture below shows the sign convention for positive stress directions. As usual, positive normal stress indicates tension.

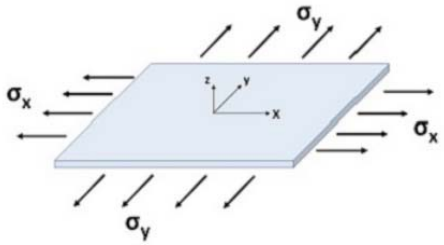

Fig. 67 - Positive stress directions

If plates in the structure can also bend, stresses may be reported at each of the top and bottom faces. Stresses at the face are combined bending and membrane stresses. If plates are subject to bending stresses only, the mid-plane is the neutral axis and therefore the normal stresses at this plane will be zero.

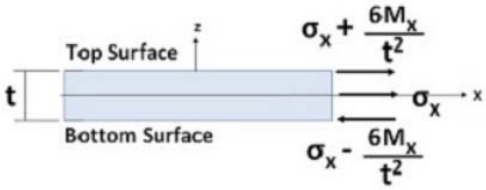

Fig. 68 - Mid plane's forces

6.2 Global plate results

Plate forces and stresses may be reported with respect to the global coordinate system. This simplifies result interpretation when the local axes of elements in a complex mesh are not identically aligned. The global forces follow the right-hand-rule for sign convention. That is, a positive M_X moment is at the global X edge of the plates and rotates about the global Z-axis.

6.3 Checking the quality of the plates model

6.3.1 Free edges

A free edge on a plate is defined as an edge that is not shared by any other plates. Normally plate free edges are found on the outer edges of plate meshes and these define the physical boundary of the structure, rather than the boundary of the elements. If a free edge is found in the middle of a mesh, it usually indicates an unzipped mesh or an incompatible boundary.

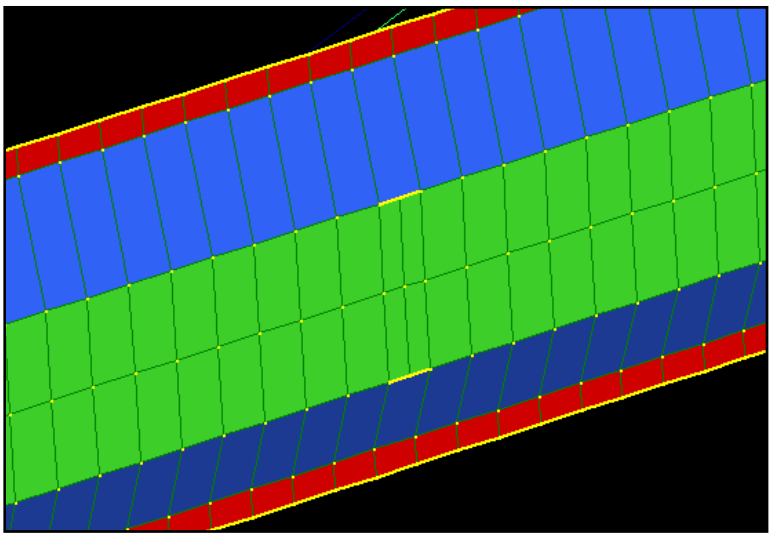

Fig. 69 - Free edges

6.3.2 Orientation

The plate orientation option is used to visually check for consistent normals on plate elements. The local z axis on a plate is defined by the node numbering order so it is important to number plates in a consistent manner, especially on 3D plate and shell models.

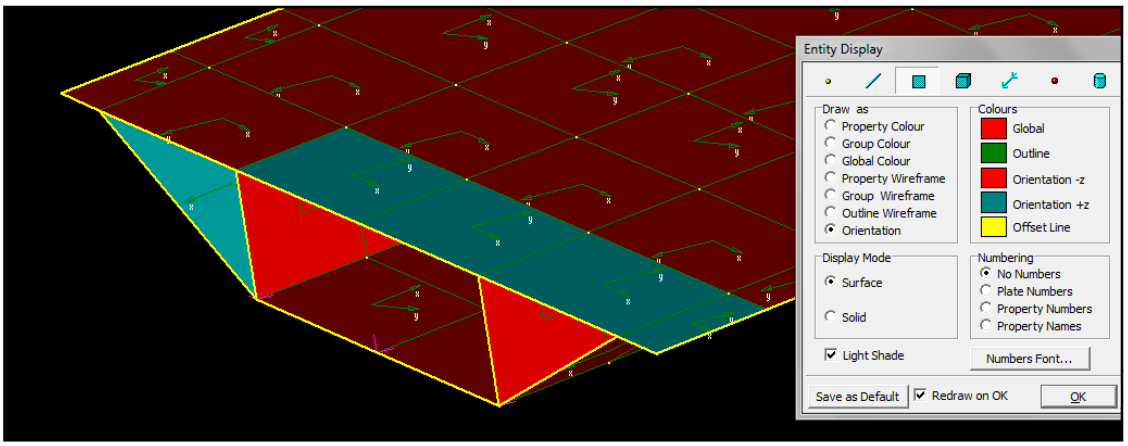

Fig. 70 - Different orientations of the plates

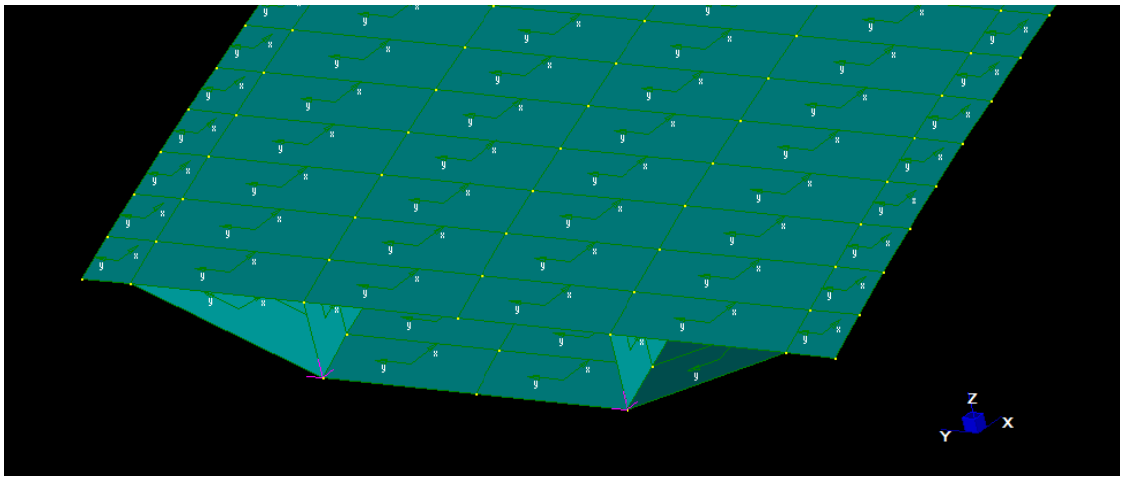

Fig. 71 - Common orientation of the plates

6.3.3 Element aspect ratio

The aspect ratio of a plate is the ratio between its longest edge length and its shortest edge length. Finite elements perform best when their aspect ratio is one. A square element has an aspect ratio of 1 while a rectangular element has an aspect ratio greater than 1 as shown in the following figure.

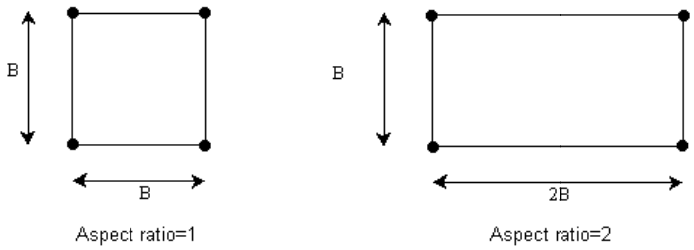

Fig. 72 - Aspect ratios for a square and a rectangle

The QUAD4 element can tolerate aspect ratios up to 4 in most situations however this is dependent on the state of stress. If the element is in an area of high stress gradient, then an aspect ratio closer to 1 is desirable.

One of the problems with high aspect ratio elements, when used in areas of stress concentration, is that they will produce inaccurate results due to the extrapolation of the Gauss point stresses to the corner nodes. On high aspect ratio elements, the extrapolation must be carried out over a longer distance and this combined with a rapidly changing stress field means that the element may not capture the real stress field.

Particularly useful is the contour Aspect (Min/Max) since this allows easy identification of collapsed elements. A collapsed element will generate a zero value.

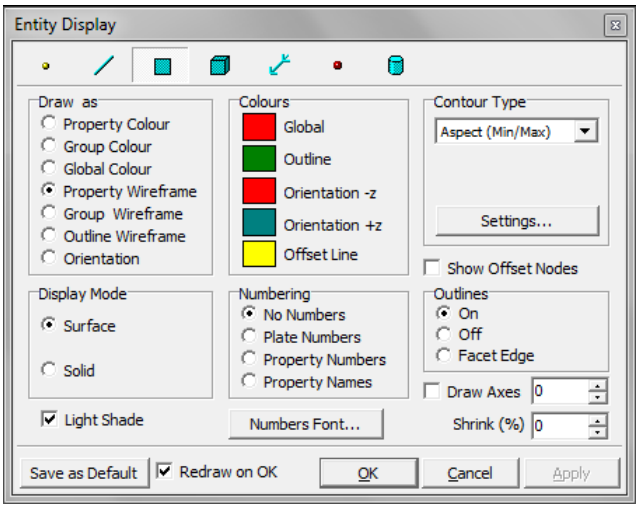

Fig. 73 - Contour type

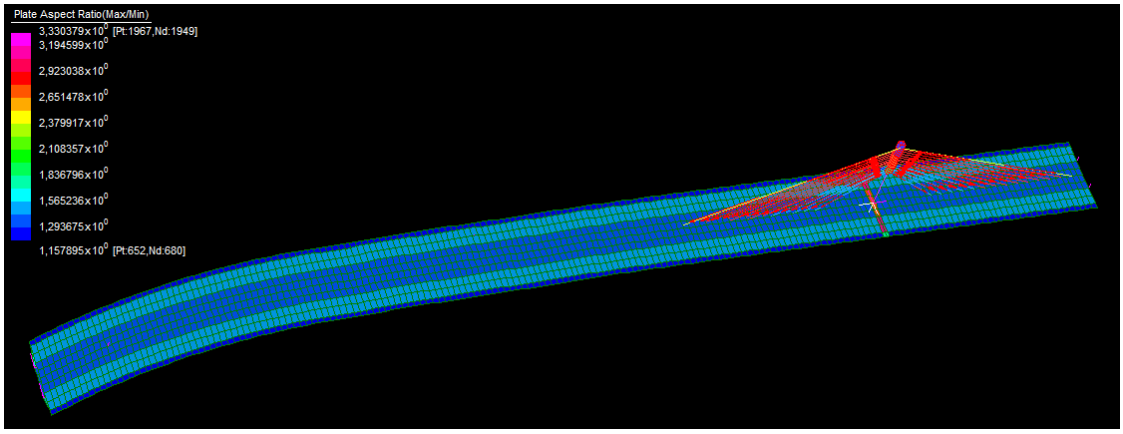

Fig. 74 - Element aspect ratio

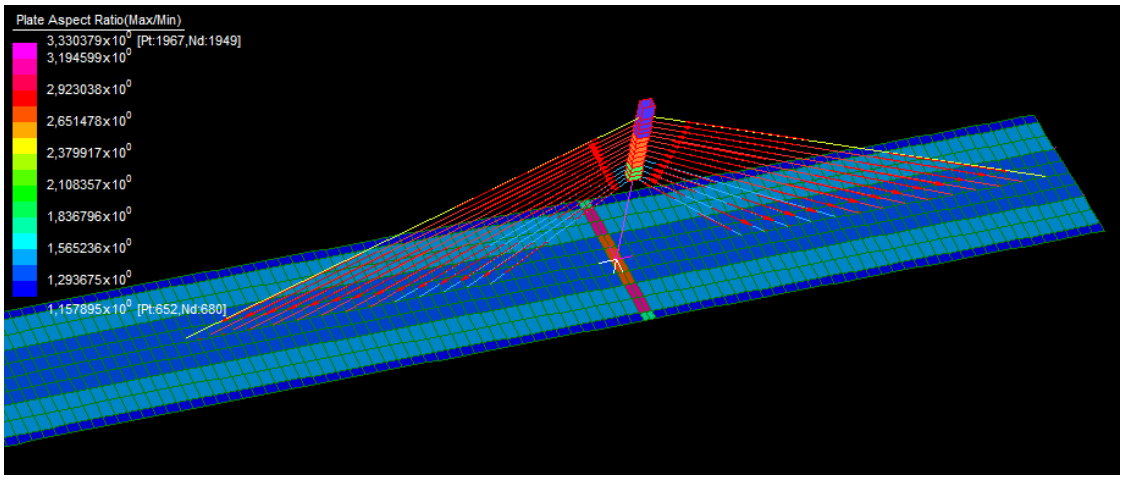

Fig. 75 - Element aspect ratio's detail

6.3.4 Plate warping ratio

When modeling shells with 4 node quadrilateral elements, all four nodes on the element should lie on the same plane. For irregular meshes on these surfaces or any mesh on a more general compound curved shell, it is unlikely that all four nodes will lie on the same plane. In this case the element is called warped.

Considering that any three nodes can uniquely define a plane, the element is warped when the forth node does not lie on the plane defined by the other three nodes.

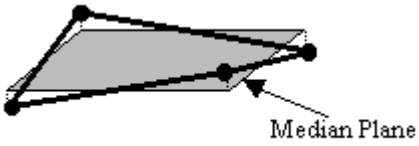

Fig. 76 - Warped plate element

The warping ratio is defined as the ratio of the maximum normal distance between the nodes and an average plane through the nodes. A warping ratio of zero is desirable although the elements in the Strand7 library can tolerate some warping.

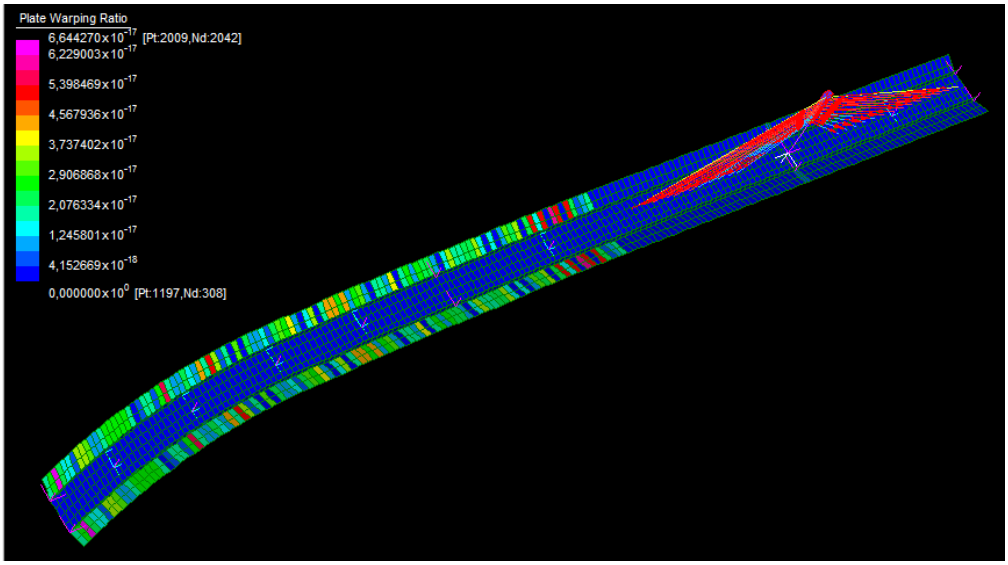

Fig. 77 - Plate warping ratio

In the curve part of the bridge the warping ration is a little bit higher because of the inherent definition.

7. COMPARISON OF THE THREE MODELS

In the following table the characteristics of mass and inertia of the three models are reported.

	Mass (T)	Ixx (mm^4)	Iyy (mm^4)	Izz (mm^4)
Beams model	2,121733E+04	1,124167E+17	1,090874E+17	2,215039E+17
Beams masses model	3,063706E+04	1,623035E+17	1,581592E+17	3,204625E+17
Plates model	2,860814E+00	1,515476E+17	1,477271E+17	2,992745E+17

Tab. 16 - Properties of the models

The simple beam model without the slab cannot always guarantee adequate bridge properties for lateral and torsional vibration.

A comparative study clearly shows that the concrete slab will significantly influence the nature of vibration in bridge transverse and torsional modes. It is verified that the simple beam element model results in the distortion of the transverse and torsional vibration modes of the bridge deck. The concrete slab has a smaller effect on the vertical bending modes of the bridge deck. To represent the bridge dynamic behavior well, a full three dimensional finite element model is essential that uses several types of elements representing different components of cable-stayed bridges. As a baseline finite element model, however, the concrete slab must be included in the model.

The plates model describes better the behavior of the bridge in terms of displacements, forces, stresses than the other two models. In the other way it is more difficult to study, identify and select clearly the distribution of forces and moments because you can only obtain stress values from a plate element.

There is always a trade-off of performance vs accuracy when using plates. The more you use, the better (generally). But the more you use, the slower the analysis, the longer your reports, and the more time it can take to manipulate and check your models.

Plates can report moment and shear forces for out of plane bending, and normal or shear stresses for in-plane activity.

Plate forces and moments are reported per unit length of plate, moments have units of force*length/length and shears have units of force/length. Plate membrane stresses may also be output relative to the global or local axis.

Chapter III

ANALYSIS

1. STATIC ANALYSIS

The cable-stayed bridge has to be analyzed for its dead-load static response and to pretension values of the cables.

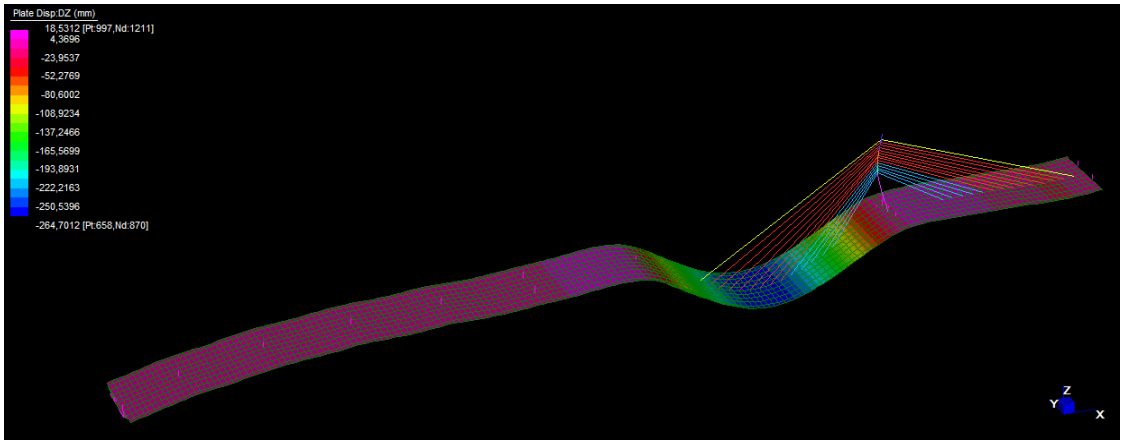

Fig. 78 - Static analysis displacements, self weight

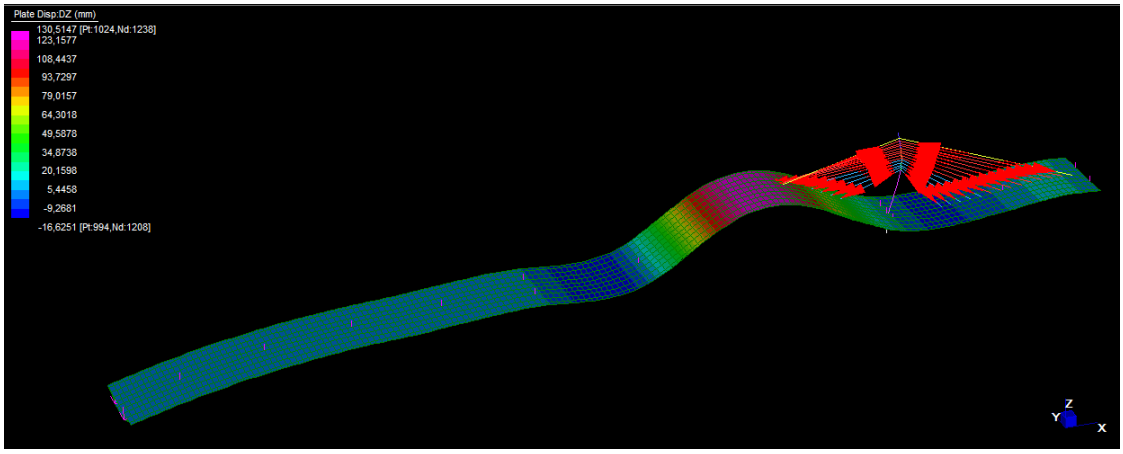

Fig. 79 - Static analysis displacements, cables pretension

The two different loads are combined in a linear load case combination with unitary coefficients.

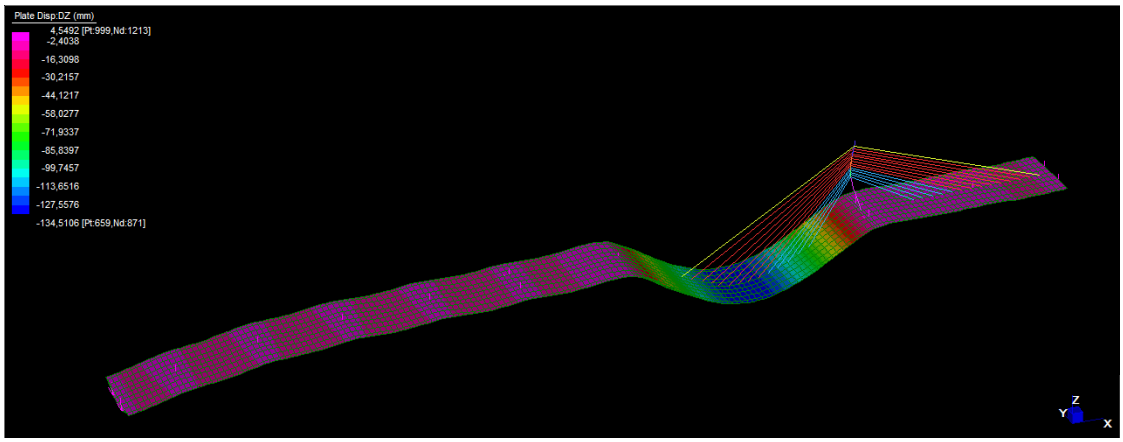

Fig. 80 - Static analysis displacements, linear load combination

In the SLU study, the pretension of the cables has the coefficient equal to $\gamma_P = 1$; at the self weight of the bridge is applied the coefficient $\gamma_{G1} = 1.3$ in the structural combination A1 of the NTC 2008.

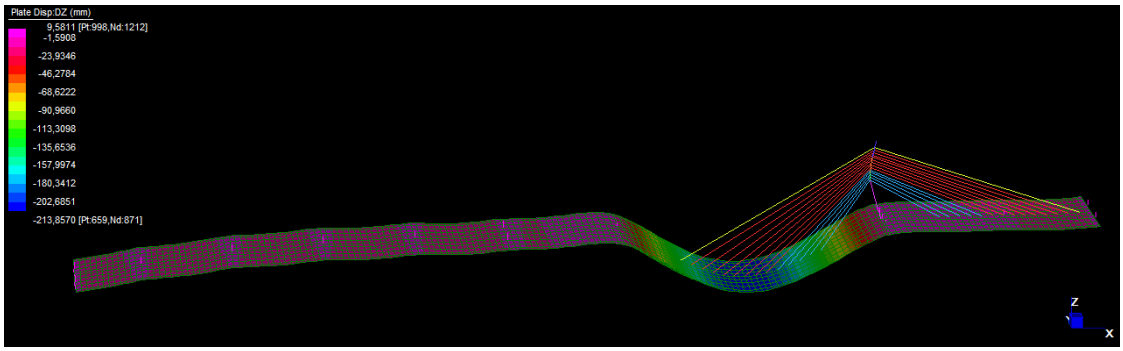

Fig. 81 - Static analysis displacements, SLU combination

The displacements are studied in the central points of the deck along the longitudinal dimension, see the figure below.

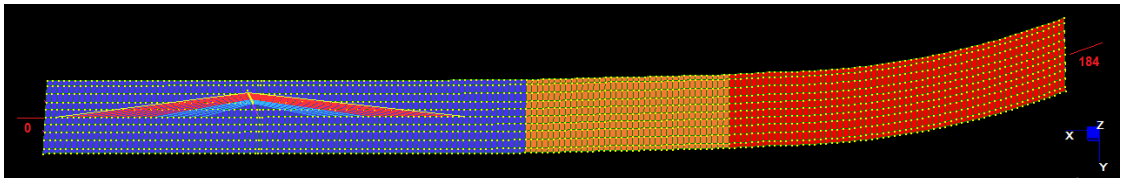

Fig. 82 - Central points of the deck

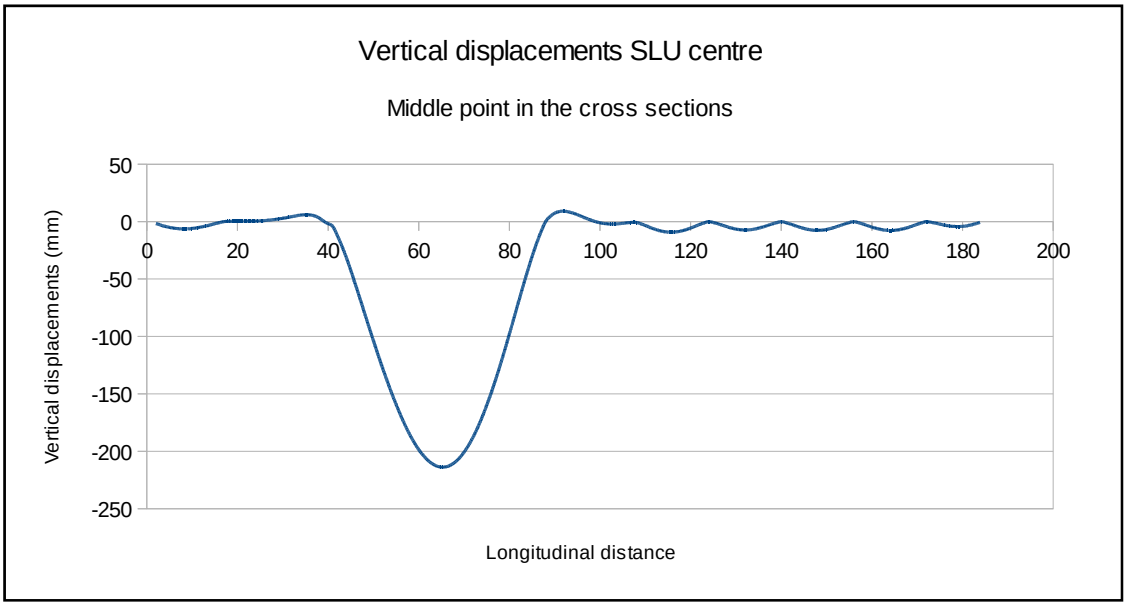

Fig. 83 - Vertical displacements SLU, centre of the deck

In the following picture some cross sections are highlighted, these are taken in consideration to evaluate the displacements along each section.

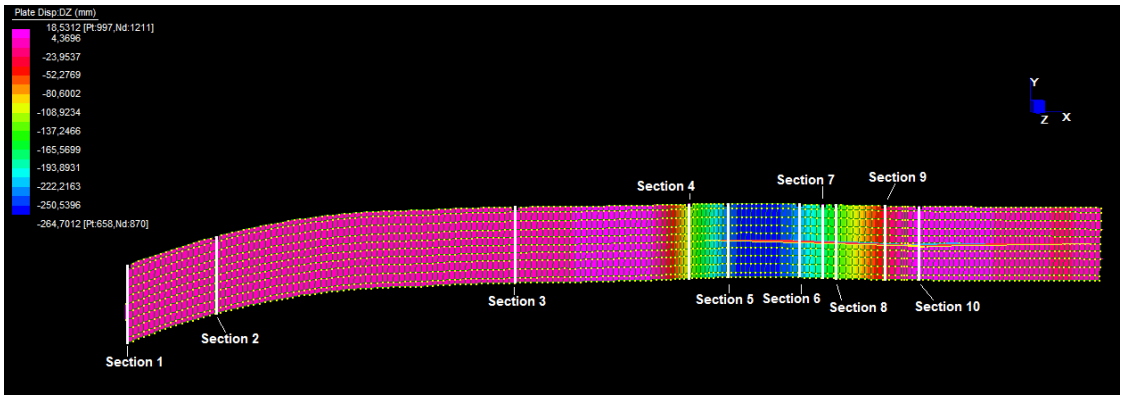

Fig. 84 - Cross sections along the slab

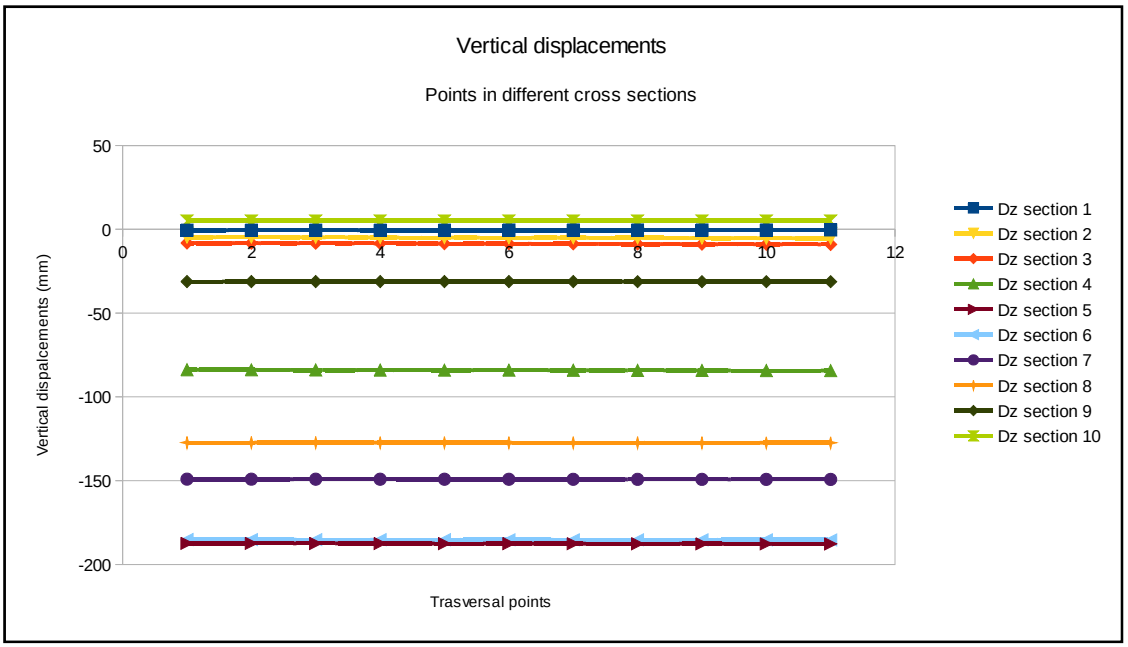

Fig. 85 - Vertical displacements in the cross sections

The displacements of the pylon are also taken into consideration; in the following figures the components and the resultant are reported.

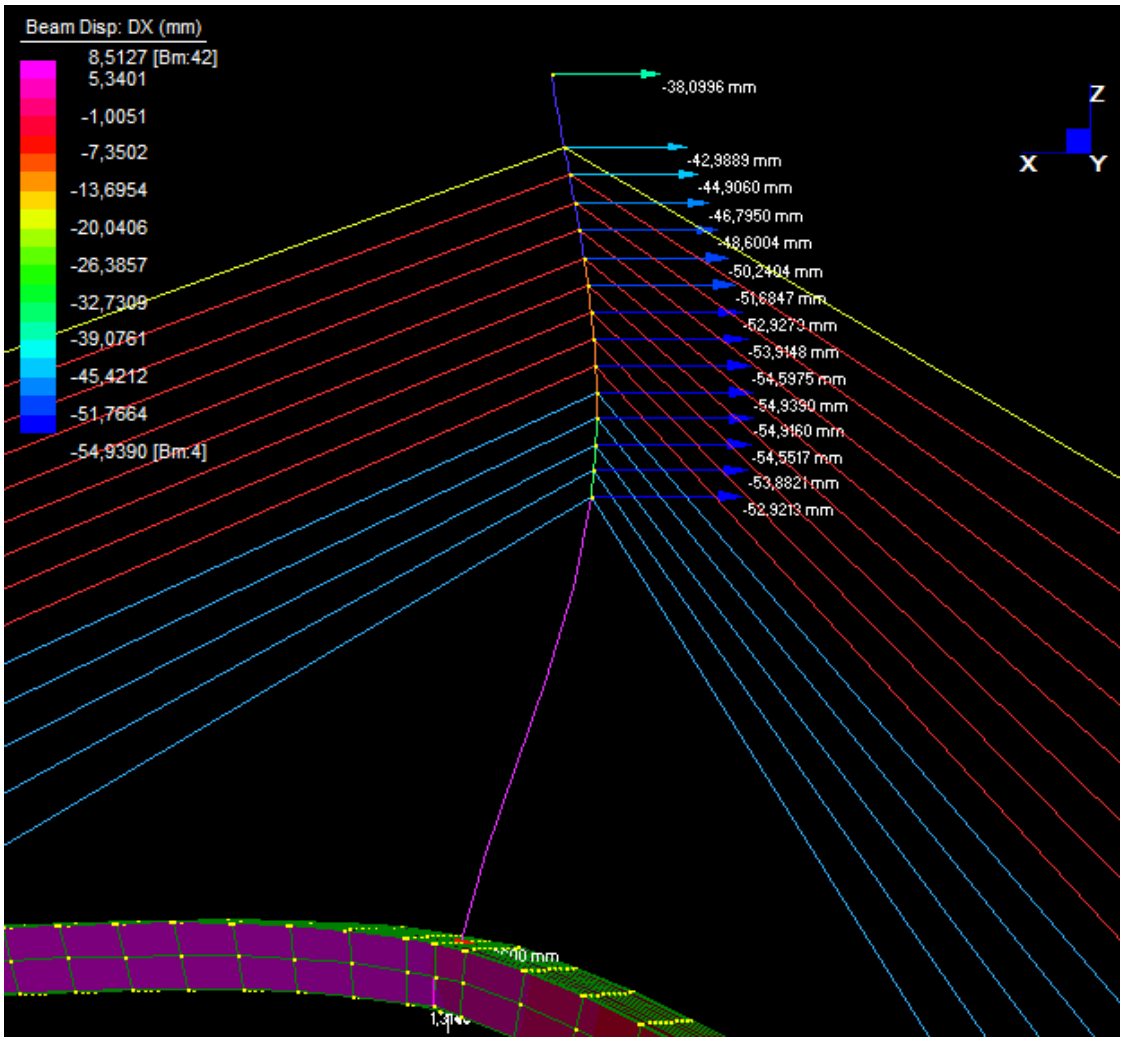

Fig. 86 - Vectors Dx of the pylon, SLU static

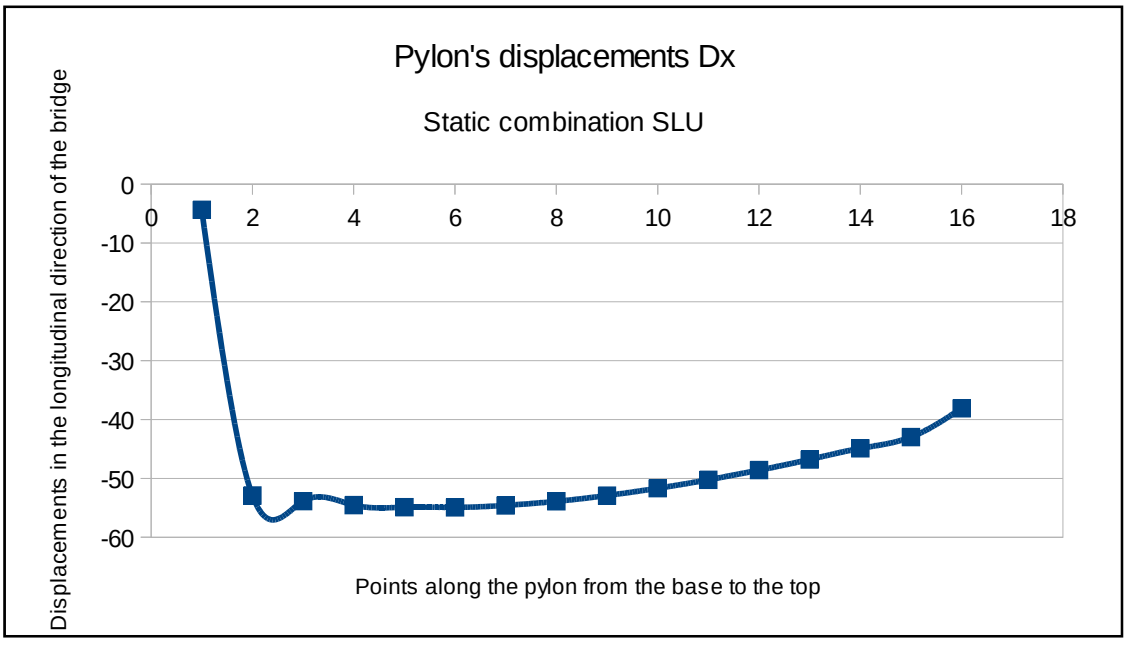

Fig. 87 - Pylon's displacements Dx, SLU static

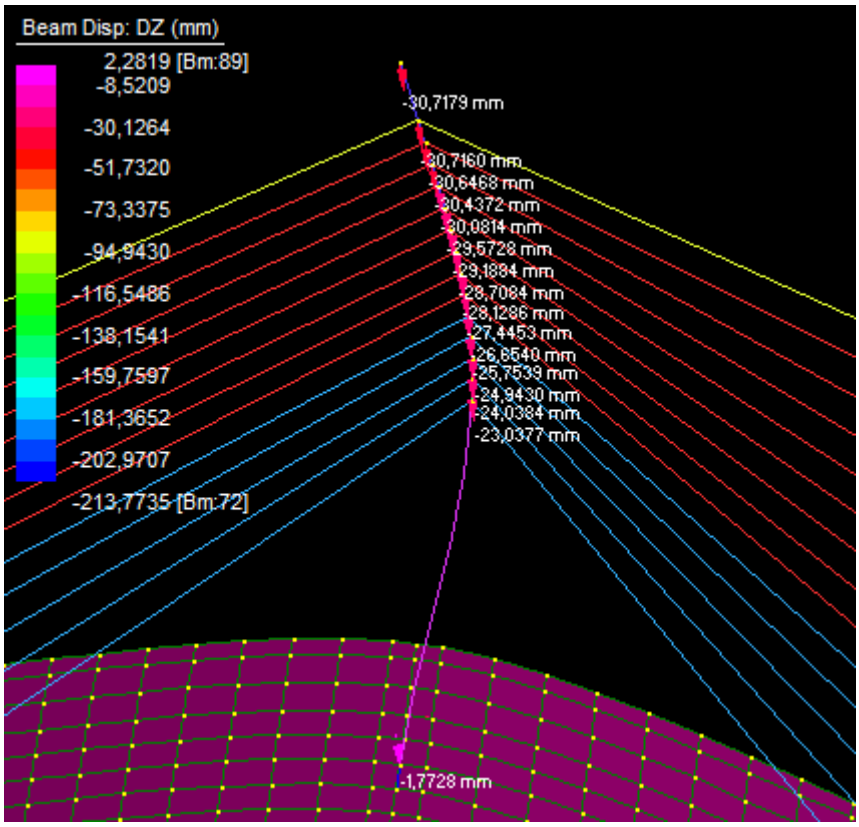

Fig. 88 - Vectors Dz of the pylon, SLU static

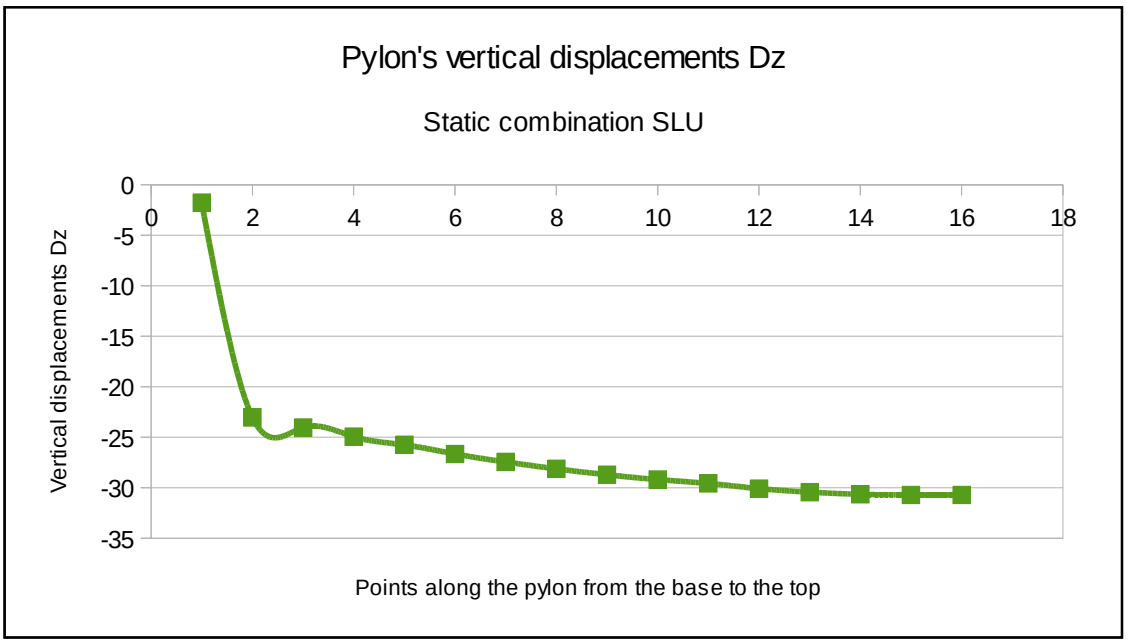

Fig. 89 - Pylon's vertical displacements Dz, SLU static

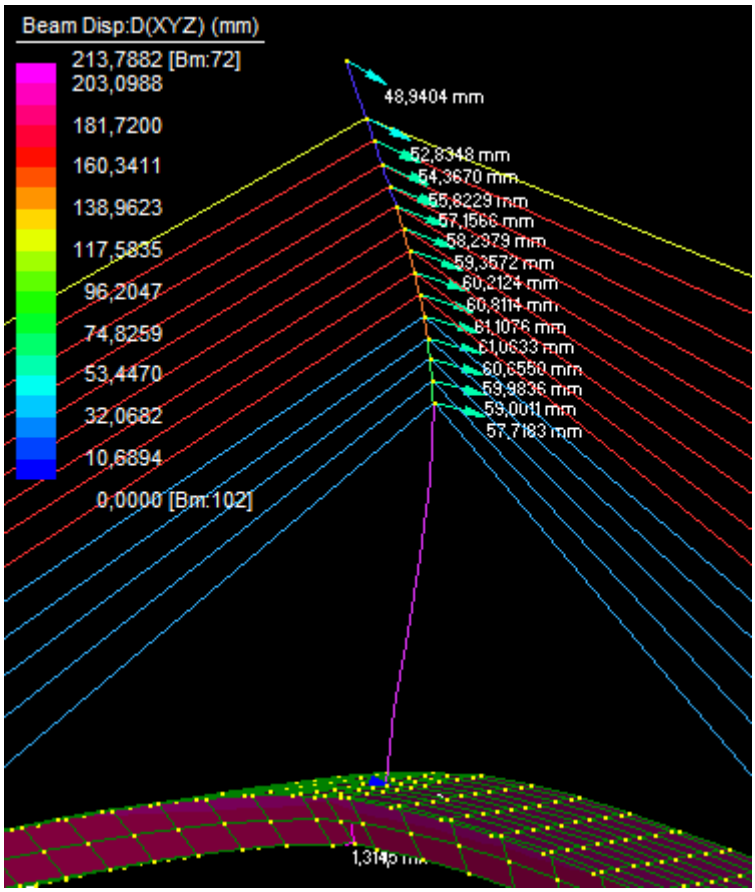

Fig. 90 - Vectors D(xyz) of the pylon SLU static

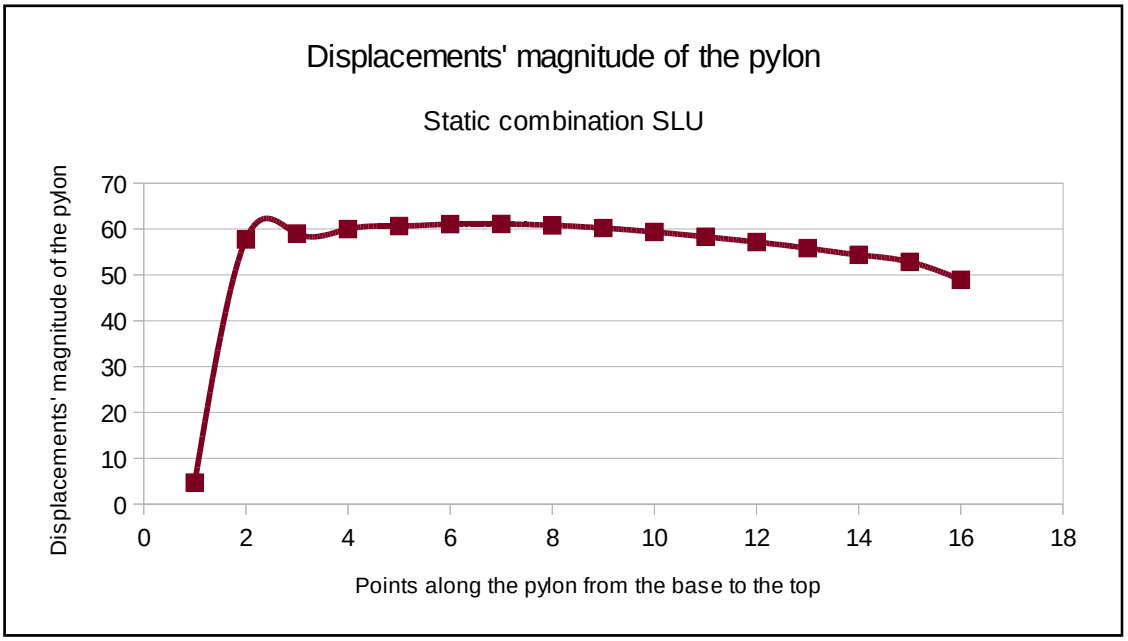

Fig. 91 - Displacements' magnitude of the pylon, SLU static

2. NATURAL FREQUENCY ANALYSIS

An accurate analysis of the natural frequencies and mode shapes of a cable-stayed bridge is fundamental to the solution of its dynamic responses due to seismic, wind and traffic loads.

Most bridges are designed using a static analysis, adjusted by a dynamic amplification factor which is a function of the first flexural frequency. This method is imprecise but continues to be used, partly because of the apparently complex processes required to estimate accurately and to provide for the levels of vibration in a bridge. While a single beam idealization is accurate for straight, nonskewed bridges and for some continuous superstructures, many other bridges require an eigenvalue analysis of a finite beam element grillage.

The Natural Frequency Solver is used to calculate the natural frequencies (or free vibration frequencies) and corresponding vibration modes of an undamped structure. The natural frequency analysis problem, is formulated as the following eigenvalue problem:

$$[K] * \{x\} = \omega^2 * [M] * \{x\}$$

Where: [K] Global stiffness matrix

[M] Global mass matrix

{*x*} Vibration mode vector

ω Circular frequency (radians/sec), natural frequency = $\omega/2\pi$ (Hertz)

The Natural Frequency Solver performs the following steps:

1. Calculates and assembles the element stiffness and mass matrices to form the global stiffness and mass matrices. In the stiffness calculation, material temperature dependency is considered through the user nominated temperature case. Either a consistent or lumped mass matrix can be used according to the solver option setting. The geometric stiffness matrix will be formed and assembled to the global stiffness matrix when an initial solution is applied. Constraints are assembled in this process. However, the constant terms for enforced displacements and shrink links are ignored.

   If the initial file is from a non linear solution, the stiffness and mass matrices calculation will be based on the current material status and geometry. More specifically, the current material modulus values will be used for nonlinear elastic material. For plastic material, the initial modulus is used.
2. The current geometry is used if geometric non linearity is considered in the initial solution.
3. Checks the mass matrix: if all diagonal entries are zero, the solution stops.

4. Modifies the stiffness matrix if a shift value is applied.
5. Solves the eigenvalue problem to get natural frequencies and the corresponding mode shapes using the Sub-Space Iteration Method.

Frequency shift can be used to calculate higher modes by excluding lower modes.
When the mode participation factors are requested, the engineering modal mass and engineering modal stiffness are also given.

2.1 Pre-stressed modal analysis

It is realized that the dead load has a significant influence on the stiffness of a cable-stayed bridge. In a finite element analysis, this influence can be taken into account through the static analysis under the dead load and cable tensions before the live load or succeeding dynamic analysis is carried out. The objective of the static analysis process is to achieve the initial deformed equilibrium configuration where the every structural member is ‘‘pre-stressed’’. Starting from the deformed equilibrium configuration, the modal analysis is followed.

The modal analysis is therefore a ‘‘prestressed modal analysis’’ that should include two key steps:

- the static analysis is first conducted to obtain the initial equilibrium configuration under dead load and cable pre-tensions;
- the modal analysis (free vibration) is then performed starting from the deformed equilibrium position.

Two types of modal analysis are carried out. Case 1 is the modal analysis with the pre-stresses effect, whereas Case 2 is the ordinary modal analysis without the pre-stresses.
The calculated natural frequencies are compared in the following tables for each models. All frequencies are increased in the pre-stressed modal analysis.
It is demonstrated that pre-stressed modal analysis might have a minimal effect on increasing the bridge natural frequencies. However, the starting position is essential to determine the responses in succeeding dynamic analysis under earthquakes, winds and vehicles.

2.2 Results from the three different models

- **Beams model**

In the following pictures are presented the 10 principal shapes of vibration.

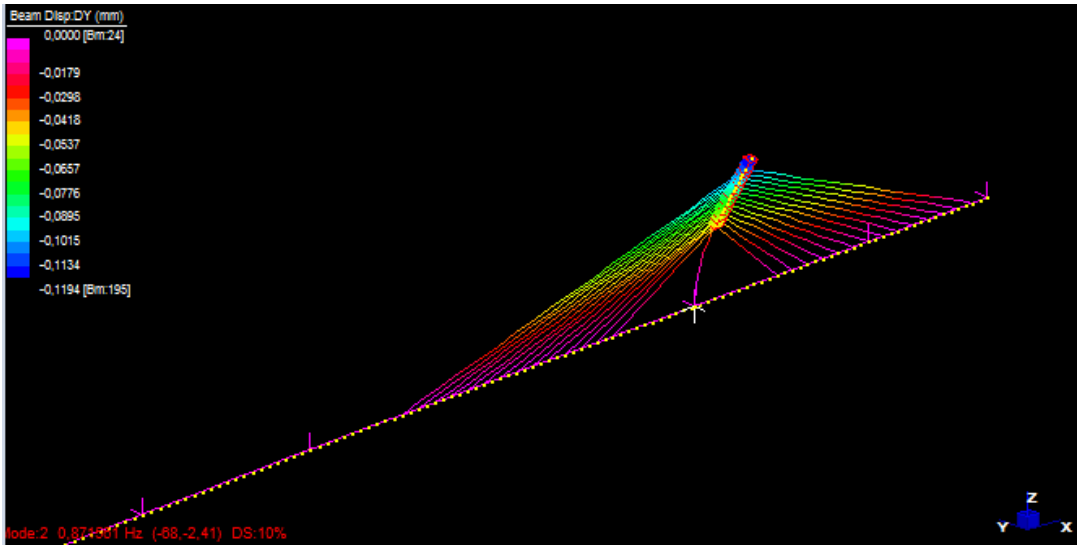

Fig. 92 - First natural mode (beams model)

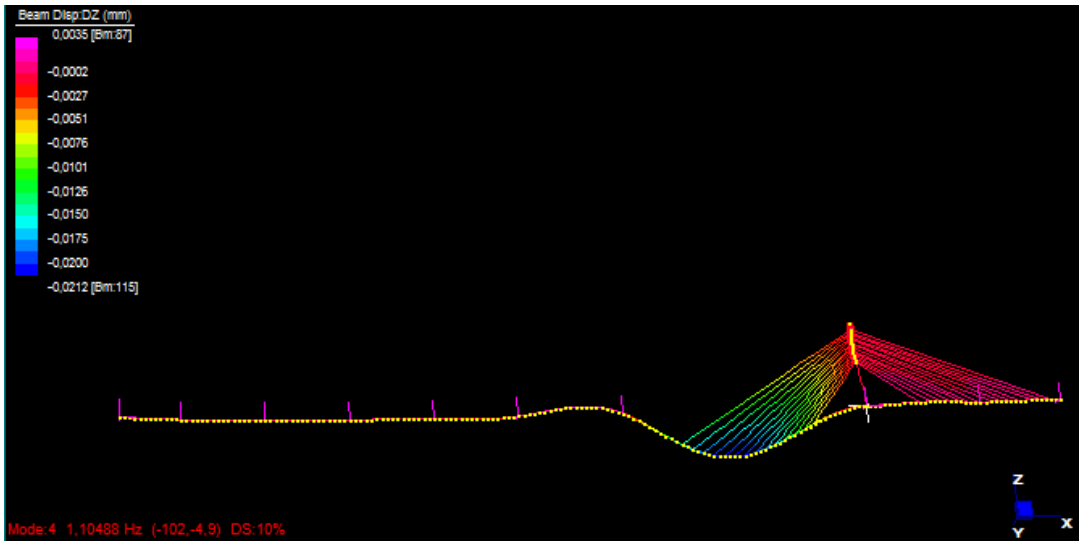

Fig. 93 - Second natural mode (beams model)

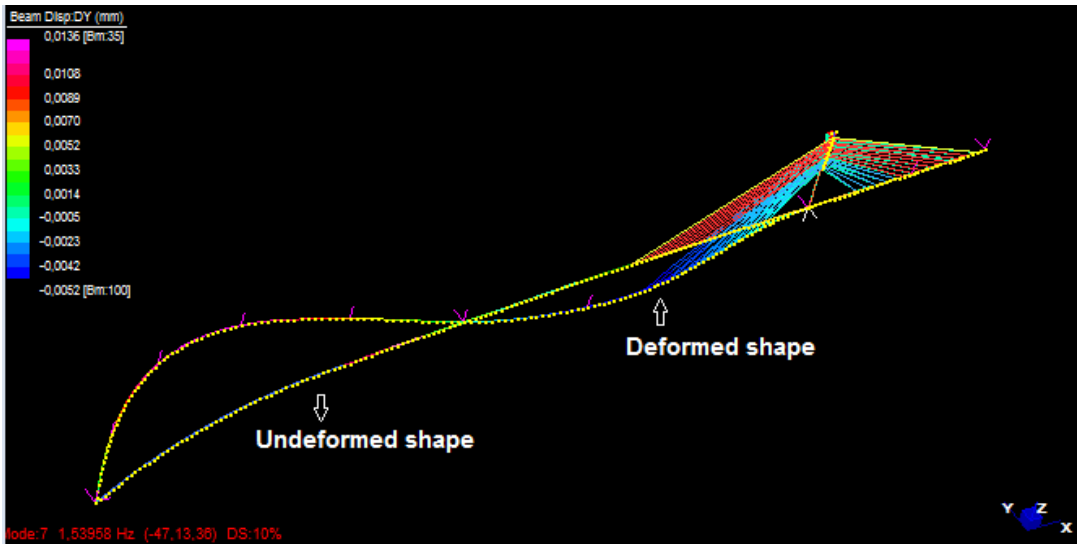

Fig. 94 - Third natural mode (beams model)

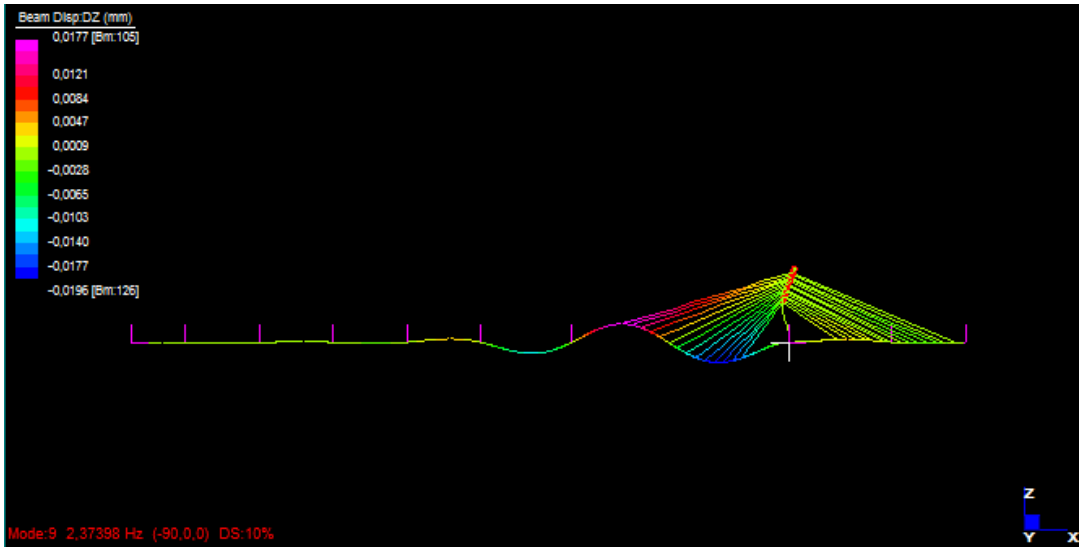

Fig. 95 - Forth natural mode (beams model)

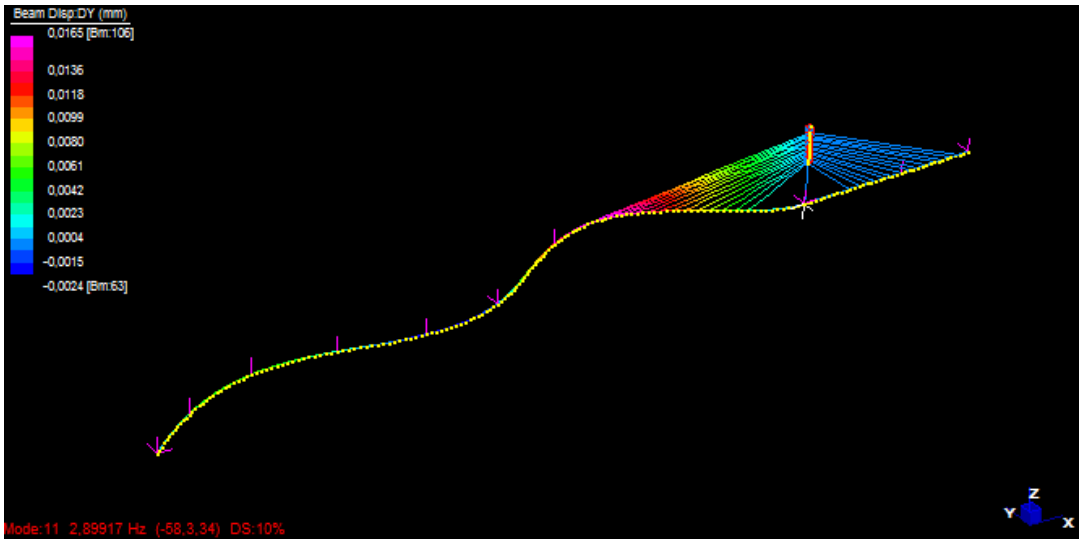

Fig. 96 - Fifth natural mode (beams model)

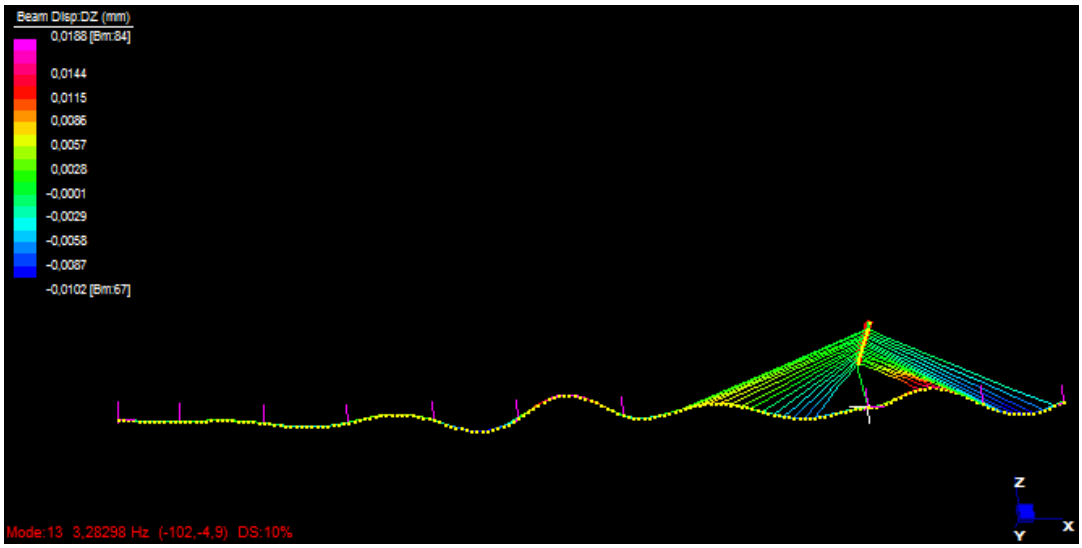

Fig. 97 - Sixth natural mode (beams model)

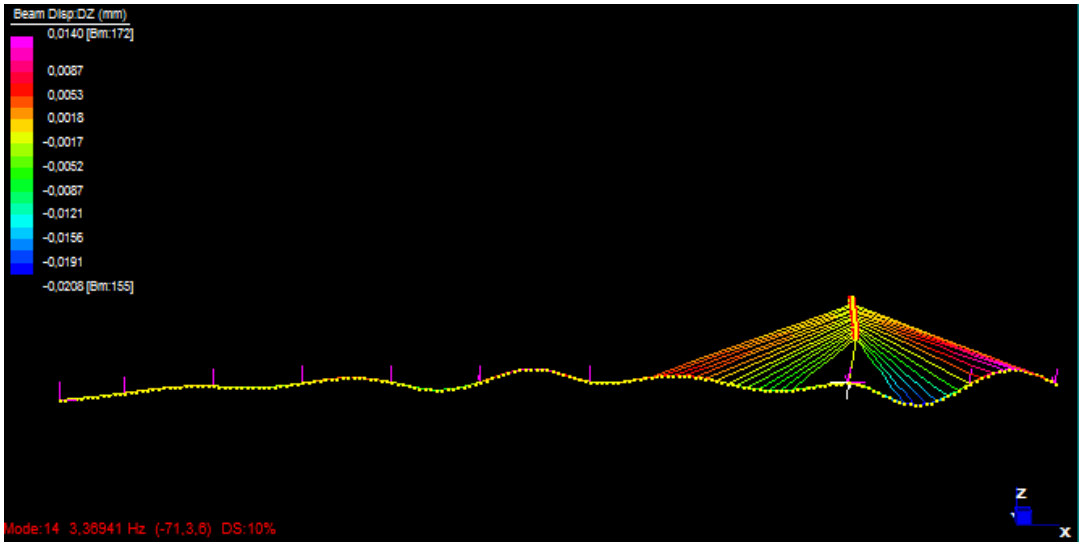

Fig. 98 - Seventh natural mode (beams model)

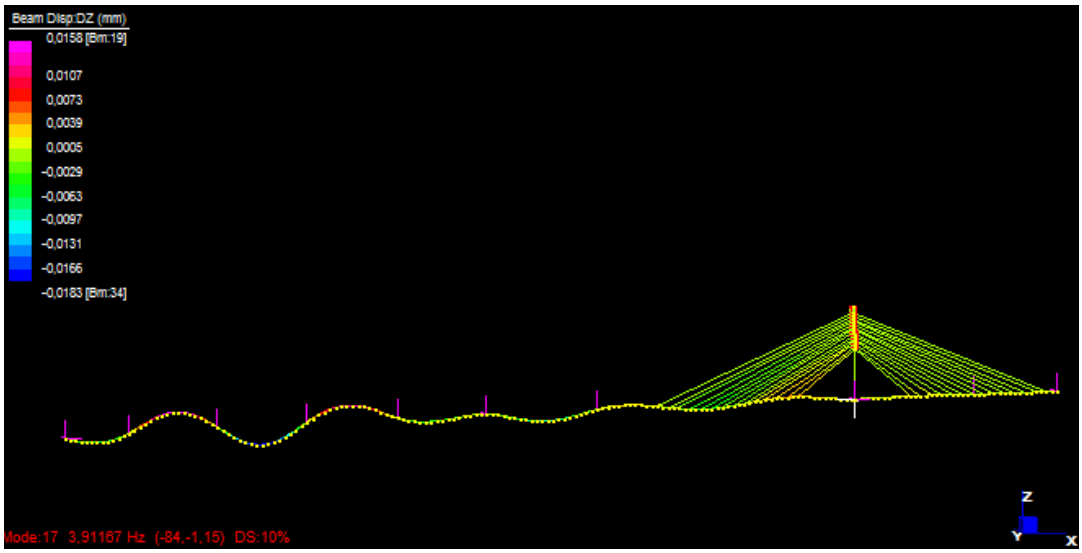

Fig. 99 - Eighth natural mode (beams model)

Beams model			
Mode	**No initial condition**	**Initial condition**	**Vibration's shapes**
1	8,716E-01	8,291E-01	Pylon out
2	1,105E+00	1,105E+00	1 Vertical bending
3	1,540E+00	1,540E+00	Horizontal
4	2,380E+00	2,374E+00	2 Vertical bending
5	/	/	Torsion
6	/	/	Torsion
7	2,899E+00	2,899E+00	Horizontal
8	3,283E+00	3,278E+00	3 Vertical bending
9	3,369E+00	3,914E+00	4 Vertical bending
10	3,912E+00	4,677E+00	5 Vertical bending

Tab. 17 - Modes of vibration (beams model)

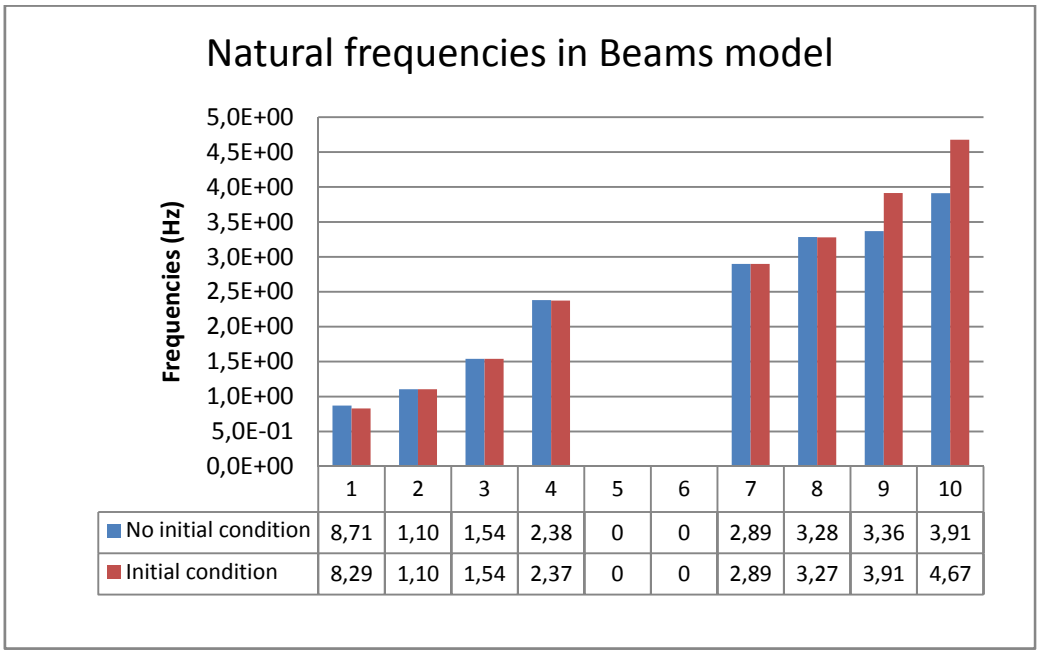

Fig. 100 - Comparison of natural frequencies (beams model)

- **Beam model with torsional degree of freedom**

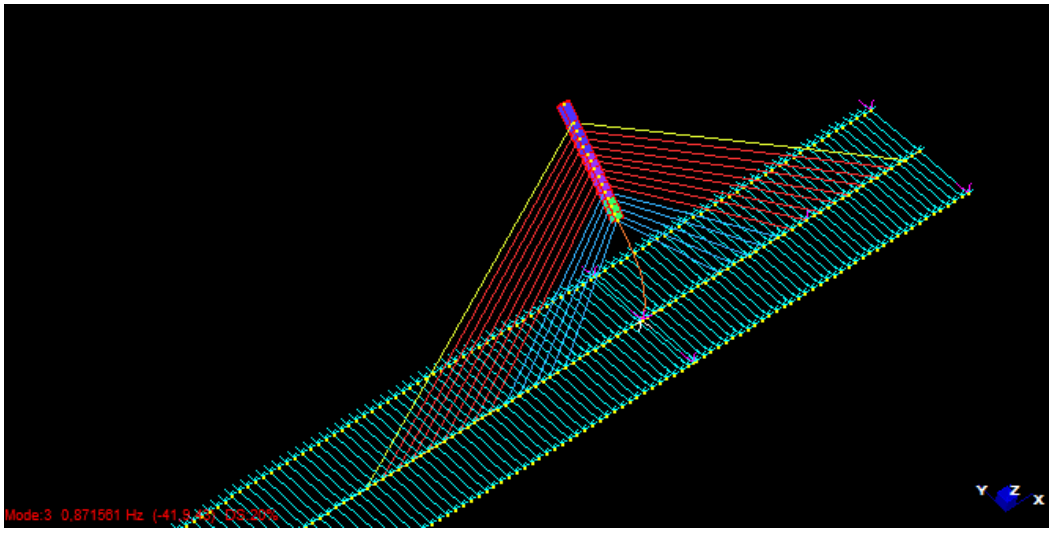

Fig. 101 - First natural mode (beams model with masses)

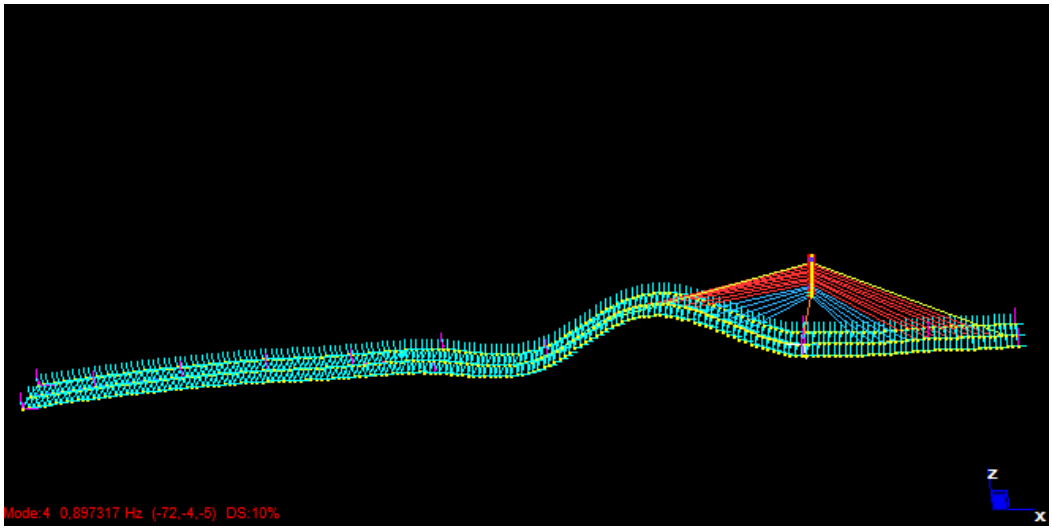

Fig. 102 - Second natural mode (beams model with masses)

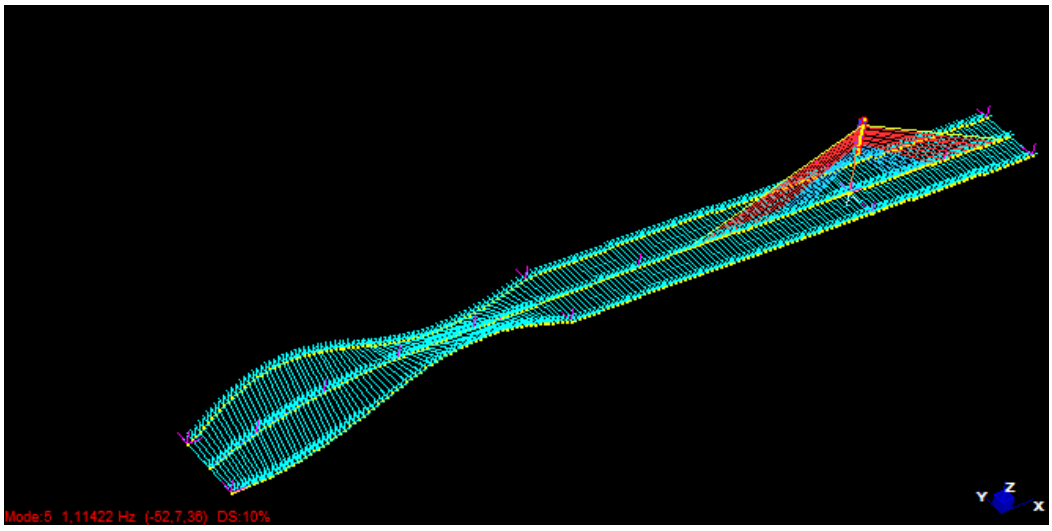

Fig. 103 - Third natural mode (beams model with masses)

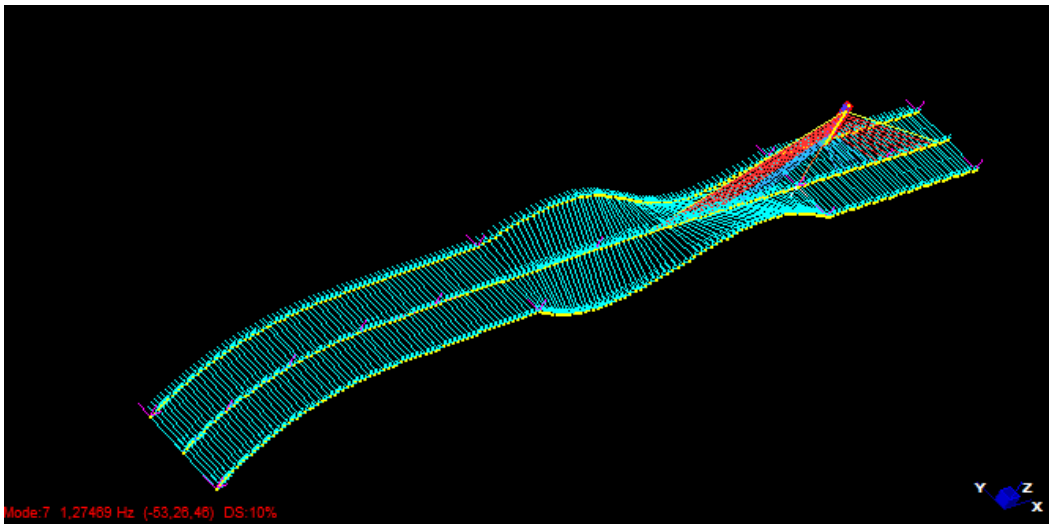

Fig. 104 - Forth natural mode (beams model with masses)

Fig. 105 - Fifth natural mode (beams model with masses)

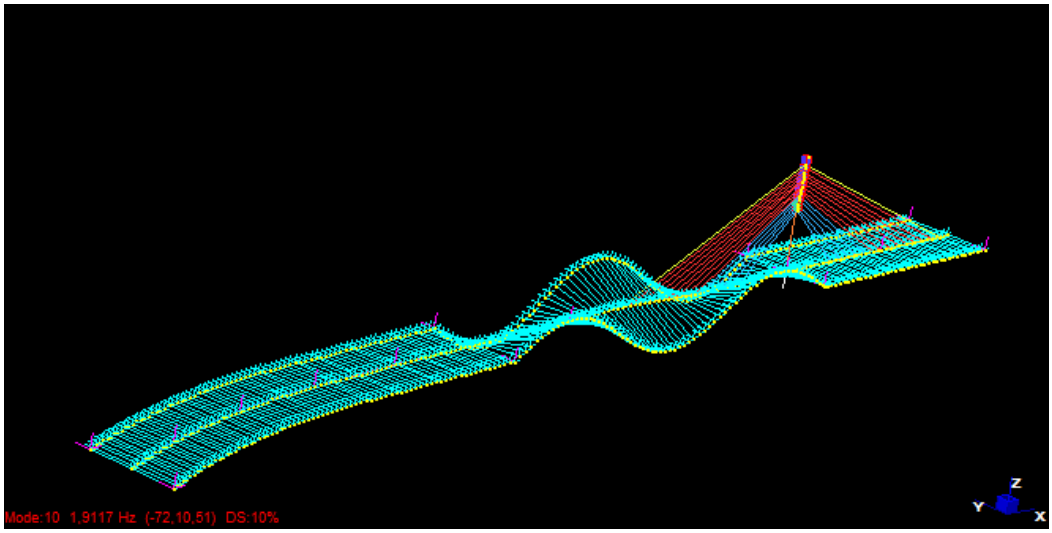

Fig. 106 - Sixth natural mode (beams model with masses)

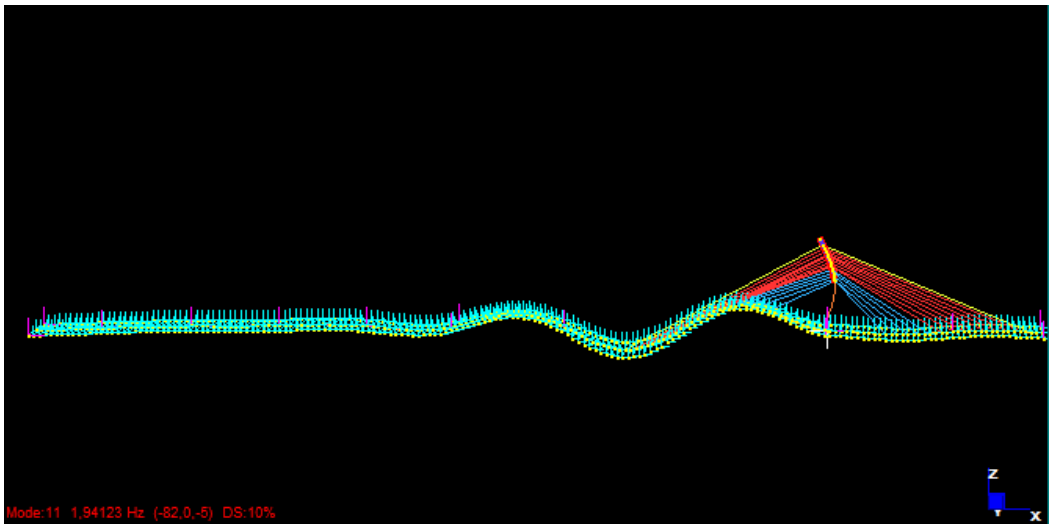

Fig. 107 - Seventh natural mode (beams model with masses)

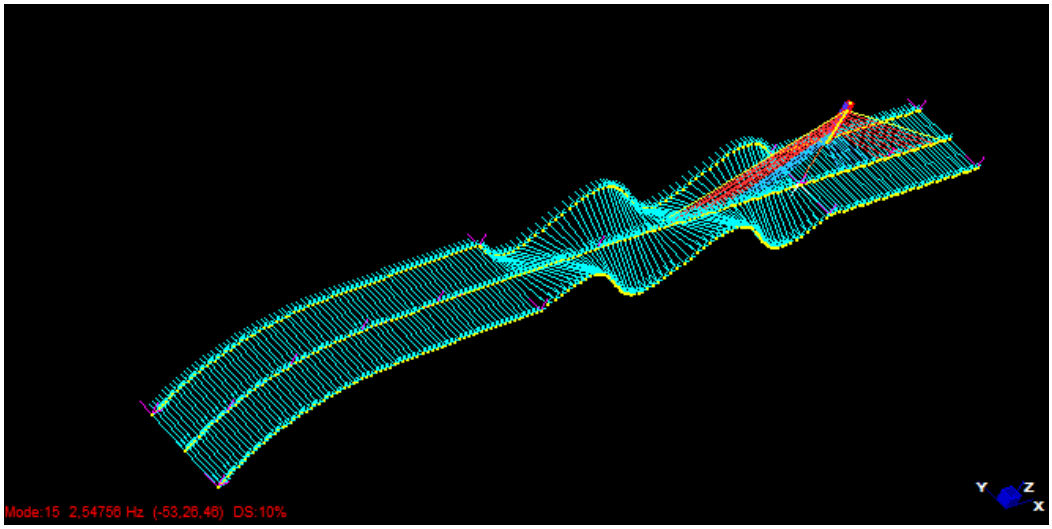

Fig. 108 - Eighth natural mode (beams model with masses)

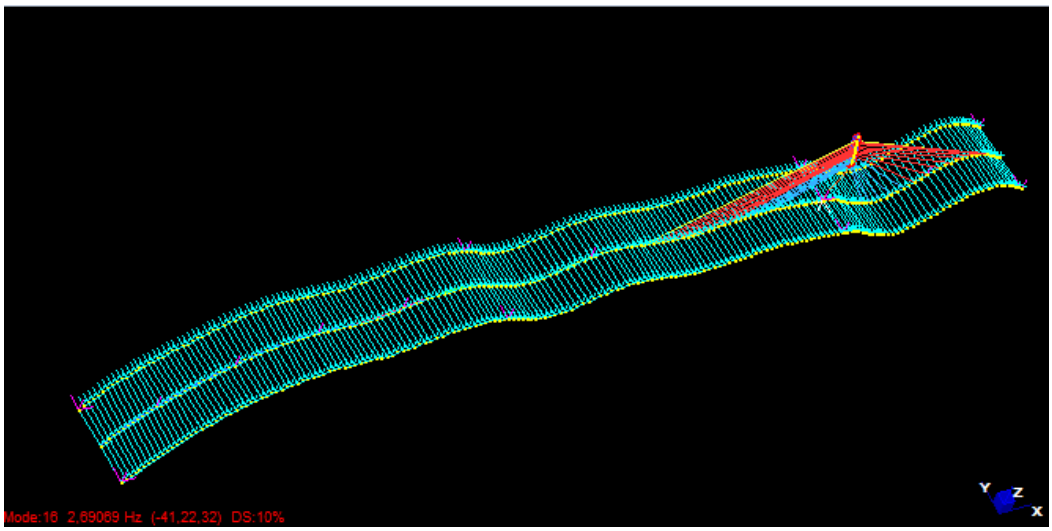

Fig. 109 - Ninth natural mode (beams model with masses)

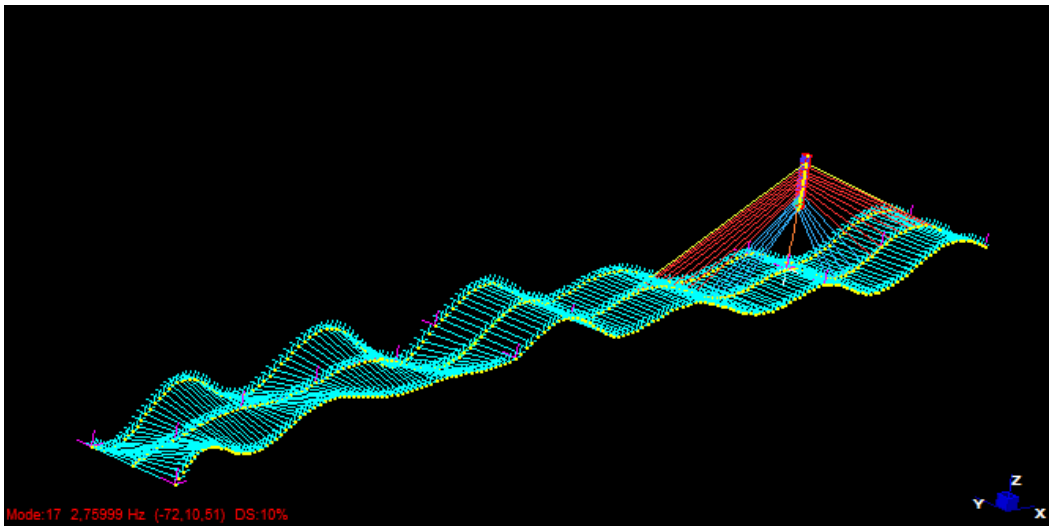

Fig. 110 - Tenth natural mode (beams model with masses)

Beam (mass added)			
Mode	**No initial condition**	**Initial condition**	**Vibration's shapes**
1	8,716E-01	8,229E-01	Pylon out
2	8,973E-01	8,966E-01	1 Vertical bending
3	1,114E+00	1,114E+00	Torsion
4	1,275E+00	1,275E+00	Torsion
5	1,685E+00	1,685E+00	Horizontal
6	1,912E+00	1,912E+00	Torsion
7	1,941E+00	1,936E+00	2 Vertical bending
8	2,497E+00	2,497E+00	Horizontal
9	2,691E+00	2,678E+00	3 Vertical bending
10	2,760E+00	2,757E+00	4 Vertical bending

Tab. 18 - Modes of vibration (beams model with masses)

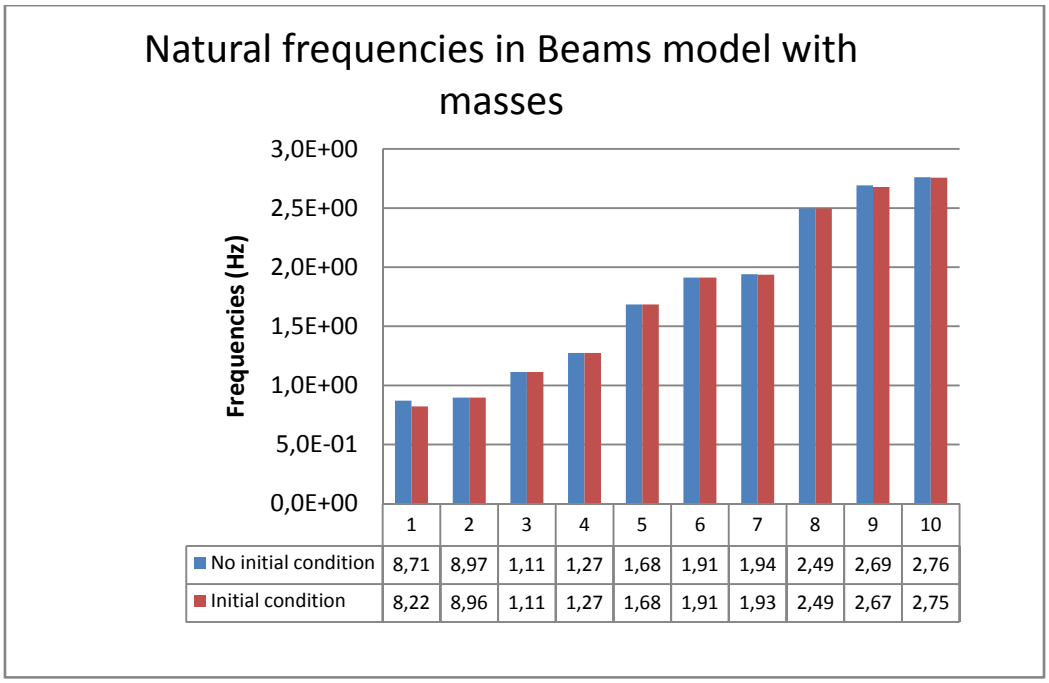

	1	2	3	4	5	6	7	8	9	10
No initial condition	8,71	8,97	1,11	1,27	1,68	1,91	1,94	2,49	2,69	2,76
Initial condition	8,22	8,96	1,11	1,27	1,68	1,91	1,93	2,49	2,67	2,75

Fig. 111 - Comparison of natural frequencies (beams model with masses)

- **Plates model**

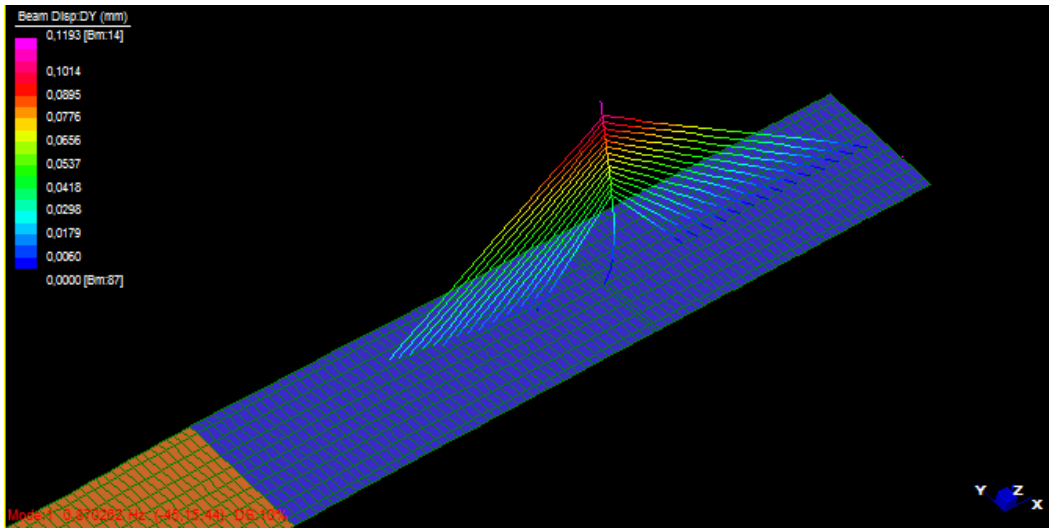

Fig. 112 - First natural mode (plates model)

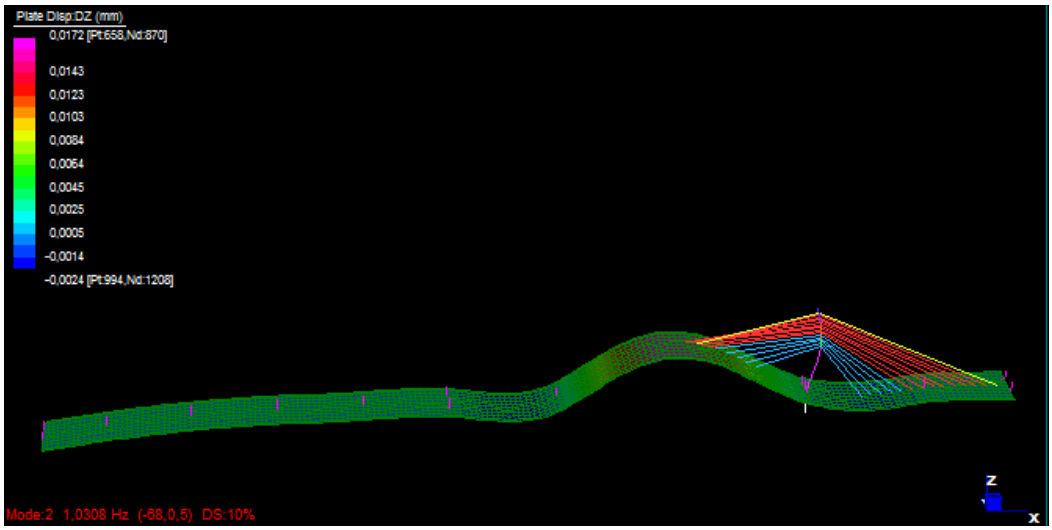

Fig. 113 - Second natural mode (plates model)

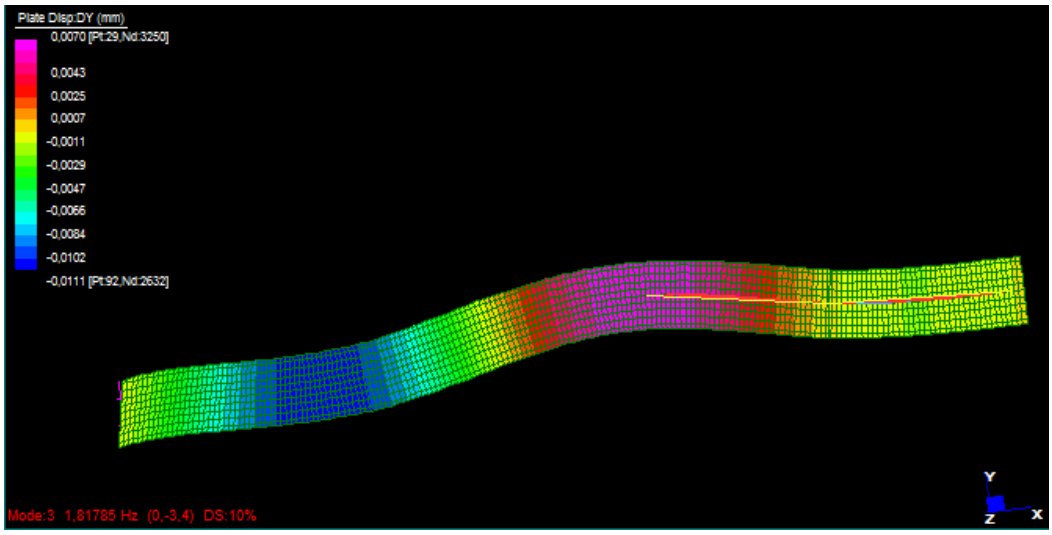

Fig. 114 - Third natural mode (plates model)

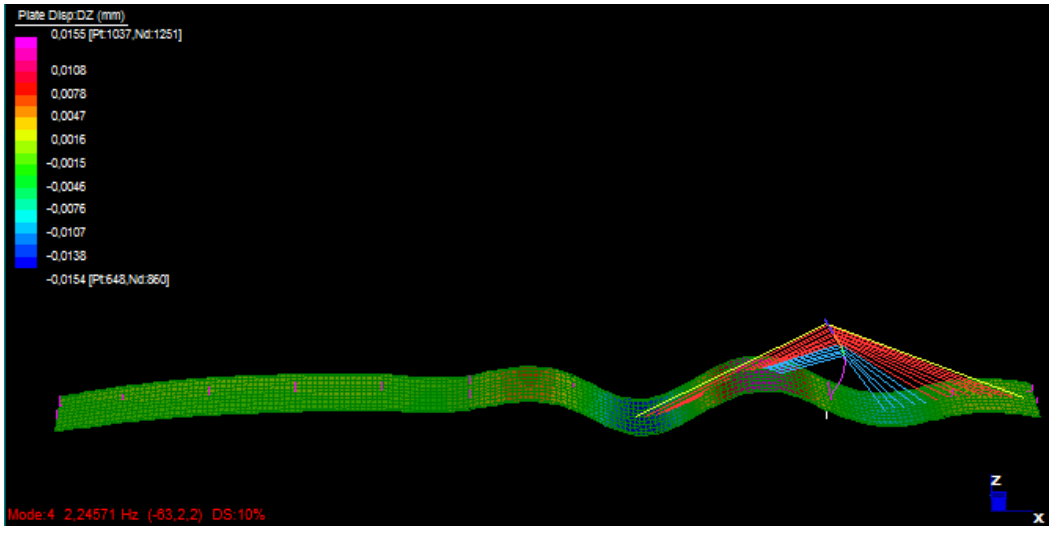

Fig. 115 - Forth natural mode (plates model)

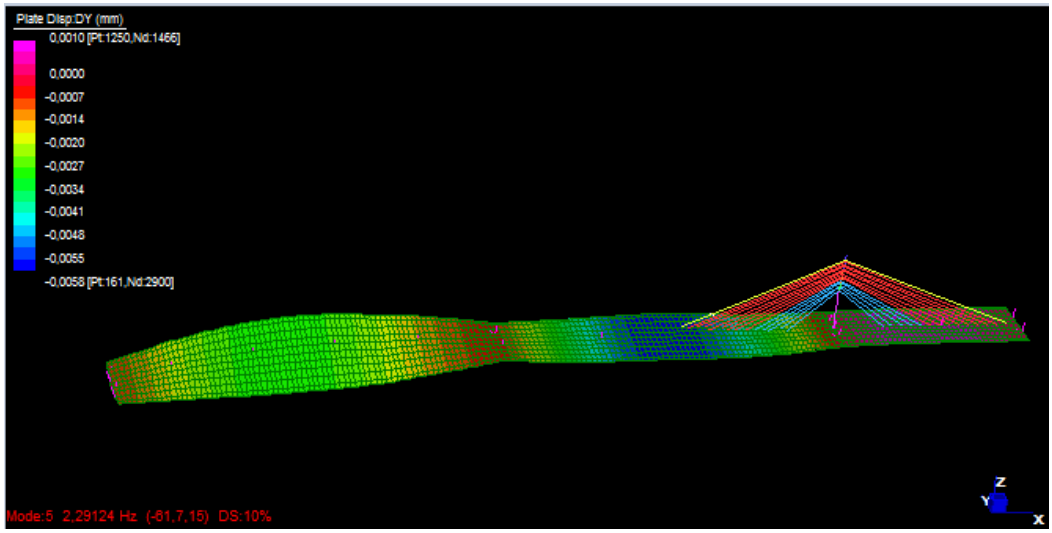

Fig. 116 - Fifth natural mode (plates model)

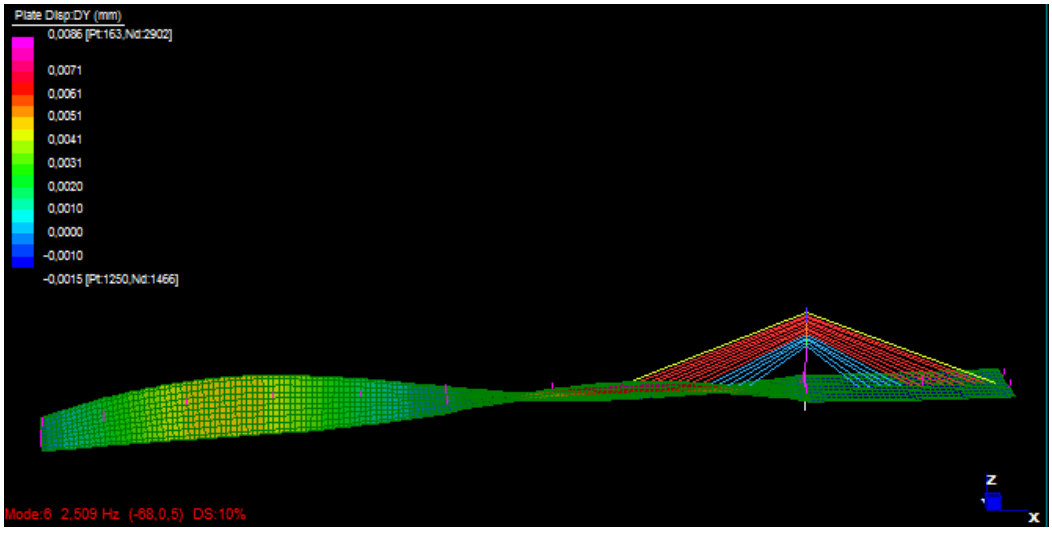

Fig. 117 - Sixth natural mode (plates model)

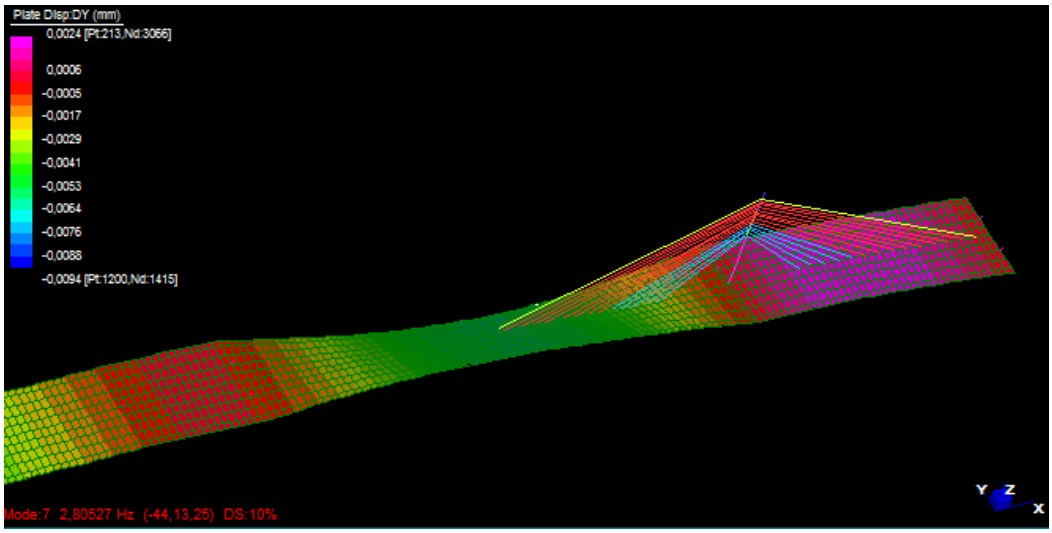

Fig. 118 - Seventh natural mode (plates model)

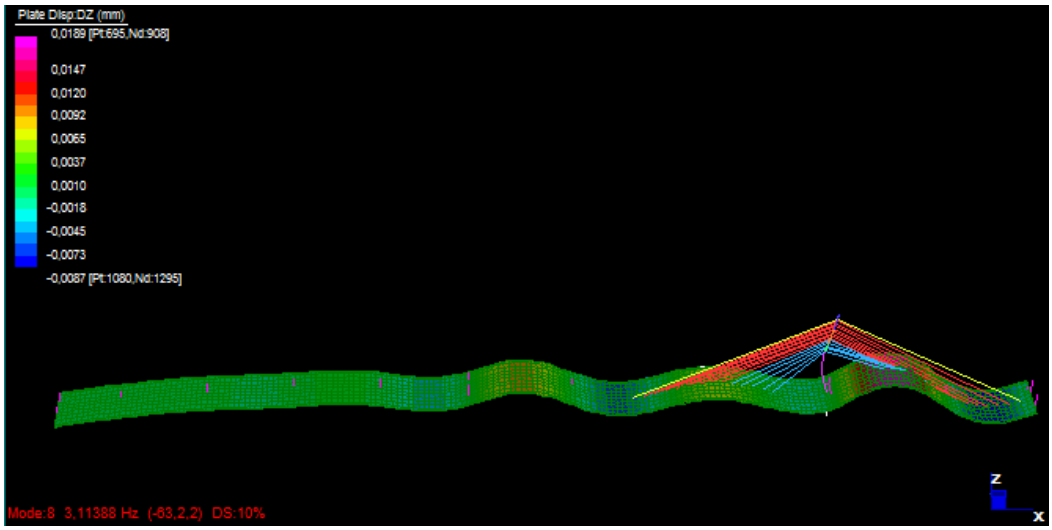

Fig. 119 - Eighth natural mode (plates model)

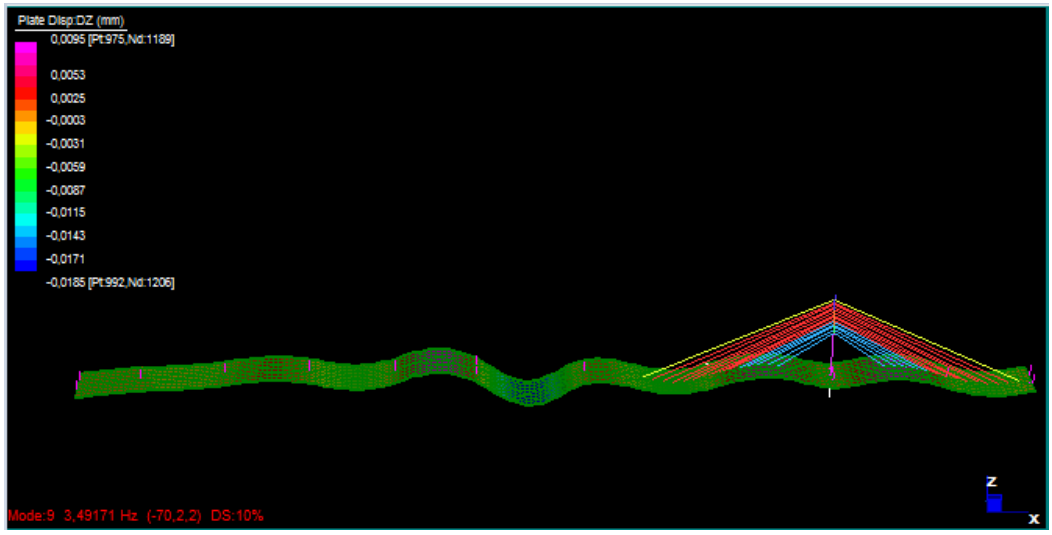

Fig. 120 - Ninth natural mode (plates model)

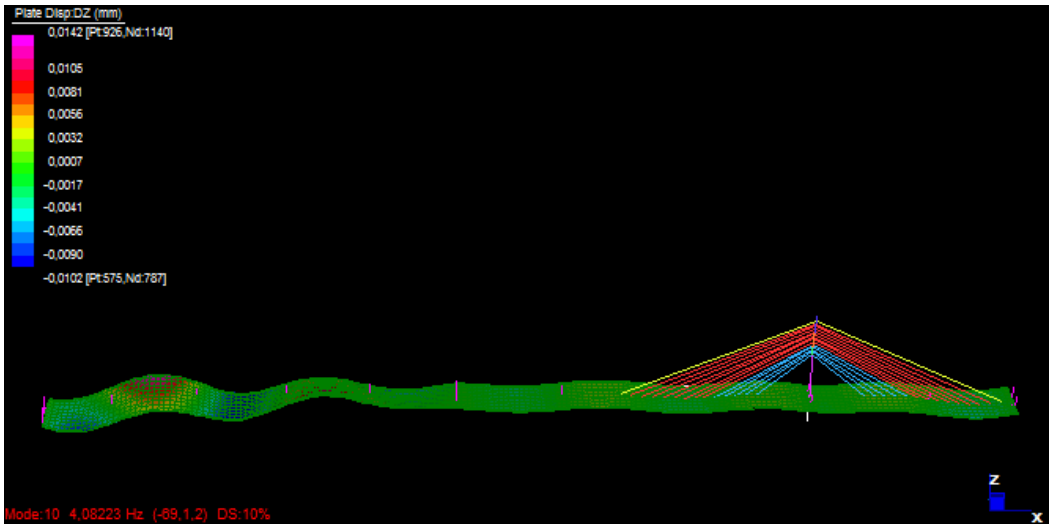

Fig. 121 - Tenth natural mode (plates model)

Plates model			
Mode	**No initial condition**	**Initial condition**	**Vibration's shapes**
1	8,703E-01	8,518E-01	Pylon out
2	1,031E+00	1,030E+00	1 Vertical bending
3	1,818E+00	1,818E+00	Horizontal
4	2,246E+00	2,241E+00	2 Vertical bending
5	2,291E+00	2,292E+00	Torsion
6	2,509E+00	2,509E+00	Torsion
7	2,805E+00	2,805E+00	Torsion
8	3,114E+00	3,109E+00	3 Vertical bending
9	3,492E+00	3,492E+00	4 Vertical bending
10	4,082E+00	4,083E+00	5 Vertical bending

Tab. 19 - Modes of vibration (plates model)

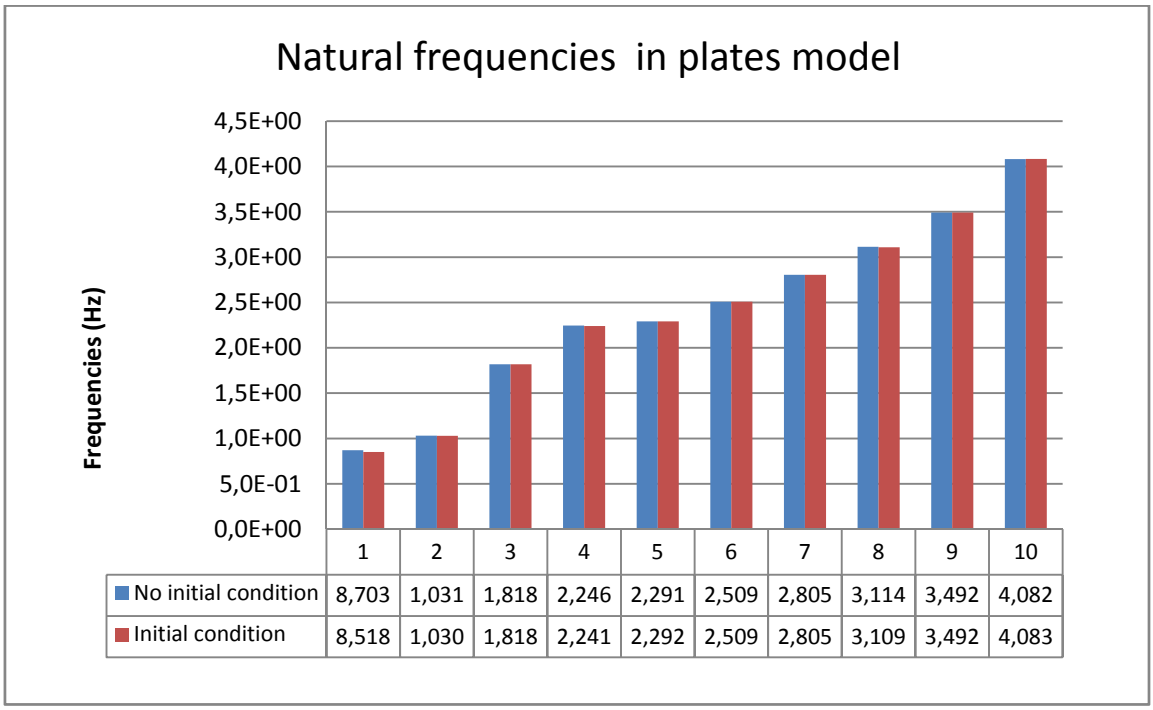

Fig. 122 - Comparison of natural frequencies (plates model)

2.3 Measured values of vibrations

Bridge maintenance consists of a combination of structural health monitoring and testing. This is regulated in country-specific engineer standards and includes an ongoing monitoring every three to six months, a simple test or inspection every two to three years and a major inspection every six to ten years. In Europe, the cost of maintenance is higher than spending on new bridges.

To evaluate the vibrations, it is possible to measure the displacement or its first and second derivatives, velocity and acceleration. The kind of parameter of evaluation depends on the frequency's range of the phenomenon.

Referring to a single harmonic wave and to any parameters, the shape and the period of the vibration remain the same, while the amplitude and the phase change. When the measures are averaged over time, the phase is not considered and the relations between the parameters are set only by the angular frequency $\omega = 2\pi f$.

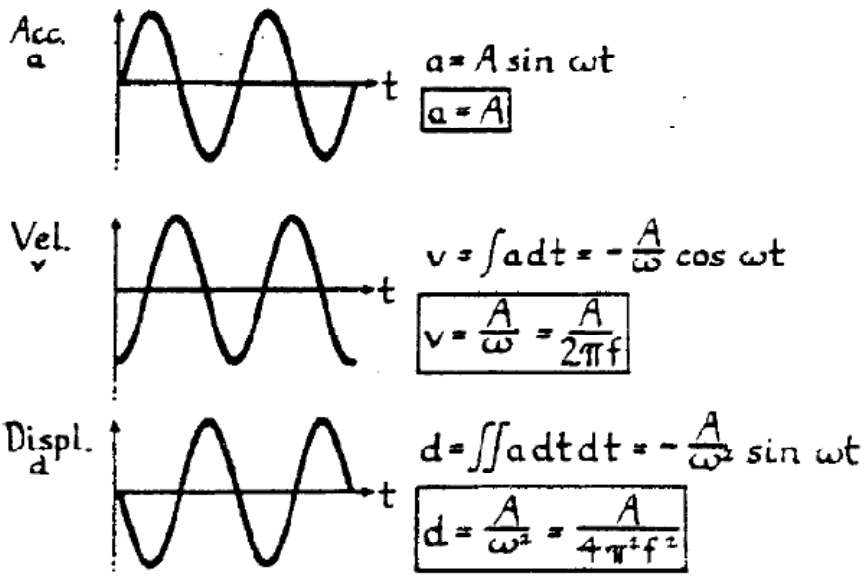

Fig. 123 - Acceleration, velocity and displacement of an harmonic wave

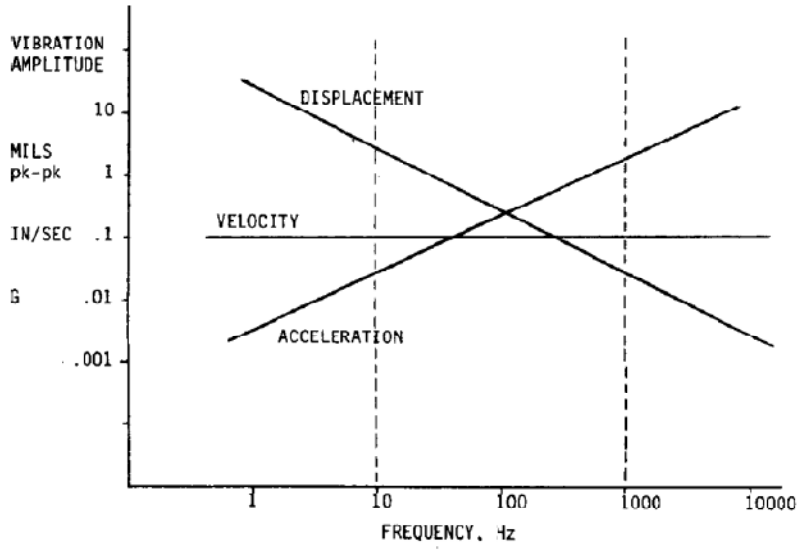

Fig. 124 - Vibration amplitude and frequency

Considering the displacements, the vibration amplitude emphasizes more the low frequency components than high frequency components. In the other hand, the acceleration emphasizes the high frequency components. The three curves are defined in the frequencies range 1 - 1000 Hz, that is the studied range for mechanical vibrations.
For low frequency measurements (<1 Hz), displacements should be determined, while for high frequency measurements (> 100 Hz) acceleration should be determined.

Sponsor demanded dynamic response measurement behavior of the bridge on the ordinary road traffic in different time intervals during one day, as was required for measurement of natural frequencies and mode shapes of vibration bridge construction in 26 sections. A separate measurements were reserved for three days and two days were used for the preparation of measurement.

Different sets of measurement were done during the life of the bridge, at the beginning during the construction and after in 2013, to determine the modal parameters of the bridge (frequencies, modes of natural vibration and corresponding damping values).

When performing vibration tests on civil engineering structures, it is often unpractical and expensive to use artificial excitation (shakers, drop weights). Ambient excitation on the contrary is freely available (traffic, wind), but it causes other challenges: the ambient input remains unknown and the system identification algorithms have to deal with output-only measurements.
The values obtained from the measurements concern about the vibration of the deck during an ordinary traffic flow.
All the measures are evaluated with accelerometers located in 26 sections in the final part of the bridge near the pylon, see the following figure.

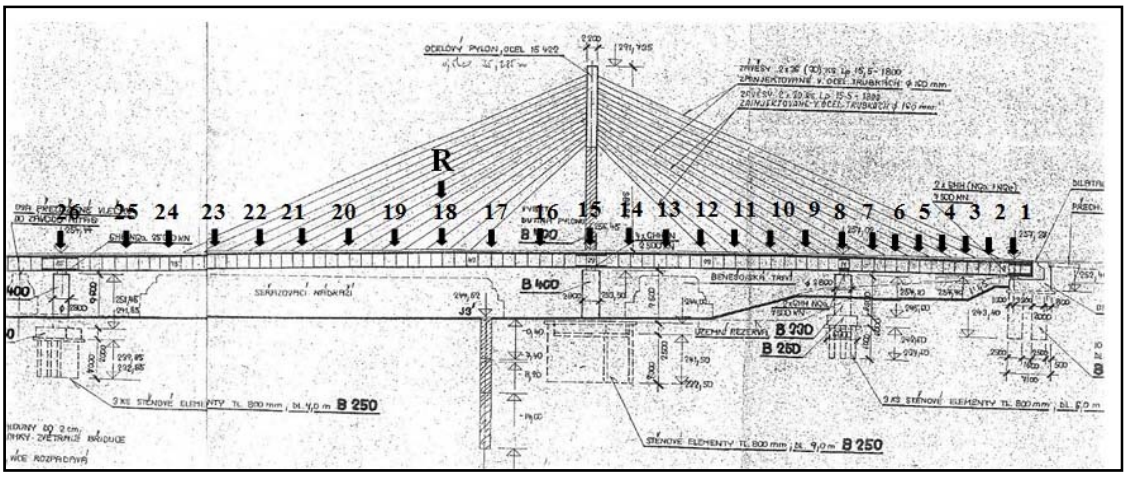

Fig. 125 - Evaluated points along the span

In the following render the type and number of piers are shown.

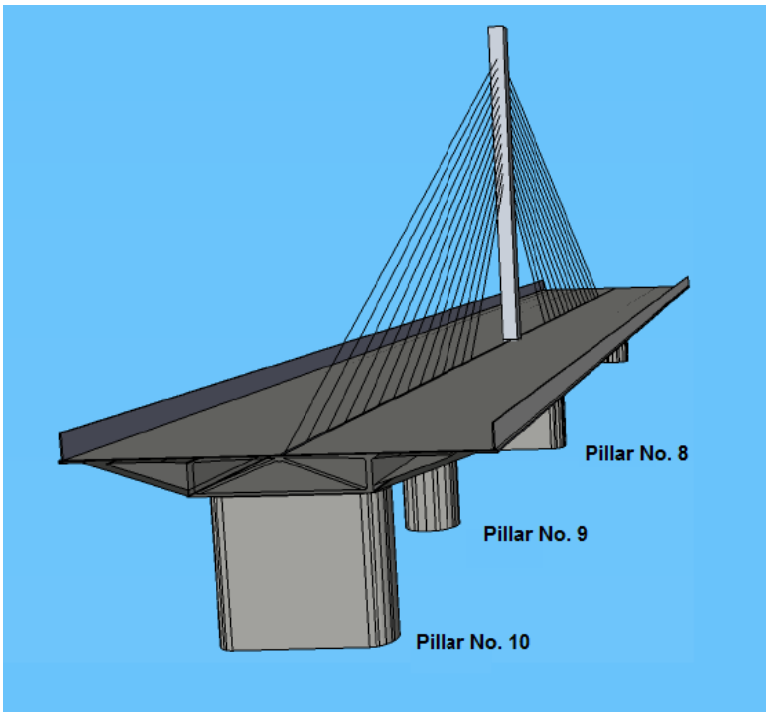

Fig. 126 - Identification of the pillars

In particular in the cross section four different points are taken as reference points for the measurements. The points are reported in the following figure: R101, R102, R103, R104.

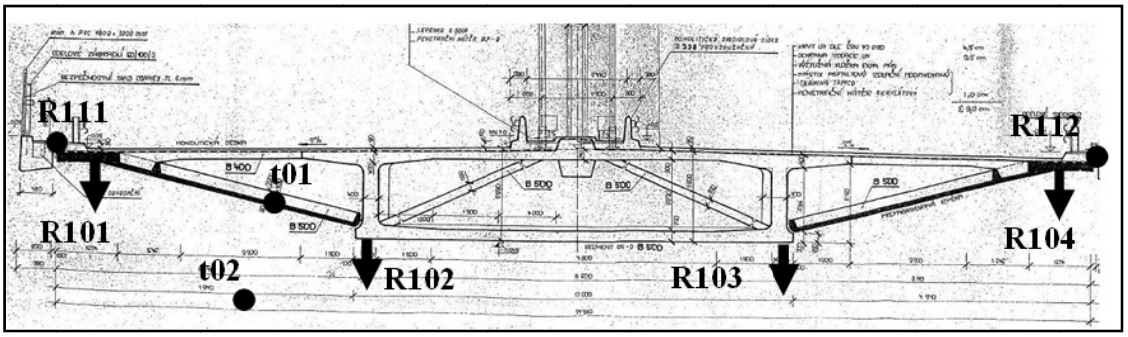

Fig. 127 - Studied points in the last cross section (Pillar No. 10)

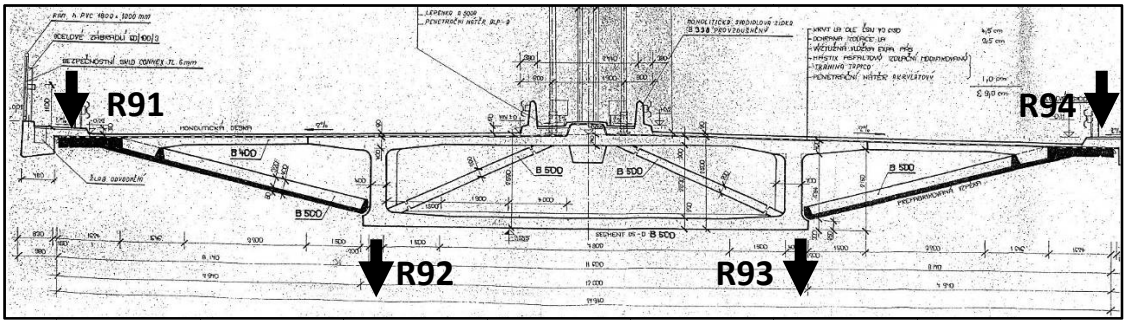

Fig. 128 - Location of monitored points in the Pillar No. 9

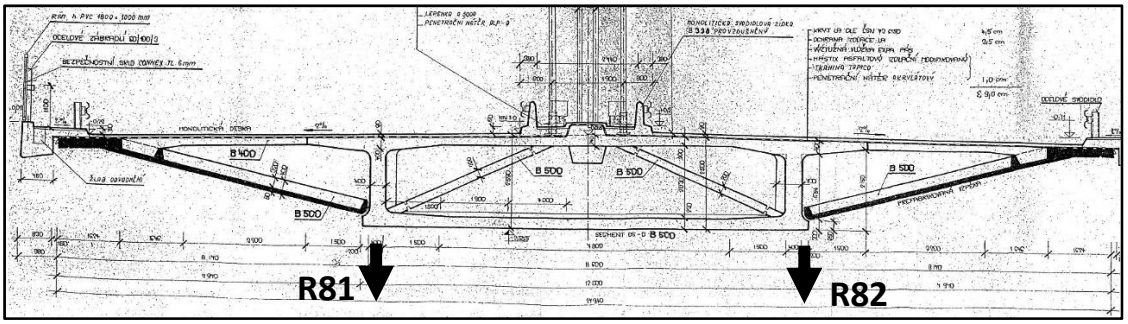

Fig. 129 - Placing the monitored points in the pillar No. 8

For data collection measuring center from the Company Dewetron was used. It was used a total of 22 channels and measuring the voltage across the bridge of concrete struts and steel rods. It was further observed behavior support bridge construction on individual pillars bearings, then tilt the whole structure in cross-section and last it was observed oscillation pylon. All channels are synchronously recorded at a time.

Eigenmodes of vibration have been investigated in both the transverse direction and in the longitudinal direction of the transverse bridge structure, so that the total number of measured slices was 52.

Fig. 130 - Measuring the vertical displacement expansion joints in section R111 of pier 10 on the left edge of the bridge

Fig. 131 - View of the sensors placed in sections R92 and R93 in Pillar No. 9

Fig. 132 - View of the sensors placed in sections R81 and R82 on pillars No. 8

Fig. 133 - The sensor tracks IWT 102 in the reporting point structure R102

Fig. 134 - View of the device for measuring relative deflection KSM-R sensor tracks WA50 captured in section R91

Fig. 135 - Measuring DEWE exchange 5000

The frequencies and modes of natural vibration are one of the most important quantities of civil engineering structure, which we can obtain by measurements. These quantities we can use further in a case of a modal analysis. The modal analysis method is not only a good tool for an identification of the basic dynamic characteristics of the bridge structure, but also a tool for the verification of the important input data to a calculation of the bridge response to the passage of vehicles.

In the following tabs are reported the measured values of displacements in the point R101, R102, R103, R104 of the cross section in the final part of the deck.

Record Numbers	Measured positions								
	R101		R104		Record Numbers	R101		R104	
	Max. [mm] ±0.026	Min. [mm] ±0.026	Max. [mm] ±0.040	Min. [mm] ±0.040		Max. [mm] ±0.026	Min. [mm] ±0.026	Max. [mm] ±0.040	Min. [mm] ±0.040
10	2,70	-0,93	1,71	-1,14	38	2,17	-1,23	2,15	-1,03
11	2,37	-0,96	1,93	-0,98	39	2,09	-0,87	1,92	-0,97
12	2,48	-1,19	2,01	**-1,31**	40	2,74	-0,97	1,85	-1,19
13	2,35	-0,92	1,77	-1,08	41	2,21	-0,93	1,99	-0,91
14	2,08	-1,00	2,08	-0,94	42	2,25	**-1,40**	2,64	-0,98
15	2,07	-0,77	1,94	-1,07	43	2,21	-1,23	2,47	-1,31
16	1,98	-0,94	2,00	-0,96	44	2,41	-1,00	2,02	-1,01
17	2,00	-0,92	1,84	-0,94	45	1,95	-1,02	1,87	-0,88
18	1,98	-1,21	**2,66**	-1,01	46	2,35	-0,63	1,50	-0,97
19	2,15	-0,85	1,77	-0,99	47	2,16	-1,06	2,03	-0,98
20	2,07	-1,03	2,15	-1,05	48	2,04	-0,96	1,73	-0,95
21	2,24	-0,95	2,27	-0,89	49	1,98	-0,97	2,15	-0,77
22	1,88	-1,23	2,32	-0,88	50	2,19	-1,02	1,88	-0,93
23	2,73	-1,05	2,25	-1,01	51	1,97	-1,00	1,94	-0,93
24	2,50	-1,11	2,44	-1,18	52	1,93	-0,84	1,77	-0,89
25	2,41	-0,90	1,90	-0,89	53	2,49	-0,83	1,70	-1,12
26	2,84	-0,90	2,09	-1,06	54	1,97	-0,82	1,99	-0,81
27	2,28	-0,79	1,66	-0,99	55	2,22	-0,86	1,77	-0,91
28	2,17	-0,95	1,82	-0,95	56	2,10	-0,91	1,62	-0,97
29	2,30	-1,23	2,02	-0,88	57	2,09	-1,18	2,00	-0,98
30	2,18	-0,89	1,89	-0,78	58	1,71	-1,08	1,95	-0,87
31	1,90	-0,95	2,05	-0,86	59	1,94	-1,07	2,13	-1,09
32	**2,91**	-1,00	2,28	-1,22	60	1,80	-0,76	1,54	-1,03
33	1,90	-1,08	2,06	-0,84	61	1,67	-1,00	1,89	-0,83
34	2,44	-0,91	1,93	-0,94	62	1,74	-1,06	1,89	-0,86
35	2,30	-0,97	2,02	-0,96	63	2,22	-0,95	2,15	-1,06
36	2,28	-0,87	1,77	-1,06	64	2,44	-1,07	2,04	-1,09
37	2,30	-0,83	1,86	-0,95					
Average	1,92	-0,84	1,79	-0,88					
ndard deviat	0,27	0,13	0,22	0,12					

Tab. 20 - Measured values for the points R101 and R104

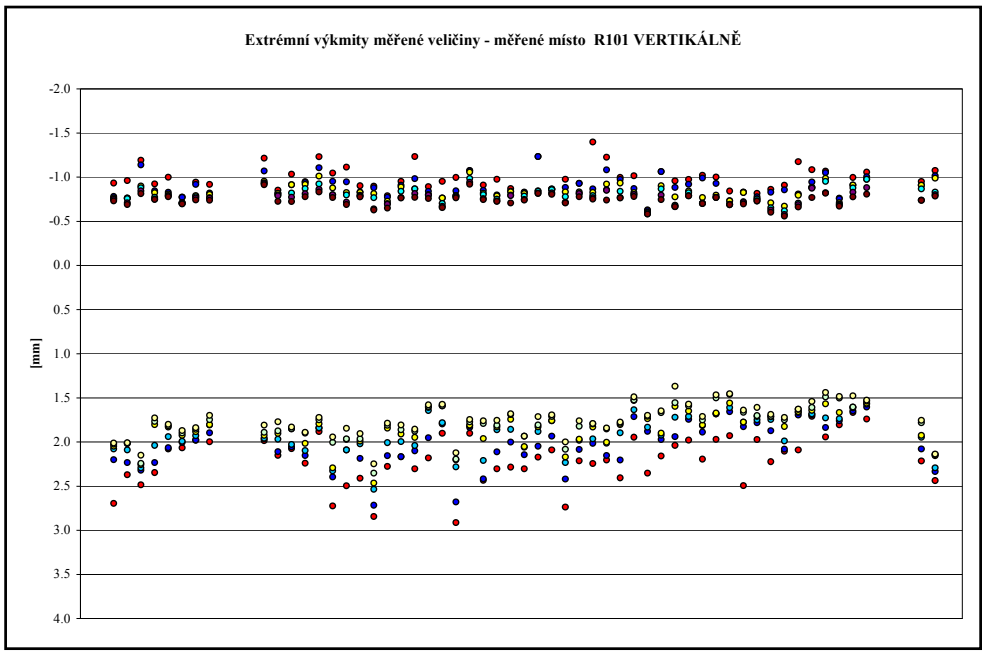

Fig. 136 - Extreme vertical deflections in the point R101 caused by traffic flow

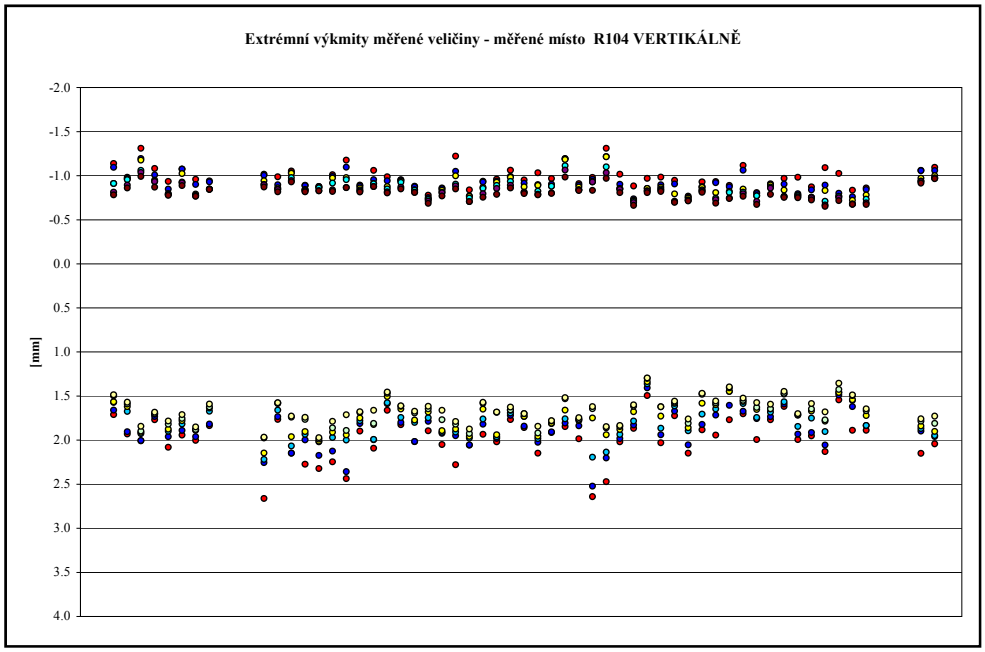

Fig. 137 - Extreme vertical deflections in the point R104 caused by traffic flow

Record numbers	Measured positions								
	R102		R103		Record. numbers	R102		R103	
	Max. [mm] ±0.010	Min. [mm] ±0.010	Max. [mm] ±0.011	Min. [mm] ±0.011		Max. [mm] ±0.010	Min. [mm] ±0.010	Max. [mm] ±0.011	Min. [mm] ±0.011
10	0,25	-0,24	0,21	-0,25	38	0,25	-0,32	0,25	-0,31
11	0,25	-0,22	0,20	-0,24	39	0,21	-0,20	0,25	-0,19
12	0,27	-0,22	0,22	-0,23	40	0,33	-0,22	0,22	-0,23
13	0,27	-0,25	0,20	-0,26	41	0,22	-0,28	0,23	-0,29
14	0,26	-0,25	0,28	-0,26	42	0,24	-0,29	**0,31**	-0,29
15	0,22	-0,23	0,23	-0,24	43	0,22	-0,33	0,25	-0,32
16	0,24	-0,22	0,23	-0,23	44	0,24	-0,25	0,23	-0,25
17	0,20	-0,27	0,22	-0,28	45	0,19	-0,18	0,22	-0,19
18	0,22	-0,25	0,22	-0,25	46	0,29	-0,20	0,17	-0,23
19	0,20	-0,22	0,20	-0,24	47	0,22	-0,25	0,17	-0,23
20	0,26	-0,23	0,23	-0,22	48	0,20	-0,27	0,19	-0,27
21	0,26	-0,28	0,25	-0,29	49	0,24	-0,16	0,25	-0,16
22	0,26	-0,25	0,26	-0,28	50	0,22	-0,18	0,16	-0,18
23	0,28	**-0,34**	0,23	**-0,34**	51	0,19	-0,25	0,18	-0,26
24	0,25	-0,21	0,25	-0,22	52	0,19	-0,22	0,18	-0,22
25	0,25	-0,20	0,23	-0,21	53	0,21	-0,20	0,18	-0,20
26	0,32	-0,20	0,22	-0,22	54	0,20	-0,15	0,19	-0,15
27	0,26	-0,21	0,19	-0,21	55	0,22	-0,21	0,19	-0,20
28	0,30	-0,28	0,19	-0,28	56	0,24	-0,19	0,19	-0,21
29	0,27	-0,30	0,21	-0,29	57	0,17	-0,17	0,21	-0,16
30	0,26	-0,22	0,24	-0,22	58	0,19	-0,16	0,26	-0,15
31	0,19	-0,24	0,19	-0,24	59	0,18	-0,16	0,19	-0,16
32	**0,34**	x	0,26	-0,27	60	0,17	-0,21	0,17	-0,21
33	0,22	-0,30	0,26	-0,30	61	0,17	-0,18	0,20	-0,18
34	0,32	-0,27	0,23	-0,23	62	0,18	-0,21	0,16	-0,19
35	0,24	x	0,24	-0,22	63	0,25	-0,20	0,22	-0,20
36	0,21	x	0,21	-0,24	64	0,29	-0,27	0,21	-0,25
37	0,24	-0,24	0,20	-0,25					
Průměr	0,20	-0,19	0,19	-0,19					
Sm. odch.	0,03	0,04	0,03	0,04					

Tab. 21 - Measured values for the points R102 and R103

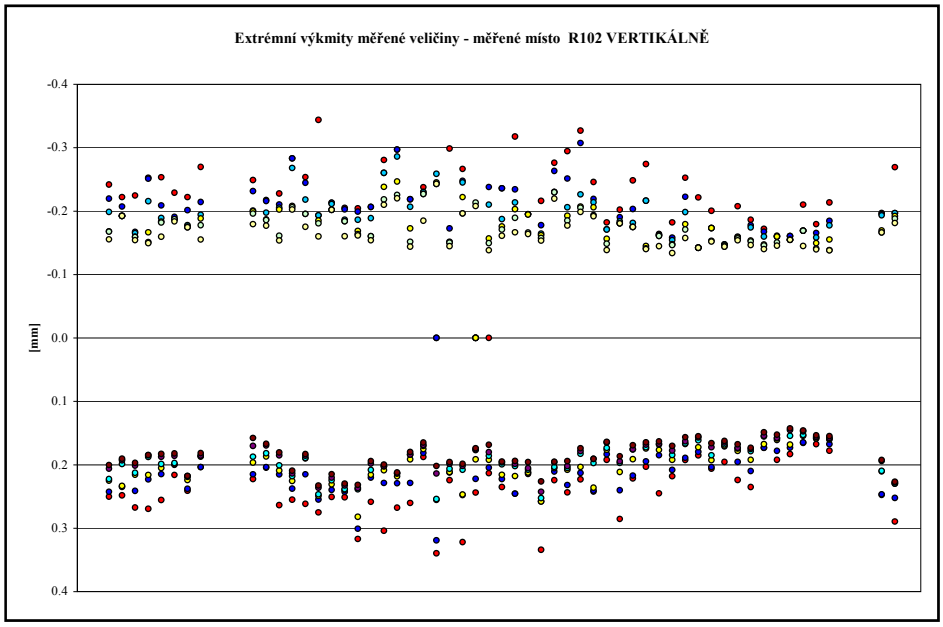

Fig. 138 - Extreme vertical deflections in the point R102 caused by traffic flow

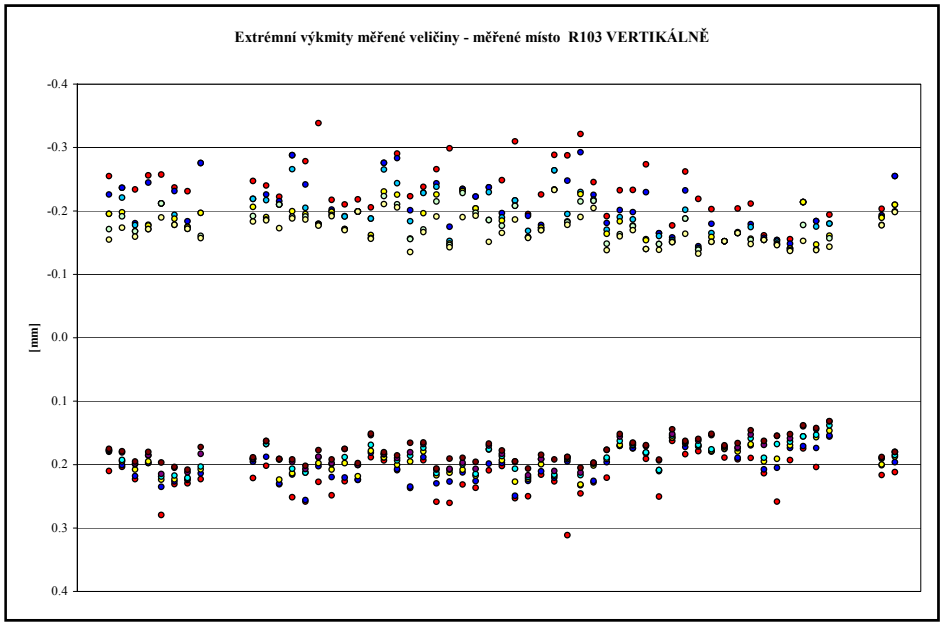

Fig. 139 - Extreme vertical deflections in the point R103 caused by traffic flow

Literature exists on several system identification methods that can identify systems excited by unknown input. A widely used method in civil engineering to determine the eigenfrequencies of a structure based on output-only measurements is the rather simple peak-picking method. In this method, the measured time histories are converted to spectra by a discrete Fourier transform (DFT). The eigenfrequencies are simply determined as the peaks of the spectra. Mode shapes can be determined by computing the transfer functions between all outputs and a reference sensor.

Another algorithm is the stochastic subspace, in which the key element is the projection of the row space of the future outputs into the row space of the past outputs. Also typical for ambient testing of

large structures is that not all degrees of freedom can be measured at once but that they are divided into several set-ups with overlapping reference sensors. These reference sensors are needed to obtain global mode shapes, used for the identification of the bridge design model.

So the experimental frequencies and modes of natural vibration were utilized for the creation of the spatial modal model of this bridge; they serve also as valuable information to verify and update a design model of the observed bridge.

The experimentally-estimated frequencies, modes of natural vibration, corresponding damping values, a dynamic coefficient, a dynamic response and static deflections realize the real immediate state of the observed structure and its spatial behavior. This is the reason for using the results of the experimental methods such as for an identification, an optimization or a verification of a bridge design model.

2.4 Finite element model validation

The correlation between modal parameters identified from the test and those calculated numerically can be evaluated by comparing the values of the natural frequencies and corresponding mode shapes.

The modal analysis carried out on the three-dimensional finite element model is capable of determining the possible modal parameters (natural frequencies and mode shapes). The analytical models of the bridge can then be validated by the corresponding measured modal parameters identified from the field ambient vibration tests. The developed full three-dimensional finite element models are validated by the results of the field ambient vibration tests that were performed just before the opening of the bridge. The finite element models reflect the built-up bridge conditions. They may serve as the baseline finite element model of the Lanovy Most cable-stayed bridge.

The results from measured test are used to optimized and validate the fem models; in the following tab the test results are quoted.

Measured values		
Mode	No initial condition	Vibration's shapes
1	8,300E-01	Pylon out
2	1,070E+00	1 Vertical bending
3	1,220E+00	Torsion
4	1,260E+00	Torsion
5	1,920E+00	Horizontal + torsion
6	2,020E+00	Torsion
7	2,100E+00	2 Vertical bending
8	2,490E+00	Torsion
9	2,800E+00	3 Vertical bending
10	2,960E+00	4 Vertical bending

Tab. 22 - Measured results of natural modes

Vertical modes are those modes dominated by the vertical bending of the bridge deck. Transverse modes are those modes dominated by the lateral sway of the bridge deck in the horizontal plane, while torsional modes are dominated by the torsional behavior of the bridge deck around the longitudinal axis of the bridge.

The analytical results are compared in the tab below.

Mode	Plates model	Beams model	Beam Masses model
	No initial condition	No Initial condition	No Initial condition
1	8,703E-01	8,716E-01	8,716E-01
2	1,031E+00	1,105E+00	8,973E-01
3	1,818E+00	1,540E+00	1,114E+00
4	2,246E+00	2,380E+00	1,275E+00
5	2,291E+00	/	1,685E+00
6	2,509E+00	/	1,912E+00
7	2,805E+00	2,899E+00	1,941E+00
8	3,114E+00	3,283E+00	2,497E+00
9	3,492E+00	3,369E+00	2,691E+00
10	4,082E+00	3,912E+00	2,760E+00

Tab. 23 - Empirical results

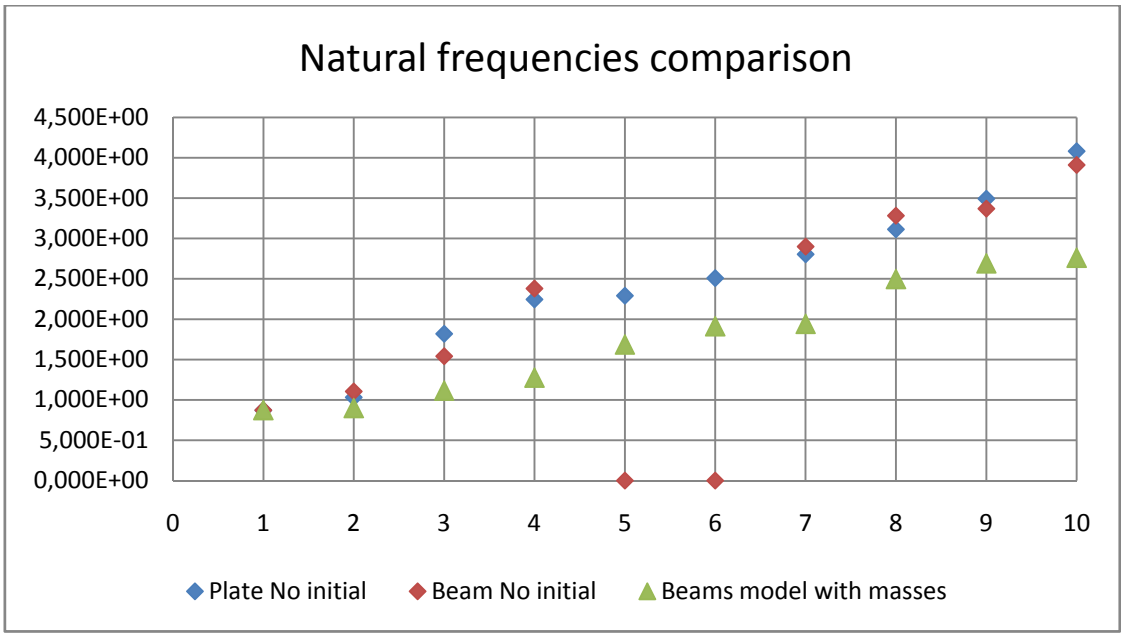

Fig. 140 - Comparison of empirical results

Tab. 24 shows the comparison of the numerically calculated frequencies from the three-dimensional finite element analysis and experimentally identified frequencies from the field ambient vibration tests.

Modes	Measured values	Plates model	Beams model	Beams model with masses
Pylon out	8,300E-01	8,703E-01	8,716E-01	8,716E-01
1 Vertical bending	1,070E+00	1,031E+00	1,105E+00	8,973E-01
Horizontal	1,920E+00	1,818E+00	1,540E+00	1,685E+00
2 Vertical bending	2,100E+00	2,246E+00	2,380E+00	1,94E+00
3 Vertical bending	2,800E+00	3,114E+00	3,283E+00	2,691E+00

Tab. 24 - Principal natural modes with measured results

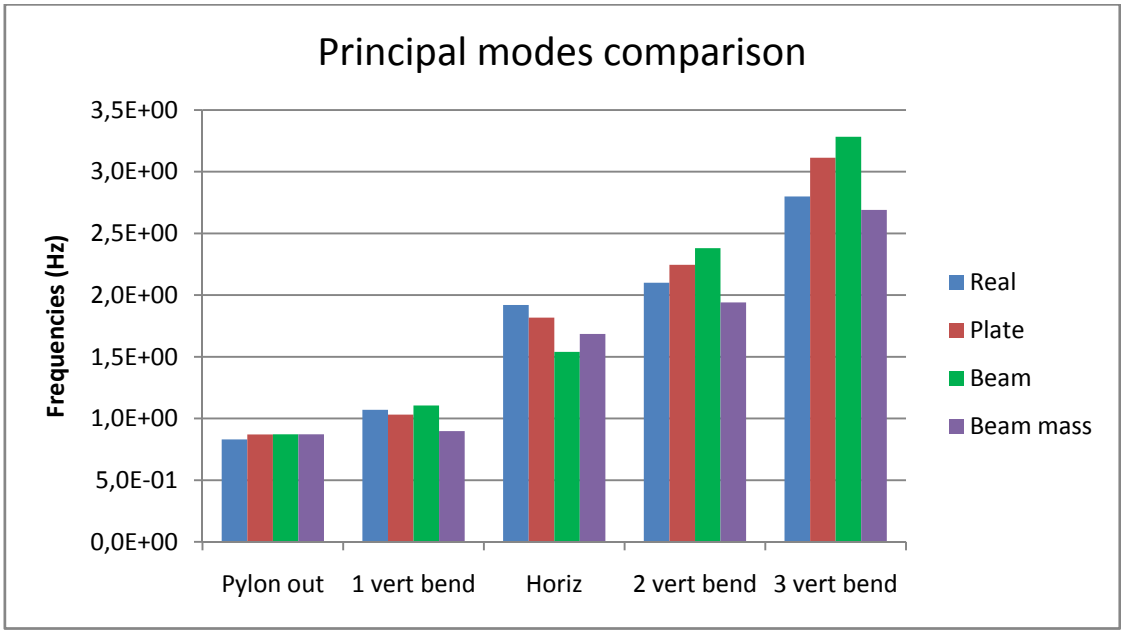

Fig. 141 - Comparison of principal natural modes with measured results

In the graph below, the percentage error between measured values and the plates model is shown.

$$\Delta\% = 100 * (f_{FEA} - f_{EMA})/f_{EMA}$$

Where: f_{FEA} are the analytical modes of vibration (with fem models)

f_{EMA} are the empirical modes of vibration (measured values)

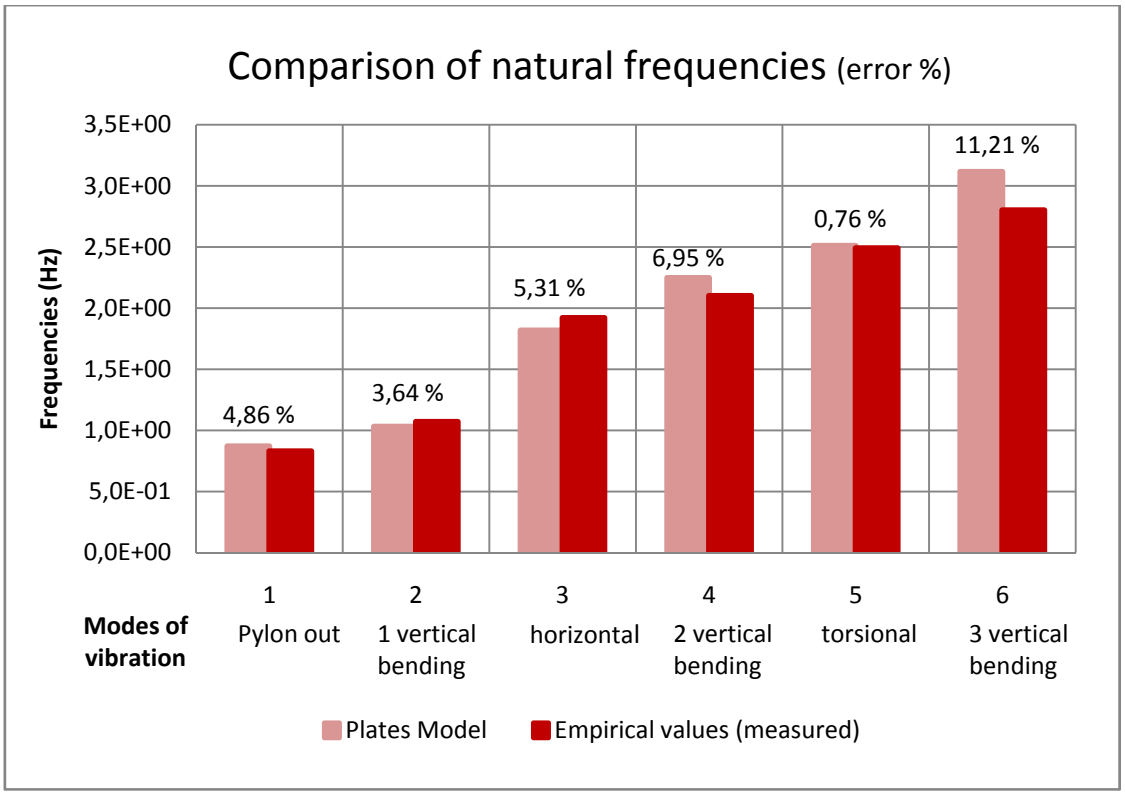

Fig. 142 - Comparison plates model vs measured values (error %)

As discussed above, the beam idealization for a straight, nonskewed bridge is an intrinsically stiffer system than the two-dimensional grillage. It is suggested that the additional stiffness which occurs when using a single beam idealization for nonskewed bridges compensates for the additional stiffness of supports in reality. This is the primary reason that the single beam idealization at times appears to correlate with reality. It is not because the idealization is theoretically accurate or representative of bridge superstructure behaviour.

Single beam idealizations do not incorporate torsional and transverse modes of vibration that occur between longitudinal modes. Therefore, one-dimensional analytical simulations will never realistically portray vehicle-bridge systems.

The difference between the observed and computed frequencies of free vibration can also be attributed to other factors such as errors in estimating the static modulus of concrete, errors resulting from modelling the support fixity, etc.

As final step, the modal shapes are obtained and compared through the correlation of the points between the fem model and the 26 measured sections.

This operation is made by the software Visual Modal Pro only introducing the numbers and coordinates of the fem model, the number of modes of vibration and the relative displacements.

The output of the software, referred to the fem results, is reported in the following figures, these represent the shapes of the modes of vibration for each analyzed section.

The comparison of the principal numerically calculated frequencies, with the plates model, and experimentally identified frequencies is shown overlapped in following figures.

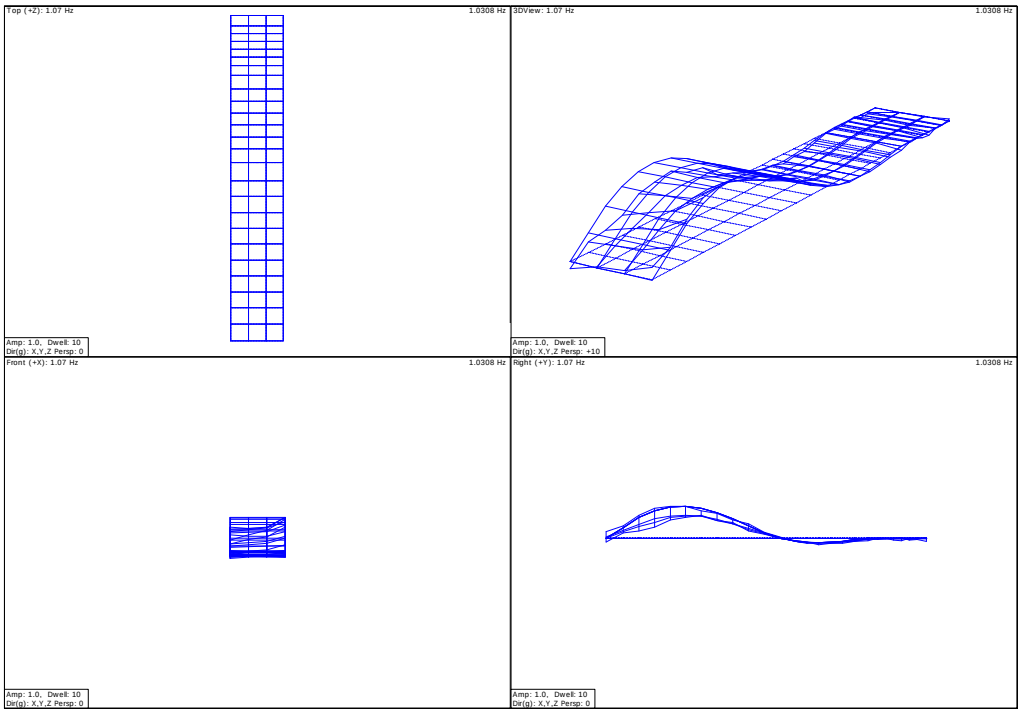

Fig. 143 - 1 vertical bending f = 1,07 Hz (measured) and 1,03 Hz

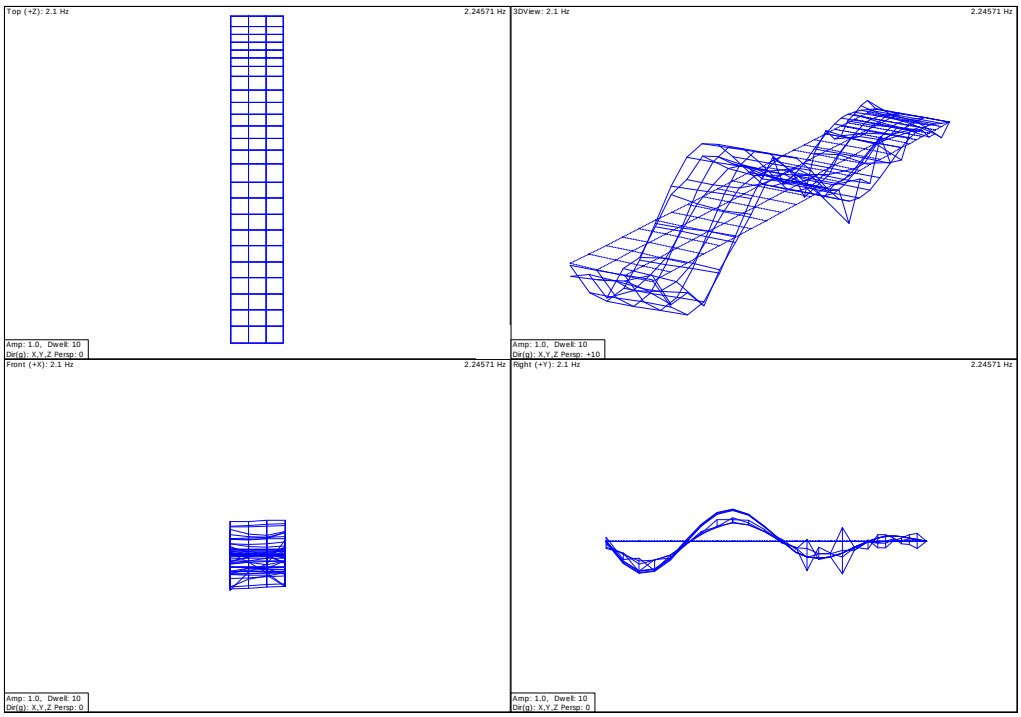

Fig. 144 - 2 vertical bending f = 2,1 Hz (measured) and 2,25 Hz

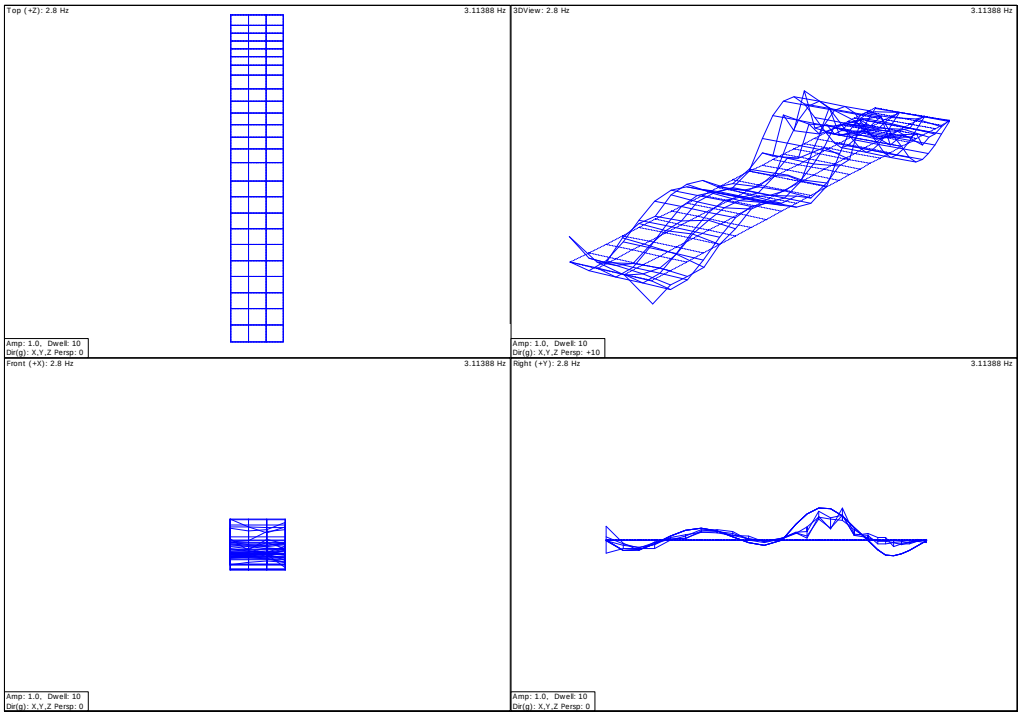

Fig. 145 - 3 vertical bending f = 2,8 Hz (measured) and 3,11 Hz

3. LINEAR BUCKLING SOLVER

Buckling is a mathematical instability, leading to a failure mode. Theoretically, buckling is caused by a bifurcation in the solution to the equations of static equilibrium. At a certain stage under an increasing load, further load is able to be sustained in one of two states of equilibrium: an undeformed state or a laterally-deformed state.

In practice, buckling is characterized by a sudden failure of a structural member subjected to high compressive stress, where the actual compressive stress at the point of failure is less than the ultimate compressive stresses that the material is capable of withstanding.

Mathematical analysis of buckling makes use of an axial load eccentricity that introduces a moment, which does not form part of the primary forces to which the member is subjected. When load is constantly being applied on a member, such as column, it will ultimately become large enough to cause the member to become unstable. Further load will cause significant and somewhat unpredictable deformations, possibly leading to complete loss of load-carrying capacity. The member is said to have buckled, to have deformed.

The linear buckling solver calculates the buckling load factors and corresponding mode shapes for a structure under given loading conditions. It is based on the assumptions that exists a bifurcation point where the primary and secondary loading paths intersect, and before this point is reached, all element stresses change proportionally with the load factor.

The buckling solution requires an existing static load solution as a basis for calculating the element geometric stiffness matrix. In Strand7, linear static, non-linear static and quasi-static solutions can be used as a basis for a linear buckling solution.

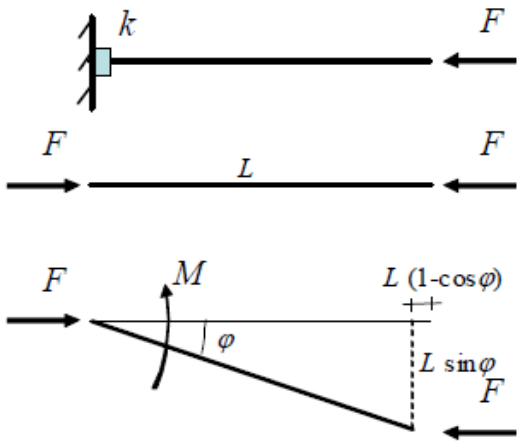

Fig. 146 - Cantilever with axial force

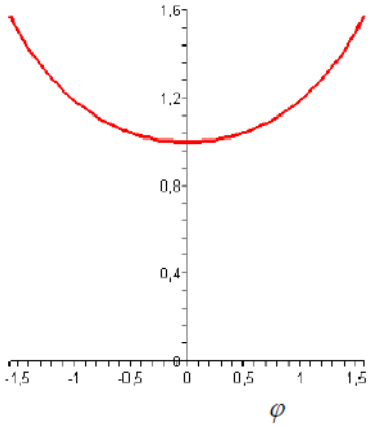

Fig. 147 - Equilibrium path of cantilever with axial force

A linear buckling solution is obtained by solving the following eigenvalue problem:

$$[K] * \{x\} = \lambda * [Kg] * \{x\}$$

Where: $[K]$ is the global stiffness matrix

$\{x\}$ buckling mode vectors

λ buckling load factor

$[Kg]$ global geometric stiffness matrix

The geometric stiffness matrix, also known as the initial stress stiffness matrix, is a symmetric matrix dependent on the element stress level. It reflects the effect of geometric change on the element force vector from a known stress state. For beam and plate bending structures, the geometric stiffness matrix represents the stiffening effect of the tensile axial/membrane stresses.

The buckling solution is possible only when an existing solution is available for determining the current stress state of the structure, which is required for the calculation of the element geometric stiffness matrix. In Strand7, both linear static and nonlinear static solutions can be used to as the initial conditions for a linear buckling solution.

The linear buckling solver performs the following steps:

a) Calculates and assembles the element stiffness and geometric stiffness matrices to form the global stiffness and geometric stiffness matrices. Constraints are assembled in this process; however, the constant terms for enforced displacements and shrink links are ignored.

b) If the initial file is from a non-linear solution, the stiffness matrix calculation is based on the current material status and geometry. In other words, a yield modulus will be used if the material has yielded and the deformed geometry will be used if the initial solution included geometry non-linearity.

c) Checks the geometric stiffness matrix. If all diagonal entries are zero, the solution stops.
d) Modifies the stiffness matrix when a shift value is applied.
e) Solves the eigenvalue problem to get buckling load factors and the corresponding buckling modes using the Sub-Space Iteration Method.

The linear buckling analysis assumes the existence of a bifurcation point where the primary and secondary loading paths intersect (point A in the figure below). At this point, more than one equilibrium position is possible. The primary path is not usually followed after loading exceeds this point and the structure is in the post-buckling state. The slope of the secondary path at the bifurcation point determines the nature of the post-buckling. A positive slope indicates that the structure will have post buckling strength whilst a negative slope means that the structure will snap through or simply collapse.

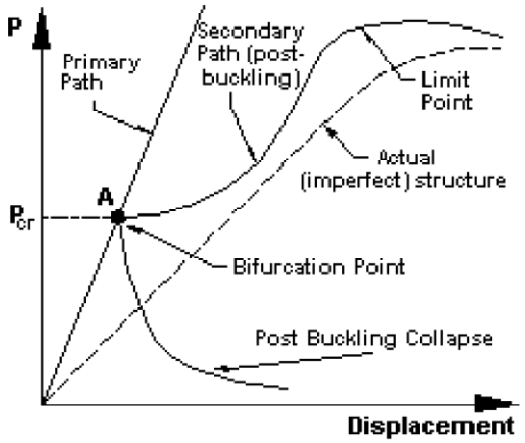

Fig. 148 - Displacement with increasing load

Real structures have geometric and loading imperfections, often causing the primary path curve and the bifurcation point to disappear.

Another assumption for the linear buckling analysis is that the stresses in the structure increase proportionally with the load. When the deformation is large enough to disturb the stress distribution, linear buckling results will no longer be valid. In this case, a nonlinear solution is more appropriate for a realistic prediction of the structure's capacity.

If a more accurate estimate of the buckling load is required, it is recommended that a nonlinear analysis be carried out so that the effect of pre-buckling deformation can be included and the post buckling capacity predicted.

The theoretical solution of Eulero is given by:

$$P_{cr} = \pi^2 * \frac{E * I}{l_0^2}$$

Where: E is the modulus of the elasticity of the material (E_{steel} = 2,10*E05 MPa)

I is the moment of inertia of the cross section

l_0 is the free length of deflection (for cantilever beam $l_0 = 2 * l$)

l is the effective length of the column ($l = 3{,}91 * E04\ mm$)

Examination of this formula reveals the following interesting facts with regard to the load-bearing ability of slender columns.

- Elasticity and not compressive strength of the materials of the column determines the critical load.
- The critical load is directly proportional to the second moment of area of the cross section.
- The boundary conditions have a considerable effect on the critical load of slender columns. The boundary conditions determine the mode of bending and the distance between inflection points on the deflected column. The closer together the inflection points are, the higher the resulting capacity of the column.

The strength of a column may therefore be increased by distributing the material so as to increase the moment of inertia. This can be done without increasing the weight of the column by distributing the material as far from the principal axis of the cross section as possible, while keeping the material thick enough to prevent local buckling. This bears out the well-known fact that a tubular section is much more efficient than a solid section for column service.

Another bit of information that may be gleaned from this equation is the effect of length on critical load. For a given size column, doubling the unsupported length quarters the allowable load. The restraint offered by the end connections of a column also affects the critical load. If the connections are perfectly rigid, the critical load will be four times that for a similar column where there is no resistance to rotation (hinged at the ends).

The pylon is made of four parts with different values of inertia, so to evaluate the inertia I of the all pylon was used a medium value of the 4 parts.

Part	Inertia	
I1	1,5608E+11	mm^4
I2	1,8720E+11	mm^4
I3	1,4730E+11	mm^4
I4	9,2423E+10	mm^4
I pylon medium	**1,4575E+11**	**mm^4**

Tab. 25 - Inertia of the pylon

The theoretical value of the critic load is:

E =	210000	MPa
L =	3,91E+04	mm
Lo =	7,82E+04	mm
Pcr =	**4,9399E+07**	**N**

Tab. 26 - Calculation of the critical load

In the numerical software the only load applied is the unitary force at the top of the pylon as in the following figure.

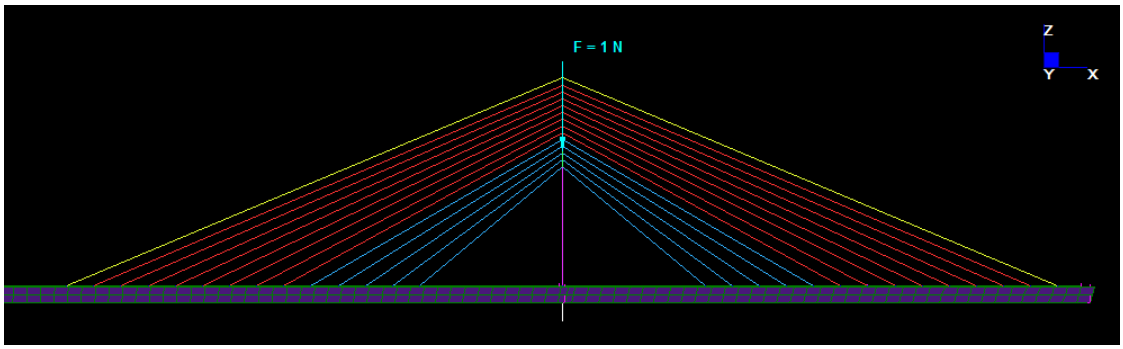

Fig. 149 - Unitary force at the top of the pylon

The numerical results is given by the first buckling load factor, that correspond to the first buckling load because of the unitary force applied and it is 6,0967E+07 N.

In the next figure is represented the shape of the pylon deformation; the displacement at the top is about 173 mm.

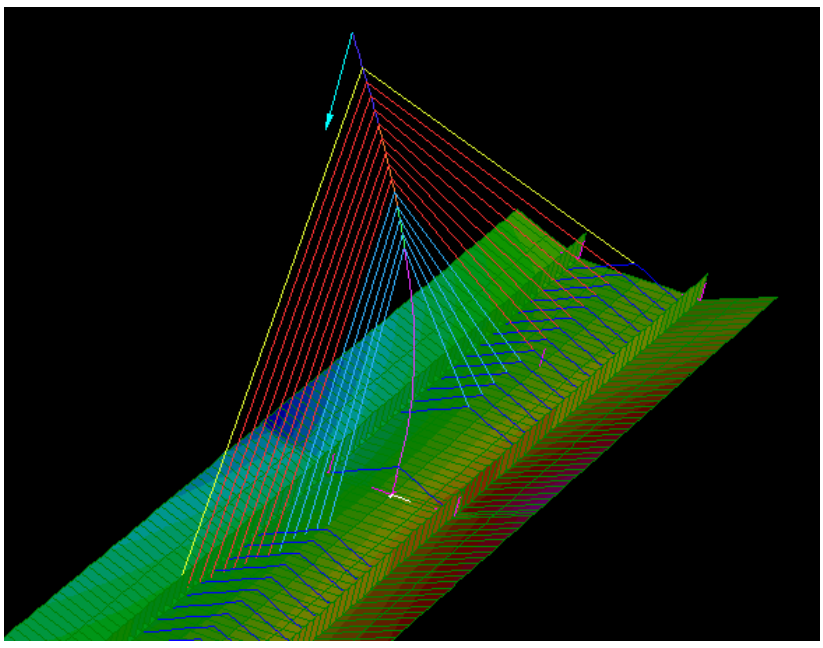

Fig. 150 - First buckling load factor

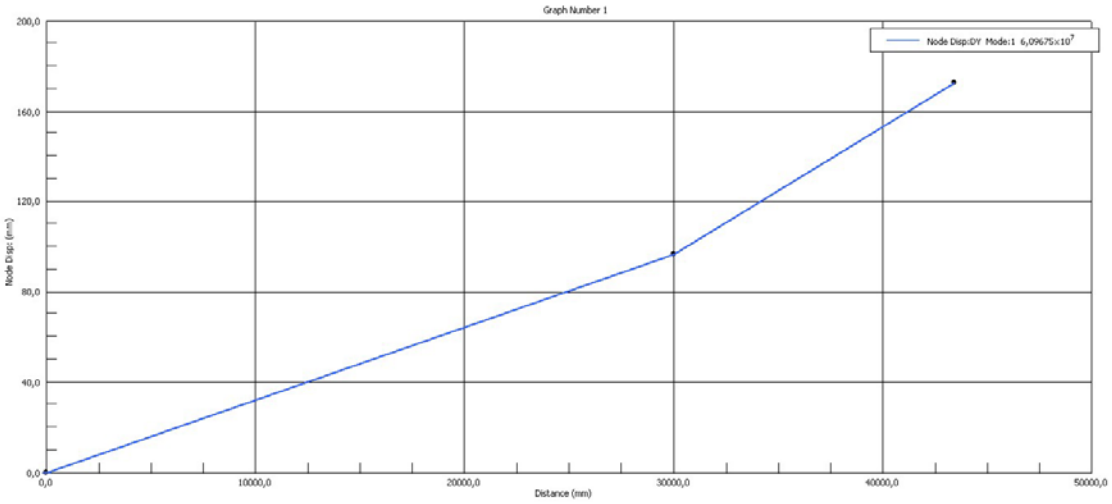

Fig. 151 - Displacement DY from the base to the top of the pylon

4. LINEAR DYNAMIC ANALYSIS

4.1 Single degree of freedom systems

The simplest vibratory system can be described by a single mass connected to a spring and possibly a dashpot. The mass is allowed to travel only along the spring elongation direction. Such systems are called Single Degree-of-Freedom (SDOF) systems and are shown in the following figure.

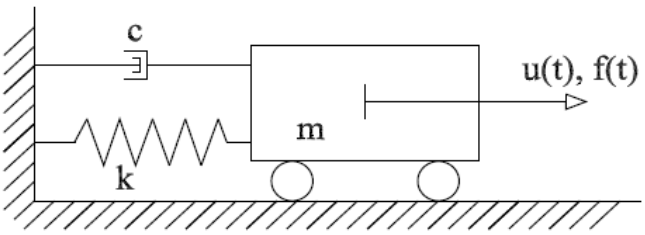

Fig. 152 - Single d.o.f. dynamic system

SDOF vibration can be analyzed by Newton's second law of motion, F = m*a. The analysis can be easily visualized with the aid of a free body diagram:

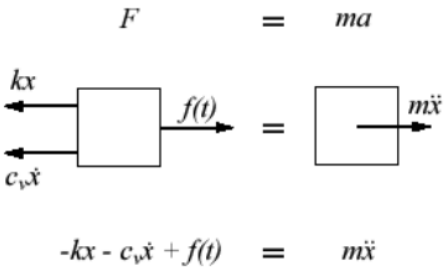

Fig. 153 - Free body diagram

The resulting equation of motion is a second order, non-homogeneous, ordinary differential equation:

$$m\ddot{u}(t) + c\dot{u}(t) + ku(t) = f(t)$$

With the initial conditions in displacement $u(0) = u_0$ and in velocity $\dot{u}(0) = \dot{u}_0$

The dot stands for derived in time and the other quantities are:

u = displacement of the center of mass of the moving object

$\dot{u}$ = velocity

$\ddot{u}$ = acceleration

m = mass of the moving object

c = linear viscous damping coefficient

k = linear elastic stiffness coefficient

$f(t)$ = external excitation force

$m\ddot{u}(t)$ = inertia force

$c\dot{u}(t)$ = damping force

$ku(t)$ = elastic recall force

For this kind of problem not always exist close solutions; it's possible to solve the equation analytically only for some type of simple-harmonic forcing. In these cases the solution u to equation is the sum of a homogeneous part u_g (free response obtain for $f(t)$ = 0) and a particular part u_p (forced response depending on the type of external excitation force $f(t) \neq 0$). The first part represents the transient state and it's influenced by initial conditions, while the second part represents the full speed behavior.

Therefore the general solution is composed by the sum $u_g + u_p$, on which has to be fix the initial conditions to obtain the displacement value u.

4.1.1 Case f = 0, c = 0

In this case the equation of motion is a constant-amplitude oscillation, defined by:

$$m\ddot{u}(t) + ku(t) = 0$$

The previous equation has the particular part equal to zero and the homogeneous equation is:

$$u(t) = Acos(\omega t) + Bsin(\omega t)$$

With:

$$\dot{u}(t) = -\omega A\, sin(\omega t) + \omega Bcos(\omega t)$$
$$\ddot{u}(t) = -\omega^2 Acos(\omega t) - \omega^2 Bsin(\omega t)$$

Putting these two expressions in the equation of motion, we obtain:

$$-\omega^2 m[Acos(\omega t) + Bsin(\omega t)] + k[Acos(\omega t) + Bsin(\omega t)] = 0$$

The previous equation is satisfied by $\omega^2 = \frac{k}{m}$.

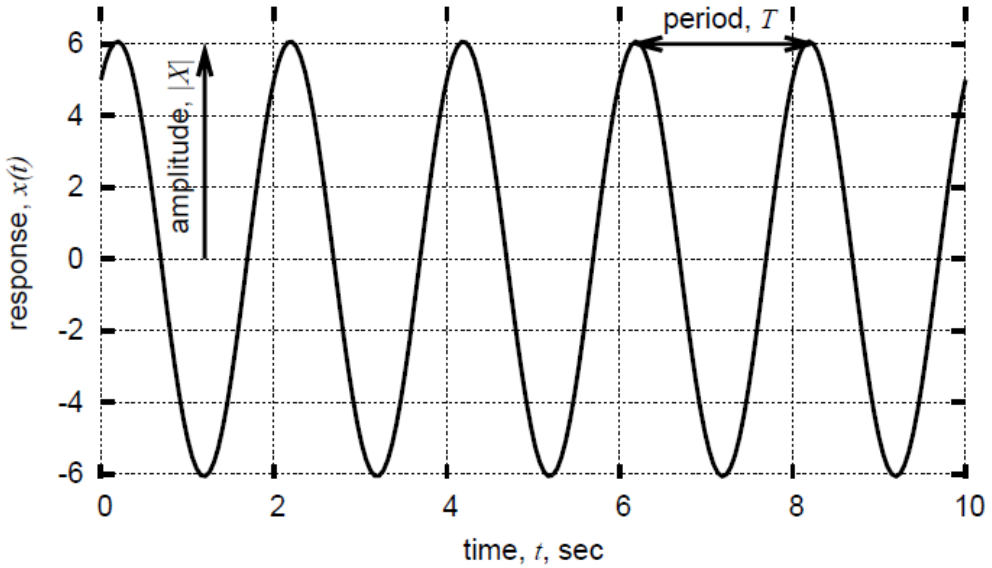

Fig. 154 - u(t) with f=0, c=0

As we see in Fig. 154 the system is excited by the initial conditions and the oscillations amplitude's remains the same forever.

The value $\omega = \sqrt{k/m}$ defines the circular natural frequency of vibration of the system. $T = 2\pi/\omega$ is the natural period of vibration of the mass, evaluated with the minimum time to obtain $u(T + t) = u(t), \forall\, t$. The two constants A and B depend on the initial conditions.

Using the initial condition at time t = 0, we obtain the following two relations:

$$A = u_0 \qquad B = \dot{u}_0/\omega$$

And the solution of the system is:

$$u(t) = u_0\, cos(\omega t) + \frac{\dot{u}_0}{\omega}\, sin(\omega t)$$

4.1.2 Case f = 0, c ≠ 0

The equation of motion in this case becomes:

$$m\ddot{u}(t) + c\dot{u}(t) + ku(t) = 0$$

This type of solution is supposed:

$$u(t) = Ge^{\lambda t}$$

From which:

$$\dot{u}(t) = \lambda G e^{\lambda t}$$

And

$$\ddot{u}(t) = \lambda^2 G e^{\lambda t}$$

Replacing them in the equation of the motion we obtain:

$$m\lambda^2 Ge^{\lambda t} + c\lambda Ge^{\lambda t} + kGe^{\lambda t} = 0$$

$$(m\lambda^2 + c\lambda + k)Ge^{\lambda t} = 0$$

Note that m, c, k, λ and G do not depend on time. For the previous equation to be true for all time,

$$(m\lambda^2 + c\lambda + k)G = 0$$

The equation before is trivially satisfied if G = 0. The non-trivial solution is:

$$m\lambda^2 + c\lambda + k = 0$$

The previous equation is called “characteristic equation”, quadratic equation in λ which has the roots:

$$\lambda_{1,2} = \frac{-c \pm \sqrt{c^2 - 4mk}}{2m}$$

The solution to an homogeneous second order ordinary differential equation requires two independent initial conditions, an initial displacement and an initial velocity. These two initial conditions are used to determine the coefficients A and B of the two linearly independent solutions corresponding to λ_1 and λ_2.

The amount of damping *c* qualitatively affects the quadratic roots $\lambda_{1,2}$ and the free response solutions.

Introducing the critical damping:

$$c_{cr} = 2\sqrt{km} = 2m\omega$$

And calling ξ the ration between the viscous and the critical damping:

$$\xi = \frac{\mathrm{c}}{c_{cr}}$$

The solution becomes (with $k = \omega^2 m$):

$$\lambda_{1,2} = -\omega\xi \pm \omega\sqrt{\xi^2 - 1}$$

In function of the value of ξ, there are three different cases:

1. critically damped: $\xi = 1 \rightarrow \lambda_1 = \lambda_2 = -\omega$
2. over-damped: $\xi > 1 \rightarrow \lambda_{1,2} = -\omega\xi \pm \omega_s \quad \omega_s = \omega\sqrt{\xi^2 - 1}$
3. under-damped: $\xi < 1 \rightarrow \lambda_{1,2} = -\omega\xi \pm i\omega_d \quad \omega_d = \omega\sqrt{1 - \xi^2}$

The frequency $\omega\sqrt{1-\xi^2}$ is called the damped natural frequency ω_d and it is the frequency at which under-damped SDOF systems oscillate freely.

- ***Critically damped response***

For $\xi = 1$, the solution is:

$$u(t) = (G_1 + G_2 t)e^{-\omega t}$$

With:

$$\dot{u}(t) = G_2 e^{-\omega t}(G_1 + G_2 t)e^{-\omega t}$$

$$\ddot{u}(t) = -\omega G_2 e^{-\omega t} - \omega G_2 e^{-\omega t} + \omega^2 (G_1 + G_2 t)e^{-\omega t}$$

The constants G_1 and G_2 are determined through the initial conditions:

$$u_0 = G_1$$

$$\dot{u}_0 = [G_2 e^{-\omega t} - \omega(G_1 + G_2 t)e^{-\omega t}]_{t=0} = G_2 - \omega G_1 \quad \rightarrow \quad G_2 = \dot{u}_0 + \omega u_0$$

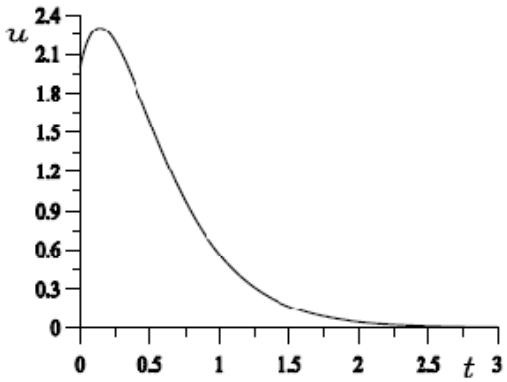

Fig. 155 - u(t) with f = 0, c = c_{cr}

So the solution is:

$$u(t) = [u_0 + (\dot{u}_0 + \omega u_0)t]e^{-\omega t}$$

In this case the damping effect permits only to turn the system back to the initial position.

- ***Over-damped response***

For $\xi > 1$ we obtain $c > 2\omega m$ and the solution is:

$$u(t) = (G_1 e^{\omega_s t} + G_2 e^{-\omega_s t})e^{-\xi\omega t}$$

Using the initial conditions it's possible to evaluate the two constants G_1 and G_2:

$$u_0 = G_1 + G_2$$

$$\dot{u}_0 = \left[[(\omega_s G_1 e^{\omega_s t} - \omega_s G_2 e^{-\omega_s t}) - \omega\xi(G_1 e^{\omega_s t} + G_2 e^{-\omega_s t})] \cdot e^{-\omega_s t}\right]_{t=0} =$$
$$= \omega_s G_1 - \omega_s G_2 - \omega\xi(G_1 + G_2)$$

And so:

$$G_1 = \frac{1}{2}\frac{\omega\xi u_0 + \omega_s u_0 + \dot{u}_0}{\omega_s} \quad G_2 = -\frac{1}{2}\frac{\omega\xi u_0 - \omega_s u_0 + \dot{u}_0}{\omega_s}$$

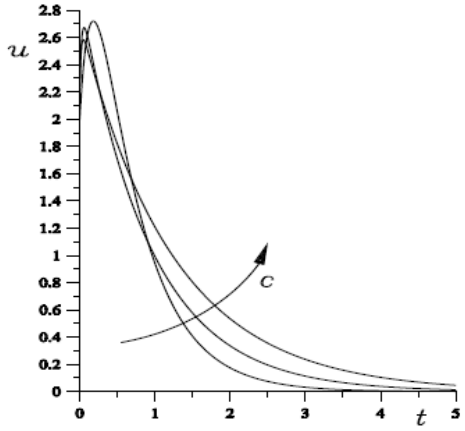

Fig. 156 - u(t) with f = 0, $c \geq c_{cr}$

From Fig. 156 we can see that with an increasing damping, the maximum displacement *u* is increasing, but the solution dampens faster.

- ***Under-damped response***

For $\xi < 1$ we have $c < 2\omega m$ and the solution is like:

$$u(t) = e^{-\omega\xi t}[Acos(\omega_d t) + Bsin(\omega_d t)]$$

With the initial conditions it's possible to calculate the constants A and B:

$$\begin{matrix} u_0 = A \\ \dot{u}_0 = -\omega\xi A + B\omega_d \end{matrix} \rightarrow \begin{matrix} A = u_0 \\ B = (\omega\xi u_0 + \dot{u}_0)/\omega_d \end{matrix}$$

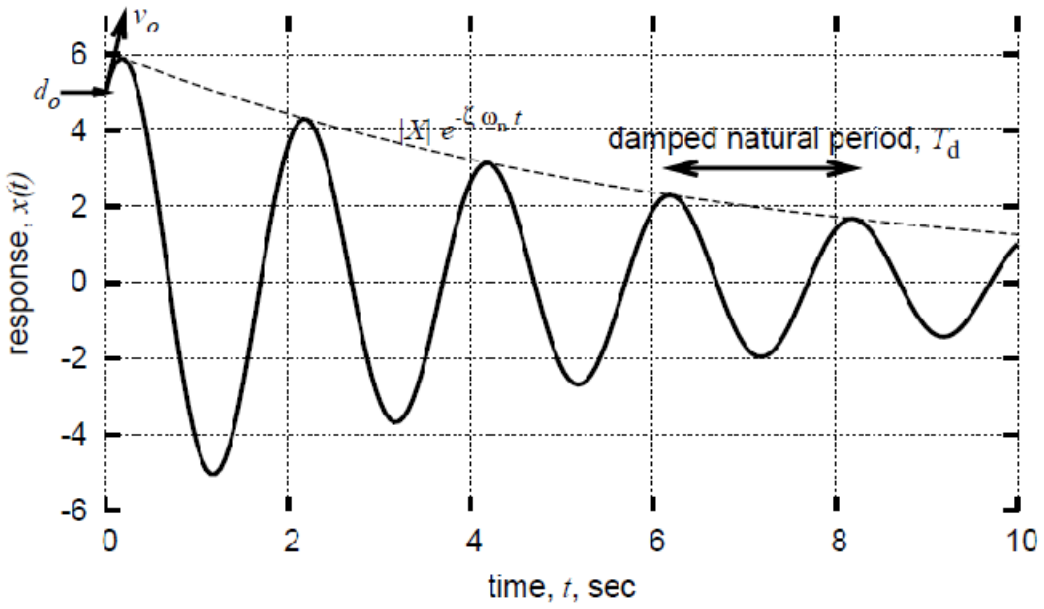

Fig. 157 - u(t) with f = 0, c < c_{cr}

In Fig. 157 it is shown the harmonic solution. Two subsequent peaks are separated by the period $T_d = 2\pi/\omega_d$. Seeing that $0 < \xi < 1$, we have $\omega_d < \omega$. The oscillatory motion is decreasing faster when the damping is rising. In an infinite time the mass is going to stabilize in the equilibrium position at the zero value's.

Until now we have determined the analytical solutions of one degree liberty system considering a null force and exciting them with the displacement and the force at the initial time.
From the previous cases we can see how a system starts to oscillate with a frequency value such as the natural frequency of the system, despite the initial conditions.

4.1.3 Case f = cost, c = 0

For constant force is simple to find the particular solution:

$$u_p(t) = \frac{\bar{f}}{k}$$

The homogeneous part for $c = 0$ is given by:

$$u(t) = Acos(\omega t) + Bsin(\omega t)$$

And introducing the following initial conditions:

$$\begin{Bmatrix} u_0 = A + \bar{f}/k & \rightarrow & A = u_0 - \bar{f}/k \\ \dot{u}_0 = \omega B & \rightarrow & B = \dot{u}_0/\omega \end{Bmatrix}$$

We obtain the general solution of the problem:

$$u(t) = (u_0 - \bar{f}/k)\cos(\omega t) + (\dot{u}_0/\omega)\sin(\omega t) + \frac{\bar{f}}{k}$$

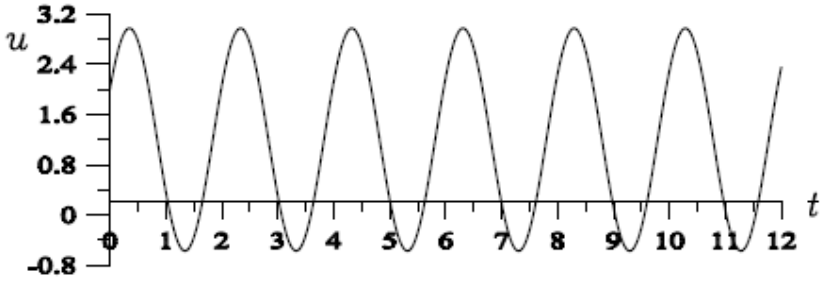

Fig. 158 - u(t) with $f = \bar{f} = cost, c = 0$

4.2 Case f = cost, c ≠ 0, ξ < 1

In this case the homogeneous part is given by:

$$\mathrm{u_g(t) = [A\cos(\omega_d t) + B\sin(\omega_d t)]e^{-\omega\xi t}}$$

The particular solution is equal to the case before so the general solution is given by:

$$\mathrm{u(t) = [A\cos(\omega_d t) + B\sin(\omega_d t)]e^{-\omega\xi t} + \frac{\bar{f}}{k}}$$

Through the initial conditions we can calculate the two constants A and B:

$$u_0 = A\,\bar{f}/k \quad \rightarrow \quad A = (-\bar{f} + u_0 K)/k$$

$$\dot{u}_0 = -\omega\xi A + B\omega_d \quad \rightarrow \quad B = (-\omega\xi\bar{f} + \omega\xi u_0 k + \dot{u}_0 k)/\omega_d k$$

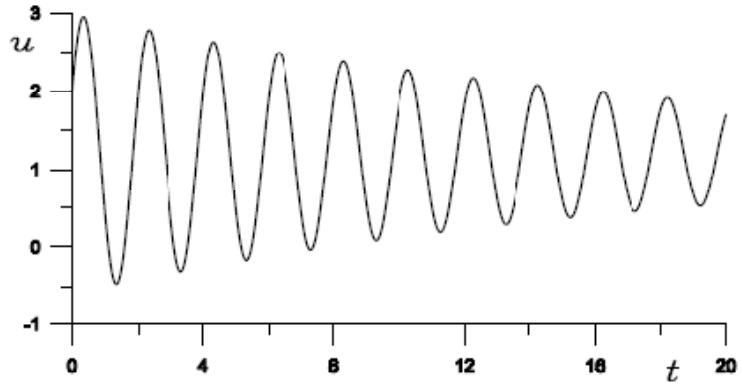

Fig. 159 - u(t) with $f = \bar{f}$=cost, $c < c_{cr}$

From Fig. 159 we can see that the mass oscillates around the static equilibrium's value $\bar{f}/k$ with an oscillation that dampens in the time.

As we saw before, without damping the mass has a medium position $\bar{f}/k$ and oscillates around this value without end. While, with the damping, the oscillations are going to end, taking back the structure in the position $\bar{f}/k$.

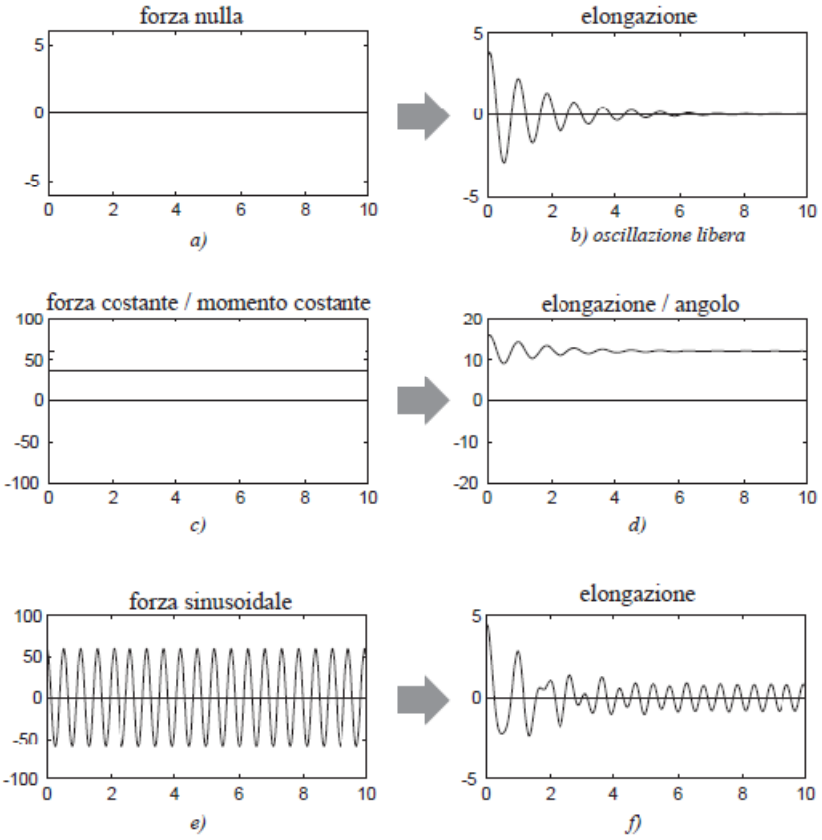

Fig. 160 - Oscillatory motions

In all vibratory systems there are resistive influences, those reduce the energy of the harmonic oscillator and the result is that the amplitude of the vibration decreases and the oscillator stops.

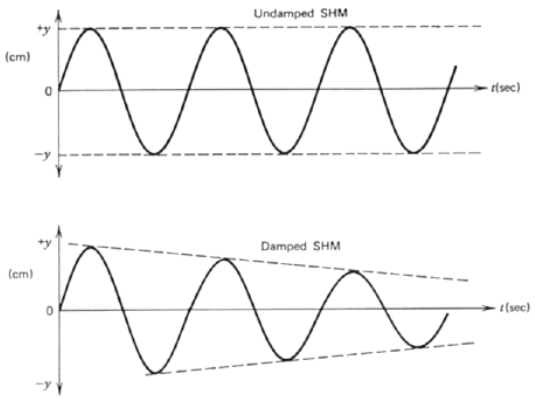

Fig. 161 - Undamped and damped oscillator

4.3 Straus analysis

Transient dynamic analysis is a technique used to determine the dynamic response of a structure, subjected to any arbitrary forcing function and initial conditions, under a time-varying load.

The time frame for this type of analysis is such that inertia or damping effects of the structure are considered to be important. Cases where such effects play a major role are under step or impulse loading conditions, for example, where there is a sharp load change in a fraction of time.

If inertia effects are negligible for the loading conditions being considered, a static analysis may be used instead.

We have to apply a load over a discrete amount of time dt.

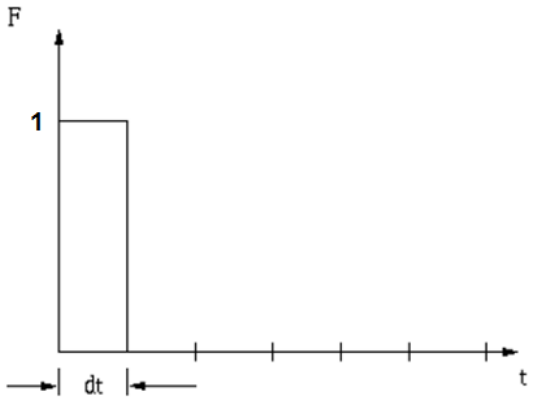

Fig. 162 - Load's law

After the application of the load, we track the response of the beam at discrete time points for as long as we like (depending on what it is that we are looking for in the response).

The size of the time step is governed by the maximum mode frequency of the structure we wish to capture. The smaller the time step, the higher the mode frequency we will capture.

Time Step Requirements Straus

Generally, given a maximum frequency of interest f_{max} the maximum time step should be small enough that about 10 sample points are taken through time in a single vibration cycle. Thus there should be 10 points per period. This means that the maximum accurate time step is given by:

$T_{min} = 1/f_{max}$.

$$\Delta t_{max} = \frac{T_{min}}{10} = \frac{1}{10\, f_{max}}$$

The termination of f_{max} requires some engineering judgment. For instance, if the structure exhibits natural modes up to 5 Hz which excite it globally, and the loading is a large load which is also likely to produce such a response, then perhaps including modes which are greater than 5 Hz is not important. So the time step could be set at a maximum of 1/50 Hz = 0,02 s.

On the other hand, if there is a vibrating machine which is likely to excite local modes in the structure, f_{max} may be taken as some frequency far enough above the forcing frequency to resolve the natural modes of the structure around the forcing frequency. This may produce a very fine time step requirement for transient analysis, which is why we provide alternative solvers (harmonic response, spectral response) to get fast solutions in such cases.

Between each time step in a transient analysis, the applied load is considered constant by the solver. This means that for an input table which has entries every N seconds, you should have an analysis time step of at most N/2 seconds for accurate integration of the loading through time.

If the time step is too large then much of the higher frequency response of the structure will be missed and the solution may not adequately represent the real behavior of the structure, see the figure below.

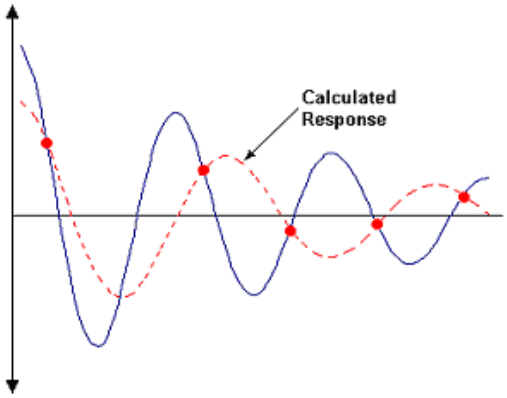

Fig. 163 - Time step too large

Linear dynamic equilibrium equations are in the following form:

$$[M]\{\ddot{x}(t)\} + [C]\{\dot{x}(t)\} + [K]\{x(t)\} = \{R(t)\}$$

Where:

- $[M]$ Mass matrix
- $[C]$ Damping matrix
- $[K]$ Stiffness matrix
- $\{x(t)\}$ Nodal displacement vector
- $\{\dot{x}(t)\}$ Nodal velocity vector (first derivative of $\{x(t)\}$)
- $\{\ddot{x}(t)\}$ Nodal acceleration vector (second derivative of $\{x(t)\}$)
- $\{R(t)\}$ Load vector

4.4 Forcing function

Two types of loading conditions can be applied: dynamic loads and base acceleration excitation.

- Dynamic loads applied to the model are factored by factor vs time tables, which can be any time history. Loads can be point forces and moments, element loads, body loads or thermal loads. Multiple freedom cases may also be included if the full system option is used. The constant terms in the freedom cases may be factored in the same way as the loads in the load cases, this provides support for time dependent displacements.
- Acceleration of the base of the model may be specified to define the excitation, that may act in any general direction defined through the direction vector. The time history can be arbitrary and is specified in the factor vs time table.

In this analysis a dynamic load approach is used.

4.5 Initial conditions

Four types of initial conditions can be specified:

- A linear static solution which specifies the displacement of a structure initially under certain static loads.
- A transient solution, which specifies the dynamic response of the structure at a time instance. The solution will start from any selected time step.
- Initial velocity and acceleration of all free nodes in the structure.
- Initial velocity and zero acceleration as specified independently at each node in one or more load cases.

4.6 Solution techniques

Two approaches to transient dynamic solutions are available:

1. Mode Superposition

Using the mode superposition method, responses of the individual modes of the structure are calculated separately and then combined to produce the total response of the structure. This is only applicable to linear transient dynamic analysis.

In addition to the other advantages of the mode superposition technique, this method offers more in a transient dynamic analysis. One of the advantages is that modal damping can be used in addition to Rayleigh damping. When experimental data is available, modal damping gives a more accurate representation of the damping in the system.

The mode superposition method is best suited to structures where the lower frequencies dominate the response (i.e. earthquakes). Typically, 10 modes will provide good accuracy for these problems. Modal superposition is not suitable for problems such as shock loads or impacts where the higher

frequency modes are excited. In these cases, 50 or more modes may be required and the cost to calculate this many modes can significantly offset the saving in the transient solution. The most serious disadvantage of this approach is that it is not capable of handling any nonlinearity in the solution.

2. Full System

This approach does not have the limitations of mode superposition, but can be computationally very expensive, as all nodal displacements are numerically integrated at the specified time steps. This method is also referred to as direct integration.

The Linear Transient Dynamic Solver performs the following steps:

a) Initializes the nodal displacement, velocity and acceleration vectors according to the specified initial conditions.
b) For mode superposition calculates and assembles equivalent element force vectors and external nodal force vectors. If base acceleration is included, the global mass matrix is also formed for the calculation of the pseudo load vector.
c) For direct integration, calculates and assemble element stiffness, mass and damping matrices, equivalent element force vectors and external nodal force vectors. In the stiffness calculation, material temperature dependency is considered (see Temperature). The element geometric stiffness matrix is also included if initial conditions are used. Rayleigh damping and element material damping can be included (see Damping). Either consistent or lumped element equivalent load vectors can be calculated according to the option setting (see Element Load). Constraints are also assembled in this process, and the constant terms in enforced displacement and shrink links are combined and applied (see Enforced Displacements and Shrink Links). At the end of this assembly procedure, the three global matrices in the equation of dynamic equilibrium are formed.
d) Loops through the specified time steps and calculates displacement, velocity and acceleration using either the Wilson theta or Newmark beta method (see Time Integration). When base acceleration is applied, either relative or absolute values of displacement, velocity and acceleration may be calculated.
e) Calculates element results such as stress and strain.

In the fem model the studied cable is taken out and the correspondent axial force is put in the two ending points instead of that cable. The force is obtained from the static analysis, in particular from the linear combination of two different forces: self weight of the bridge and the pretension values in the cables.

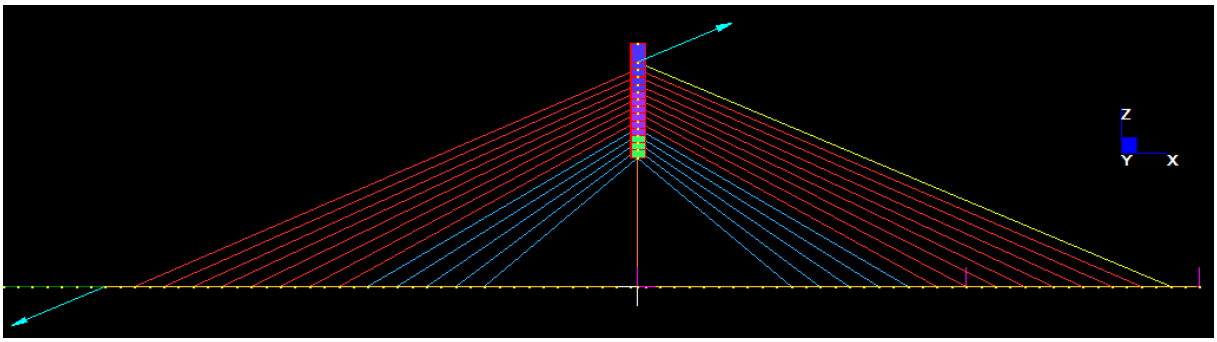

Fig. 164 - Reaction force applied instead of the cable

Model	Axial force N (N)	Horizontal component Fx (N)	Vertical component Fz (N)
Beams model	147898,3774	136375,417	57233,5187
Beams model with masses	2499292,331	2304569,124	967172,8451
Plates model	120730,7357	111324,4427	46720,2206

Tab. 27 - Static forces applied in the models

The axial force applied to the cable follow the function given by a factor vs time table with a unitary value of the force, see the figure below.

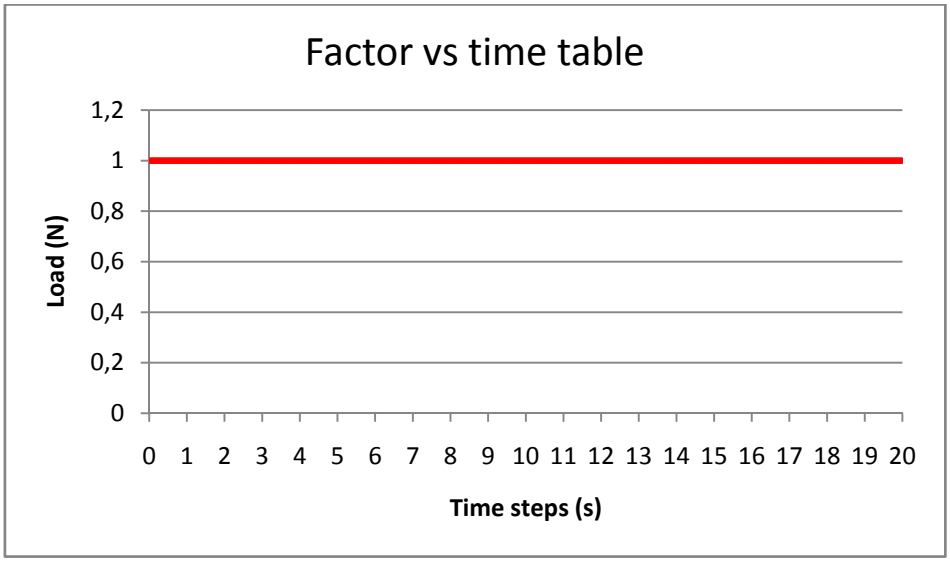

Fig. 165 - Load vs time table

4.7 Rayleigh damping

In dynamic analysis of structures and foundations, damping plays an important role. However due to the limitation in our knowledge about damping, the most effective way to treat damping within modal analysis framework is to treat the damping value as an equivalent Rayleigh Damping in form of:

$$[C] = \alpha[M] + \beta[K]$$

in which:

[C] = damping matrix of the physical system;

[M] = mass matrix of the physical system;

[K] = stiffness matrix of the system;

α and β are pre-defined constants.

The major advantage gained in converting the damping matrix into an equivalent Rayleigh damping lies in the fact that using orthogonal transformation a structure having n degrees of freedom can be reduced to n-number of uncoupled equations. However, for systems with large degrees of freedom, it is difficult to guess meaningful values of α and β at the start of the analysis.

As such in most of the practical engineering analysis the analyst makes simplifying assumptions in selecting damping ratios (constant for all significant modes) based on his experience or standard literature that would hopefully be valid for the overall system. It is a fact that modal mass participation decreases with increase in modes.

A system having multi-degrees of freedom, the equation of motion under externally applied time dependent force is given by:

$$[M]\{\ddot{X}\} + [C]\{\dot{X}\} + [K]\{X\} = \{P_t\}$$

Where $\{P_t\}$ is the force vector which is a function of time.

The orthogonal transformation of the damping matrix reduces the matrix [C] to the form:

$$2\xi_i\omega_i = \alpha + \beta{\omega_i}^2$$

This, on simplification reduces to:

$$\xi_i = \frac{1}{2}\left(\frac{\propto}{\omega_i} + \beta * \omega_i\right)$$

Where ω_i are the frequencies that involve the major part of the structure's mass and ξ is the damping ratio in uncoupled mode.

From the previous equation it can be observed that the damping ratio is proportional to the natural frequencies of the system.

For the linear dynamic analysis is used the Rayleigh damping, which is assumed to be proportional to the mass and stiffness matrix. It only offers two damping coefficients which only makes correct tuning of two modes possible and possibly leads to unrealistic damping levels of the remaining modes.

The two coefficients are calculated for the three models by the previous formula, assuming the damping value equal to ξ = 1 %, value used for concrete structures under the splitting limit.

Model	ω1 (Hz)	ω2 (Hz)
Beams model	1,105	1,54
Beams model with masses	0,8973	2,497
Plates model	2,509	4,082

Tab. 28 - Frequencies used for Rayleigh coefficients

Model	α	β
Beams model	0,012867	0,007561
Plates model	0,031078	0,003034
Beams model masses	0,013202	0,005892

Tab. 29 - Rayleigh coefficients

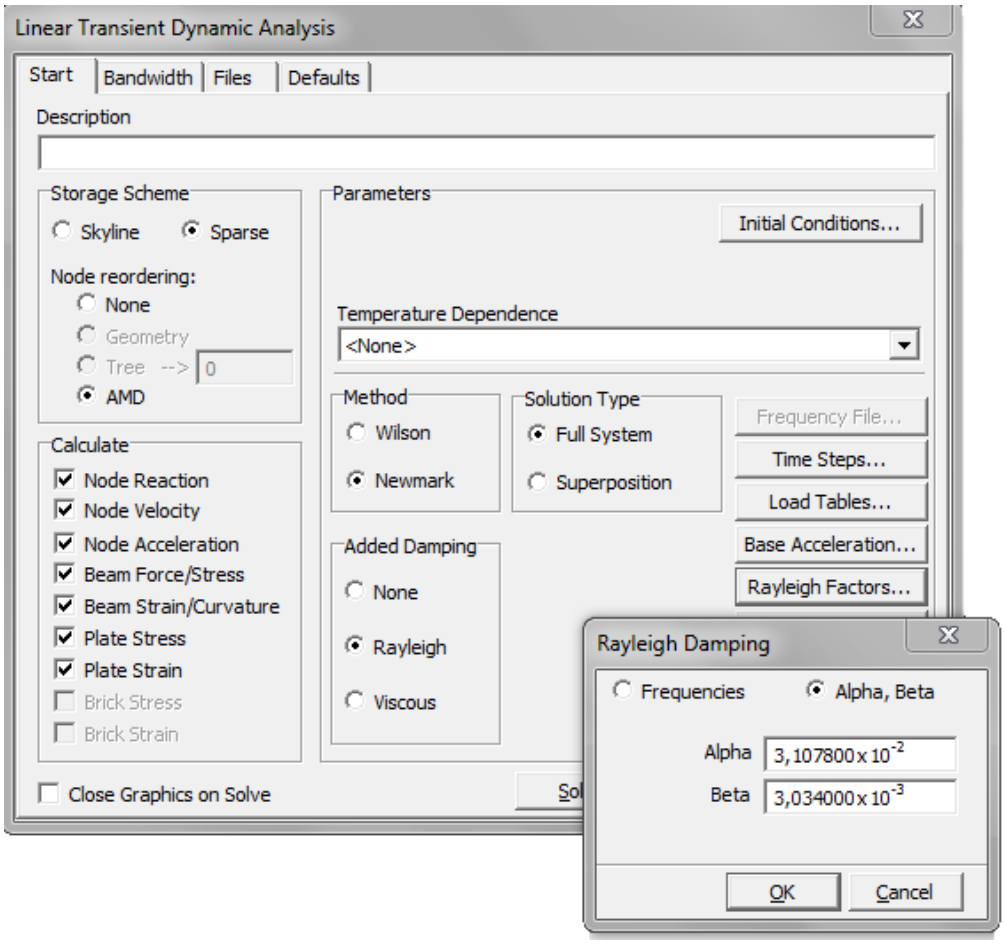

Fig. 166 - Linear transient dynamic solver (plates model)

- ***Beams model results***

The dynamic study of the break cable is studied in some particular points of the deck, near the missing cable, as shown in the figure.

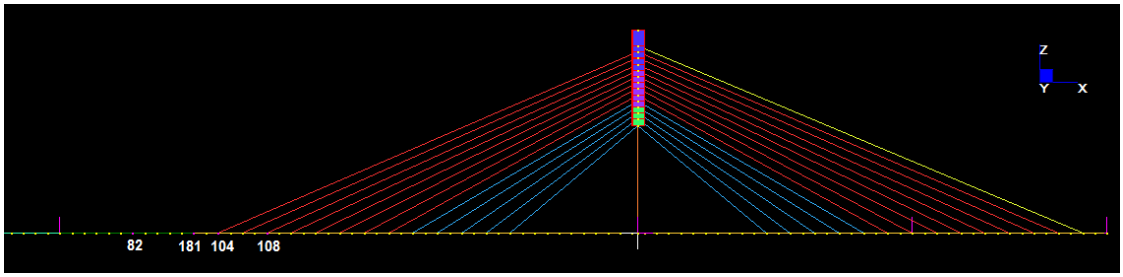

Fig. 167 - Points of study in the cross section (beams model)

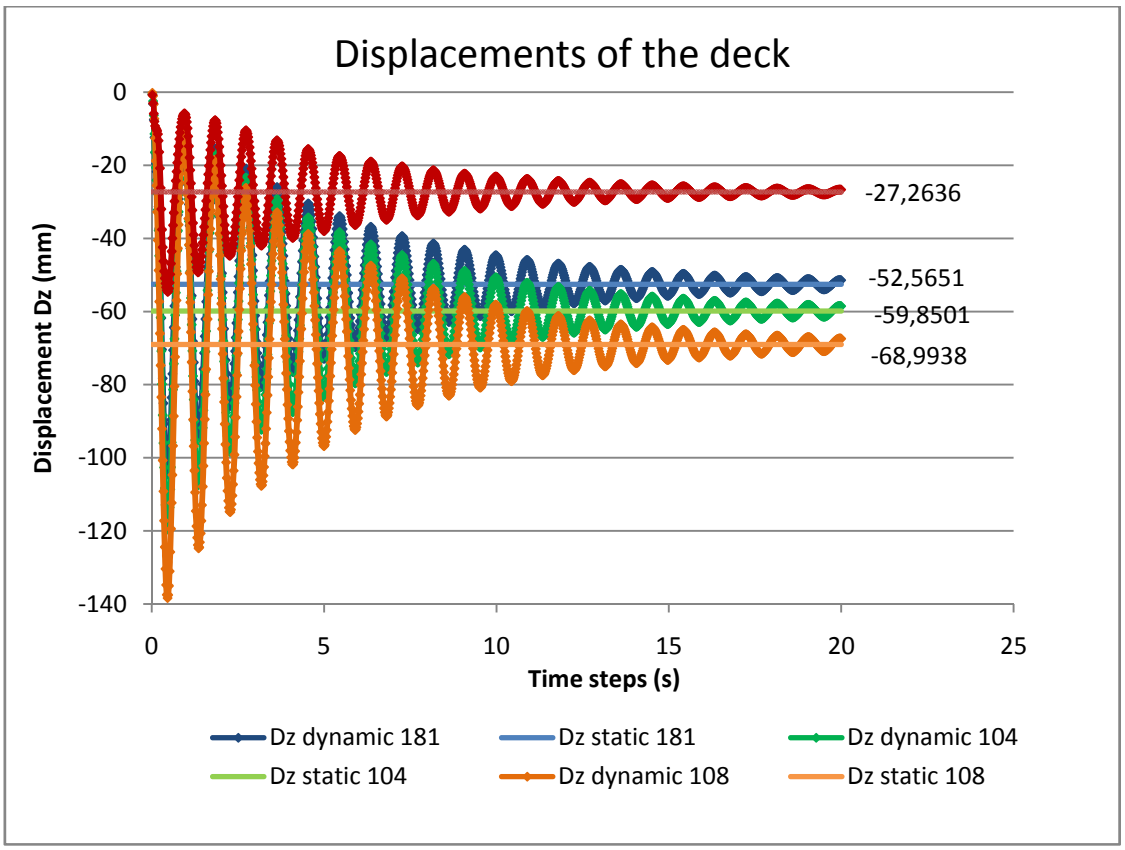

Fig. 168 - Displacements of different points in the deck (beams model)

- ***Beams model with non structural masses results***

For the beams model with the masses, the same points in the deck are studied.

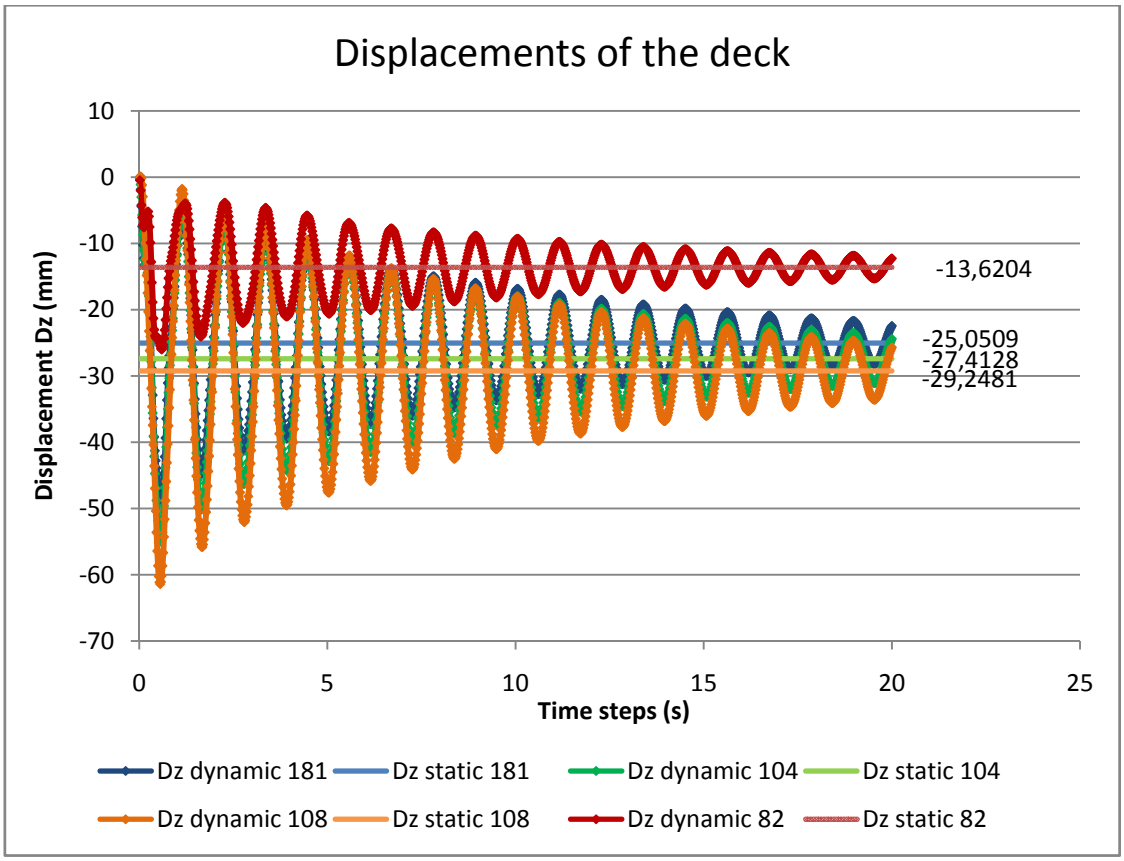

Fig. 169 - Displacements of different points in the deck (beams model with masses)

- ***Plates model results***

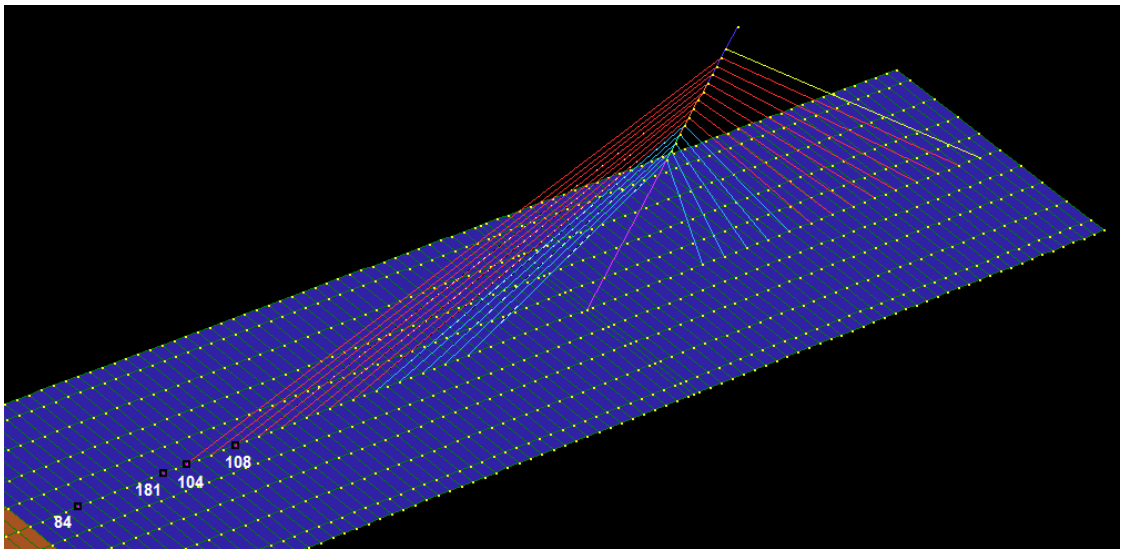

Fig. 170 - Some studied points for the dynamic analysis (plates model)

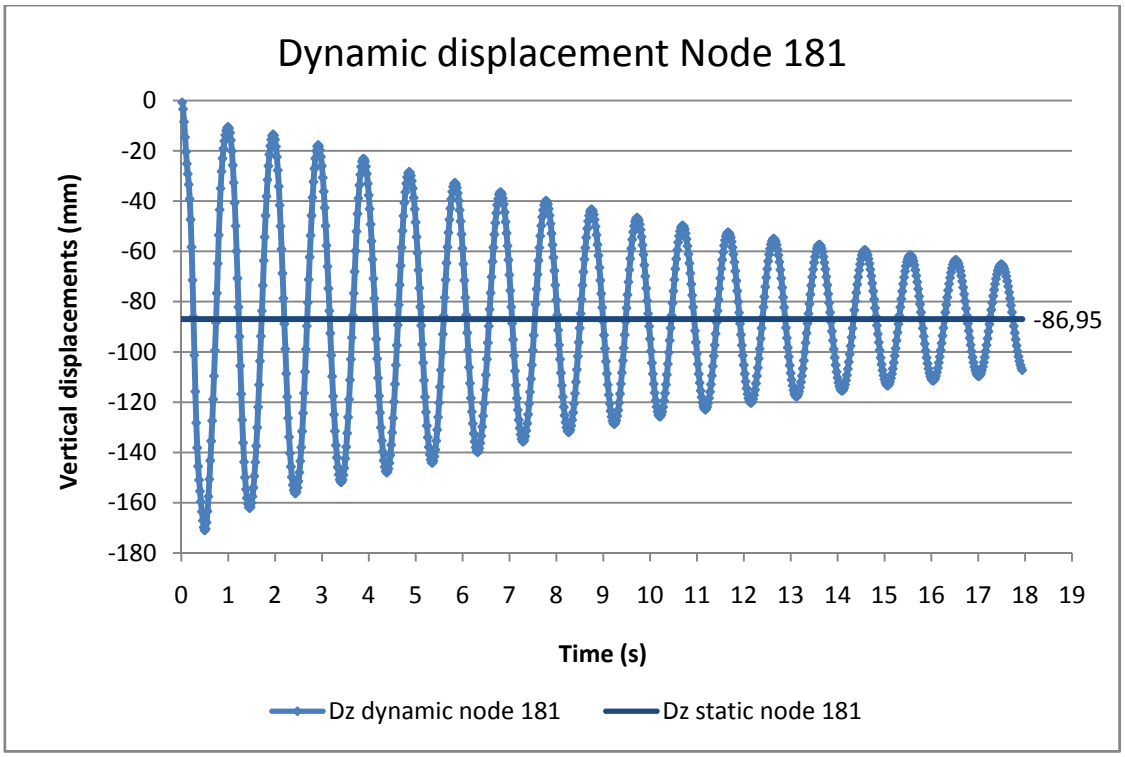

Fig. 171 - Displacements of node 181 in the linear dynamic analysis (plates model)

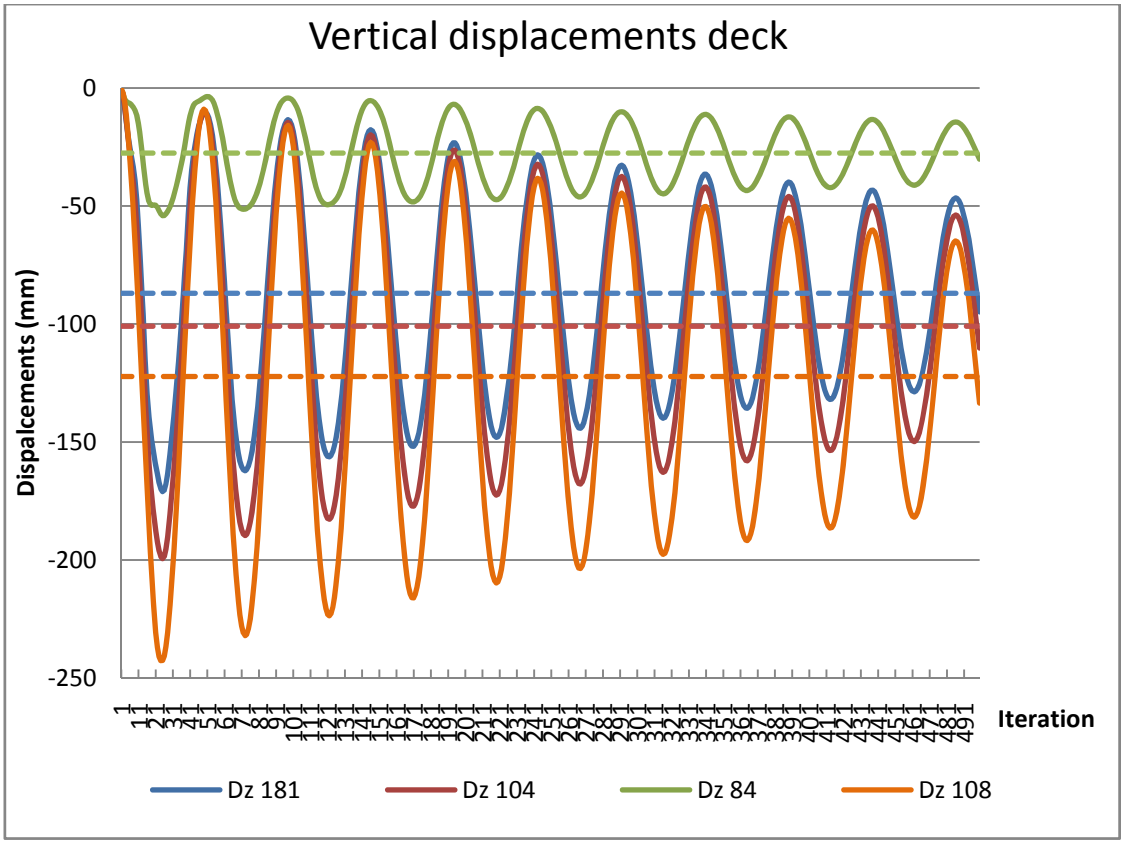

Fig. 172 - Displacements of different points in the deck (plates model)

- ***Dynamic results for the pylon***

In the following figures the studied points are shown.

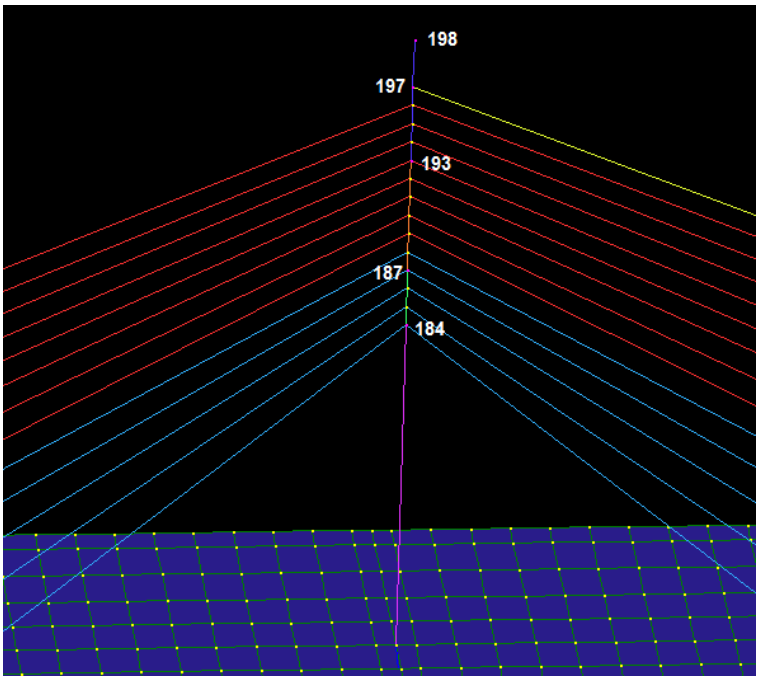

Fig. 173 - Points of study in the pylon

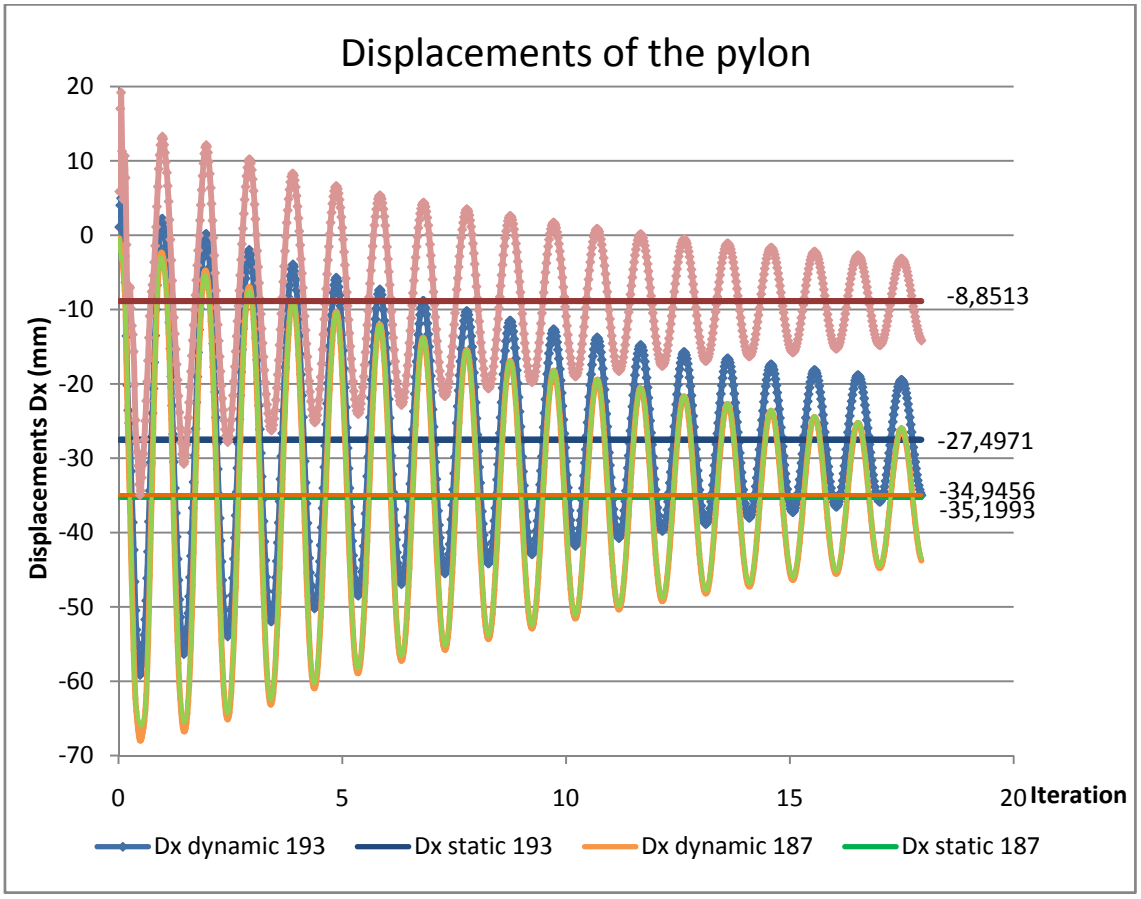

Fig. 174 - Displacements of different points in the pylon

5. VEHICLES VIBRATION

Vibration is a mechanical phenomenon whereby oscillations occur about an equilibrium point. The oscillations may be periodic such as the motion of a pendulum or random such as the movement of a tire on a gravel road.
Vibration is occasionally "desirable". More often, vibration is undesirable, wasting energy and creating unwanted sound. For example, the vibrational motions of engines, electric motors, or any mechanical device in operation are typically unwanted; careful designs usually minimize unwanted vibrations.

The vibrations caused by the passage of vehicles have become an important consideration in the design of bridges, in particular the interaction problem between the moving vehicles and the bridge.
This is in part due to the rapid increase in the proportion of heavy vehicles and high-speed vehicles in highway and railway traffic, as well as the trend towards high-performance materials and therefore more slender sections for the bridges.

The goal of the bridge engineer is to design economical structures which are safe, durable, and serviceable. Determination of the dynamic response of bridges has been the topic of numerous studies in recent years. Much of the attention has been focused on maximum dynamic displacements and moments and on the distribution loads to the floor system - information necessary to design for adequate strength. Problems associated with the rapid deterioration of bridge decks have also attracted the interest of researchers.
Another important concern, the comfort of those crossing the bridges, has received relatively little attention.

Vehicle-bridge interaction is a complex dynamic phenomenon, depending on many parameters. These parameters include the type of bridge and its natural frequencies of vibration, vehicle characteristics, vehicle speed and traversing path, the number of vehicles and their relative positions on the bridge, roadway surface irregularities, the damping characteristics of bridge and vehicle, etc.
The first recorded research into bridge vibration appears to be a report published in 1849 by Willis, which discussed the reasons for the collapse of the Chester Railway Bridge.
The moving-force model, the moving-mass model and the moving-vehicle model are three common choices used in the studies.
The moving-force model, in which a vehicle is modeled as a force, is the simplest model whereby researchers can capture the essential dynamic characteristics of a bridge under the action of a moving vehicle, but the interaction between the vehicle and bridge is ignored. Where the inertia of the vehicle cannot be regarded as small, a moving-mass model, in which a vehicle is modeled as a

mass, is often adopted. However the moving-mass model suffers from its inability to consider the bouncing effect of the moving mass, which is significant in the presence of road surface irregularities or for vehicles running at high speeds. At last in the moving-vehicle model, a vehicle was modeled as a single-axle or multi-axle mass-spring-damper dynamic system.

Pavement surfaces of roads on bridges have some irregularities, however, carefully they are prepared. It may be attributed to the inaccuracies in casting concrete, assembling pre-cast segments and the subsequent overlaying of water proofing membrane and bituminous surfacing. Newly constructed pavement may be poorly finished or may have design features, such as construction joint, thermal expansion joints, etc. Pavements that have been in-service for sometimes often develop localized distresses due to application of heavy wheel load and environmental changes. Moving vehicles exert fluctuating forces on the bridge deck caused by its vibration resulted from surface unevenness.
The fluctuating nature of the dynamic wheel load with increase in number of load repetitions may cause pavement degradation and fatigue damage.

Many studies have been reported for the analysis of bridge response due to vehicles passing over at constant and variable speed. The development and application of computers opened up new and practically unlimited possibilities for the exact solution for highly statically indeterminate systems.

5.1 Introduction to Program Prejezdy

The purpose of Program Prejezdy, software for vehicle passages of Prof. Polak Micha, is the cognition of dynamic effects caused by the transport of the structures. It is used to simulate the interaction between the traffic flow and the bridge and was implemented for the last 25 years in the CTU, Faculty of Civil Engineering in Prague.

In this study, a vehicle-bridge system is divided into two subsystems: the vehicle subsystem and the bridge subsystem. Dynamic equilibrium equations for each of these two subsystems are then established. The connection between these two subsystems is considered by the wheel-street contact condition.

5.1.1 Model of vehicle

A vehicle is a complex mechanical system, which is modeled by the suitable plane or space (Fig. 175) model to determine the vertical vehicle effects on the bridge structure by their interaction. In the formulation of the physical model of the analyzed system it is necessary to abandon the formerly used simple vehicle models (one or two d.o.f) and to introduce into the computation more adequate models of vehicles as planar or space systems of n degrees of freedom.

The model formulation for the vehicles is based on the following simplifies assumptions:

- the model is based on the small deformation theory;
- the vehicle consists of a system of rigid bodies or plates and mass points mutually interconnected by deformable massless links acting in vertical direction only;
- the mutual horizontal displacement of the individual members is prevented by the design;
- the masses of wheels are concentrated in mass points.

The vehicle is modeled as a non linear dynamic system of mass elements mutually interconnected by massless force links.
In particular the vehicle used is a track TATRA T815: three axle trucks with 230 KN gross weight.

For a sprung mass system moving along the bridge deck, two equations of motion have to be solved simultaneously. The first equation represents the dynamic equilibrium for the bridge. The second equation is for the dynamic equilibrium of the sprung mass system. The interaction force between the pavement and the sprung mass system depends upon the deck displacement. Hence the two equations are coupled and need to be solved simultaneously.
The coupled sets of equations of motions are solved by using Newmark-β with predictor–corrector algorithm.

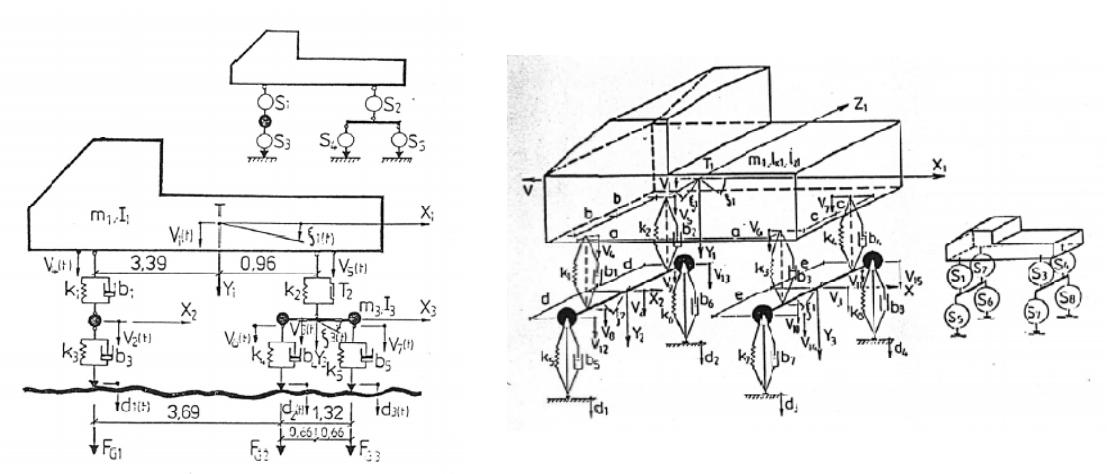

Fig. 175 - Plane and space model of the truck type TATRA T815

5.1.2 Procedure of calculation of the bridge response

The moving load of the bridge is modeled as a traffic flow, a group of real vehicles. The vehicles are modeled as a non linear space system of mass elements mutually interconnected by immaterial force links by means of the component element method.
Since the position of the vehicles on the bridge is the function of time, also the position of points of contact varies in time. The displacements of the structure and the unevennesses of the carriageway

surface in points of contact also vary in time. In this way a kinematics excitation of the vehicles takes place which, in return, influences the bridge structure by its forces.

The response of the modal model under the both dynamic and static influence of the moving load is calculated by the method of the expansion with the respect to the modes of natural vibration. The system of differential equations of motion both the bridge and the vehicles is integrated by direct (step by step) method. The central difference method is used.

5.2 Applications of Program Prejezdy

The main screen shows the available options of the software.

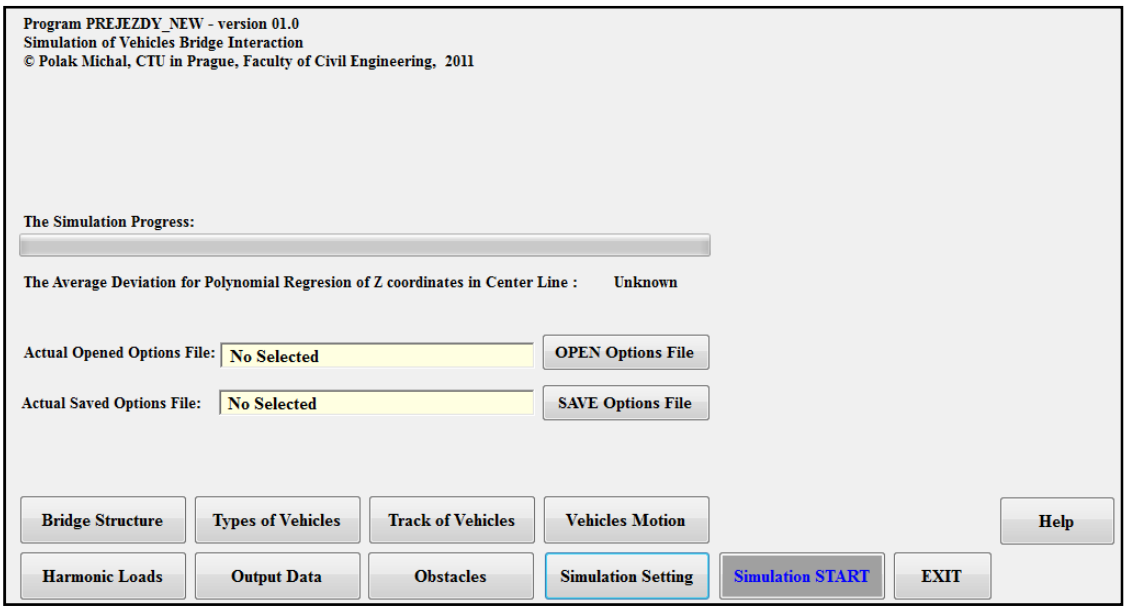

Fig. 176 - Main screen of Polàk software

Throw an excel file, reporting the coordinates of all the nodes of the fem model, the modes of vibration and the relative displacements and rotations, it was possible to import the fem model into this software.

The importation screen appears as in Fig. 177.

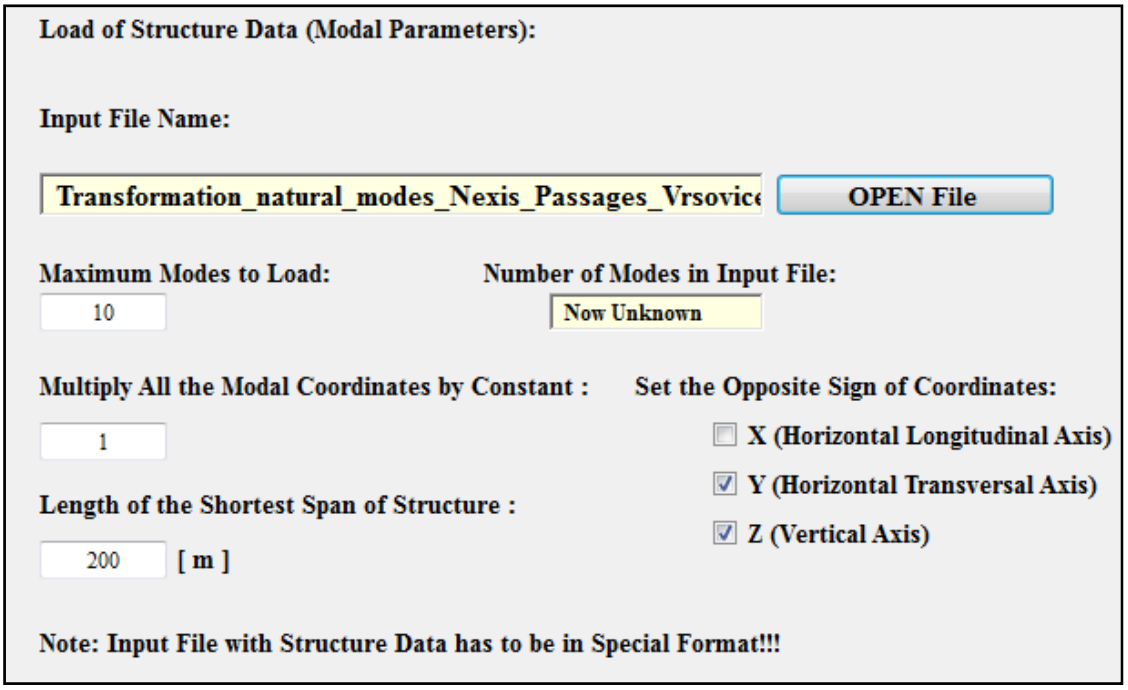

Fig. 177 - Importation screen

It is possible to define the vehicles motion (speed, position, type) like in the figure below.

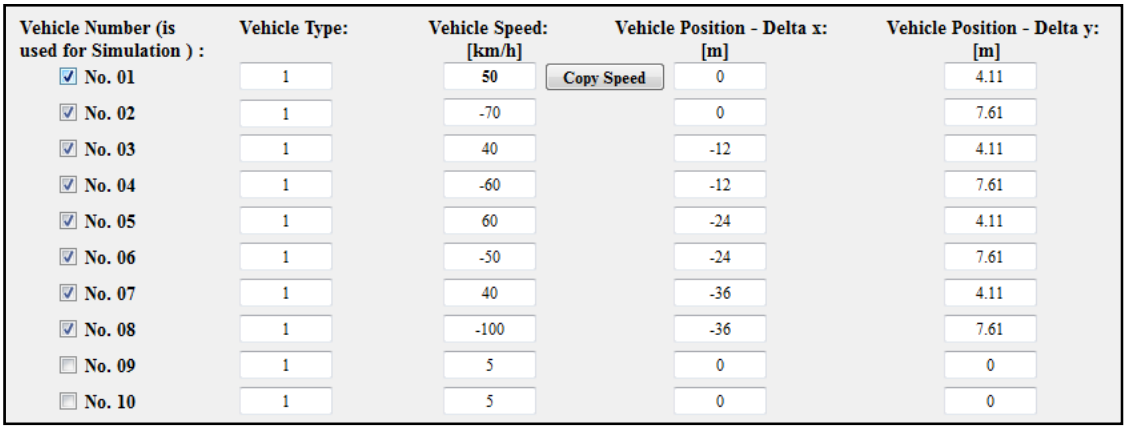

Fig. 178 - Vehicles motion

The kind of roughness is fixed as the following, no obstacles are positioned in the road.

The random unevennesses of the carriageway surface in the computation can be simulated on the basis of the measurements on the carriageway surface by the use of a two-parametric random unevennesses generator. The principal characteristics are the depth and the length of unevennesses.

The standard obstacle imitates a deterministic solitary unevennesses on a carriageway surface.

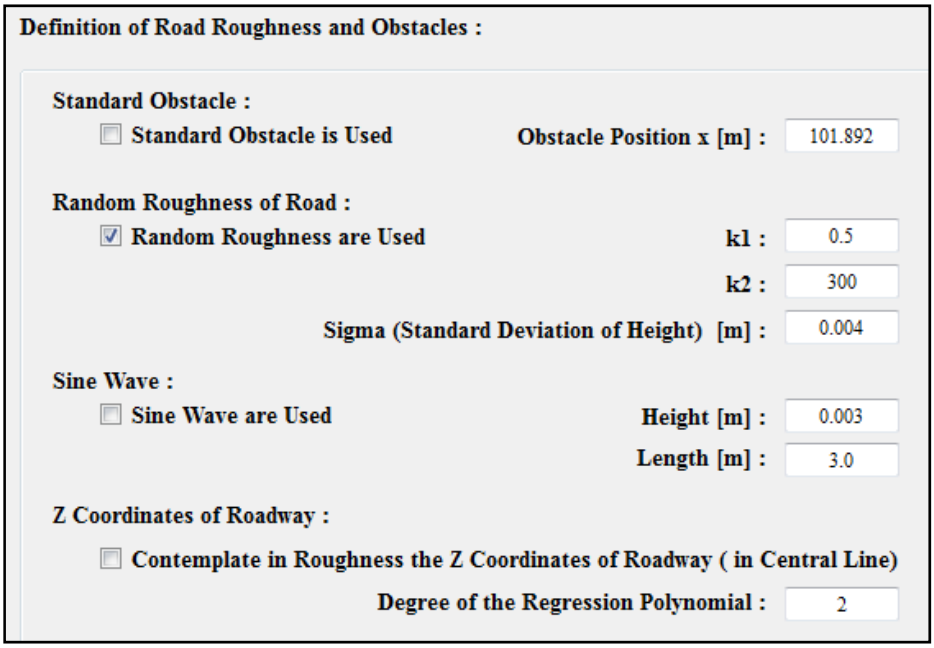

Fig. 179 - Road roughness and obstacles

In the last step, it is necessary only to define the output points, where we are interested in the study of vibrations, and the simulation parameters.

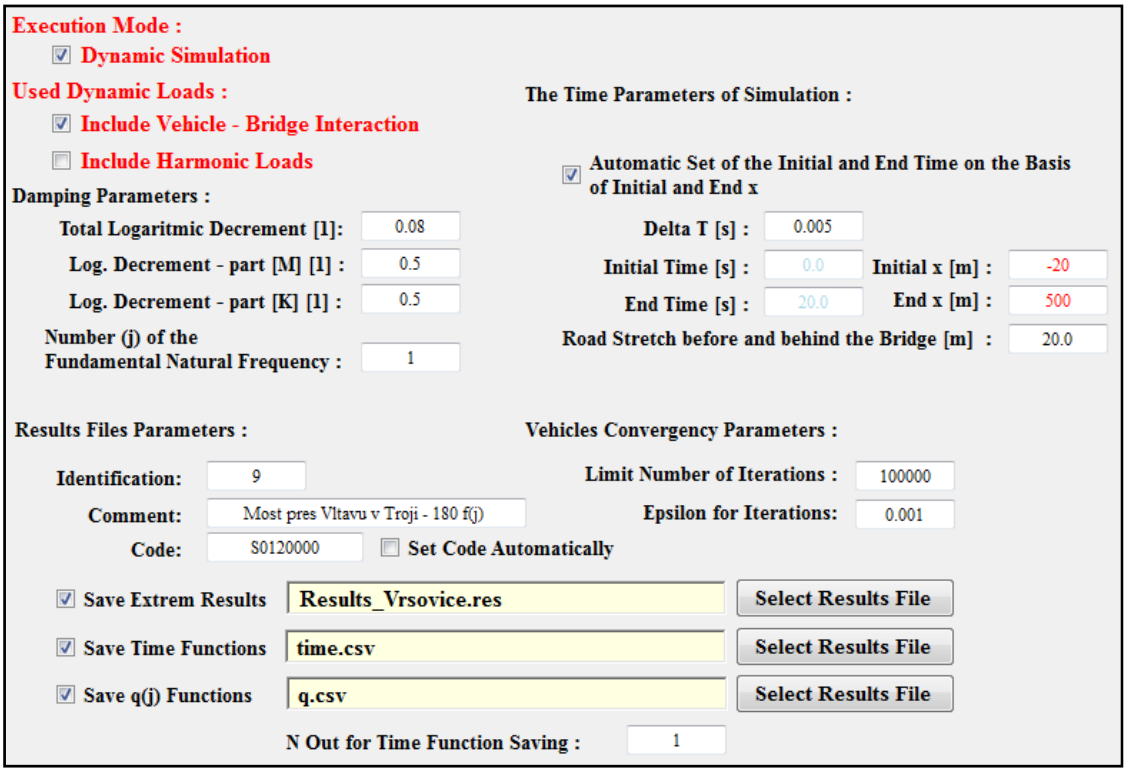

Fig. 180 - Definition of simulation parameters

The dumping parameters are defined as:

- Total logarithmic decrement equal to 0.08, estimate values for concrete bridge;
- Log. Decrement - part [M] means the α coefficient for the mass;
- Log. Decrement - part [K] means the β coefficient for the stiffness.

The software gives three kinds of output files: two excel files and one graph.

One excel file displays the vertical displacements of the deck during the time, the other one contains the multiplicative values of the vertical displacements for each mode of vibration.

The graph shows the progress of the vertical displacements throw the time in all the chosen points.

5.3 Analyzed cases of traffic

The response of the bridge structure was measured in the selected network of points on the upper bridge surface (see Fig. 181). The total number of network points was 104, 26 points in four lines of the cross section.

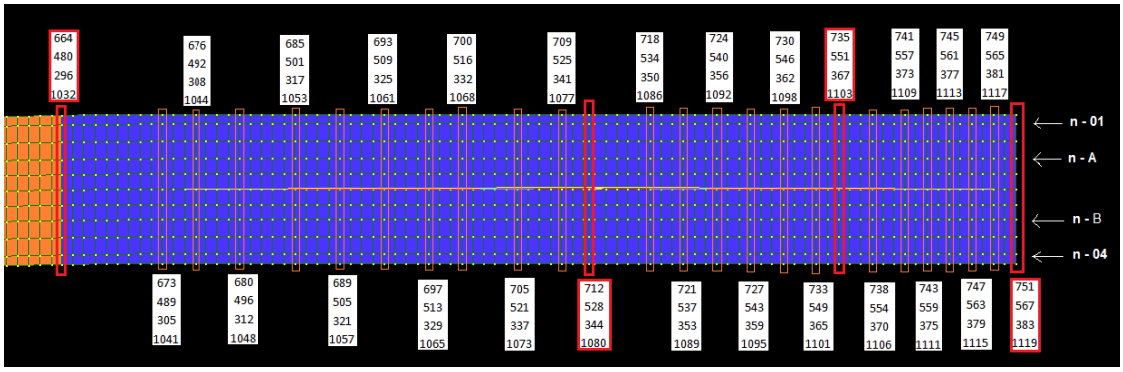

Fig. 181 - Analyzed sections for the vibration

The output of the software is defined for 4 kinds of points in each cross section, as shown in the figure below.

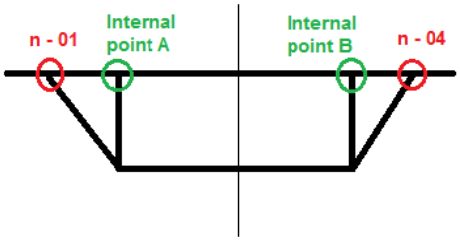

Fig. 182 - Output points in each cross section

5.3.1 Case 1: two vehicles in the same direction at 50 Km/h

The first case studies the behavior of the bridge under two vehicles at 50 km/h along the longitudinal dimension of the bridge, running parallel.

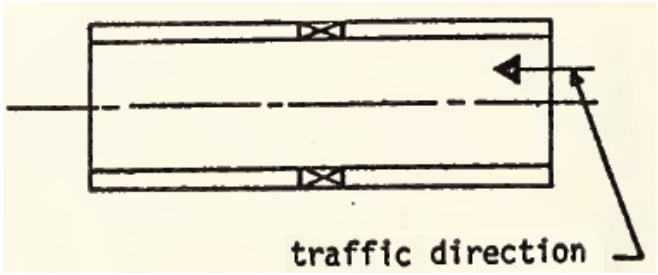

Fig. 183 - Traffic's direction

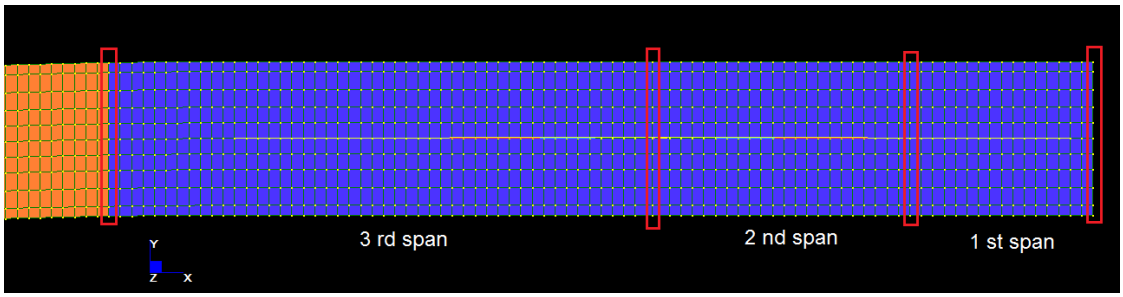

Fig. 184 - Definition of the spans

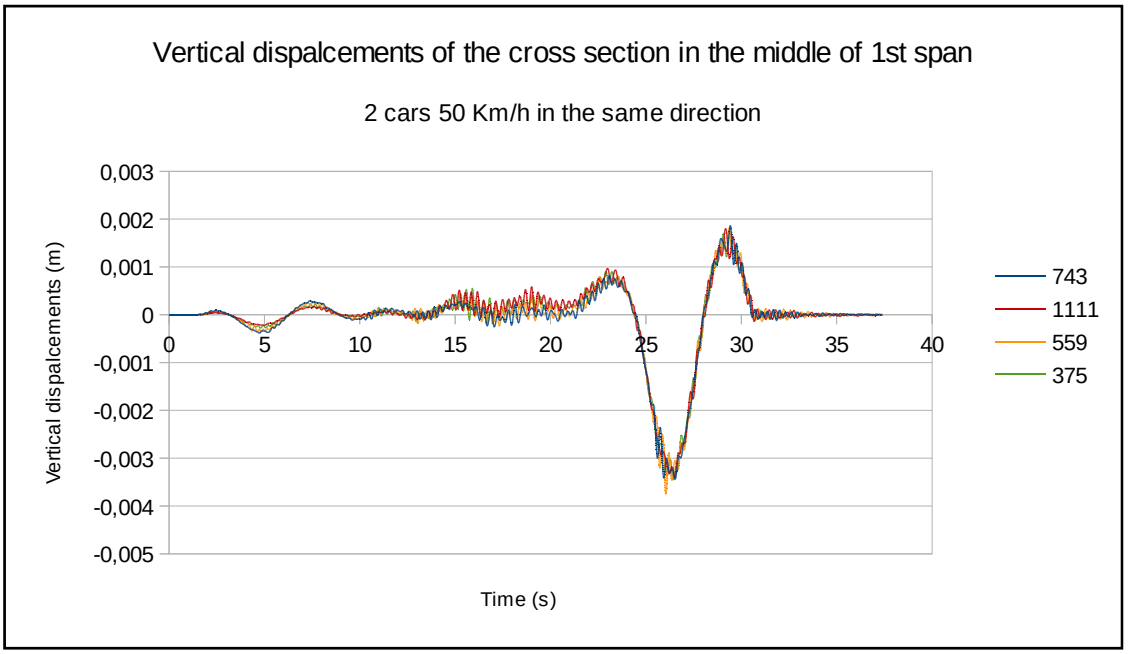

Fig. 185 - Vertical displacements of the cross section in the middle of the 1st span (case 1)

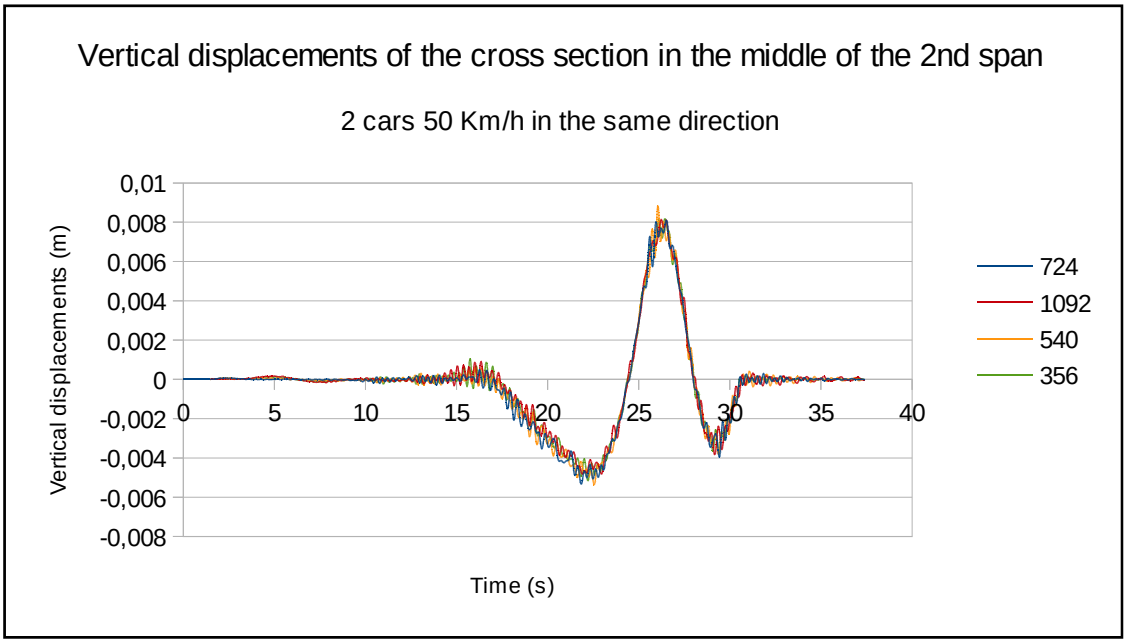

Fig. 186 - Vertical displacements of the cross section in the middle of the 2nd span (case 1)

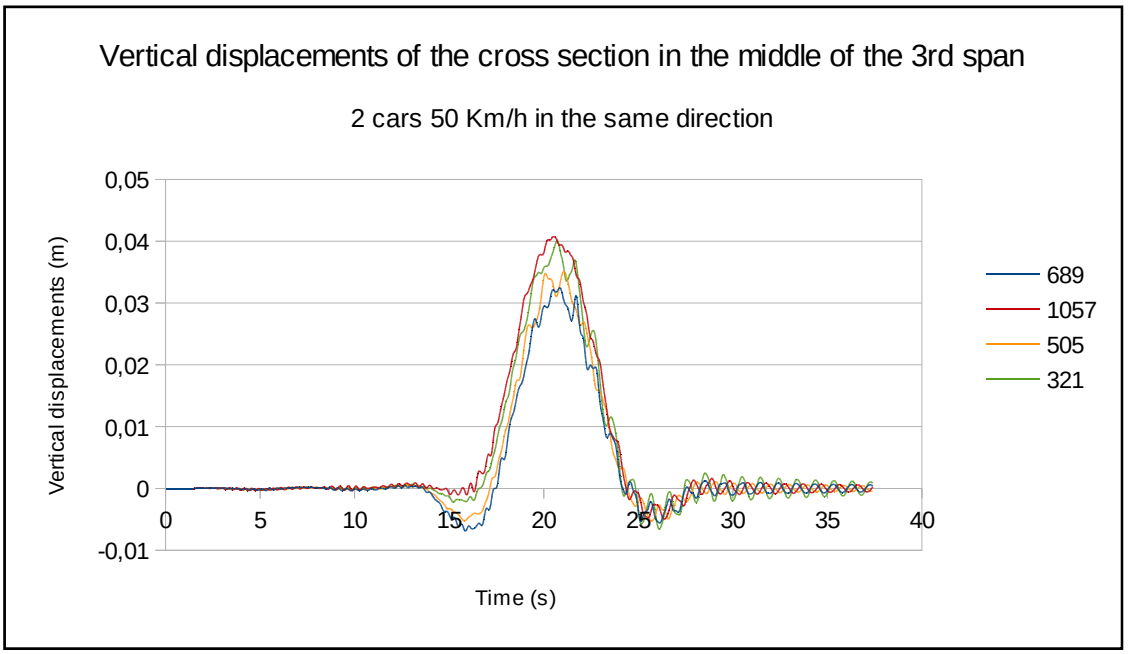

Fig. 187 - Vertical displacements of the cross section in the middle of the 3rd span (case 1)

In the following pictures different kinds of diagrams are reported to represent:

- the time history at a certain point of the bridge;
- the maximum and minimum values of the transversal dynamic deflection induced at different points along the bridge;
- the dynamic deflection induced at different points along the bridge at particular instants of time.

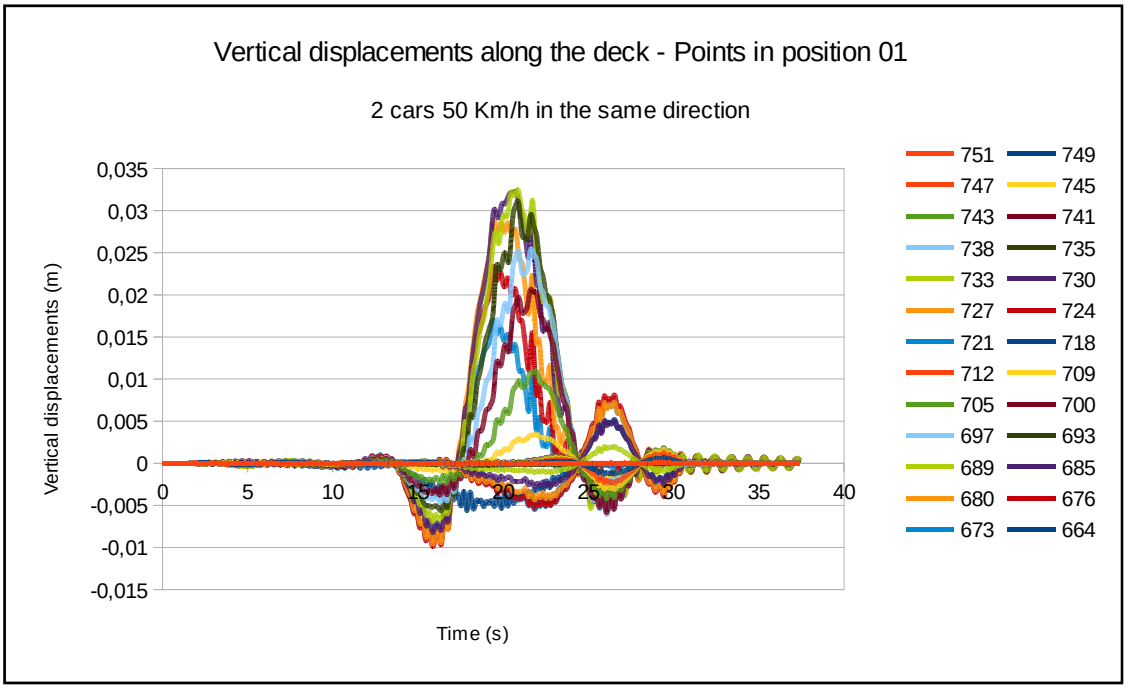

Fig. 188 - Vertical displacements along the deck - Points in position 01 (case 1)

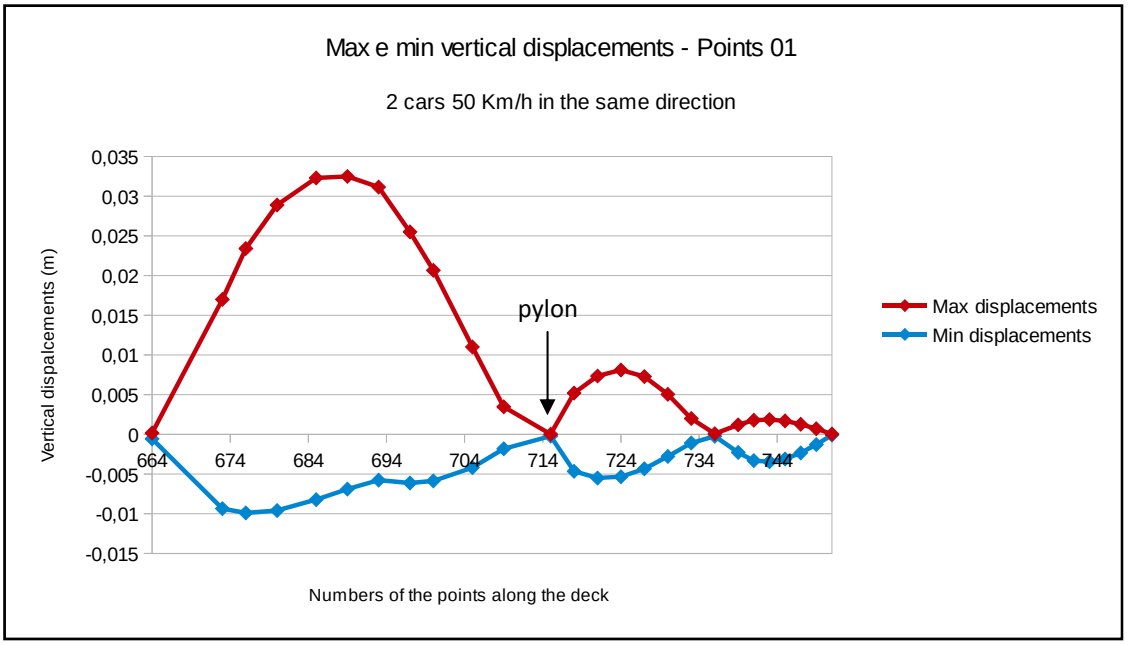

Fig. 189 - Max e min vertical displacements - Points 01 (case 1)

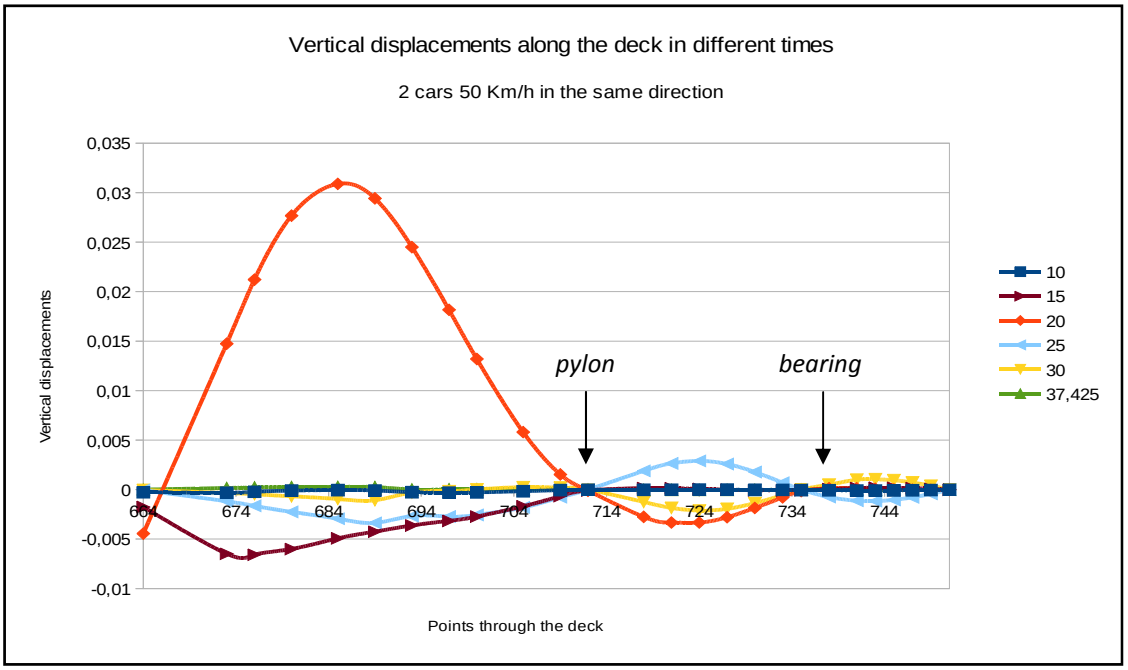

Fig. 190 - Vertical displacements along the deck in different times - position 01 (case 1)

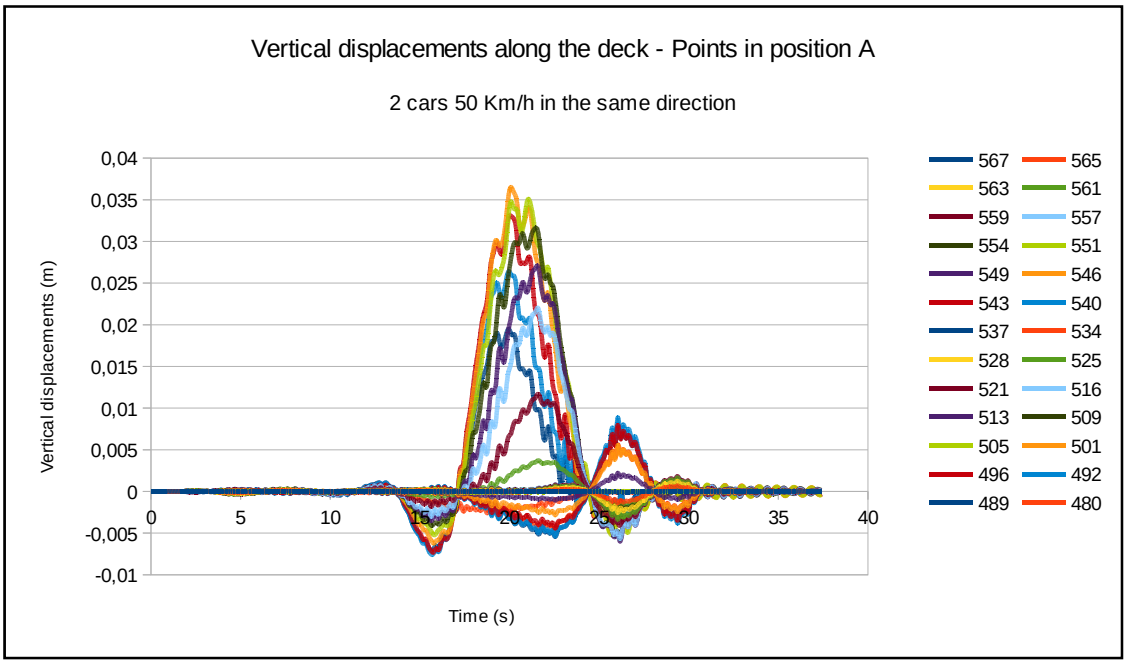

Fig. 191 - Vertical displacements along the deck - Points in position A (case 1)

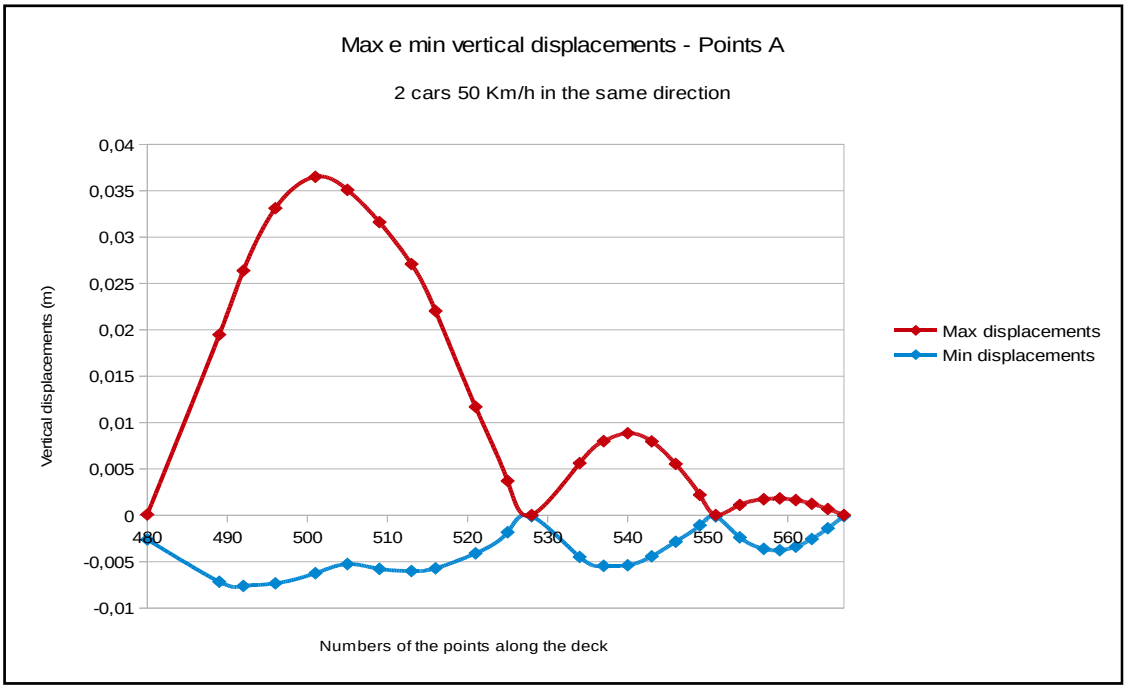

Fig. 192 - Max e min vertical displacements - Points A (case 1)

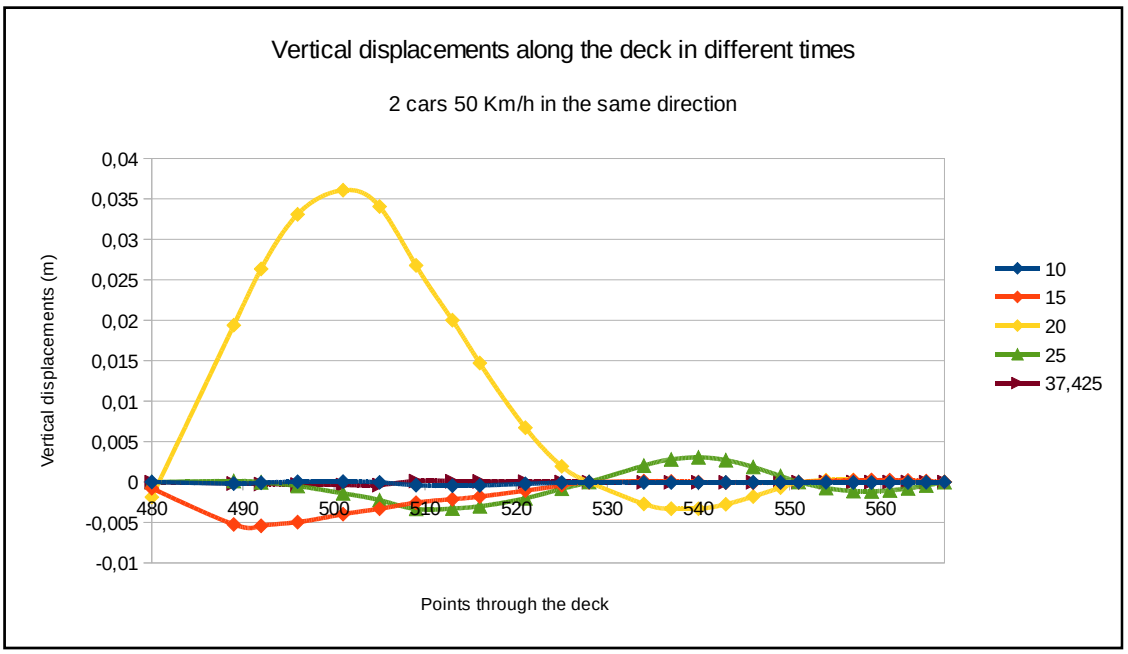

Fig. 193 - Vertical displacements along the deck in different times - position A (case 1)

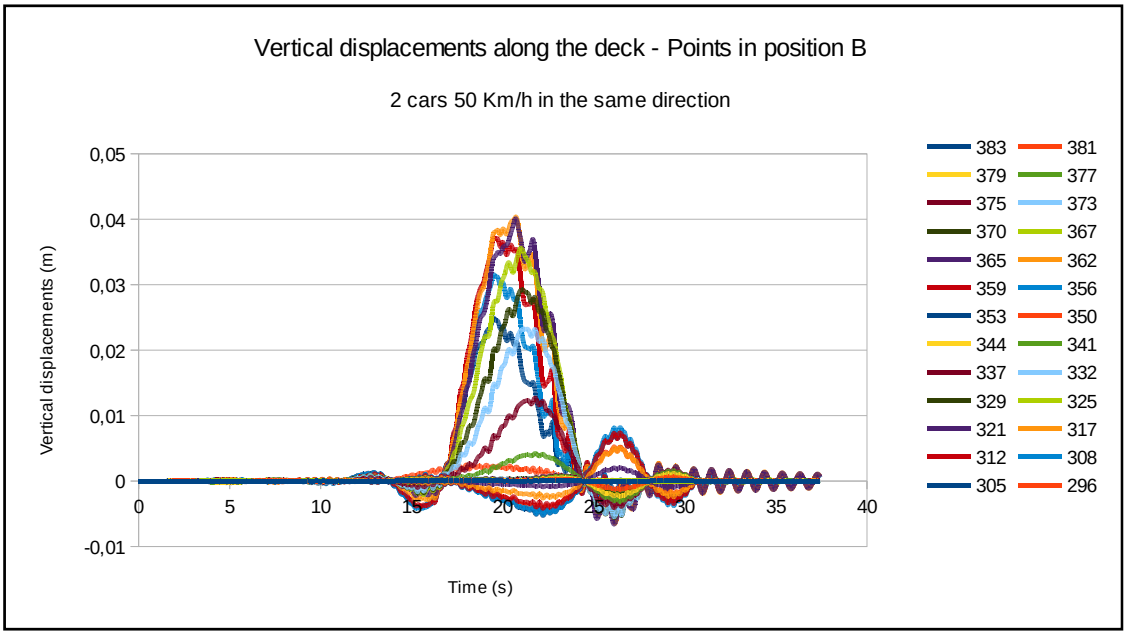

Fig. 194 - Vertical displacements along the deck - Points in position B (case 1)

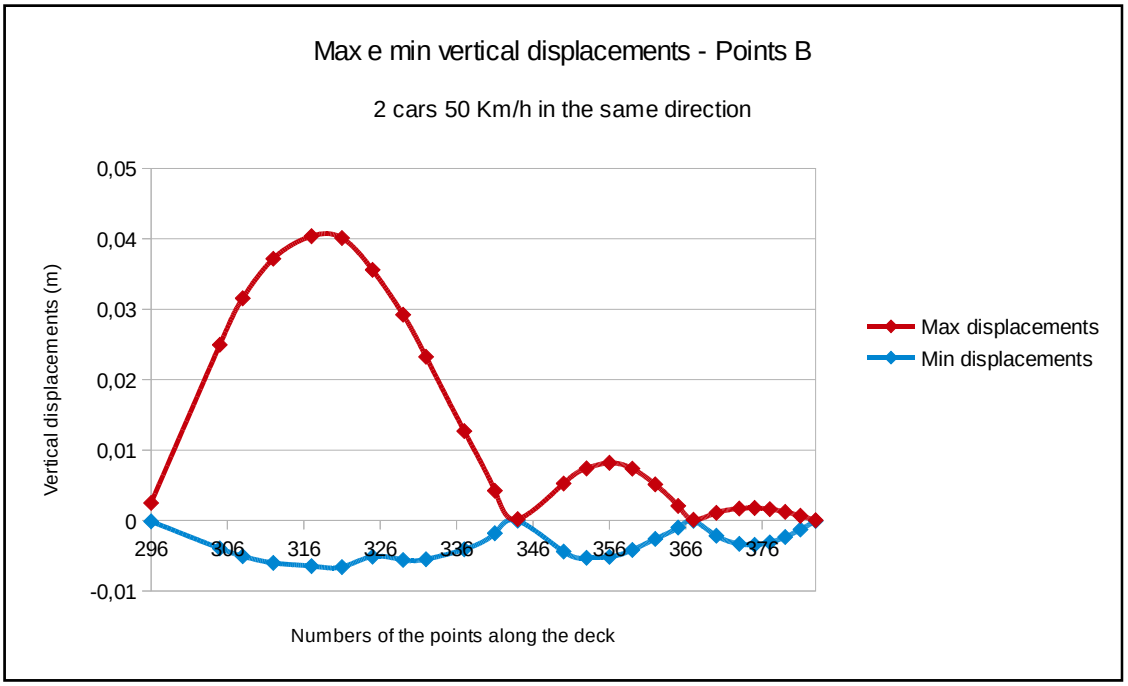

Fig. 195 - Max e min vertical displacements - Points B (case 1)

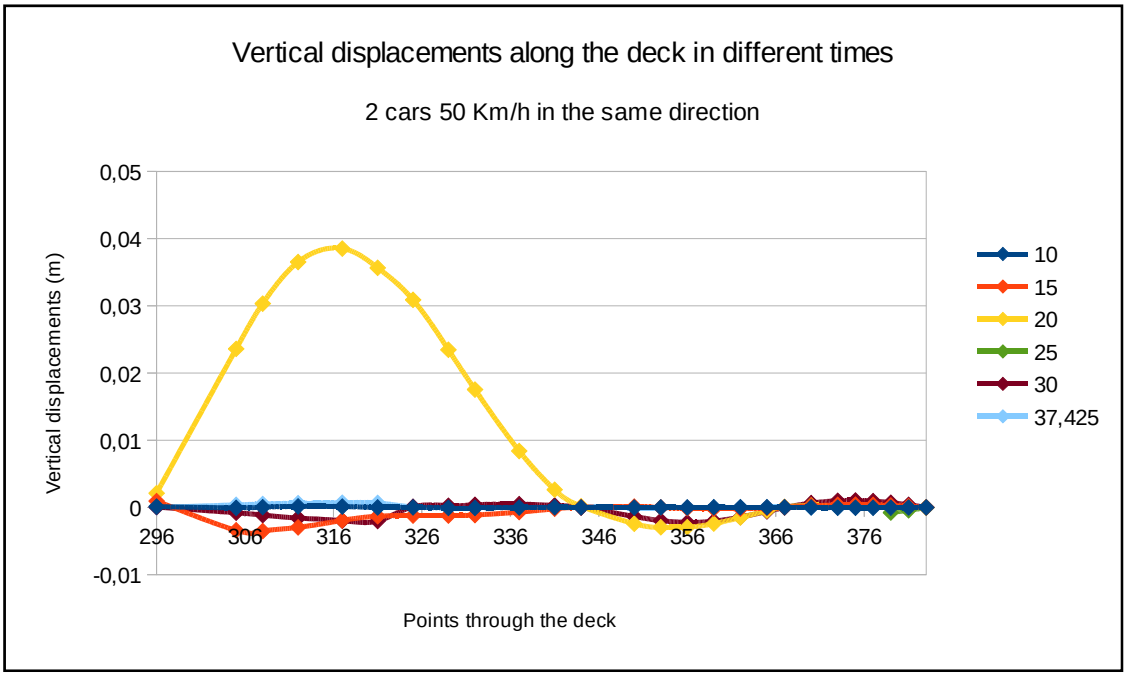

Fig. 196 - Vertical displacements along the deck in different times - position B (case 1)

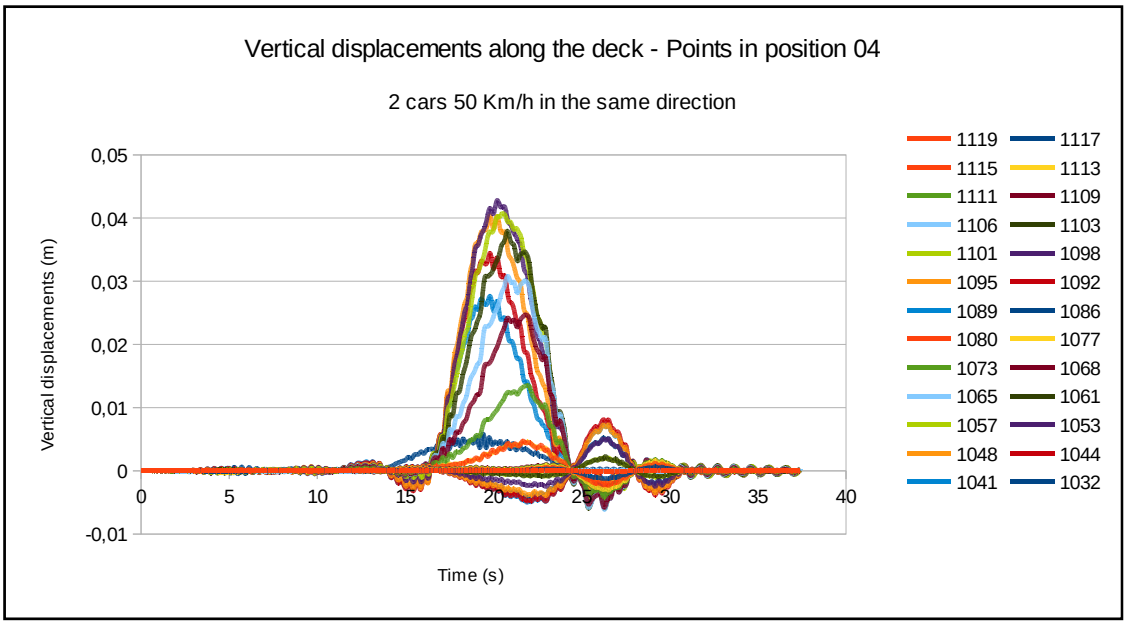

Fig. 197 - Vertical displacements along the deck - Points in position 04 (case 1)

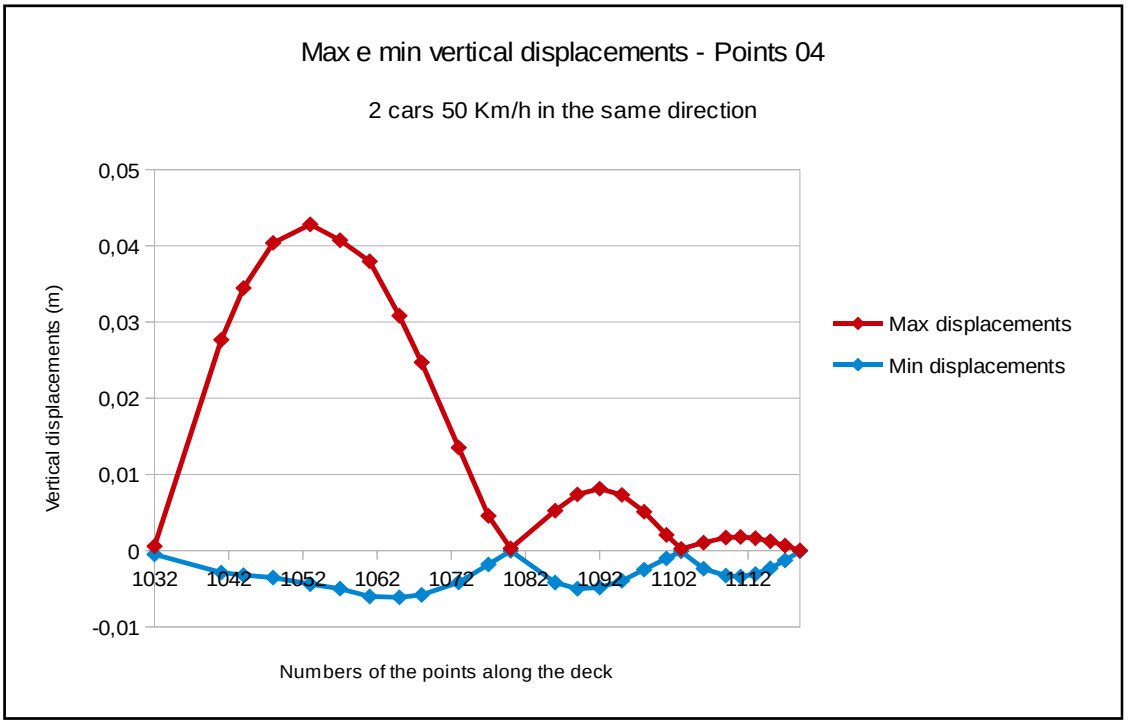

Fig. 198 - Max e min vertical displacements - Points 04 (case 1)

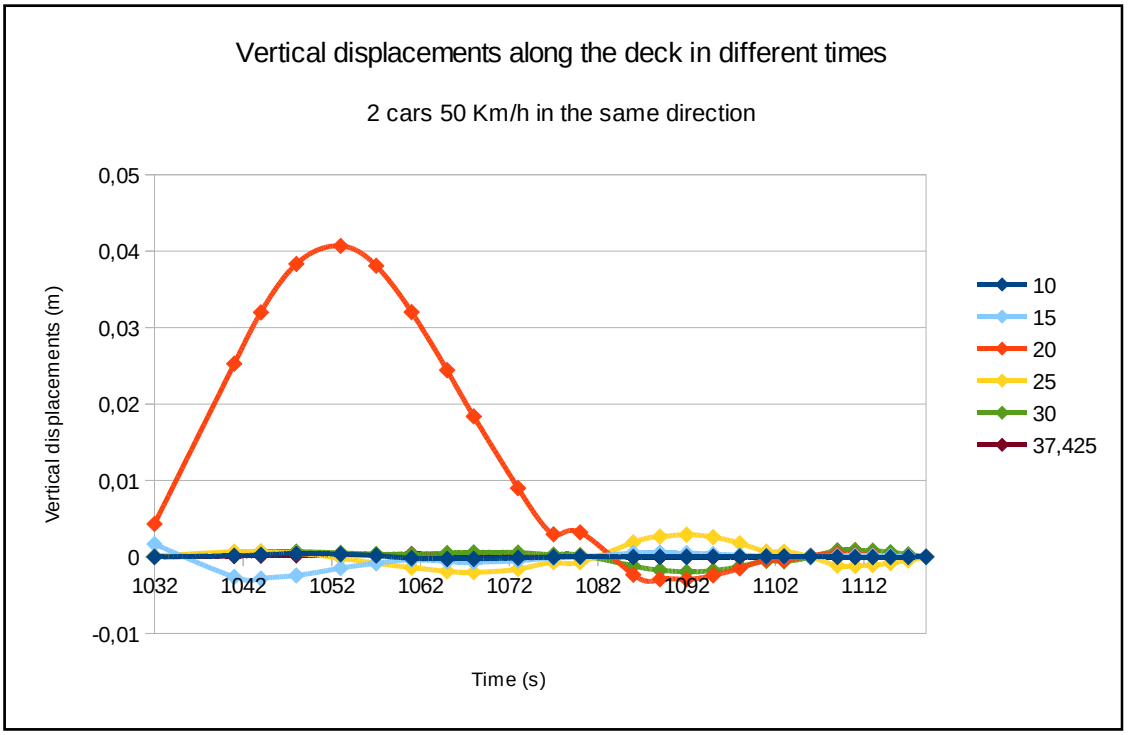

Fig. 199 - Vertical displacements along the deck in different times - positions 04 (case 1)

5.3.2 Case 2: two vehicles in the same direction at 100 Km/h

The second case studies two vehicles at 100 km/h running parallel along the longitudinal dimension of the bridge.

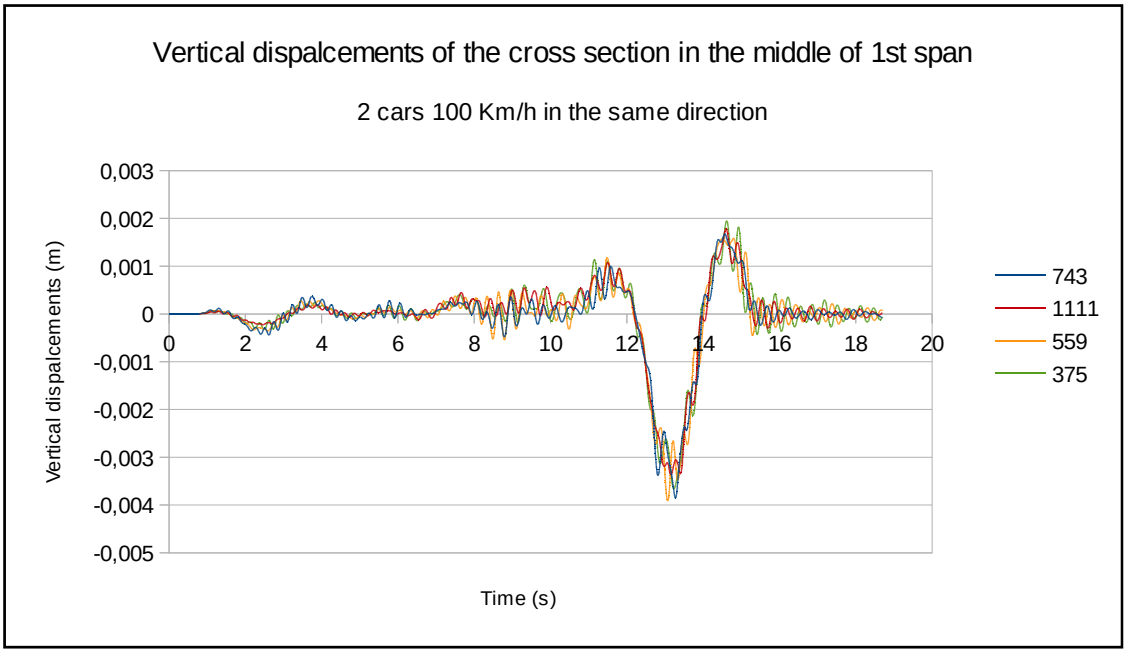

Fig. 200 - Vertical displacements of the cross section in the middle of the 1st span (case 2)

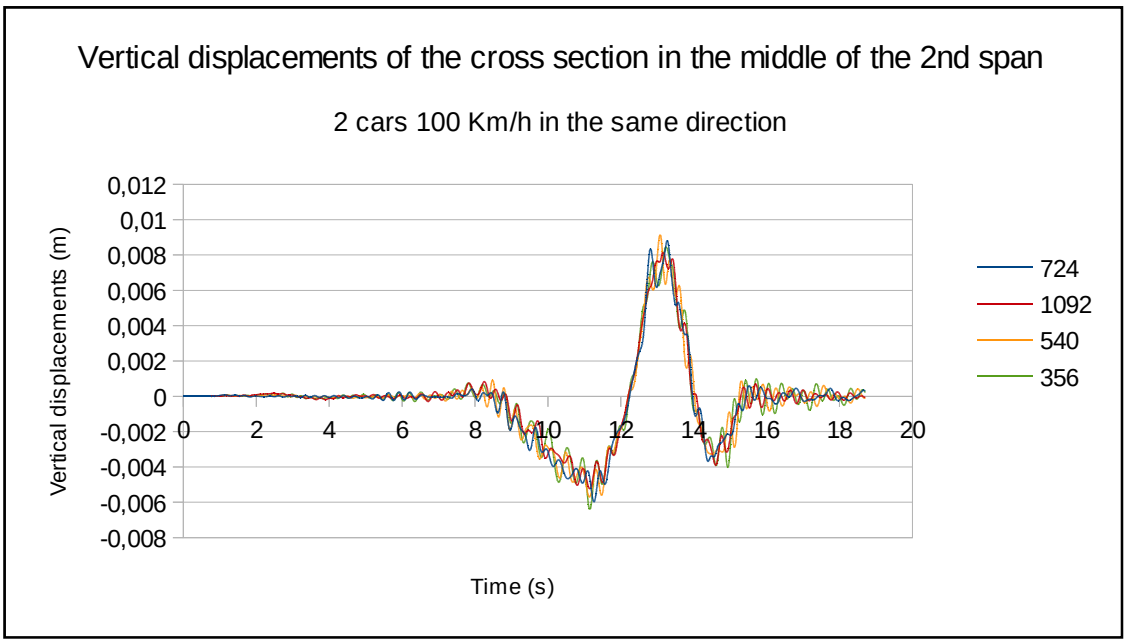

Fig. 201 - Vertical displacements of the cross section in the middle of the 2nd span (case 2)

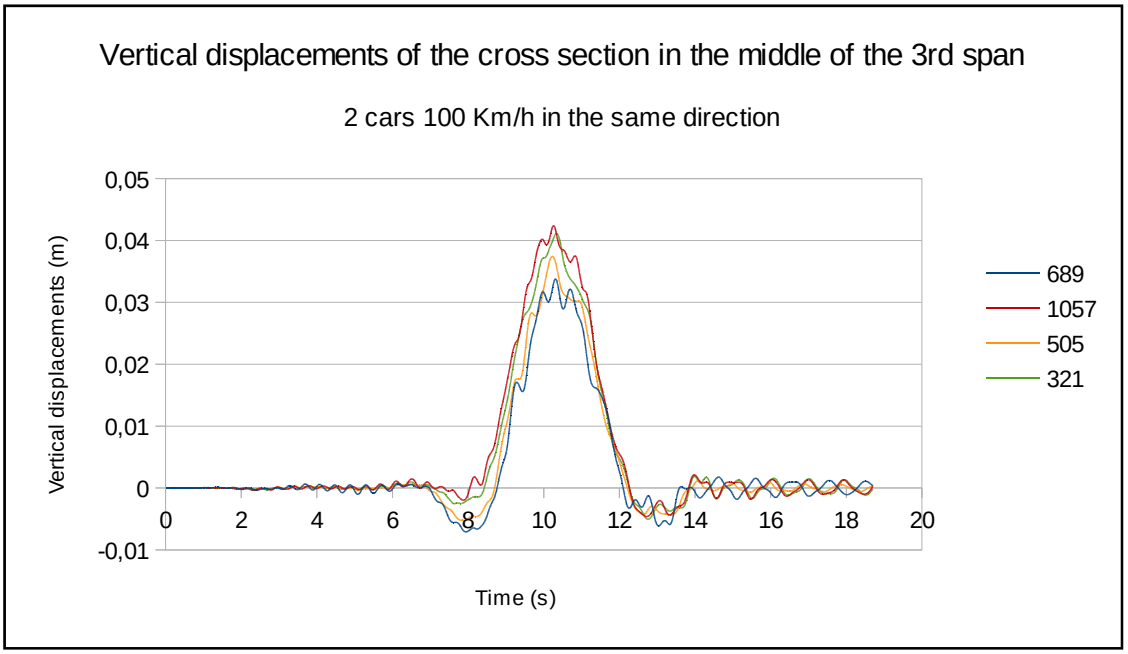

Fig. 202 - Vertical displacements of the cross section in the middle of the 3rd span (case 2)

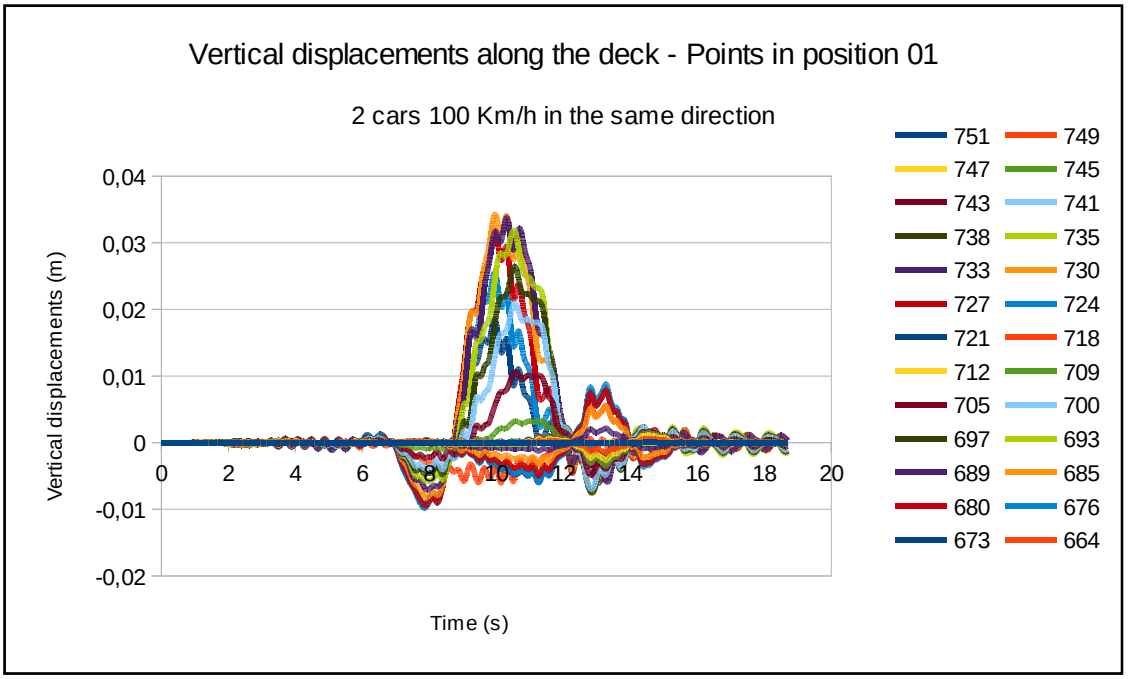

Fig. 203 - Vertical displacements along the deck - Points in position 01 (case 2)

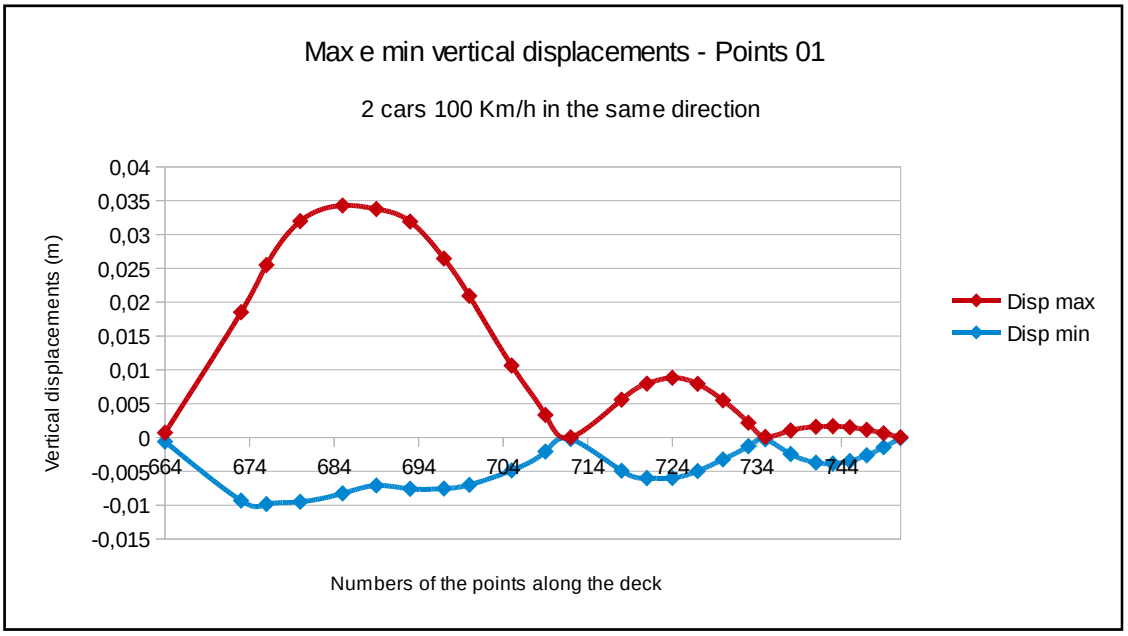

Fig. 204 - Max e min vertical displacements - Points 01 (case 2)

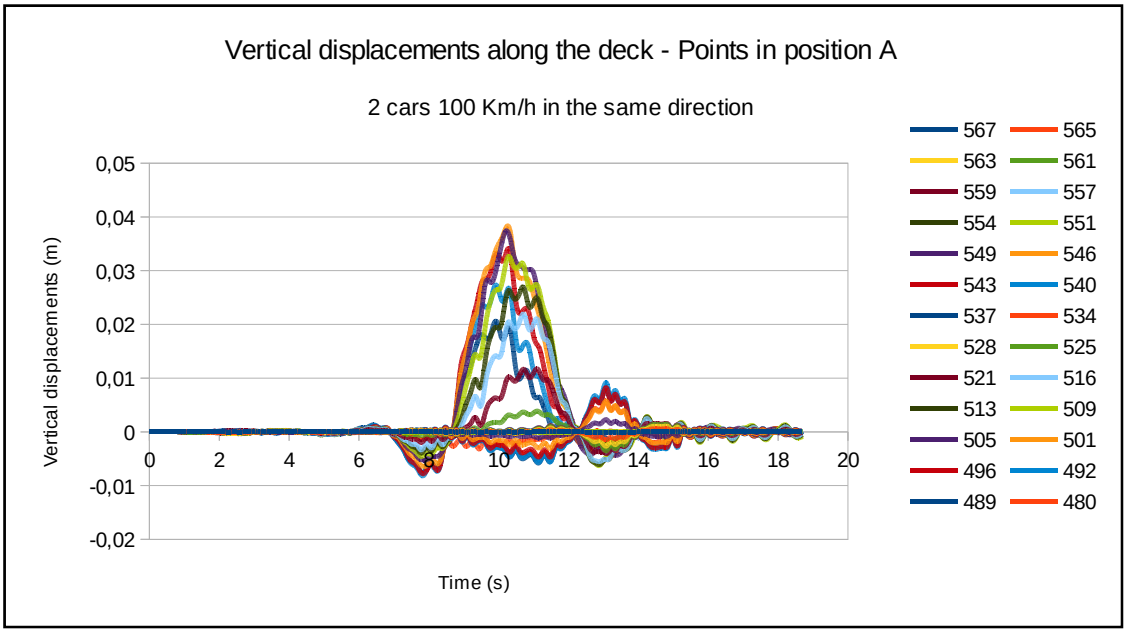

Fig. 205 - Vertical displacements along the deck - Points in position A (case 2)

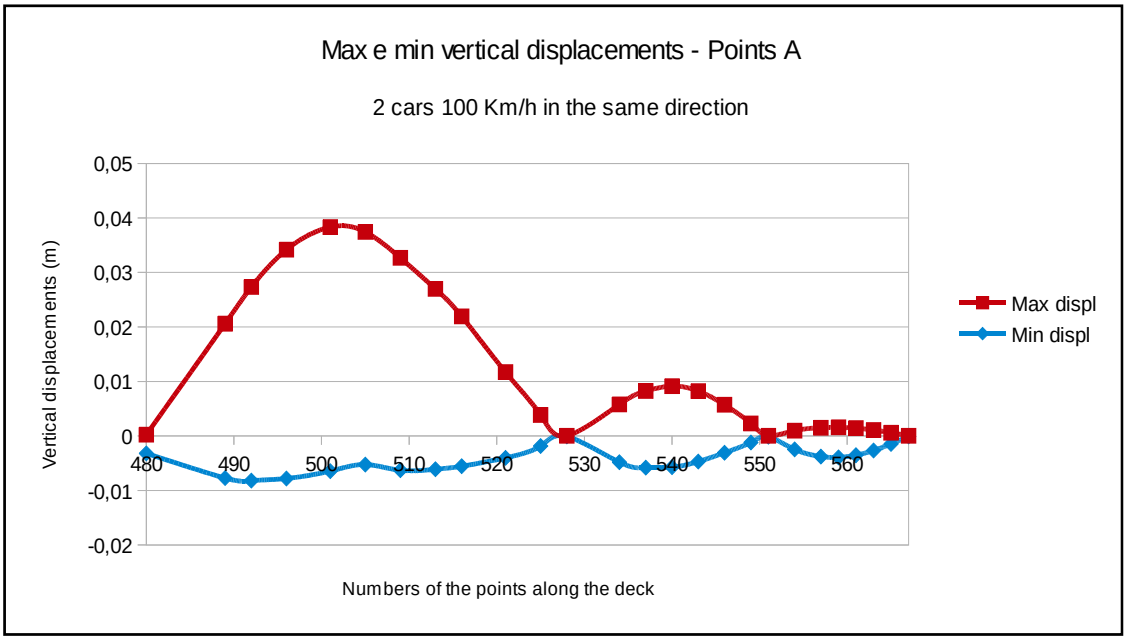

Fig. 206 - Max e min vertical displacements - Points A (case 2)

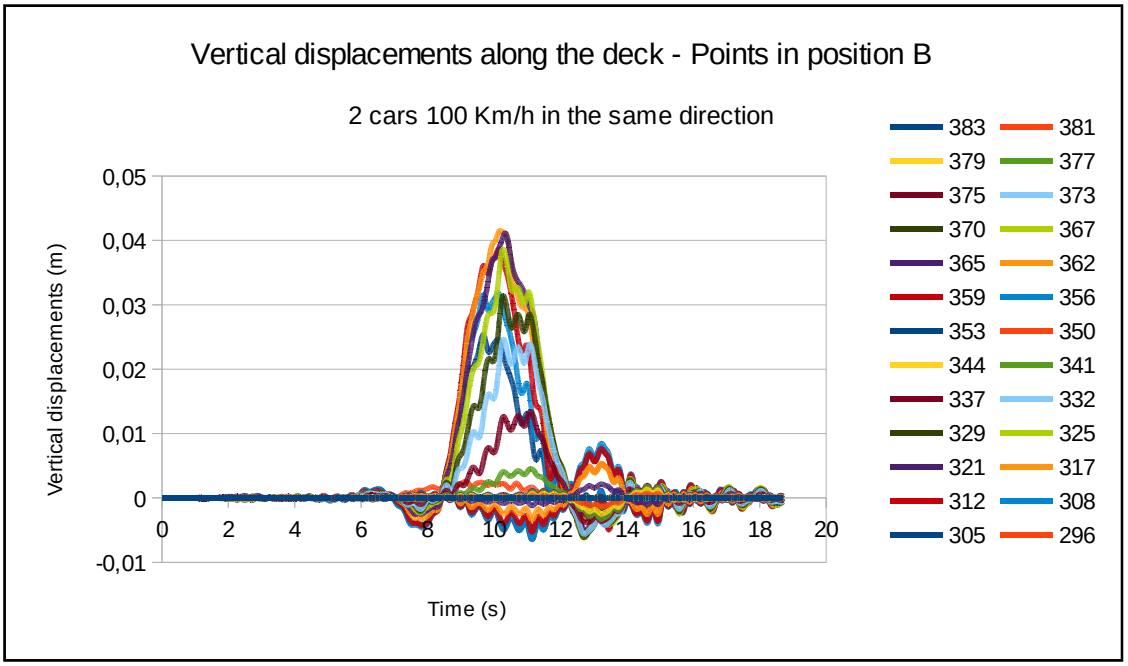

Fig. 207 - Vertical displacements along the deck - Points in position B (case 2)

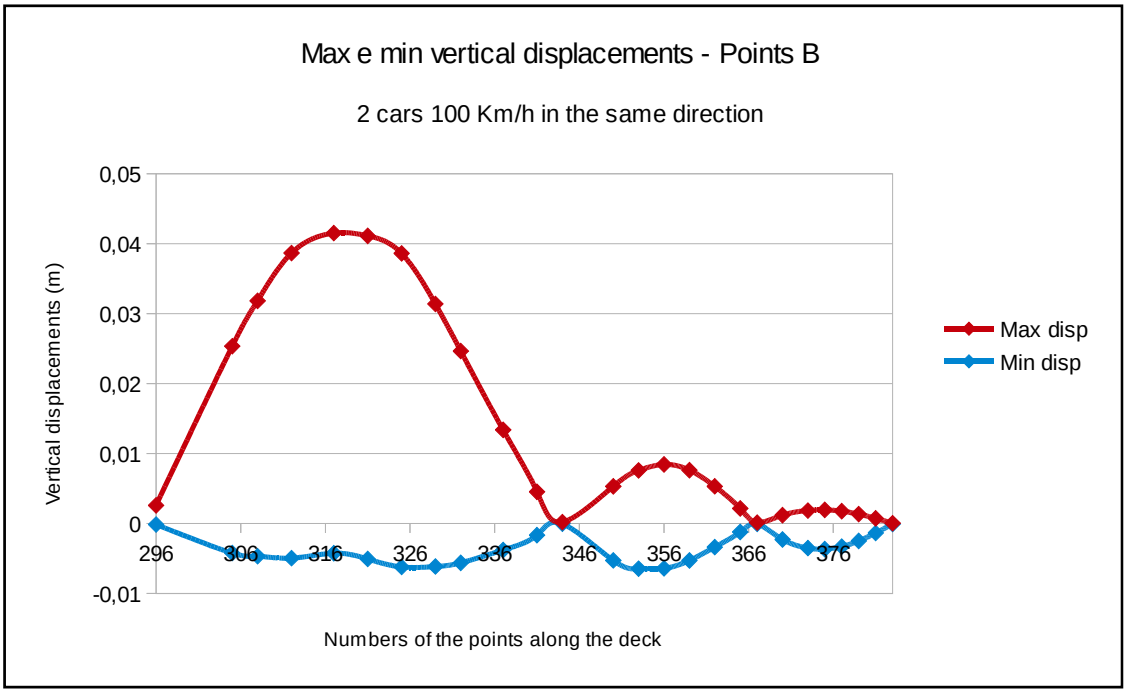

Fig. 208 - Max e min vertical displacements - Points B (case 2)

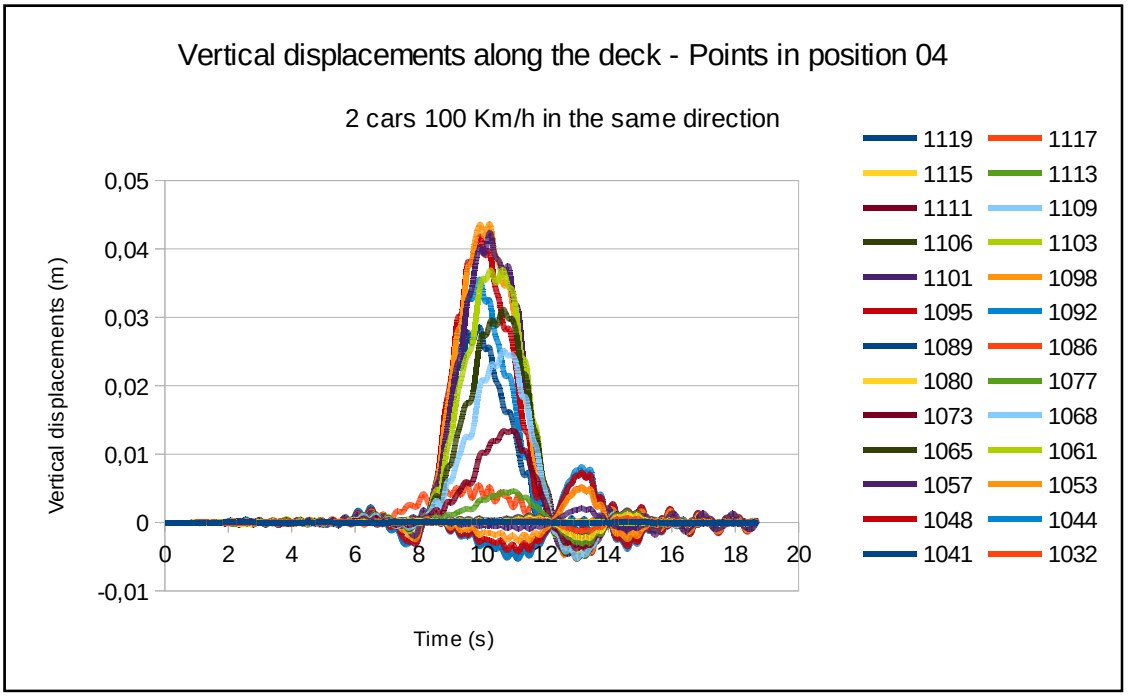

Fig. 209 - Vertical displacements along the deck - Points in position 04 (case 2)

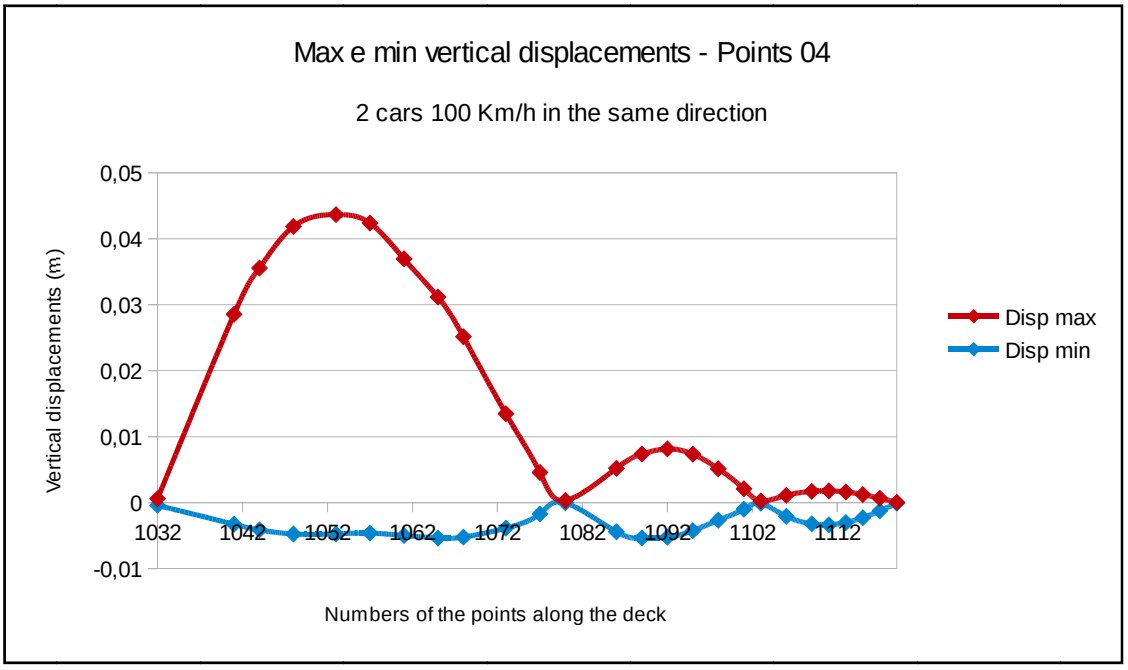

Fig. 210 - Max e min vertical displacements - Points 04 (case 2)

In general, the responses tend to increase with the increase in vehicle speed.

5.3.3 Case 3: traffic flow

The traffic flow is simulated by a random group of cars with different velocities and directions like reported in the figure below.

Definition of Vehicles Motion (Speed, Position, Type) :

Vehicle Number (is used for Simulation) :	Vehicle Type:	Vehicle Speed: [km/h]	Vehicle Position - Delta x: [m]	Vehicle Position - Delta y: [m]
☑ No. 01	1	50	0	4.11
☑ No. 02	1	-70	0	7.61
☑ No. 03	1	40	-12	4.11
☑ No. 04	1	-60	-12	7.61
☑ No. 05	1	60	-24	4.11
☑ No. 06	1	-50	-24	7.61
☑ No. 07	1	40	-36	4.11
☑ No. 08	1	-100	-36	7.61
☑ No. 09	1	120	-46	4.11
☑ No. 10	1	-100	-46	7.61
☑ No. 11	1	100	-55	4.11
☑ No. 12	1	-130	-55	7.61
☑ No. 13	1	80	-65	4.11
☑ No. 14	1	-70	-65	7.61
☑ No. 15	1	90	-80	4.11
☑ No. 16	1	-90	-80	7.61
☑ No. 17	1	70	-90	4.11
☑ No. 18	1	-120	-90	7.61
☑ No. 19	1	90	-100	4.11
☑ No. 20	1	-90	-100	7.61

Tab. 30 - Vehicles motion (traffic flow)

The three following pictures show the vertical displacements time-history at the midspan of each parts, subjected to the traffic flow. The vehicle has a point contact with the bridge deck and maintains that contact as it moves along the deck.

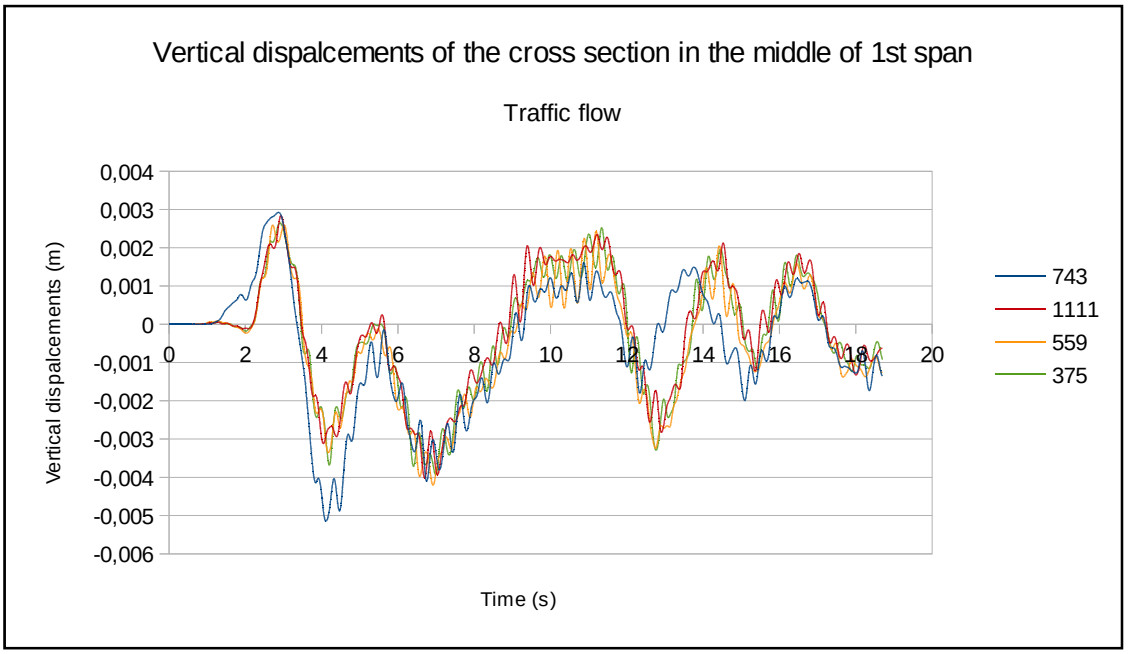

Fig. 211 - Vertical displacements of the cross section in the middle of the 1st span (case 3)

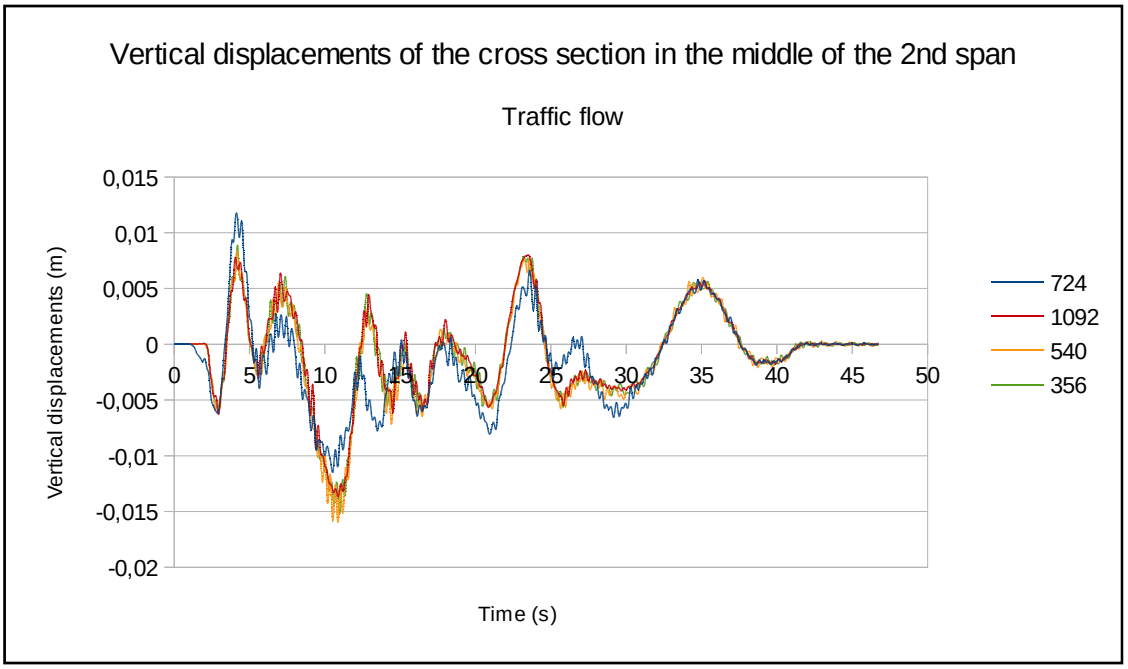

Fig. 212 - Vertical displacements of the cross section in the middle of the 2nd span (case 3)

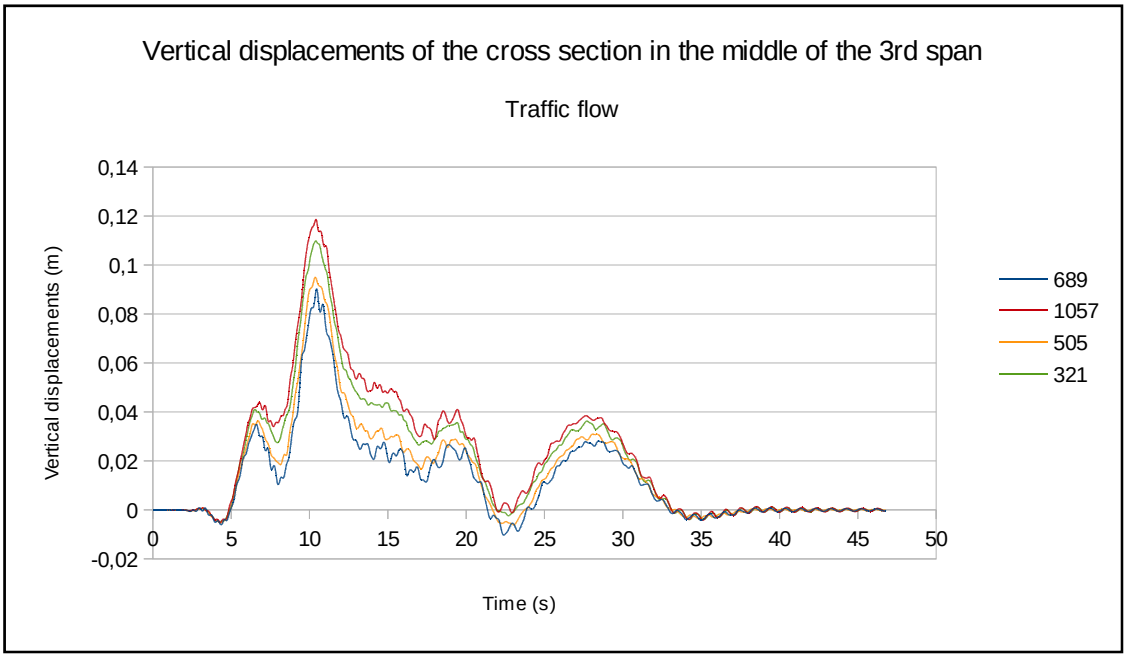

Fig. 213 - Vertical displacements of the cross section in the middle of the 3rd span (case 3)

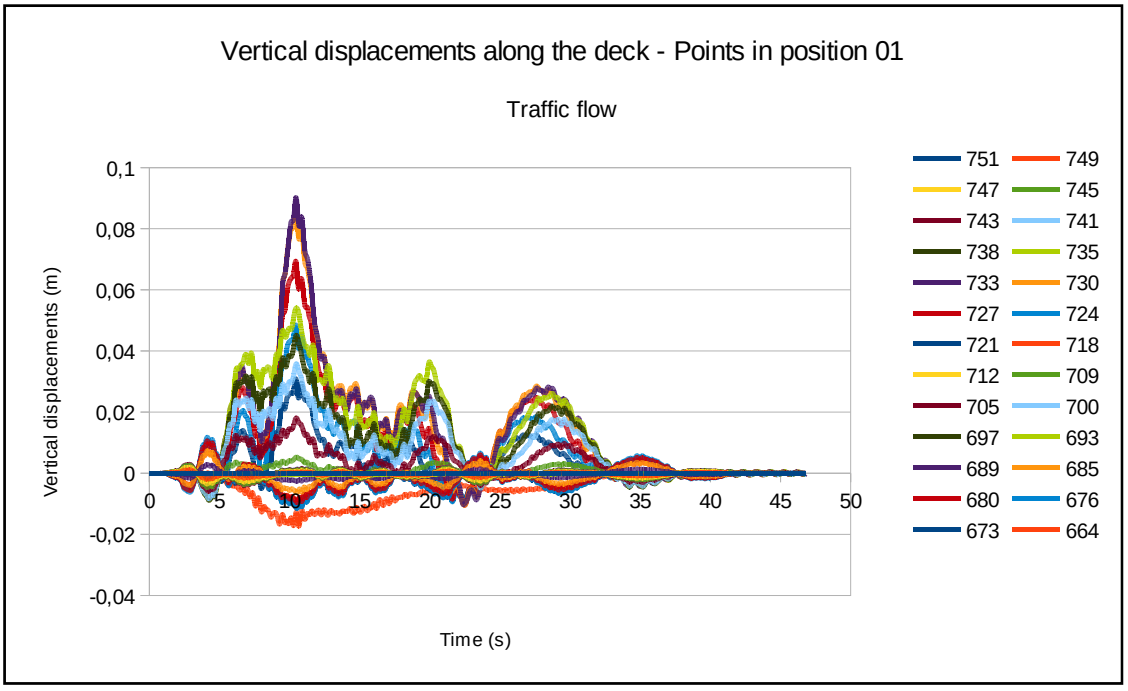

Fig. 214 - Vertical displacements along the deck - Points in position 01 (case 3)

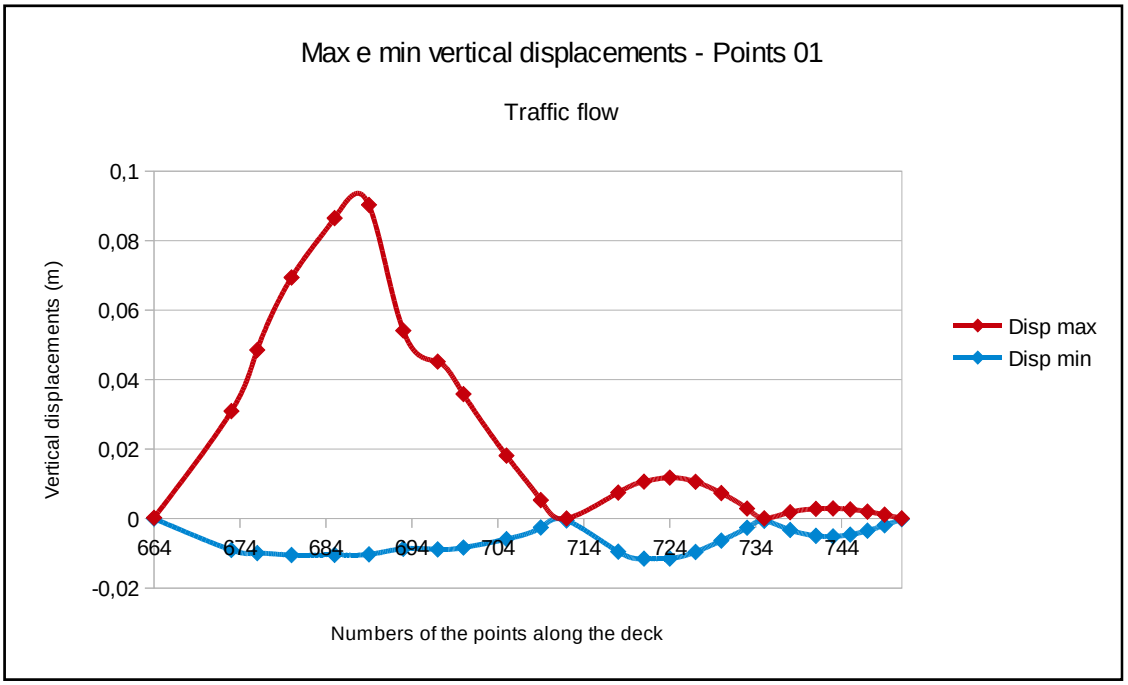

Fig. 215 - Max e min vertical displacements - Points 01 (case 3)

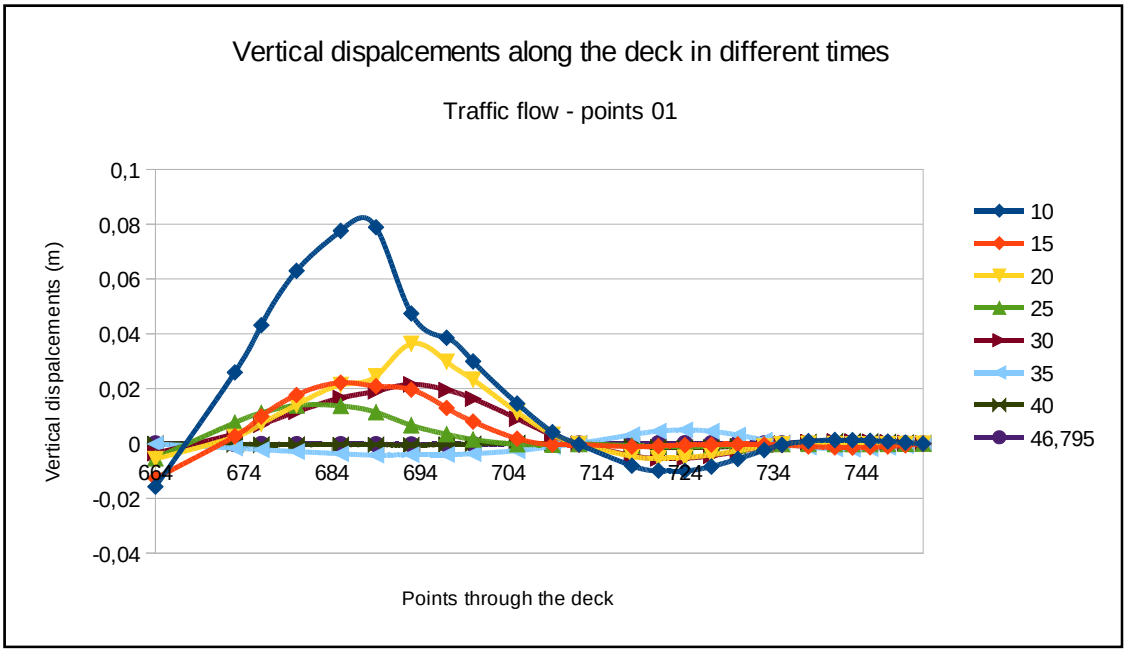

Fig. 216 - Vertical displacements along the deck in different times - position 01 (case 3)

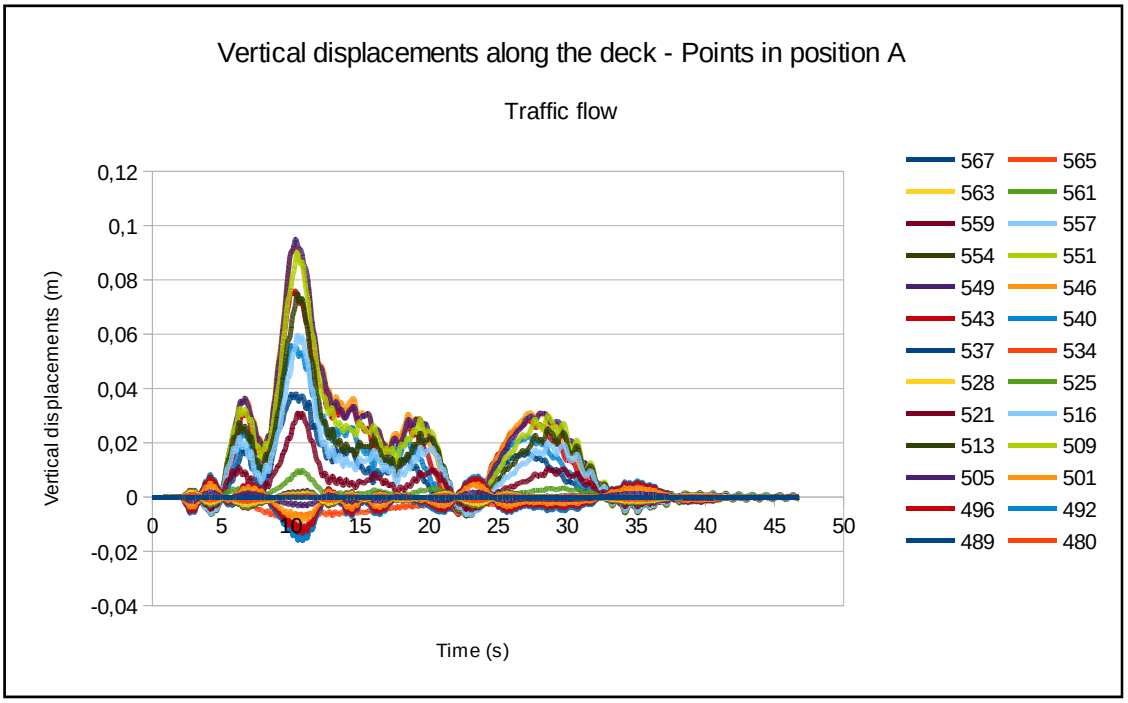

Fig. 217 - Vertical displacements along the deck - Points in position A (case 3)

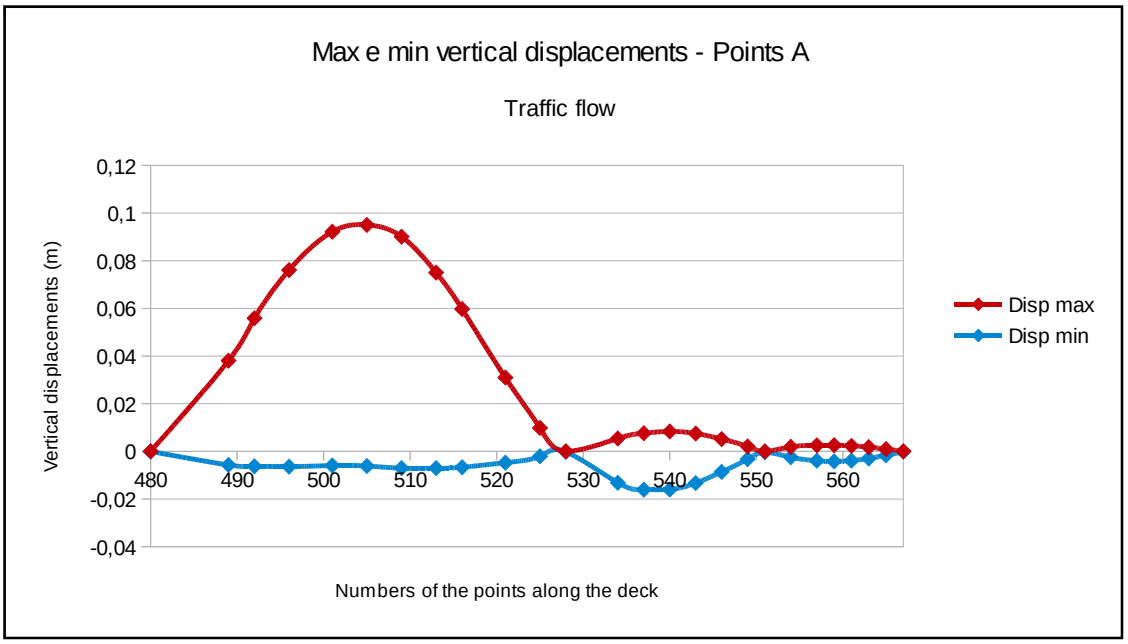

Fig. 218 - Max e min vertical displacements - Points A (case 3)

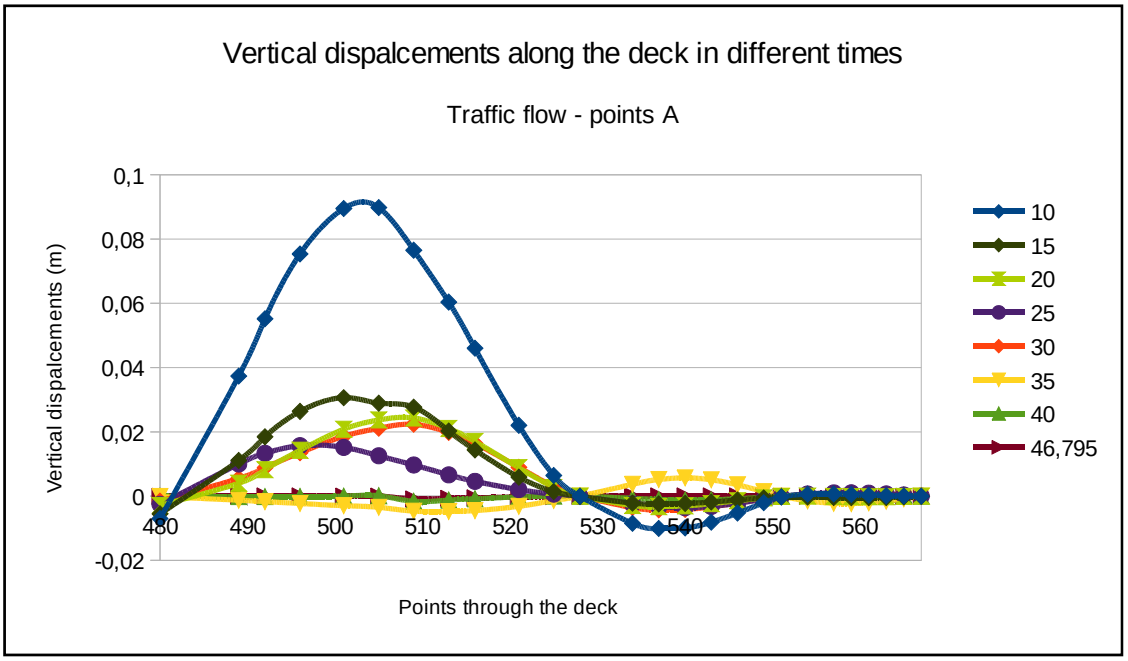

Fig. 219 - Vertical displacements along the deck in different times - position A (case 3)

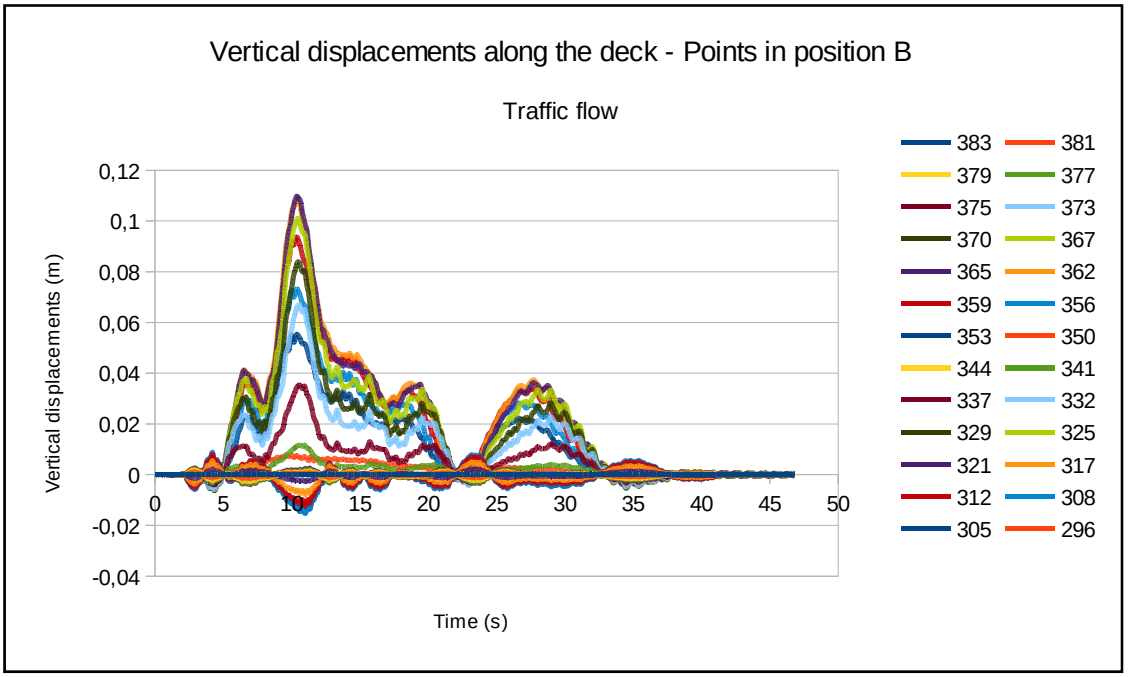

Fig. 220 - Vertical displacements along the deck - Points in position B (case 3)

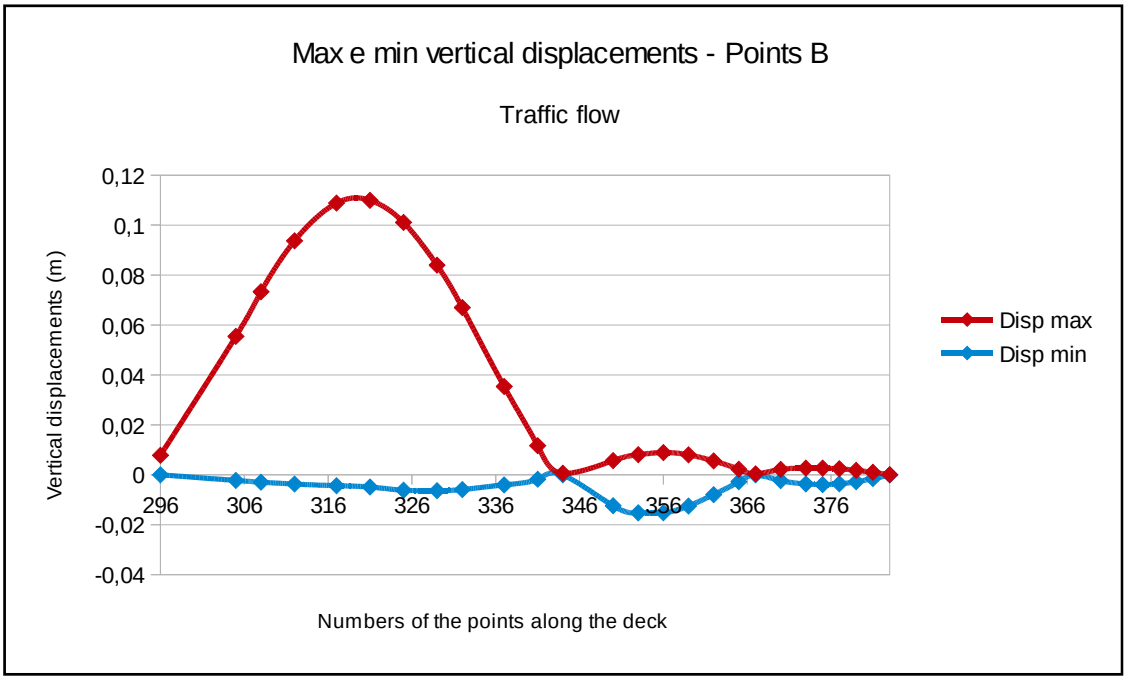

Fig. 221 - Max e min vertical displacements - Points B (case 3)

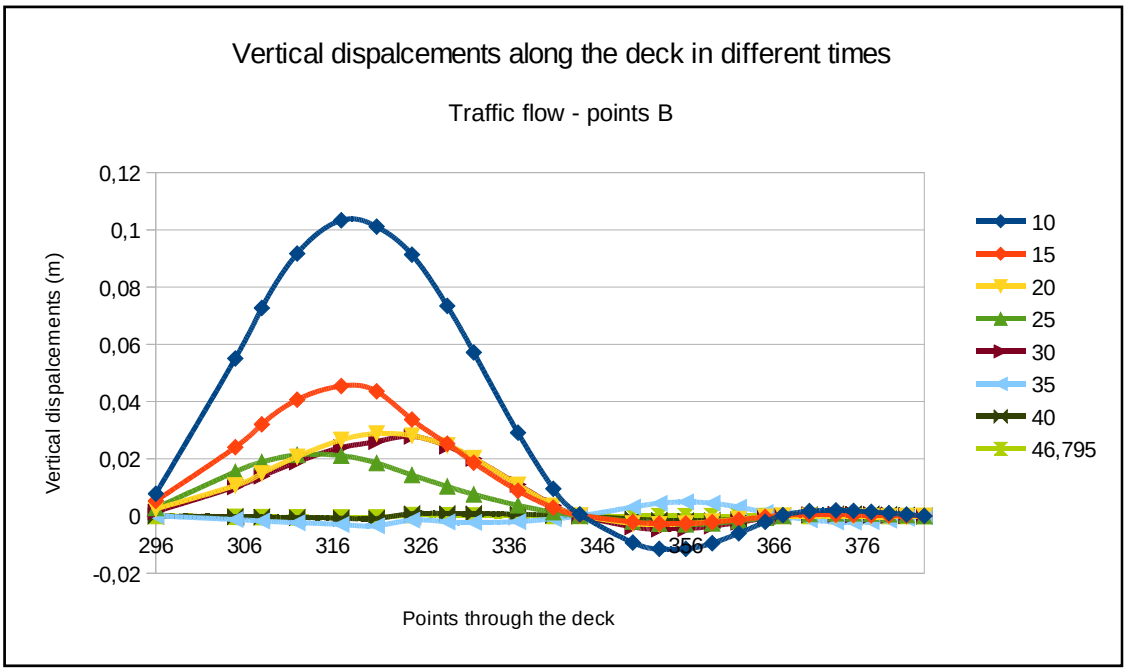

Fig. 222 - Vertical displacements along the deck in different times - position B (case 3)

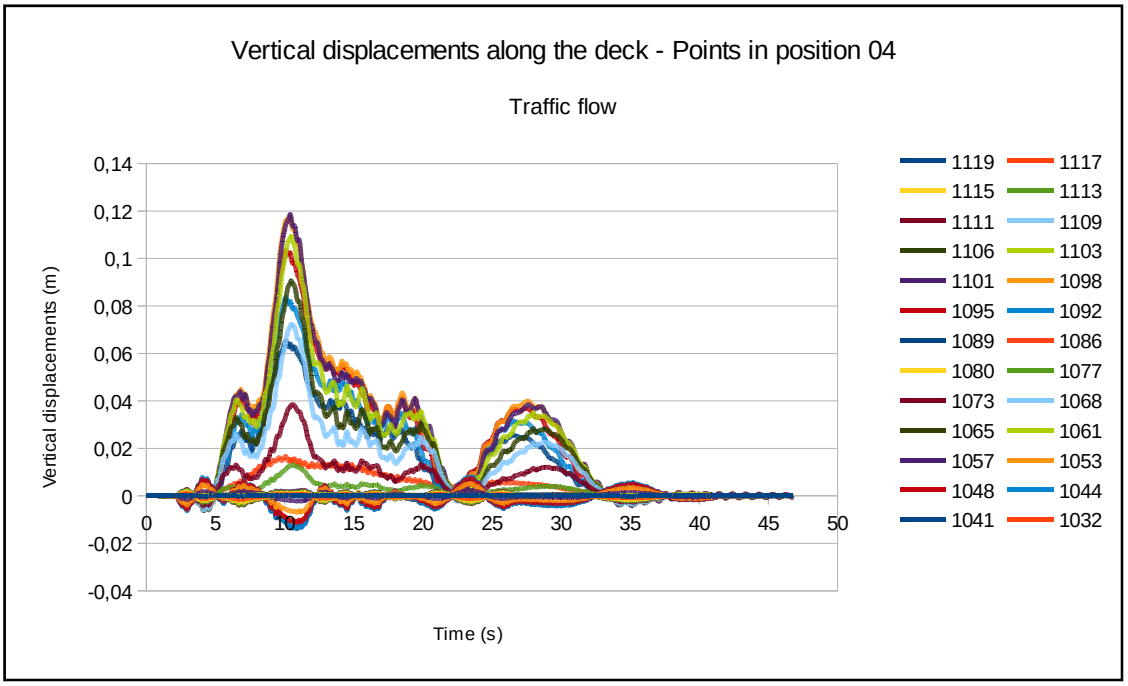

Fig. 223 - Vertical displacements along the deck - Points in position 04 (case 3)

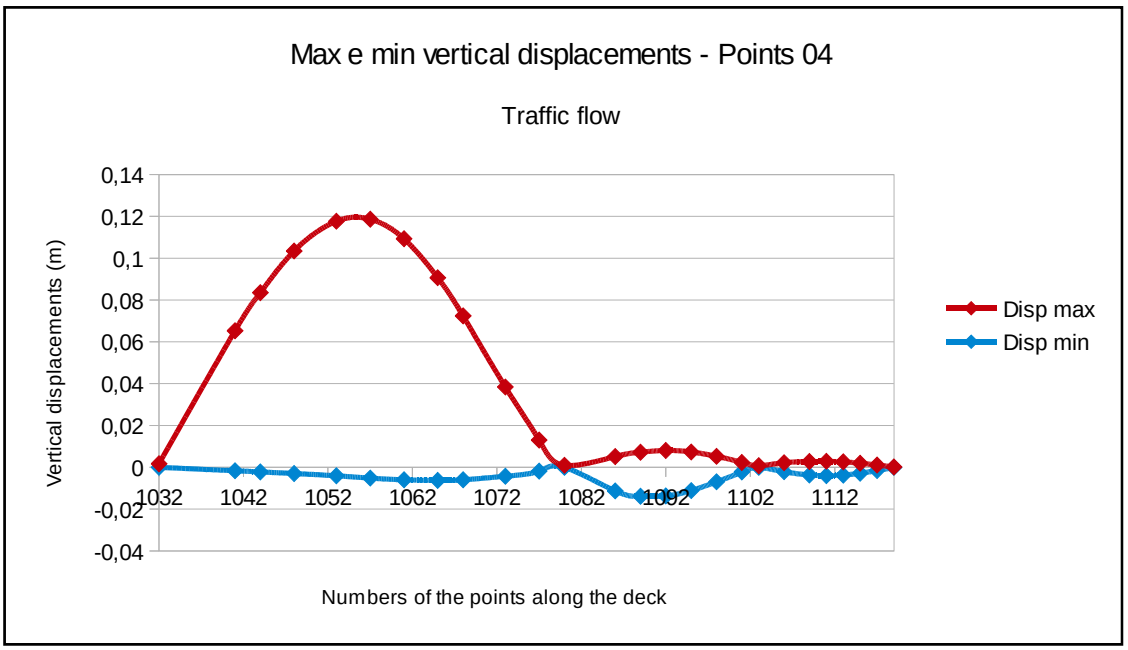

Fig. 224 - Max e min vertical displacements - Points 04 (case 3)

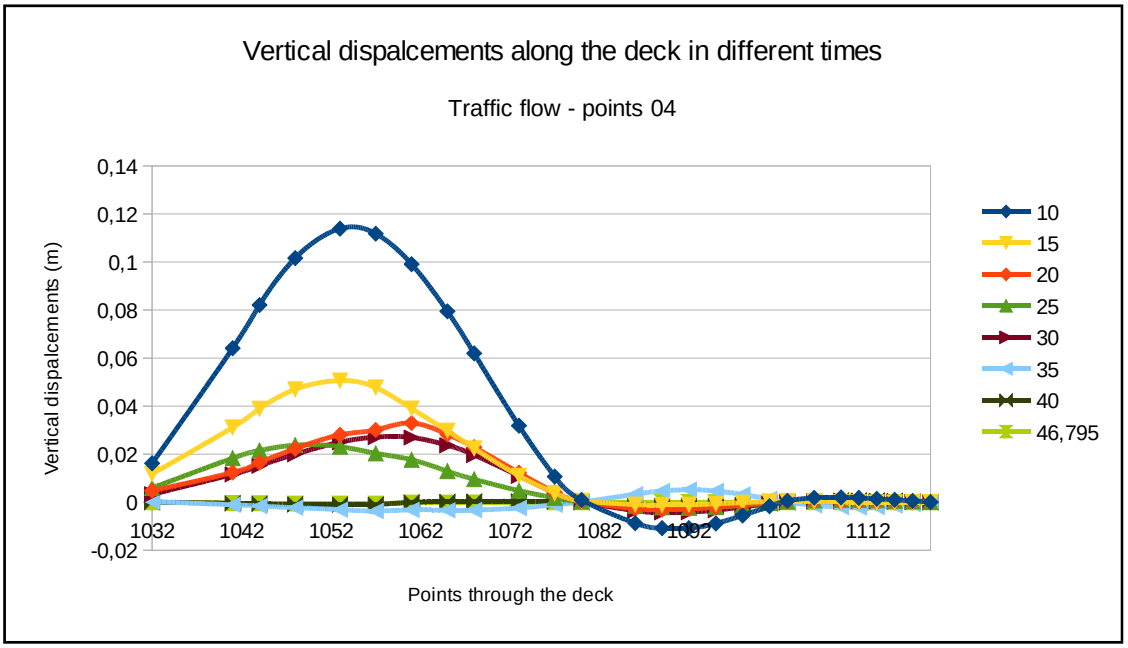

Fig. 225 - Vertical displacements along the deck in different times - position 04 (case 3)

In the following two figures the comparison between measured values with accelerometers and simulated one with the software is reported.

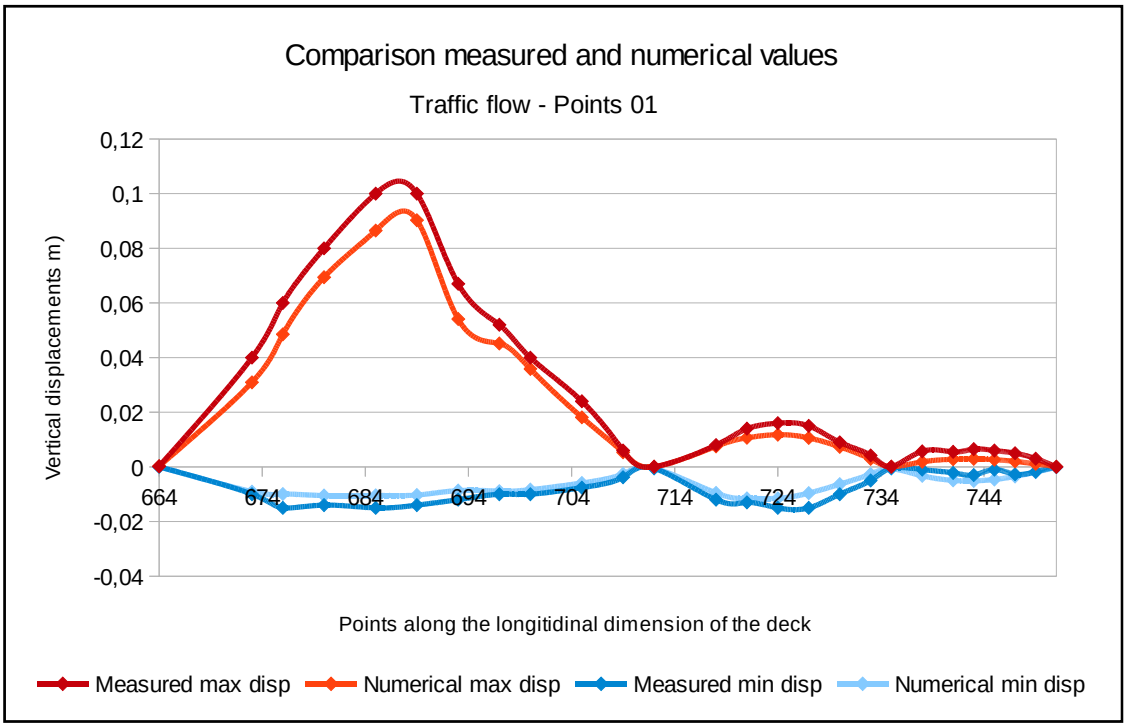

Fig. 226 - Comparison measured and numerical values (Points 01)

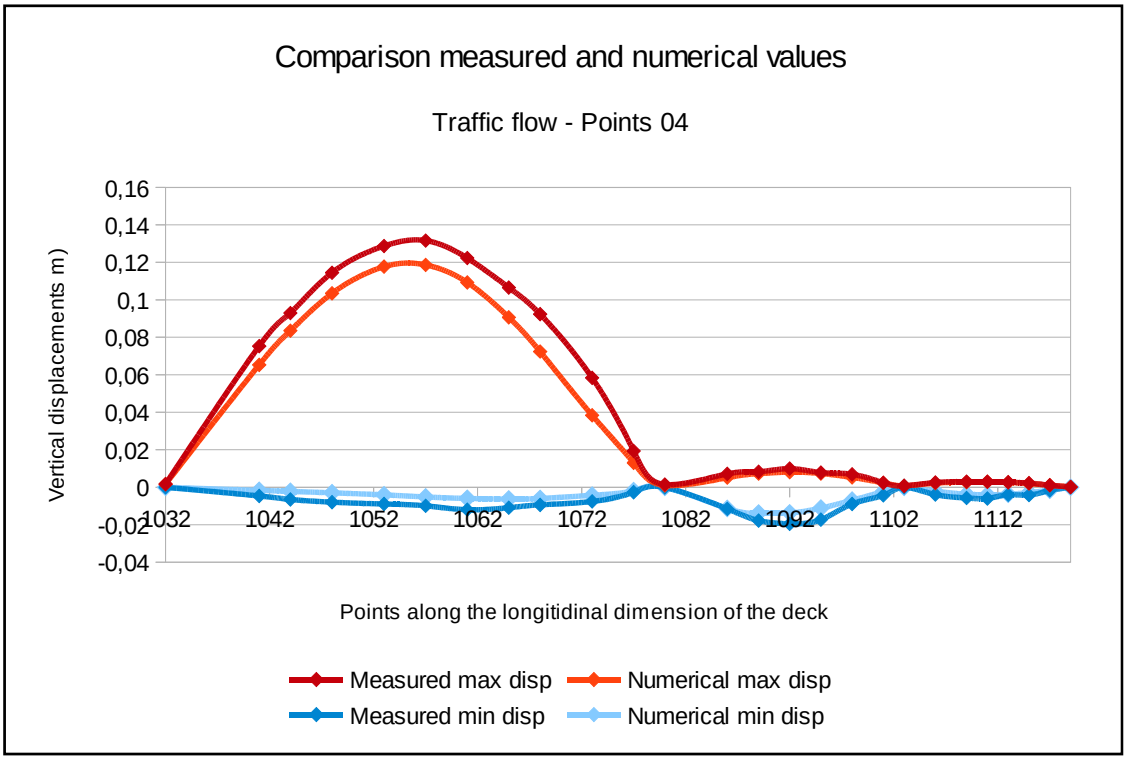

Fig. 227 - Comparison measured and numerical values (Points 04)

The comparison is done for the maximum and minimum displacements along the deck in the two main positions.

The figures show that the traffic flow's simulation approximates well the real behavior of the bridge with little errors that can be neglected.

6. CONCLUSIONS

This research is focused towards understanding the dynamic characteristics of the highway bridge Lanovy Most.

Creation of the three fem models.

Base on previous research and static analysis of the bridge, three 3-dimensional numerical models are created; on one of these a dynamic analysis of the bridge is conducted in order to find frequencies and mode shapes.

The three fem models developed are:

- a simple fem model composed by a sequence of beams representing the deck of the bridge;
- the same beam model with additional masses connected by rigid links to the central beams;
- an accurate plates model in which the cross section is divided and composed by plate elements.

The beam model is mostly adopted as it is simple and it can account for the essential characteristics of the bridge. In particular the simple beam element models of the bridge deck that neglect the deck slab cannot effectively represent the three-dimensional vibration behavior of cable-stayed bridges.

The plate model may be necessary for slab bridges and some cases in which the traversing path of the vehicles is not along the centre-line.

The finite element and experimental modal analysis provide a comprehensive investigation on the dynamic properties of cable-stayed bridges. The analytical modal analysis through three-dimensional finite element modeling gives a detailed description of the physical and modal characteristics of the bridge, while the experimental modal analysis through the field dynamic tests provides a valuable source of information to validate the drawing-based idealized finite element model.

Optimization and validation of the fem models.

These three analytical models of the bridge are validated and optimized by the corresponding measured modal parameters identified from the field ambient vibration tests. Validation of all FE models was based on comparison between numerical results and experimental data of displacements, strains, and accelerations recorded during the field test.

In particular the experimental frequencies and modes of natural vibration were utilized for the creation of the spatial modal model of this bridge; they serve also as valuable information to verify and update a design model of the observed bridge.

The set of measurements was recorded in 26 sections along the deck, four points for each sections, for a total of 104 points.
Accelerometers were placed on the bridge to measure and determine its vibration. The accelerometers logged data as ambient traffic traveled over the bridge, the overall goal of these measurements is to aid in understanding the bridge response.

The final baseline finite element model was the full three-dimensional model, plates model, that reflects the dynamic behavior well in every aspect.
A good correlation is achieved between the numerically calculated modal parameters from three dimensional finite element analysis and identified ones from field ambient vibration tests. The validated finite element model that reflects the built-up structural conditions can serve as the baseline model for a more precise dynamic response prediction, damage identification and long-term health monitoring of the bridge.

The initial equilibrium configuration of cable-stayed bridge is important since it is the starting position from which to perform the succeeding dynamic analysis. The modal analysis of cable-stayed bridges and succeeding dynamic analysis under earthquakes, winds and vehicles involves two steps: the static analysis due to the dead load and cable tensions, and the subsequent dynamic analysis.
Comparison of analytical (finite element) model predictions and full-scale measurements on the Lanovy Most bridge show that the best match of measured modes is with a finite element (FE) model that uses a deck composed by a series of plates to represent deck bending and torsional properties.

In the following figure the comparison between the “plates fem model” and the measured values of natural frequencies is reported. In particular the percentage errors between the two are presented.
The errors are always less than 6% for the most of the modes and not high also for the other modes.

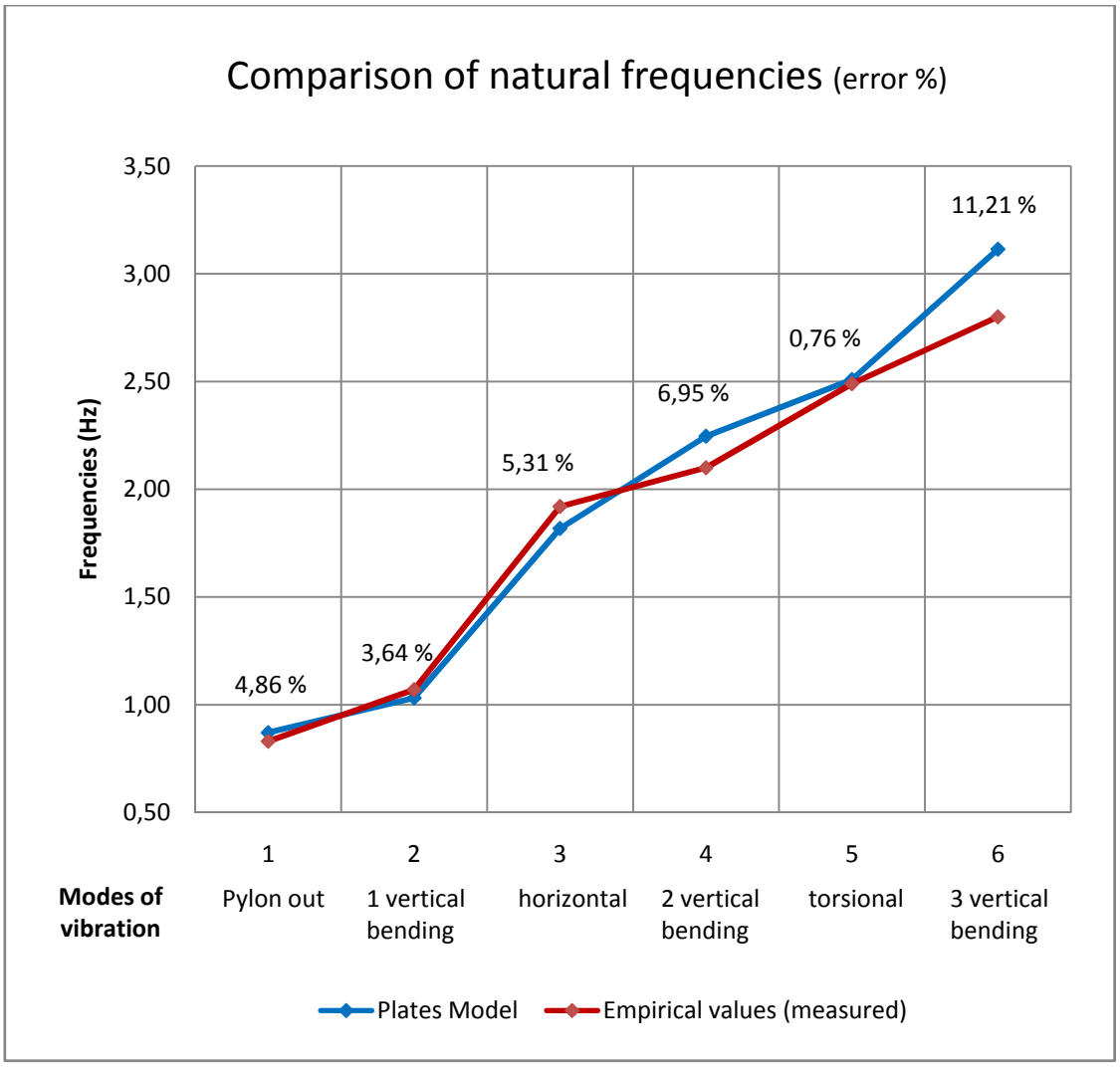

Fig. 228 - Comparison of natural frequencies "plates model" and measured values

Break of one cable.

A special event was also studied, the break of one cable, situation happened just after the construction of the cable stayed bridge. A dynamic analysis was carried on from the initial static condition.

From the evaluation of the displacements through time it is possible to see how the vibrations of every points of the bridge (deck, pylon, cables) are damped to the static configuration.

Traffic flow vibrations.

The vehicle-structure interaction problem of a bridge traversed by a moving vehicle has been investigated.

Moving vehicles and trains have often been modeled as either moving forces, moving masses or moving mass-spring-damper systems.

The vehicle in this work was modelled as a non linear dynamic system of mass elements mutually interconnected by massless force links. Thus the vehicle is a space 2 axle system like schematized in the figure below.

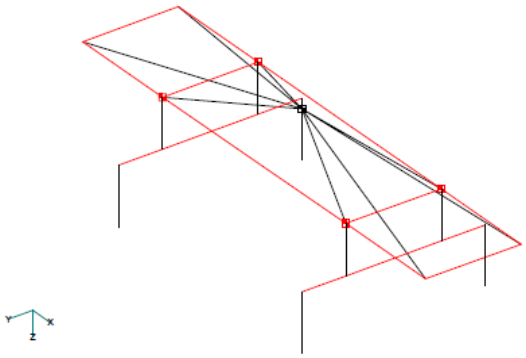

Fig. 229 - 2 axle space system for the vehicle

The relationship between the bridge vibration characteristics and the vehicle speed was determined.

The interaction between the moving vehicles and the bridge is a nonlinear problem. The significant parameters affecting the dynamic response of a bridge include the natural frequencies of the bridge, vehicle characteristics, vehicle velocity and traversing path, the number of vehicles and their relative positions on the bridge, roadway surface roughness, as well as the damping characteristics of the bridge and vehicles. etc.
The analysis has been performed in time domain by considering the interaction between the vehicle and the bridge pavement, coupling of vertical and torsional motion of the deck due to eccentrically placed vehicles and the randomness of the bridge surface irregularity.
Road surface roughness affects the impact value of vehicle loads significantly. The impact value of vehicle loads increases with the road surface roughness.
The traffic load patterns play an important role in simulating the dynamic responses of box-girder bridge.

In general, the dynamic responses of bridge tend to increase with the increase of vehicle speed. The dynamic amplification factors due to bridge-vehicle interaction associated with higher vehicle speed are much more pronounced than lower vehicle speed.
Results at different vehicle speeds demonstrated that the maximum dynamic deflection occurs at the vicinity of the bridge mid-span.

The results of this investigation could be applied to verify the integrity of the structure along its life.

References

[1] Wei-Xin Ren, Xue-Lin Peng. Baseline finite element modeling of a large span cable-stayed bridge through field ambient vibration tests. Available online 12 January 2005.

[2] D.C.D. Oguamanam. *Free vibration of beams with finite mass rigid tip load and flexural torsional coupling*. Department of Mechanical and Industrial Engineering, Ryerson University, Toronto, Ont., Canada 2002.

[3] Wei-Xin Ren, Xue-Lin Peng, You-Qin Lin. *Experimental and analytical studies on dynamic characteristics of a large span cable-stayed bridge*.

[4] R. Karoumi. Some *modeling aspects in the non linear finite element analysis of cable-supported bridges*. Comput. Struct. 71 (1999).

[5] Animesh Das, Anjan Dutta, Sudip Talukdar. *Effcient dynamic analysis of cable-stayed bridges under vehicular movement using space and time adaptivity*. Department of Civil Engineering, Indian Institute of Technology, Guwahati India.

[6] J.T. Gaunt, C.D. Sutton. *Joint highway research project - highway bridge vibration studies*. Purdue University.

[7] Ewins, D.J. 2000. *Modal Testing: Theory, Practice and Application*. 2° edizione, Research Studies Press LTD, England.

[8] D. P. Thambiratnam and G. H. Brameld. *Free vibration analysis of bridges*. School of Civil Engineering, Queensland University of Technology, Australia 1994.

[9] James M.W. Brownjohn, Jeffery Lee, Bernard Cheong. *Dynamic performance of a curved cable-stayed bridge*. School of Civil and Structural Engineering, Nanyang Technological University, Singapore 1998.

[10] E. Esmailzadeh, N. Jalili. *Vehicle-passenger-structure interaction of uniform bridges traversed by moving vehicles*.

[11] F T K Au, Y S Cheng and Y K Cheung. *Vibration analysis of bridges under moving vehicles and trains*. Republic of China 2001.

[12] F.T.K. Au, Y.S. Cheng, Y.K. Cheung, D.Y. Zheng. *On the determination of natural frequencies and mode shake of cable-stayed bridges*. Republic of China 2000

[13] Lei Gong, Moe S. Cheung. *Computer simulation of dynamic interactions between vehicle and long span box girder bridges*. Department of Civil Engineering, University of Ottawa, Ottawa, Canada.

[14] W. Baumgaertner. *Bridge-truck interaction: simulation, measurements and load identification.*

[15] P. Galvín and J. Domínguez*. Dynamic Study of the Barqueta Cable-Stayed Bridge*. Escuela Superior de Ingenieros Universidad de Sevilla.

[16] He Zhang, Xu Xie. *Dynamic responses of cable-stayed bridges to vehicular loadingincluding the effects of the local vibration of cables*. Department of Civil Engineering, Zhejiang University, Hangzhou, China.

[17] Liuchuang Wei, Heming Cheng, Jianyun Li. *Modal Analysis of a Cable-stayed Bridge*. Faculty of Civil Engineering and Architecture. Kunming University of Science and Technology, China.

[18] Dr. Michael Chajes. *Dynamic Analysis of Delaware's Smart Bridge*. Research Experience for Undergraduates in Bridge Engineering, University of Delaware 2006.

[19] Wendy E. Daniell, John H.G. Macdonald. I*mproved finite element modelling of a cable-stayed bridge through systematic manual tuning.* Department of Civil Engineering, University of Bristol, UK 2005.

[20] Hugo C. Gomez, Paul J. Fanning, Maria Q. Feng, Sungchil Lee. *Testing and long-term monitoring of a curved concrete box girder bridge.* Journal of Engineering Structures 2011.

[21] Qi LI, Dingjun WU, Xiaobin Huang. *Vibration analysis of medium and small span bridges subjected to mixed marshalling freight trains*. Front. Archit. Civ. Eng. China 2008.

[22] Leslaw Kwasniewski, Hongyi Li, JerryWekezer, Jerzy Malachowski. *Finite element analysis of vehicle–bridge interaction*. Science and direct 2005.

[23] G. H. Tan, G. H. Brameld and D. P. Thambiratnam. *Development of an analytical model for treating bridge-vehicle interaction*. Engineering Structures 1998.

[24] Chul Woo Kim, Mitsuo Kawatani, Ki Bong Kim. *Three-dimensional dynamic analysis for bridge-vehicle interaction with roadway roughness*. Computers and Structures 2004.

[25] Xinfeng Yin, Zhi Fang, C.S. Cai, Lu Deng. *Non-stationary random vibration of bridges under vehicles with variable speed*. Engineering Structures 2009.

[26] X. He, Y. Noda, T. Hayashikawa, M. Kawatani, T. Matsumoto. *An analytical approach to coupled vibration of curved rationalized girder bridges and running vehicles.* Science Direct.

[27] Bart Peeters and Guido De Roeck. *Reference-based stochastic subspace identification for output-only modal analysis.* Department of Civil Engineering, Katholieke Universiteit Leuven, Belgium 1999.

[28] P.H. Rattigan, E.J. O. Brien, A. Gonzalez. *The Dynamic Amplification on Highway Bridges due to Traffic Flow*. Dept. of Civil Engineering, University College Dublin, Dublin 2, Ireland.

[29] M. Polàk. *Study of dynamic behaviour of a prestressed concrete road bridge*. Structural Dynamics – EURODYN 1999. Czech Technical University, Prague, Czech Republic.

[30] Miloslav Bat'a, Vladimìr Bìly, Michal Polàk. *Models to assess vehicle/bridge interaction*. International Journal Heavy Vehicle Systems, Special Issue 1996. Czech Technical University, Prague, Czech Republic.